HETEROGENEOUS PORPHYRIN-BASED CATALYSTS FOR ELECTROCHEMICAL ENERGY APPLICATIONS

By Aleksei N. Marianov

Supervisor

Dr. Yijiao Jiang

The thesis is submitted in fulfillment of

the requirements for the degree of

Doctor of Philosophy

Macquarie University

Faculty of Science and Engineering

Department of Engineering

October 2019

I certify that the work in this thesis has not previously been submitted for a degree nor has it been submitted as part of requirements for a degree to any other university or institution other than Macquarie University.

Aleksei N. Marianov 18 October 2019

ACKNOWLEDGEMENTS

I would like to express my gratitude to Macquarie University for generous financial support of my research through iMQRES scholarship and School of Engineering research budget. Also, PGRF grant that allowed me to present my research at the ACS National meeting and visit to the University of Binghamton is gratefully acknowledged. I am infinitely grateful to Dr Yijiao Jiang for continuous support and encouragement during three years of my candidature. Undoubtedly, without her help this thesis would have never happen. Also, I express my deepest gratitude to my co-supervisor Prof. Candace Lang who always kept me inspired by her positive attitude and who provided me with useful advice multiple times thanks to her vast research experience.

Additionally, without the support of Prof. Yves DeDeene, Dr. Nicole Cordina, Dr. Chao Shen, Dr. Timothy Murphy and Dr. Matthew McKay who helped me to perform NMR, SEM analysis, Raman spectroscopy and mass spectrometry this research would surely not be possible. I would like to thank the team of Macquarie Engineering & Technical Services, especially Walter Adendorff and Sam Borg for their timely and professional help with the mechanical issues.

Also, only unconditional support of my dear wife and parents allowed me to stay on track and keep the spirit high during numerous setbacks. Thank you, Alena, Nikolai and Tatiana for your endless love and encouragement throughout this difficult time. Support of my colleagues, group members and friends, especially Susan Law, Alexander Arriola, Mark Tran, Mark Gatus, Sviatoslav Eliseenko, Haimei Xu, Wenwen Zhang, Xiaoxia Yang, Shengshen Gu, Amanj Kheradmand, Maria Kovaleva, Timo Mayer, Kay-Dennis Boom, Cristo Suárez, Morgan Wheatley and Neil Anderson all of whom have helped me in many ways, is also gratefully acknowledged.

Last but not least, I express my sincere gratitude to the examiners for reviewing my thesis and for their valuable comments.

LIST OF PUBLICATIONS

Journal publications included in the thesis

[1] Marianov, A. N.; Jiang, Y., Covalent ligation of Co molecular catalyst to carbon cloth for efficient electroreduction of CO_2 in water, *Appl. Catal. B,* **2019**, 244, 881-888

[2] Marianov, A.; Jiang, Y., Effect of manganese porphyrin covalent immobilisation on electrocatalytic water oxidation and oxygen reduction reactions, *ACS Sustainable Chem. Eng.,* **2019**, 7, 3838-3848

[3] Marianov, A.; Jiang, Y., In pursuit of a stable electrocatalyst: kinetic inhibition of Co porphyrin degradation in CO_2 reduction in aqueous medium, *Submitted to Appl. Catal. B.*

Other publications

[1] Zhang, X.; Marianov, A.; Jiang, Y.; Cazorla C.; Chu D., Hierarchically Constructed Silver Nanowire@ Nickel-Iron Layered Double Hydroxide Nanostructures for Electrocatalytic Water Splitting, *ACS Appl. Nano Mater.*, **2020**, 3, 887-895.

[2] Kheradmand, A.; Zhu, Y.; Zhang, W.; Marianov, A.; Jiang, Y., Cobalt oxide on mesoporous carbon nitride for improved photocatalytic hydrogen production under visible light irradiation, *Int. J. Hydrogen Energy*, **2019**, 44, 17930-17942.

[3] Xu, H.; Wang, Z., Miao, Z.; Zhu, Y.; Marianov, A.; Wang, L.; Castignolles, P.; Gaborieau, M.; Huang, J. and Jiang, Y., Correlation between acidity and catalytic performance of mesoporous zirconium oxophosphate in phenylglyoxal conversion, *ACS Sustainable Chem. Eng.,* **2019**, 7, 8931-8942.

[4] Zhu, Y.; Marianov, A.; Xu, H.; Lang, C. and Jiang, Y., Bimetallic Ag-Cu supported on graphitic carbon nitride nanotubes for improved visible-light photocatalytic hydrogen production, *ACS Appl. Mater. Interfaces.*, **2018**, 10, 9468-9477

[5] Mayer, T.; Marianov, A. N. and Inglis, D. W., Comparing fusion bonding methods for glass substrates, *Mater. Res. Express*, **2018**, 5, 085201.

[6] Gu, S.; Marianov, A. N.; Zhu, Y.; Jiang, Y., Cobalt porphyrin immobilised on the TiO2 nanotube electrode for CO_2 electroreduction in aqueous solution, *Submitted to ChemCatChem*.

Conference proceedings

[1] A.N. Marianov, Y. Jiang: "Covalent ligation of Co molecular catalyst to carbon cloth for efficient electroreduction of CO_2" International Symposium on Advancement and Prospect of Catalysis Science & Technology, Sydney, Australia, 25-27 July 2018, oral presentation

[2] A.N. Marianov, Y. Jiang: "Rational design of heterogeneous Co porphyrin-based catalysts for CO_2 electroreduction in aqueous medium" ACS National meeting, Orlando, USA, 31 March – 04 April 2019, oral presentation

LIST OF ACRONYMS

CO	carbon monoxide
CO_2	carbon dioxide
CO_2ERR	CO_2 electrochemical reduction reaction
COSY	homonuclear correlation spectroscopy
CoTPP	cobalt (II) tetraphenylporphyrin
CPE	controlled potential electrolysis
CV	cyclic voltammetry
DMF	*N,N*-dimethylformamide
EDS	energy dispersive X-ray spectroscopy
EIS	electrochemical impedance spectroscopy
EPR	electron paramagnetic resonance
ETN	electron transfer number
Fc	ferrocene
FE(CO)	faradic yield of CO
FeTPP	iron (III) tetraphenylporphyrin
FTIR	Fourier transform infrared spectroscopy
GC	gas chromatography
HMBC	heteronuclear multiple bond correlation
HRMS	high resolution mass spectrometry
HSQC	heteronuclear single quantum correlation
LSV	linear scan voltammetry
MnTPP	manganese (III) tetraphenylporphyrin
NHE	normal hydrogen electrode
NMR	nuclear magnetic resonance
NOESY	nuclear Overhauser effect spectroscopy
OER	oxygen evolution reaction
ORR	oxygen reduction reaction
Py	pyridine
SEM	scanning electron microscopy
TBAP	tetrabutylammonium hexafluorophosphate
TOCSY	total correlation spectroscopy
TOF	turnover frequency
TON	turnover number
TPP	tetraphenylporphyrin
UV/Vis	ultraviolet-visible spectroscopy
Γ_{EA}	electrochemically active amount of complex

ABSTRACT

Complexes of the first row transition metals are a promising class of tunable and inexpensive catalysts for electrochemical energy applications. Although considerable efforts have been devoted to the structure-activity relationships, little attention has been paid to the effects of immobilisation mode on their performance. This thesis shows that covalent grafting of porphyrin-based catalysts to the surface of carbon electrodes could be used as an efficient and simple method that allows to significantly improve rates and selectivities of electrochemical reactions relevant for electrochemical energy applications.

In the first part of this dissertation a reliable procedure for covalent immobilisation of metalloporphyrins onto the surface of carbon electrodes was established. To achieve this, electroreduction of corresponding diazonium salts was chosen as it allows to create an extremely durable C-C bond of a complex with the supporting electrode. Indeed, the reduction of tetraphenylporphyrin diazonium salt under mild conditions on carbon electrodes followed by treatment with hot solution of $Mn(OAc)_2$ in DMF/CH_3COOH proved to be a reliable tool for immobilisation of MnTPP on carbon cloth. The resulting hybrid materials were studied using CV and Raman spectroscopy and the resulting layer of complex was found to possess all signature CV and spectral features characteristic for MnTPP while showing complete lack of solubility signifying the success of covalent immobilisation. Variation of electrodeposition time was found to be a convenient tool to control the density of organometallic layer which in turn allows to shorten the Mn···Mn distance and thus increase the probability of two Mn atoms taking part in a concerted electrochemical process. The use of covalent immobilisation proved to be highly beneficial for ORR in which we achieved significantly higher reduction current density and nearly 100 % selectivity towards $4e^-$ pathway under low overpotentials after 5 min-long TPP electrodeposition. This feature could be explained by the stepwise reduction of O_2 to H_2O_2 and then to H_2O. At the same time the rate of OER appears to be independent of the immobilisation mode and proportional to the amount of electrochemically active complex on the surface. The study of MnTPP-modified electrodes in CO_2ERR did not result in a significant CO_2 reduction current due to inherently low activity of the catalyst itself. At the same time, significant suppression of the hydrogen evolution upon covalent immobilisation of MnTPP was observed. This phenomenon was ascribed to the blocking effect of well-formed organic layer and much better surface coverage compared to analogous electrode prepared via drop-casting.

Following the assessment of MnTPP-based design the electrodeposition technique was used for the synthesis of covalently immobilised CoTPP which is known for its excellent activity in electrocatalytic reduction reactions. This material showed 2.4 times higher density of electrochemically active species compared to the noncovalently immobilised analogue and the activity of the resulting electrodes shows dramatic improvement of CO formation rate during CO_2ERR in neutral electrolyte under an overpotential of 500 mV. Indeed, a TOF of 8.3 s^{-1} was achieved contrary to the drop-cast analogue which exhibited TOF of 4.5 s^{-1} only. Furthermore, in full agreement with the previous results, the maximum average FE(CO) increased from 50 % to 67 % upon introduction of a covalent link with the surface. Also, the optimum potential corresponding to the highest FE(CO) was achieved under 50 mV less negative potential compared to noncovalent immobilisation. The catalyst exhibited excellent cumulative TON of $3.9 \cdot 10^5$ in a 24 h long electrolysis surpassing performance of the drop-cast counterpart by the factor of 3. We must note here that the TON and TOF values measured in our study are among the highest to date surpassing those reported for Fe hydroxyporphyrins and Co porphyrin-based covalent organic frameworks. Apparently, the kinetics of CO_2ERR under low overpotentials is highly dependent on the rate of the electron transfer between the electrode surface and the complex while the resulting phenylene linker is playing the role of a "molecular wire" within the catalytic layer.

Further, the activity of covalently immobilised Co tetraphenylporphyrin in ORR was evaluated. The assessment showed that the observations made for covalently immobilised MnTPP are applicable to CoTPP as covalent ligation improves selectivity to $4e^-$ reduction pathway from 0 % for drop-cast complex to 55 % for a material after 10 min-long electrodeposition. Also, covalent immobilisation significantly increases the rate of H_2O_2 reduction, and the effect is more pronounced with the electrochemical immobilisation times longer than 5 min. This change is also believed to take place due to the participation of multicentred reduction reaction.

Considering its outmost importance, in the final part of this dissertation the problem of catalyst stability in CO_2ERR in aqueous electrolyte was studied. For this work CoTPP was chosen as one of the most active catalysts available. In strong contrast to earlier reports, the results show that the leaching, demetallation, poisoning by CO and reduction to chlorins are not responsible for the deactivation process. Moreover, recyclability was found to be independent of the heterogenisation mode. Surprisingly, it is uptake of two oxygen atoms from the CO_2 molecule that renders the porphyrin catalytically inactive. Based on the insight into the degradation mechanism a strategy for the development of more stable porphyrin-based catalysts was

established. The most successful approach is based on kinetic suppression of unwanted oxygen insertion reaction. Indeed, introduction of steric protection in the form of eight bulky -OMe groups into the porphyrin core furnished 100 % recyclable heterogeneous molecular catalyst. Furthermore, lateral proton donors also significantly improve catalyst longevity due to favourable proton delivery to the CO_2-complex adduct and thus lower probability of oxygen uptake by the macrocyclic core. In strong contrast to Fe analogues, thermodynamic stabilisation of Co^I active form by electronegative substituents or additional axial ligands such as pyridine renders the catalyst almost inactive. Thus, it was proven that the careful analysis of degradation pathway is a crucial step in the rational development of industrially viable electrocatalysts.

In summary, covalent immobilisation of molecular catalysts on conductive electrodes provides higher amount of the catalytically active complex, better rate of interfacial electron transfer and shortened M···M distance. These effects are quite general and provide numerous advantages for energy-related applications. In turn, the longevity of molecular catalysts is defined by their structure rather than heterogenisation technique. Hence, careful design of a ligand can be used to significantly enhance the lifetime of an electrocatalyst. The results described below provide solid background for the future development of not only highly active, but also more durable molecular electrocatalysts which is of paramount significance for the field of electrocatalysis.

TABLE OF CONTENTS

CHAPTER 1. INTRODUCTION

1.1 Background

Fossil fuels depletion and greenhouse emissions have long been recognised as one of the key problems the humanity is facing.[1-4] The mean concentration of CO_2 in the atmosphere has been rising since the start of systematic measurements and exceeded by far the pre-industrial and prehistoric levels of 180-300 ppm.[5-7] Based on this, it is expected that the major climate changes will take place by 2050 due to the departure of air and ocean temperatures from the historic variability with the tropical regions being affected the most.[8] These factors underpin the development of sustainable emission-free energy economy which will allow to mitigate the impact of humankind on the environment and help to resolve major issues of economic and national security.[9-11] A wide range of power sources such as photovoltaics and wind turbines are already commercially available, however, inherent intermittent nature of these generators undermines their widespread utilisation.[12-13] Hence, efficient conversion of electrical energy into storable fuels and vice versa would allow to fully exploit the benefits of sustainable power generation. In this regard, electrochemistry provides an excellent opportunity to convert electricity into energy-rich chemicals and later utilise them to release the accumulated potential with zero net emissions through a cascade of redox reactions under near ambient conditions (Figure 1.1).[3, 10, 14]

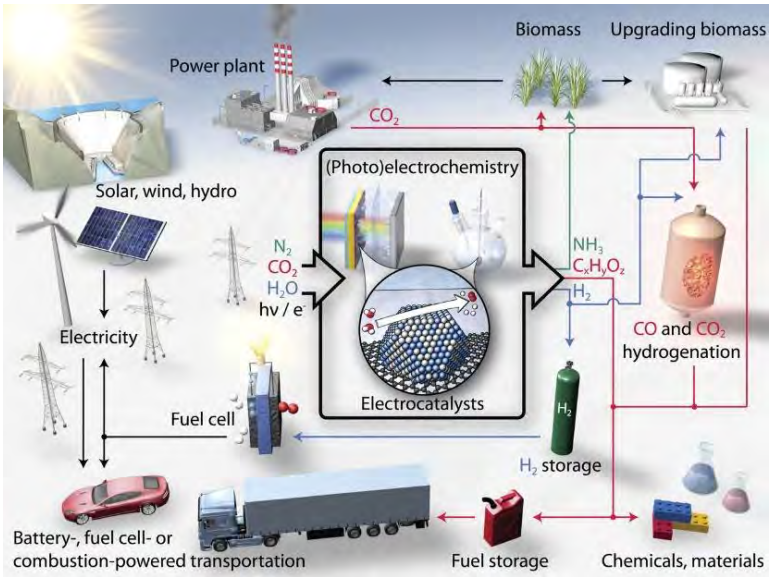

Figure 1.1 The model of sustainable energy economy.[14]

The model described above implies two successive steps. First, renewable electrical energy must be supplied to power an electrolyser where fuel generation on a cathode and oxygen evolution reaction (OER) on an anode take place (Figure 1.2a).[11, 15] Cathodic CO_2 electrochemical reduction reaction (CO_2ERR) to CO is an extremely useful process which could serve as entry point for the synthesis of long-chain hydrocarbons using well-developed Fischer-Tropsch process.[15-19] The resulting organic products could be directly used as fuels in modern transportation or as raw materials in the production of polymers and construction materials. Moreover, carbonylation reactions open numerous opportunities to utilize CO_2ERR in preparation of fine chemicals for pharmaceutical industry.[20] Stoichiometrically the overall process is the equivalent of CO_2 splitting into CO and O_2.

The second part of the infrastructure includes energy production via controlled oxidation of fuels. In this regard proton exchange membrane (PEM) fuel cells are excellent generators where a controlled low-temperature anodic oxidation of hydrogen, methanol or formic acid and cathodic oxygen reduction reaction (ORR) occur (Figure 1.2b).[21-24] PEM fuel cells provide chemical-to-electrical energy conversion efficiency of up to 65 % thus allowing to complete the model of an emission-free system.[25]

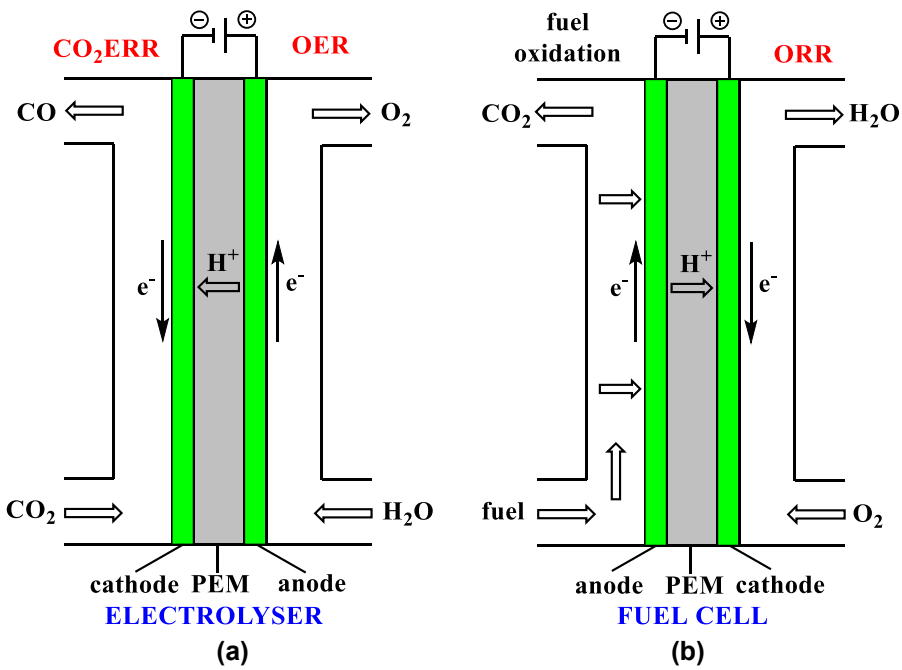

Figure 1.2 (a) Scheme of CO_2 electrolyser and (b) hydrogen fuel cell.

Although the prospects of the economic model described above are great, there are several major challenges to overcome. First, CO_2ERR, ORR and OER as multielectron proton coupled electrode reactions are characterised by sluggish kinetics and thus require significant

overpotentials to achieve practical current densities.[10, 26-28] Second, they often could lead to a multitude of different products such as CO, HCOOH, CH_3OH etc. in case of CO_2ERR or H_2O and H_2O_2 for ORR.[26, 29-30] More than that, the water discharge reaction might exacerbate the selectivity problem due to competing hydrogen evolution reaction taking place under negative potentials in aqueous media.[31] The problems of low reaction rate and selectivity could be resolved by careful design of electrocatalysts that bind favorably to the reactants and intermediates thus lowering the overpotentials and improving the process selectivity.[32-34] However, the development of effective catalysts requires significant advancement in understanding of the reaction mechanisms and factors affecting the performance of electrochemical devices.

The engineering and economic aspects impose stringent requirements on the choice of a reaction medium and the catalyst physical state. Clearly, CO_2ERR, ORR and OER could be performed both in organic solvents by means of homogeneous catalysis and in aqueous medium where catalysts are usually not readily soluble thus forming heterogeneous systems.[35-36] Use of homogeneous catalysts in non-aqueous electrolytes such as *N,N*-dimethylformamide (DMF) or acetonitrile (ACN) provides certain advantages for fundamental studies such as good solubility of CO_2 and O_2, the lack of competing solvent discharge reaction and simplified analysis of solutions using NMR, FTIR or HRMS.[37-38] However, high cost and toxicity of organic solvents necessitate the employment of heterogeneous water-based systems.[35, 39] Moreover, heterogeneous catalysis provides great advantage of simplified catalyst reuse thus lowering the overall cost of the process.

1.2 Introduction

There are several classes of heterogeneous electrocatalysts for CO_2ERR, ORR and OER available. Purely inorganic materials are quite a popular choice due to their accessibility and good theoretical understanding of the reaction mechanisms. As such, CO_2 could be reduced to CO with high selectivity on Ag electrodes while Cu is a unique electrode material that can produce more complex products, though not selectively.[40-41] Regarding ORR, pure Pt is an excellent benchmark catalyst which is extremely close to the top of the theoretical Sabatier volcano curve and drives this process almost exclusively through the desirable $4e^-$ reduction pathway.[42] OER is generally quite difficult to catalyse at low overpotentials and such materials as IrO_2 and RuO_2 are the most active candidates.[43] However, inorganic catalysts do not provide sufficient structural flexibility of the active sites thus making it difficult to

achieve simultaneously high selectivities and current densities due to so-called scaling relationships. Further, noble metal-based catalysts for ORR or OER are extremely expensive which renders them unfeasible for widespread use.

At the same time, the emergent class of molecular catalysts based on organometallic complexes of first row transition metals (Mn, Fe, Co and Ni) comprise unsurpassed tunability by means of organic synthesis, excellent activity in the transformations described above and relatively low price.[44-45] Across numerous classes of organometallics, porphyrins are among the most promising candidates thanks to simplicity of their synthesis and stability under ambient conditions.[46-48] Furthermore, some of them possess exceptionally high activity due to the simultaneous presence of redox-noninnocent aromatic ligand and metal atom (Scheme 1.1).[49-50]

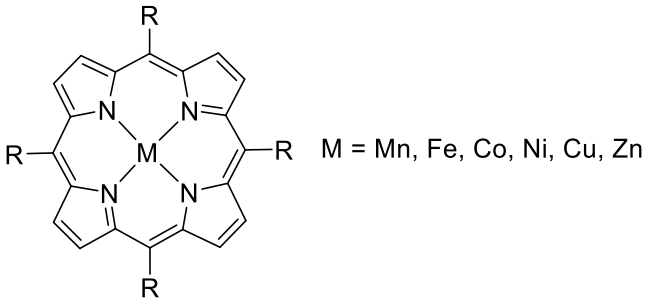

Scheme 1.1 Structure of metalloporphyrins.

Though macrocyclic complexes are excellent catalysts, two major drawbacks are holding up their industrial utilisation. First, these materials are dielectrics and most of them are not soluble in water. Thus, they must be either used as solutions in organic solvents or immobilised on the conductive electrodes. As we noted above, nonaqueous electrolytes are hardly suitable for widespread use and the practical applications require CO_2ERR, ORR and OER to be performed in aqueous medium.[32, 47] Hence, the only viable option is heterogenisation which generally could be achieved by covalent and noncovalent methods (Scheme 1.2).[32] The fundamental difference between these techniques is the presence of a direct covalent link between the conductive surface and the molecule of the catalyst in the first case while simple physisorption is used to immobilise molecular catalyst on the electrode in the latter method.[32, 51] Generally, noncovalent heterogenisation is synthetically simpler while covalent ligation to the electrode surface could provide ideal protection against leaching and enhance the rate of electron transfer. Though great examples of both strategies have been published, their advantages and disadvantages have not been formally elucidated until recently.[52-53]

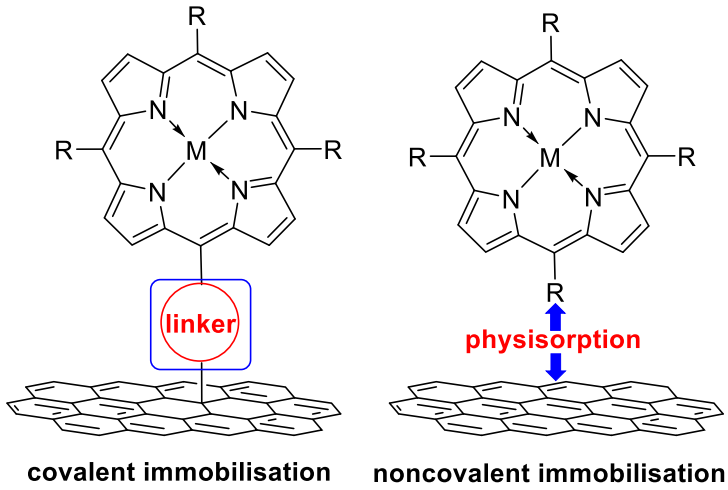

Scheme 1.2. Covalent and noncovalent immobilisation modes of porphyrin-based catalysts.

Second, the stability of molecular catalysts is usually quite low, and this problem has only recently started to draw attention.[32, 54] This major impediment, though usually not explicitly emphasised in the literature, largely negates the great progress achieved in the direction of catalyst activity. The degradation pathways have often been assumed rather than experimentally verified which led to the limited amount of controversial information being scattered across a big number of reports.

A general pathway for the development of a molecular catalyst could be described as a succession of the following steps (Scheme 1.3):

1. Proof of concept. At this stage a catalyst's suitability for a target reaction is assessed. This step could be performed both in homogeneous and heterogeneous systems. As a rule of thumb, CV is used to observe the increase of faradic current in the presence of a substrate while a following CPE study confirms the formation of desirable products.

2. A study of the reaction mechanism and the design of the most active catalyst within the class structurally similar complexes. This is usually done in homogeneous solutions to allow detection of reaction intermediates with advanced spectroscopic techniques such as NMR, FTIR, Raman spectroscopy, UV/Vis or EPR. Also, kinetics of the reaction could be conveniently studied using CV.

3. Heterogenisation of the catalyst. At this stage the catalytic activity is transferred into aqueous solution. Optimisation of the catalyst loading and heterogenisation methods usually follow. Finally, troubleshooting of stability and activity issues furnishes desirable hybrid electrocatalyst.

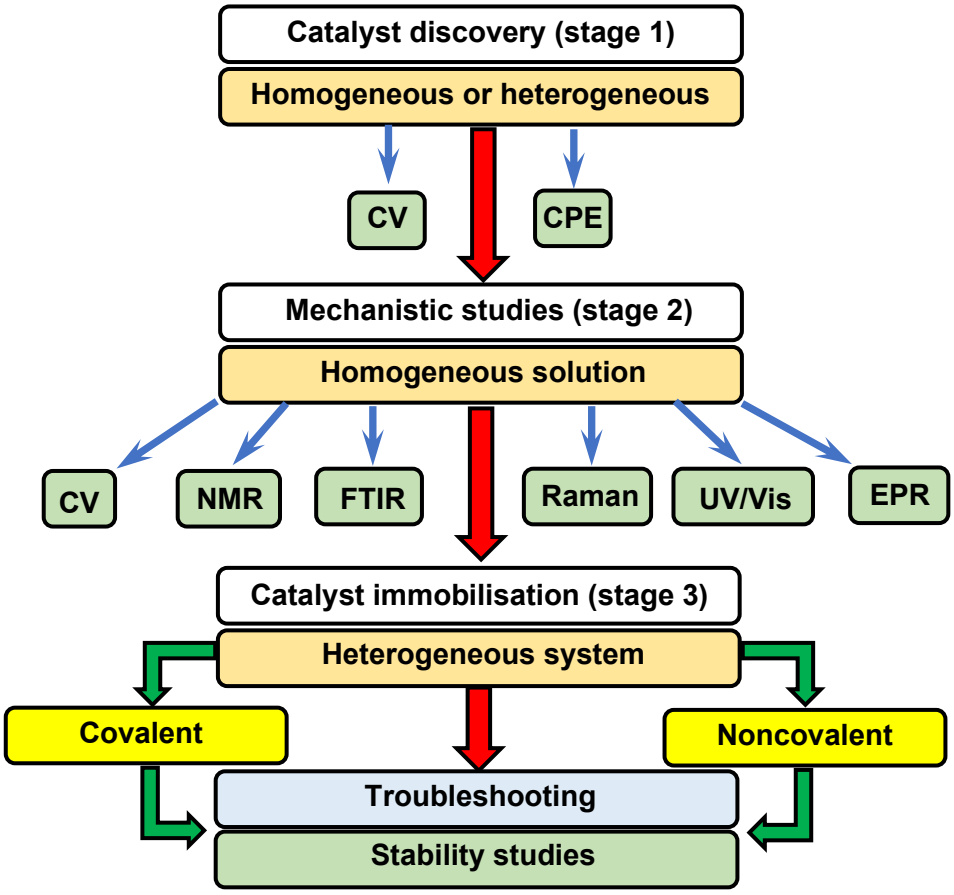

Scheme 1.3. A typical workflow of the catalyst development. The focus of current research is shown in green.

As the number of active porphyrin-based catalysts reported to date for CO_2ERR, ORR and OER is already significant, the research described below is dedicated to the third stage of the catalyst development (Scheme 1.3). Of special interest here is the influence of heterogenisation methods on the activity, stability and selectivity of molecular electrocatalysts.

1.3 Aims and thesis outline

This thesis is focused on the synthesis and electrocatalytic behaviour of covalently and noncovalently heterogenized Co and Mn metalloporphyrins in CO_2ERR, ORR and OER. The major research question it answers could be formulated as follows: "*Is it possible to influence the activity, selectivity and stability of porphyrin-based catalysts in electrocatalytic reactions using various immobilisation strategies?*"

To answer this question the following specific objectives were put forth:

1) Develop a reliable procedure for covalent and noncovalent immobilisation of Mn and Co porphyrins onto the surface of carbon cloth electrodes.

2) Perform the in-depth analysis of the resulting materials, compare their structural characteristics and confirm the validity of the comparison between covalent and noncovalent immobilisation modes.

3) Study the activity of the complexes in CO_2ERR, ORR and OER in aqueous medium and make the conclusions regarding the influence of immobilisation mode on electrocatalytic properties.

4) Thoroughly analyse the decomposition pathway for Co porphyrin upon repetitive reuse in CO_2ERR and deduce the mechanism of this process.

5) Based on the deactivation mechanism, devise and test the strategic framework for the development of more stable molecular catalysts.

This thesis consists of the following chapters: introduction, literature review, methods, three results and discussion chapters followed by conclusions and outlook. The findings of the research described above have been presented as three first author manuscripts listed at the beginning of the dissertation. Chapter 1 gives the background information on the place of electrochemical energy storage and conversion technologies in the modern economy followed by general overview the key problems in the field. Chapter 2 is a literature review which describes synthesis of porphyrins and the reported achievements in the field of porphyrin catalysed CO_2ERR, ORR and OER. Chapter 3 provides thorough description of experimental techniques used in this research. Chapter 4 deals with synthesis, characterisation and activity of covalently and noncovalently immobilised Mn tetraphenylporphyrin in ORR and OER. Activity of Mn porphyrin in CO_2ERR was evaluated as well. Chapter 5 describes the influence of immobilisation mode on the activity and selectivity of CoTPP in CO_2ERR and ORR. Chapter 6 is focused on the problem of stability of heterogeneous Co porphyrin-based catalysts in CO_2ERR in aqueous medium. Chapter 7 covers the key research outcomes of this project and features discussion on the prospects and challenges of heterogeneous molecular catalysts for electrochemical industry.

1.4 References

[1] Marcus, R. J., Chemical Conversion of Solar Energy, *Science* **1956,** 123 (3193), 399-405
[2] Capellán-Pérez, I.; Mediavilla, M.; de Castro, C.; Carpintero, Ó.; Miguel, L. J., Fossil fuel depletion and socio-economic scenarios: An integrated approach, *Energy* **2014,** 77, 641-666
[3] Chu, S.; Majumdar, A., Opportunities and challenges for a sustainable energy future, *Nature* **2012,** 488, 294
[4] Turner, J. A., Sustainable Hydrogen Production, *Science* **2004,** 305 (5686), 972
[5] Tans, P.; Keeling, R. Trends in atmospheric carbon dioxide. http://www.esrl.noaa.gov/gmd/ccgg/trends/data.html.
[6] Petit, J. R.; Jouzel, J.; Raynaud, D.; Barkov, N. I.; Barnola, J. M.; Basile, I.; Bender, M.; Chappellaz, J.; Davis, M.; Delaygue, G.; Delmotte, M.; Kotlyakov, V. M.; Legrand, M.; Lipenkov, V. Y.; Lorius, C.; PÉpin, L.; Ritz, C.; Saltzman, E.; Stievenard, M., Climate and atmospheric history of the past 420,000 years from the Vostok ice core, Antarctica, *Nature* **1999,** 399 (6735), 429-436
[7] Siegenthaler, U.; Stocker, T. F.; Monnin, E.; Lüthi, D.; Schwander, J.; Stauffer, B.; Raynaud, D.; Barnola, J.-M.; Fischer, H.; Masson-Delmotte, V.; Jouzel, J., Stable Carbon Cycle-Climate Relationship During the Late Pleistocene, *Science* **2005,** 310 (5752), 1313
[8] Mora, C.; Frazier, A. G.; Longman, R. J.; Dacks, R. S.; Walton, M. M.; Tong, E. J.; Sanchez, J. J.; Kaiser, L. R.; Stender, Y. O.; Anderson, J. M.; Ambrosino, C. M.; Fernandez-Silva, I.; Giuseffi, L. M.; Giambelluca, T. W., The projected timing of climate departure from recent variability, *Nature* **2013,** 502, 183
[9] Lewis, N. S.; Nocera, D. G., Powering the planet: Chemical challenges in solar energy utilization, *Proc. Nat. Acad. Sci.* **2006,** 103 (43), 15729
[10] Jiao, Y.; Zheng, Y.; Jaroniec, M.; Qiao, S. Z., Design of electrocatalysts for oxygen- and hydrogen-involving energy conversion reactions, *Chem. Soc. Rev.* **2015,** 44 (8), 2060-2086
[11] Agarwal, A. S.; Zhai, Y.; Hill, D.; Sridhar, N., The Electrochemical Reduction of Carbon Dioxide to Formate/Formic Acid: Engineering and Economic Feasibility, *ChemSusChem* **2011,** 4 (9), 1301-1310
[12] Dunn, B.; Kamath, H.; Tarascon, J.-M., Electrical Energy Storage for the Grid: A Battery of Choices, *Science* **2011,** 334 (6058), 928
[13] Ravestein, P.; van der Schrier, G.; Haarsma, R.; Scheele, R.; van den Broek, M., Vulnerability of European intermittent renewable energy supply to climate change and climate variability, *Renew. Sust. Energ. Rev.* **2018,** 97, 497-508
[14] Seh, Z. W.; Kibsgaard, J.; Dickens, C. F.; Chorkendorff, I.; Nørskov, J. K.; Jaramillo, T. F., Combining theory and experiment in electrocatalysis: Insights into materials design, *Science* **2017,** 355 (6321), 4998
[15] Ross, M. B.; Dinh, C. T.; Li, Y.; Kim, D.; De Luna, P.; Sargent, E. H.; Yang, P., Tunable Cu Enrichment Enables Designer Syngas Electrosynthesis from CO2, *J. Am. Chem. Soc.* **2017,** 139 (27), 9359-9363
[16] Van Der Laan, G. P.; Beenackers, A. A. C. M., Kinetics and Selectivity of the Fischer–Tropsch Synthesis: A Literature Review, *Catal. Rev,* **1999,** 41 (3-4), 255-318
[17] Jahangiri, H.; Bennett, J.; Mahjoubi, P.; Wilson, K.; Gu, S., A review of advanced catalyst development for Fischer–Tropsch synthesis of hydrocarbons from biomass derived syn-gas, *Catal. Sci. Technol.* **2014,** 4 (8), 2210-2229
[18] Henrici-Olivé, G.; Olivé, S., The Fischer-Tropsch Synthesis: Molecular Weight Distribution of Primary Products and Reaction Mechanism, *Angew. Chem. Int. Ed.* **1976,** 15 (3), 136-141
[19] Foit, S. R.; Vinke, I. C.; de Haart, L. G. J.; Eichel, R.-A., Power-to-Syngas: An Enabling Technology for the Transition of the Energy System?, *Angew. Chem. Int. Ed.* **2017,** 56 (20), 5402-5411
[20] Jensen, M. T.; Rønne, M. H.; Ravn, A. K.; Juhl, R. W.; Nielsen, D. U.; Hu, X.-M.; Pedersen, S. U.; Daasbjerg, K.; Skrydstrup, T., Scalable carbon dioxide electroreduction coupled to carbonylation chemistry, *Nat. Comm.* **2017,** 8 (1), 489
[21] Jacobson, M. Z.; Colella, W. G.; Golden, D. M., Cleaning the Air and Improving Health with Hydrogen Fuel-Cell Vehicles, *Science* **2005,** 308 (5730), 1901
[22] Sebastián, D.; Baglio, V.; Aricò, A. S.; Serov, A.; Atanassov, P., Performance analysis of a non-platinum group metal catalyst based on iron-aminoantipyrine for direct methanol fuel cells, *Applied Catal. B* **2016,** 182, 297-305
[23] Czaun, M.; Kothandaraman, J.; Goeppert, A.; Yang, B.; Greenberg, S.; May, R. B.; Olah, G. A.; Prakash, G. K. S., Iridium-Catalyzed Continuous Hydrogen Generation from Formic Acid and Its Subsequent Utilization in a Fuel Cell: Toward a Carbon Neutral Chemical Energy Storage, *ACS Catal.* **2016,** 6 (11), 7475-7484
[24] Zhang, J.; Chen, M.; Li, H.; Li, Y.; Ye, J.; Cao, Z.; Fang, M.; Kuang, Q.; Zheng, J.; Xie, Z., Stable palladium hydride as a superior anode electrocatalyst for direct formic acid fuel cells, *Nano Energy* **2018,** 44, 127-134
[25] Stambouli, A. B., Fuel cells: The expectations for an environmental-friendly and sustainable source of energy, *Renew. Sustain. Energy Rev.* **2011,** 15 (9), 4507-4520

[26] Savéant, J.-M., Molecular Catalysis of Electrochemical Reactions. Mechanistic Aspects, *Chem. Rev.* **2008,** 108, 2348–2378
[27] Koper, M. T. M., Theory of multiple proton–electron transfer reactions and its implications for electrocatalysis, *Chem. Sci.* **2013,** 4 (7), 2710-2723
[28] Nørskov, J. K.; Rossmeisl, J.; Logadottir, A.; Lindqvist, L.; Kitchin, J. R.; Bligaard, T.; Jónsson, H., Origin of the Overpotential for Oxygen Reduction at a Fuel-Cell Cathode, *J. Phys. Chem. B* **2004,** 108 (46), 17886-17892
[29] Jiang, K.; Sandberg, R. B.; Akey, A. J.; Liu, X.; Bell, D. C.; Nørskov, J. K.; Chan, K.; Wang, H., Metal ion cycling of Cu foil for selective C–C coupling in electrochemical CO2 reduction, *Nature Catal.* **2018,** 1 (2), 111-119
[30] Gewirth, A. A.; Varnell, J. A.; DiAscro, A. M., Nonprecious Metal Catalysts for Oxygen Reduction in Heterogeneous Aqueous Systems, *Chem. Rev.* **2018,** 118 (5), 2313-2339
[31] Zhang, X.; Wu, Z.; Zhang, X.; Li, L.; Li, Y.; Xu, H.; Li, X.; Yu, X.; Zhang, Z.; Liang, Y.; Wang, H., Highly selective and active CO2 reduction electrocatalysts based on cobalt phthalocyanine/carbon nanotube hybrid structures, *Nature Comm.* **2017,** 8, 14675
[32] Dalle, K. E.; Warnan, J.; Leung, J. J.; Reuillard, B.; Karmel, I. S.; Reisner, E., Electro- and Solar-Driven Fuel Synthesis with First Row Transition Metal Complexes, *Chem. Rev.* **2019,** 119 (4), 2752-2875
[33] Corbin, N.; Zeng, J.; Williams, K.; Manthiram, K., Heterogeneous molecular catalysts for electrocatalytic CO2 reduction, *Nano Res.* **2019**,
[34] Cometto, C.; Chen, L.; Lo, P.-K.; Guo, Z.; Lau, K.-C.; Anxolabéhère-Mallart, E.; Fave, C.; Lau, T.-C.; Robert, M., Highly Selective Molecular Catalysts for the CO2-to-CO Electrochemical Conversion at Very Low Overpotential. Contrasting Fe vs Co Quaterpyridine Complexes upon Mechanistic Studies, *ACS Catalysis* **2018,** 8 (4), 3411-3417
[35] Costentin, C.; Robert, M.; Savéant, J.-M., Molecular catalysis of electrochemical reactions, *Curr. Opin. Electrochem.* **2017,** 2 (1), 26-31
[36] Kang, P.; Cheng, C.; Chen, Z.; Schauer, C. K.; Meyer, T. J.; Brookhart, M., Selective Electrocatalytic Reduction of CO2 to Formate by Water-Stable Iridium Dihydride Pincer Complexes, *J. Am. Chem. Soc.* **2012,** 134 (12), 5500-5503
[37] Passard, G.; Dogutan, D. K.; Qiu, M.; Costentin, C.; Nocera, D. G., Oxygen Reduction Reaction Promoted by Manganese Porphyrins, *ACS Catal.* **2018,** 8 (9), 8671-8679
[38] Machan, C. W.; Sampson, M. D.; Chabolla, S. A.; Dang, T.; Kubiak, C. P., Developing a Mechanistic Understanding of Molecular Electrocatalysts for CO2 Reduction using Infrared Spectroelectrochemistry, *Organometallics* **2014,** 33 (18), 4550-4559
[39] Lei, H.; Liu, C.; Wang, Z.; Zhang, Z.; Zhang, M.; Chang, X.; Zhang, W.; Cao, R., Noncovalent Immobilization of a Pyrene-Modified Cobalt Corrole on Carbon Supports for Enhanced Electrocatalytic Oxygen Reduction and Oxygen Evolution in Aqueous Solutions, *ACS Catal.* **2016,** 6 (10), 6429-6437
[40] Weng, Z.; Wu, Y.; Wang, M.; Jiang, J.; Yang, K.; Huo, S.; Wang, X.-F.; Ma, Q.; Brudvig, G. W.; Batista, V. S.; Liang, Y.; Feng, Z.; Wang, H., Active sites of copper-complex catalytic materials for electrochemical carbon dioxide reduction, *Nature Comm.* **2018,** 9 (1), 415
[41] Kim, C.; Jeon, H. S.; Eom, T.; Jee, M. S.; Kim, H.; Friend, C. M.; Min, B. K.; Hwang, Y. J., Achieving Selective and Efficient Electrocatalytic Activity for CO2 Reduction Using Immobilized Silver Nanoparticles, *J. Am. Chem. Soc.* **2015,** 137 (43), 13844-13850
[42] Gasteiger, H. A.; Kocha, S. S.; Sompalli, B.; Wagner, F. T., Activity benchmarks and requirements for Pt, Pt-alloy, and non-Pt oxygen reduction catalysts for PEMFCs, *Appl. Catal. B* **2005,** 56 (1), 9-35
[43] Lee, Y.; Suntivich, J.; May, K. J.; Perry, E. E.; Shao-Horn, Y., Synthesis and Activities of Rutile IrO2 and RuO2 Nanoparticles for Oxygen Evolution in Acid and Alkaline Solutions, *J. Phys. Chem. Lett.* **2012,** 3 (3), 399-404
[44] Zhang, W.; Lai, W.; Cao, R., Energy-Related Small Molecule Activation Reactions: Oxygen Reduction and Hydrogen and Oxygen Evolution Reactions Catalyzed by Porphyrin- and Corrole-Based Systems, *Chem. Rev.* **2017,** 117 (4), 3717-3797
[45] Costentin, C.; Drouet, S.; Robert, M.; Savéant, J.-M., A Local Proton Source Enhances CO2 Electroreduction to CO by a Molecular Fe Catalyst, *Science* **2012,** 338 (6103), 90-94
[46] Benson, E. E.; Kubiak, C. P.; Sathrum, A. J.; Smieja, J. M., Electrocatalytic and homogeneous approaches to conversion of CO2 to liquid fuels, *Chem. Soc. Rev.* **2009,** 38 (1), 89-99
[47] Pegis, M. L.; Wise, C. F.; Martin, D. J.; Mayer, J. M., Oxygen Reduction by Homogeneous Molecular Catalysts and Electrocatalysts, *Chem. Rev.* **2018,** 118 (5), 2340-2391
[48] Lin, S.; Diercks, C. S.; Zhang, Y.-B.; Kornienko, N.; Nichols, E. M.; Zhao, Y.; Paris, A. R.; Kim, D.; Yang, P.; Yaghi, O. M.; Chang, C. J., Covalent organic frameworks comprising cobalt porphyrins for catalytic CO2 reduction in water, *Science* **2015,** 349 (6253), 1208-1213
[49] Lash, T. D., Origin of aromatic character in porphyrinoid systems, *J. Porphyrins Phthalocyanines* **2011,** 15 (11n12), 1093-1115

[50] Costentin, C.; Savéant, J.-M.; Tard, C., Ligand "noninnocence" in coordination complexes vs. kinetic, mechanistic, and selectivity issues in electrochemical catalysis, *Proc. Nat. Acad. Sci.* **2018,** 115 (37), 9104
[51] Tong, L.; Göthelid, M.; Sun, L., Oxygen evolution at functionalized carbon surfaces: a strategy for immobilization of molecular water oxidation catalysts, *Chem. Comm.* **2012,** 48 (80), 10025-10027
[52] Marianov, A. N.; Jiang, Y., Covalent ligation of Co molecular catalyst to carbon cloth for efficient electroreduction of CO2 in water, *Appl. Catal. B* **2019,** 244, 881-888
[53] Marianov, A.; Jiang, Y., Effect of manganese porphyrin covalent immobilization on electrocatalytic water oxidation and oxygen reduction reactions, *ACS Sustainable Chem. Eng.* **2019,** 244, 881-888
[54] Jiang, J.; Matula, A. J.; Swierk, J. R.; Romano, N.; Wu, Y.; Batista, V. S.; Crabtree, R. H.; Lindsey, J. S.; Wang, H.; Brudvig, G. W., Unusual Stability of a Bacteriochlorin Electrocatalyst under Reductive Conditions. A Case Study on CO2 Conversion to CO, *ACS Catalysis* **2018,** 8 (11), 10131-10136

CHAPTER 2. LITERATURE REVIEW

2.1 Fundamentals of electrocatalysis

Any electrochemical process is characterised by its intrinsic redox potential. The equilibrium cell potential could be calculated based on Gibbs energies of the starting materials and products using Equation 2.1 where ΔG^0 stands for the change of free energy in the redox reaction, n is the number of electrons transferred and F is Faraday's constant (96485 C/mol):[1]

$$E^0 = -\frac{\Delta G^0}{nF} \quad \textbf{(Equation 2.1)}$$

Also, since the Gibbs energy is the maximum possible value of useful work produced under reversible conditions, thermodynamics could be employed to express the maximum theoretical efficiency of a system $\zeta_{theoretical}$ using the Equation 2.2 where ΔH^0 and ΔS^0 are changes of enthalpy and entropy in the reaction and T is thermodynamic temperature.[2] It must be noted that the Equation 2.2 could be applied to both electrolysers and fuel cells since it describes an ideally reversible system and the only difference between these two is the direction of the reaction. Clearly, the $T\Delta S$ term has a considerable contribution and under standard conditions $\zeta_{theoretical}$ for a hydrogen fuel cell is 83 % (referenced to the heat of hydrogen combustion) and 82 % for an electrolyser transforming CO_2 into CO and O_2 (compared to the heat of reversed reaction of CO with O_2).[2-3]

$$\zeta_{theoretical} = \frac{\Delta G^0}{\Delta H^0} = 1 - \frac{T\Delta S^0}{\Delta H^0} \quad \textbf{(Equation 2.2)}$$

The potential derived from the equation 2.1 is applicable to a process under standard conditions, which implies gas pressure of 1 bar and the activity of solutes in the electrolyte of 1 M. However, in reality conditions often differ to those imposed by the Equation 2.1 and for non-standard cases it is possible to estimate redox potentials using the Nernst equation (Equation 2.3) based on concentrations of reduced [*Red*] and oxidised [*Ox*] species in the solution, temperature and the universal gas constant R.[4] Further, the Nernst relationship optimised for pH-dependant redox reactions could be applied for CO_2ERR, ORR and OER which generally depend on the activity of protons only (equation 2.4).[1]

$$E = E^0 - \frac{RT}{nF} ln \frac{[Red]}{[Ox]} \quad \textbf{(Equation 2.3)}$$

$$E = E^0 - 0.059pH \text{ (Equation 2.4)}$$

Thermodynamic considerations described above are valid only in equilibrium state meaning that there is no current flowing through the cell and the reaction rate is infinitely small. This scenario corresponds to an open circuit while energy applications are based on non-equilibrium systems with significant current densities. As a result of the departure from the equilibrium state, additional potential must be applied to drive the required reaction with a desirable rate. The difference between equilibrium potential E^0 and the actual bias applied to the electrode by external power supply or delivered to the lead of a fuel cell $E_{electrode}$ is called overpotential η and is defined by the Equation 2.5.

$$\eta = E^0 - E_{electrode} \text{ (Equation 2.5)}$$

It must be noted here that although the overpotential is required to drive a process, the amount of useful energy stored in the form of chemical bonds or released by the fuel cell is still determined by the change of intrinsic Gibbs energy during the transformation in question while the excess is dissipated as heat. An additional source of energy losses is the ohmic resistance of the electrochemical cell, however this is usually a minor factor compared to the limitations imposed by the redox chemistry.[5] Generally, the practical energy effectiveness of electrolyser $\zeta_{electrolyser}$ could be calculated using the Equation 2.6 while the efficiency of fuel cell $\zeta_{fuel\ cell}$ is defined by the Equation 2.7 where iR is the ohmic voltage drop.[5-6]

$$\zeta_{electrolyser} = 1 - \frac{\eta_{cathode} + \eta_{anode} + iR}{E_{cell}} \text{ (Equation 2.6)}$$

$$\zeta_{fuel\ cell} = 1 - \frac{\eta_{cathode} + \eta_{anode} + iR}{E^0} \text{ (Equation 2.7)}$$

Kinetic relationship between the current density and overpotential for an irreversible electrode reaction is described by Butler-Volmer Equation 2.8 where j is the current density, n is the number of electrons transferred in the process, F is the Faraday's constant (96485 C/mol), k_0 is the reaction rate constant, C_i is the concentration of the species i, N is the total number of species in the rate law, α is the transfer coefficient, R is the ideal gas constant (8.314 J/(mol·K)), T is the absolute temperature and η is the applied overpotential. This relationship is applicable to the reaction if the overpotential is big enough for the reverse reaction to be neglected ($\eta >$ 118 mV; negative sign corresponds to the cathodic process and positive – to the anodic one).[7]

$$j = \pm nFk_0\left(\prod_{i=1}^{N} C_i^{\nu_i}\right)exp\left(-\frac{\{1-\alpha\}F}{RT}\eta\right) \quad \textbf{(Equation 2.8)}$$

However, the potential dependence of the reaction rate is often studied and reported using simpler Tafel Equation 2.9 where n is the number of electrons transferred before rate-determining step, β is the symmetry factor (routinely assumed to be 0.5) and q is the number of electrons transferred during the rate-determining step.[7] This relationship allows to gain insight into the reaction mechanism and the nature of the rate-determining step from the values of the Tafel slope m_{Tafel}. Clearly, the electrode reactions show logarithmic dependence on the applied potential, in strong contrast to the linear Ohm's law and the higher the number of electrons transferred, the more sensitive the reaction to the changes in potential. The minimum theoretical slope derived from the Equation 2.9 is 118 mV/dec and in case of m_{Tafel} >> 118 mV/dec other factors than the charge transfer from the electrode to the reactant contribute to the reaction rate.[7-8]

$$m_{Tafel} = \left[\frac{\partial(\pm\eta)}{\partial log(\pm j)}\right]_{C_i,T} = \frac{59\ mV/dec}{n+(1-\beta)q} \ (T = 25\ ℃) \quad \textbf{(Equation 2.9)}$$

Thus, it is the kinetics of electrode reactions that define the overall efficiency of the energy system and one would desire to perform electrochemical transformations with as little overpotential as possible to assure that the significant portion of renewable electricity is stored within the fuel.[5-6, 9] In this regard, CO_2ERR, ORR and OER are characterised by sluggish kinetics and thus need significant overpotentials to proceed with practically viable rates. As such, for CO_2ERR the overpotential of 510 mV at the current density of ~ 0.35 mA/cm^2 is considered to be a good result and a recently published number of 180 mV (at the current density of 0.25 mA/cm^2) was reported as unprecedented.[9-10] For ORR and OER typical η values lie between 300 and 700 mV at the current densities below 10 mA/cm^2 depending on the catalyst.[6, 11-13] Notably, these numbers are in stark contrast to those characteristic for simpler electrode reactions such as hydrogen oxidation where anodic η can be as little as 20-50 mV at the current densities of up to 5 mA/cm^2 (as measured on a flat rotating Pt electrode).[6, 14] All the limitations described above lead to the fact that the realistic $\zeta_{fuel\ cell}$ is around 45-60 % and CO_2 electrolysers rarely boast more than 50 % transformation efficiency.[5-6, 15-16]

This behaviour comes from the fact that all these processes require stepwise rather than simultaneous transfer of at least 2 protons and 2 electrons as simultaneous transfer of 2

electrons would require 4 times higher activation energy compared to a single-electron mechanism.[17] Therefore, a redox reaction proceeds through a multitude of intermediates all of which are characterised by their respective redox potentials.[17-18] One could fully comprehend the complexity of multielectron reactions by the analysis of even a relatively simple generic $2e^-/2H^+$ process described by the equation $A + 2H^+ + 2e^- \rightarrow AH_2$. As shown in the Figure 2.1, the transformation proceeds through either concerted or decoupled proton and electron transfer (i.e. through successive PT and ET). In this case the potential barriers of each reaction step could be roughly estimated using Marcus theory based on the free energy of solvent rearrangement around reacting species.[19-21] As the solvation effects play dominant role in thermodynamics of redox reactions, the formation and annihilation of ions in the solution incurs high energy penalty and unless the reactants have a strong tendency to lose or gain protons and electrons, their transfer will more likely take place in a concerted manner as this transformation has the lowest potential barrier.[22] This condition applied to the proton-coupled reaction such as CO_2ERR, ORR and OER means that from the kinetic point of view, there is an optimum pH at which the reaction is bound to proceed via the most favourable concerted mechanism and this value is close to the pK_a of the reactant.[22]

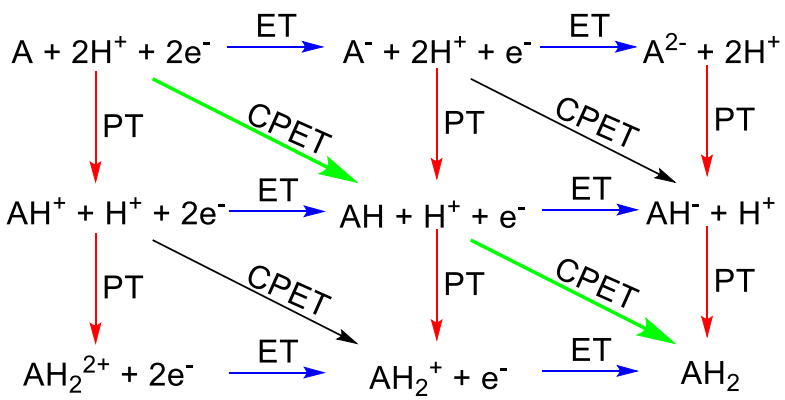

Figure 2.1. Scheme of possible transformations taking place in a generic $2e^-/2H^+$ redox reaction. ET - electron transfer; PT - proton transfer, CPET – concerted proton and electron transfer.[22]

As the rate of a reaction on an inert electrode is limited due to the weak interaction between the surface of an electrode and the reactant, active centres on its surface binding to CO_2, O_2 or H_2O are required to drive the electrochemical process.[17-18] Consequently, these electrodes must take part in the electrochemical process and not be expended. Such materials are called catalysts by definition or, in case of electrochemistry, electrocatalysts. Well-designed electrocatalysts are necessary to diminish energy losses, boost the reaction rates and improve

selectivity of a desirable process if several reactions could take place simultaneously. Moreover, from the engineering point of view, electrode materials are expected to be highly active, indefinitely stable and as cheap as possible. These requirements resulted in extensive research effort being devoted to the rational design of electrocatalysts that could satisfy these requirements.[23-24]

The underlying role of an electrocatalyst is illustrated in the Figure 2.2.[25-26] Depending on the reaction mechanism several types of electrocatalytic processes are possible: (i) reactions where a redox catalyst simply shuttles electrons from an inert electrode to a molecule via outer-sphere electron transfer (pathway 1) and (ii) chemically catalysed reactions with inner-sphere electron transfer where a catalyst actively participates in the reaction by binding to the substrate (pathways 2 and 3). Generally, a poorly catalysed reaction following a pathway 1 requires high overpotential to force the formation of energy-rich unstable transition state with the activation energy $\Delta G_1^{\neq}$. However, if the transition state is stabilised by chemical bonds in the pathway 2, this may considerably decrease the potential barrier to $\Delta G_2^{\neq}$ thus making its formation less unfavourable. At last, if there are unstable adducts formed along the reaction coordinate (pathway 3), it is possible to further lower the overpotential to $\Delta G_3^{\neq}$.

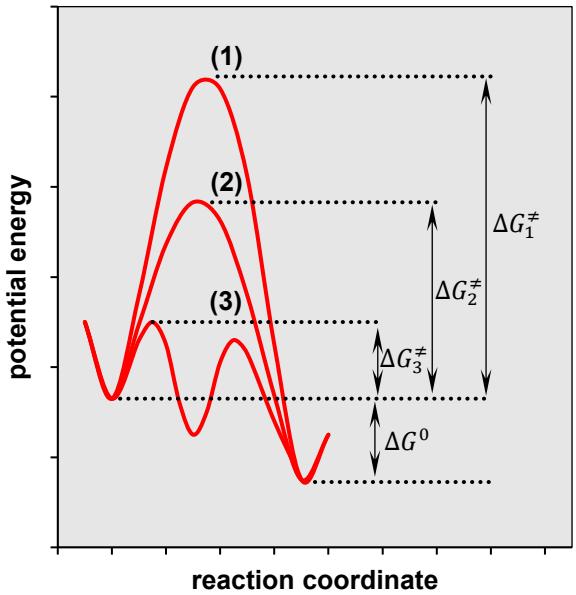

Figure 2.2. Potential barriers for: (1) uncatalysed or redox-catalysed reaction; (2) one-step chemical catalysis and (3) two-step chemical catalysis. Reaction barriers $\Delta G^{\neq}$ and overall change of Gibbs free energy ΔG^0 are shown.[25-26]

Basic thermodynamic requirements for the electrocatalyst design could be based on the Sabatier principle which states that intermediates must bind to the catalyst neither too weakly

nor too strongly. If the first condition is not satisfied, the catalyst would not function at all while in the second case the catalytically active centres would be poisoned by the intermediate. Also, for an ideal catalyst with zero overpotential the Sabatier principle requires the formation of each intermediate to proceed with zero or negative change of free energy along the reaction coordinate.[18, 27-28]

Since the role of a catalyst is to lower the energy of the transition state, it would be desirable to adjust the binding energy of the key intermediate while keeping the other parameters constant and thus arriving to the point where all steps show $\Delta G \leq 0$ (and hence overpotential is zero). However, as it was found recently, additional limitations apply to multielectron reactions. The energies of intermediates adsorbed on a catalyst are not independent and linked by linear scaling relationships.[23, 29] In other words, an attempt to enhance the affinity of an intermediate that binds too weakly to a catalytically active centre would instead induce the proportional change in other intermediates and may even modify the nature of the rate determining step. As a result, the overpotential will never decrease to zero but rather approach closer to the theoretical limit (apex of the Sabatier curve). The existence of these relationships leads to the fact that a multistep process is bound to have intrinsic overpotential due to unfavourable energy relationships between intermediates if the catalytically active site itself does not change in the course of the reaction.[29-31] For CO_2ERR, ORR and OER the existence of scaling relationships between some of the intermediates have been proven in a series of brilliant works by Nørskov who showed that any conventional catalyst will be a trade-off between binding energies of intermediates to the same catalytically active centre.[18] Essentially, this fact gives rise to the famous volcano-type graphs derived from Sabatier principle.[18, 23]

At the same time, the notion of a sole catalytically active site being unsuitable for multielectron multiphoton process provides another insight: if not one, but several catalytically active centres could participate in a reaction, it is possible to circumvent costly steps by avoiding altogether points on the reaction coordinate incurring high energy penalty. This approach could be illustrated by the example of enzymes which are excellent Nature's multicentred catalysts.[6, 32-33] Thus, in the quest for effective electrocatalysts structural tunability is vital both from fundamental and practical points of view.

2.2 Thermodynamics and kinetics of electrode reactions

2.2.1 CO_2 electrochemical reduction (CO_2ERR)

CO_2 is a very stable linear molecule with two double bonds and high Gibbs free energy of formation of ΔG^0_{298} = - 394.384 kJ/mol. Hence, any reductive CO_2 transformation requires bending of the molecule which involves an extremely high energy penalty. As a result, CO_2 has a huge electrochemical potential for one-electron reduction to corresponding anion radical $\cdot CO_2^-$ with estimated $E^0_{CO_2/\cdot CO_2^-}$= -1.90 V vs NHE in water. This massive activation barrier is the main reason of overpotential needed to drive the reaction on a catalyst with low specific affinity to CO_2.[25-26, 34-36] However, as discussed earlier, it is possible to circumvent formation of anion radical and thus significantly lower overpotential if the reduction is directed through a proton-coupled multielectron pathway.[36] The thermodynamics of this process is much more favorable compared to the uncatalysed process and the corresponding redox potentials are summarised in the Table 2.1.[37] Clearly, even the formation of simplest products such as CO and HCOOH (entries 1 and 2) decreases the equilibrium redox potential by the factor of 3.6 while involvement of higher number of electrons and protons would decrease the redox potential even further (entries 3-6).

Table 2.1. Standard redox potentials of proton-coupled multielectron CO_2ERR (pH = 7).[34]

Entry	Redox reaction	E^0(V) *vs* NHE
1	$CO_2 + e^- \rightarrow \cdot CO_2^-$	-1.90
2	$CO_2 + 2H^+ + 2e^- \rightarrow CO + H_2O$	-0.53
3	$CO_2 + 2H^+ + 2e^- \rightarrow HCOOH$	-0.61
4	$CO_2 + 4H^+ + 4e^- \rightarrow HCHO + H_2O$	-0.48
5	$CO_2 + 6H^+ + 6e^- \rightarrow CH_3OH + H_2O$	-0.38
6	$CO_2 + 8H^+ + 8e^- \rightarrow CH_4 + 2H_2O$	-0.24
7	$2H^+ + 2e^- \rightarrow H_2$	-0.41

However, from the kinetic point of view electrosynthesis of deeply reduced products is the game of diminishing returns due to scaling relationships between adsorbed CO and CHO intermediates. As shown in a series of brilliant works by Nørskov at al., conventional metallic catalysts show volcano-type plot with little room for improvement and even Cu, which is closest to the apex of the Sabatier curve for the synthesis of CH_4 and CH_3OH still requires at least ~ 0.8 V overpotential (Figure 2.3).[18, 28, 38-39] The scarcity of materials capable of overcoming this scaling relationships led to ever increasing number of reports on

nanostructured Cu-based electrodes with the aim of tuning the adsorption energies of intermediates using the size effects.[40-42]

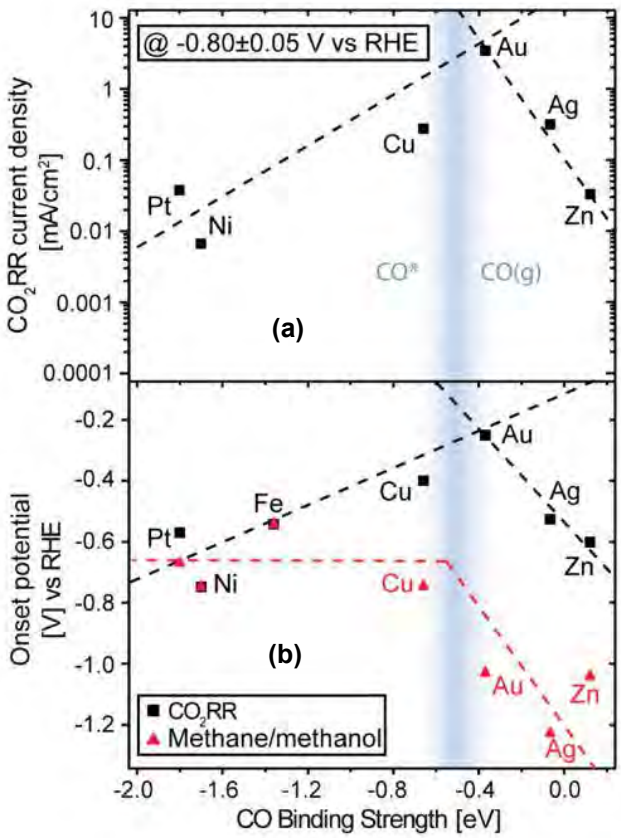

Figure 2.3. (a) Volcano plot for CO_2ERR current density and (b) onset potentials for overall CO_2ERR and CH_4/CH_3OH synthesis vs CO binding energy as measured for 7 metals.[39]

Table 2.1 also provides a clue to the second major complication, namely hydrogen evolution reaction, which is not only thermodynamically more favorable compared to CO_2ERR across all the pH range, but also has simpler kinetics.[6, 17, 39] Therefore, the most suitable pH of CO_2ERR is around 7 which directly corresponds to the maximum ratio of $[CO_2]/[H^+]$ in aqueous solution and thus the solution of CO_2 in water containing 0.1 M - 0.5 M $KHCO_3$ or $NaHCO_3$ as a background electrolyte is one of the most popular choices for practical applications.[43] The competing hydrogen evolution reaction limits the choice of supporting electrode to the conductive materials that have high overpotential of water discharge and highly stable in the reductive environment. Based on these considerations, carbon in the form of carbon fabric, carbon paper or carbon nanotubes is one of the most appropriate materials available.[44-46] Some metals such as Pb and Hg also show high water discharge overpotential and thus gained some attention, however Pb itself is an active catalyst capable of producing $HCOO^-$, while Hg is suitable only for homogeneous catalysis due to its liquid state.[16, 47-48]

These implications define the fact that CO or HCOOH accompanied by H_2 evolution is the most probable outcome of CO_2 reduction in the aqueous medium. Though one might argue that these simple products are of no economic value, this is not the case as the mixture of CO and H_2 is a perfect raw material for a well-developed Fischer-Tropsch process which leads directly to long-chain linear alkanes while HCOOH could be used in fuel cells and, in fact, might be even more feasible for this purpose than methanol due to lower crossover rate.[49]

2.2.2 Oxygen reduction (ORR) and oxygen evolution (OER) reactions

Since ORR and OER are mutually complimentary from thermodynamic point of view, it is possible to consider both processes together. However, due to high overpotentials required they are not microscopically reversible.[18, 50] As a result, the catalysts that are excellent for one process are not going to perform as well for the reversed reaction.

Reduction of molecular oxygen could proceed in two directions (Table 2.2). The first pathway is the direct reduction to water through the $4e^-$ process while the second one is a $2e^-$ reduction leading to the formation of hydrogen peroxide (H_2O_2). The $2e^-$ reduction mechanism is highly undesirable for fuel cells and air-breathing batteries as hydrogen peroxide is the strong liquid oxidant which degrades membranes, electrodes and the catalysts thus leading to irreversible damage of the electrochemical system.[25] Conversely, selective $2e^-$ pathway would be suitable for the sustainable production of H_2O_2 directly from O_2.[51]

Table 2.2. Redox potentials of oxygen reduction reaction.[25, 51]

Entry	Redox reaction	E^0(V) *vs* NHE
1	$O_2 + 4H^+ + 4e^- \rightarrow 2H_2O$	+1.23
2	$O_2 + 2H^+ + 2e^- \rightarrow H_2O_2$	+0.70
3	$H_2O_2 + 2H^+ + 2e^- \rightarrow 2H_2O$	+1.76

As one could clearly see from the entries 1 and 2 of the Table 2.2, reduction of O_2 to H_2O is more favourable in terms of thermodynamics. However, as in case of CO_2ERR, $2e^-$ pathway leading to H_2O_2 is kinetically preferable on the most of electrode materials.[25, 52] This behaviour is also determined by the fact that simultaneous transfer of 4 electrons is highly unlikely and a cascade of intermediates is required to achieve the formation of H_2O via associative or dissociative mechanisms (Table 2.3). It is believed that the breaking of the O-O bond is a very slow process and thus, even though H_2O_2 is the thermodynamically less stable product in the reaction chain, its reduction is much slower than that of O_2.[25] Based on this,

research effort is highly focused on the development of catalysts that can not only boost the reaction rates, but also shift ORR selectivity towards $4e^-$ reduction process.

Table 2.3. Mechanisms of $4e^-$ ORR.[18]

Associative [a]	Dissociative
$O_2 + * \rightarrow O_2*$	$O_2 + 2* \rightarrow 2O*$
$O_2* + H^+ + e^- \rightarrow HOO*$	$2O* + 2H^+ + 2e^- \rightarrow 2HO*$
$HOO* + H^+ + e^- \rightarrow O* + H_2O$	$2HO* + 2H^+ + 2e^- \rightarrow 2H_2O + 2*$
$O* + H^+ + e^- \rightarrow HO*$	
$HO* + H^+ + e^- \rightarrow H_2O + *$	

[a] *symbol * represents a catalytically active site.*

As with other catalytic reactions, the Sabatier principle is applicable to the ORR as well (Figure 2.3a). For ORR and OER the scaling relationship between adsorbed species HO* and HOO* was found (Figure 2.3b) which gives rise to the inherent ORR overpotential of at least 0.25-0.35 V depending on the electrode material.[18, 27, 53-54] Regarding activity of an ORR catalyst, if an active site binds too strongly to O_2, the reaction rate is limited by the electron transfer onto O* or HO* while if the adsorption energy is too small, the reduction of O_2* or O=O splitting become the slowest steps of the reaction. In an excellent agreement with theoretical predictions, Pt is the best ORR catalyst to date.[18]

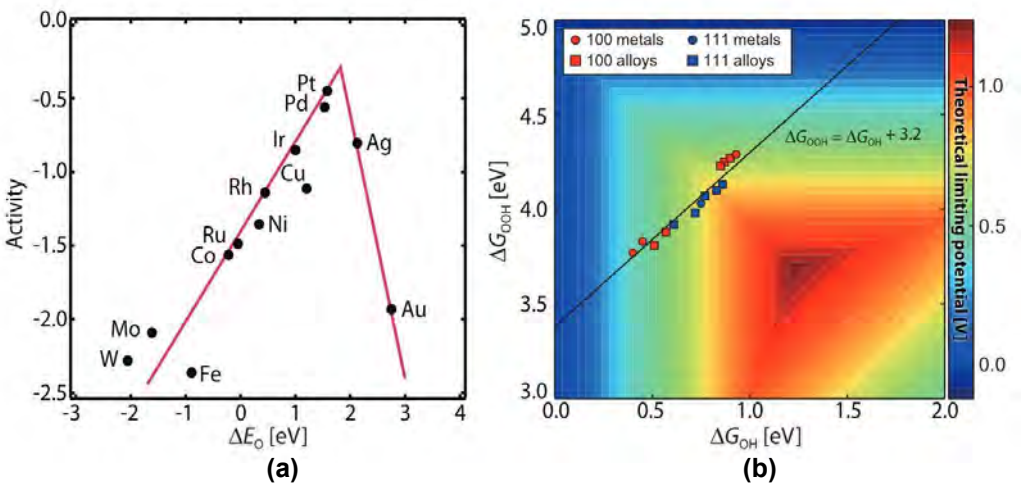

Figure 2.3. (a) Volcano plot for metal-catalysed ORR and (b) theoretical limiting potential for ORR on (111) and (100) facets of metals and alloys.[18]

In turn, OER takes place on the anode of electrolyser and supplies electrons to the cathode via an external circuit thus keeping the whole system neutral. As OER is the reversed ORR, standard electrode potential of this reaction is +1.23 V vs NHE as well. Thermodynamically, oxidation of water to O_2 (Table 2.2, entry 1) is more favourable compared to the formation of H_2O_2 (Table 2.2, entry 3) and in this case kinetics generally falls in line with thermodynamic

considerations and the formation of peroxide does not take place. The process yields O_2 molecules via $H_2O^{\cdot+}$ or ·OH, depending on the pH and these radicals recombine to form the double bond of the final product.[25]

Nevertheless, one of the major OER constraints is highly oxidative potential applied to the electrode. These conditions render any metal electrodes, including Pt, unstable and this leads to the formation of surface oxide layers.[18, 55] This observation translated into volcano-plot derived for water oxidation on oxide surfaces which shows that IrO_x to be the most active OER catalyst in great agreement with experimental results (Figure 2.4). Thus, the research is currently focused on the study of earth-abundant metal oxides and molecular catalysts that are not only capable of binding with H_2O and form O_2, but also survive in highly oxidative environment.[18, 53] While in case of metals stability hardly could be changed, for organometallics this can be achieved via introduction of oxidation-resistant substituents to the ligands or modification of immobilisation methods. Also, fine tuning of the electronic structure and the special arrangement around the active centre may lead to unprecedented activities.

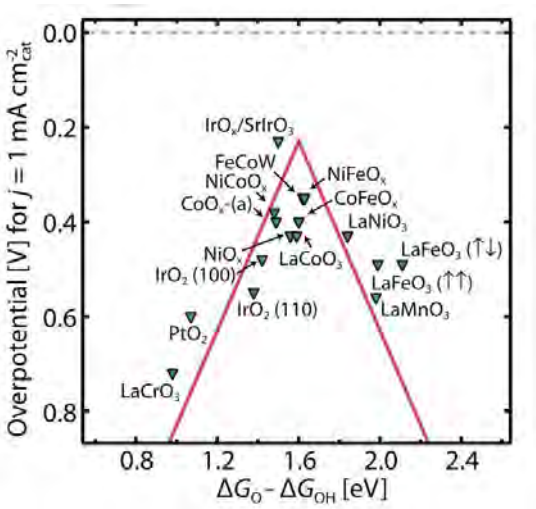

Figure 2.4. Volcano plot for metal oxide catalysed OER.[18]

2.3 Overview of electrocatalysts

The catalysts that can efficiently drive the CO_2ERR, ORR and OER may be classified into two major types according to the nature of the catalytically active site. The first class is represented by purely inorganic materials with loosely defined active centres containing a surface metal atom or metal/heteroatom cluster binding to the substrate. As one could clearly see from the theoretical discussion above, metals are among the most popular and well-studied electrocatalysts for CO_2ERR and ORR. Metal-based catalysts are normally employed in the

form of nanoparticles or nanowires to maximise the available surface area with large research effort devoted to the study of effects of crystal shape and the role of size effects, grain boundaries and facets.[6, 18, 28] Metal oxide nanoparticles have been extensively explored as electrocatalysts for reduction reactions as well with SnO_2 being a remarkable example as shown in the Table 2.4. Hybrid materials, such as heteroatom-doped carbon, are quickly gaining recognition due to their good activity and generally low cost (Tables 2.4 and 2.5). On the other hand, the OER catalysts (Table 2.6) are overwhelmingly dominated by the metal oxides since even noble metals form surface oxides under highly positive potentials required to drive water oxidation and hence the oxide layers are normally expected to be the active catalysts. For all the of materials mentioned above it is hard to define the intrinsic TOF values as the nature of catalytically active sites and the number of atoms in them are usually unknown. Hence, most of the mechanistic information is obtained in the form of current densities, faradic efficiencies and selectivities of catalytic processes. Also, since the options for the variation of electronic structure of an atom in the bulk metal are limited, the best way to enhance the overall rate of a reaction is simply to improve the surface area of the catalyst by dispersing it into nanoparticles.

Based on this information, one could argue that the maximum utilisation of a catalytically active metal may be achieved by dispersing it to single atoms. This conclusion leads directly to the idea of molecular catalysts where a metal is represented by a sole atom surrounded with a ligand. As opposed to inorganic materials, organometallics provide a unique opportunity to tune the intrinsic activity of the catalytically active centre through the variation of the ligand structure.[25] Indeed, introduction of an electron-deficient substituent will decrease the charge on the metal (desirable for oxidations) while the use of a donating group will create a centre with high electron density (generally more active is reductions). In strong contrast to nanoparticles, the TOF values and detailed kinetic information could be obtained for the molecular catalysts and the cumulative current density could be additionally improved by the increase of the surface area of a supporting electrode.

Several notable examples of CO_2ERR catalysts are shown in the Table 2.4. Clearly, the highest current densities reported for CO_2ERR (> 50 mA/cm^2) have been obtained for the metal-based electrodes or metal oxides (entries 1,3, 4 in the Table 2.4). Also, Cu was found to be the only metal supporting the deep reduction of CO_2 to alcohols and hydrocarbons (entry 1, Table 2.4). However, it does not mean that the molecular catalysts deliver low reaction rates as a very recent report showed that the CO_2ERR current densities of more than 150 mA/cm^2 could be achieved in a flow cell using Co phthalocyanine catalysts (entry 10, Table 2.4).[56] Moreover,

it appears that the molecular catalysts deliver higher current densities under low overpotentials (<500 mV) thus providing generally better performance in terms of $\zeta_{electrolyser}$ (entries 6-7 and 9, Table 2.4). Also, a recent discovery of Co-based molecular catalyst reducing CO_2 beyond CO is truly remarkable (entry 9, Table 2.4).[57]

Table 2.4. Heterogeneous CO_2ERR catalysts operating in aqueous medium.

Entry	Catalyst	*j* CO_2ERR (mA/cm^2)	*E (V vs NHE)*[a]	*Products*	*Ref.*
1	Cu nanocubes on Cu foil	~ 56	-1.38	CO, C_2H_4, CH_4, EtOH	[42]
2	Ag nanowires	3.5	-1.46	CO	[58]
3	Ag nanoparticles on carbon foam	120	-1.851.21	CO	[59]
4	SnO_2 nanoparticles	145	-2.00	$HCOO^-$, CO	[60]
5	N-doped CNTs[b]	~ 0.8	-1.19	CO	[9]
6	CoTPP-based COF[c]	5	-1.08	CO	[45]
7	CoTPP/CNTs	2.9	-1.09	CO	[8]
8	drop-cast Fe porphyrin on CNTs	~ 0.5	-1.03	CO	[46]
9	Co phthalocyanine / CNTs	~17	-1.11	CO, CH_3OH	[57]
10	Co phthalocyanine / CNTs	176	N/A[d]	CO	[56]

[a] *Potentials were converted to the NHE scale from the potential scale given in literature references.*

[b] *Carbon nanotubes.*

[c] *Covalent organic frameworks.*

[d] *Not applicable. The cited study was performed in a flow-cell (no reference electrode) with the cell voltage of 2.52 V under the total current density of 200 mA/cm^2 and a FE (CO) of 88%.*

Due to low solubility of oxygen in water the maximum ORR reaction rate is usually determined by the diffusion limitations. Thus, the Table 2.5 describing the ORR catalysts is focused on the onset potentials, selectivity to 4e$^-$ reduction and electrolyte employed in the studies, the latter being due to pH impact on the thermodynamic reduction potential E^0_{ORR}. In case or ORR, the carbon-supported Pt is undeniably the most active catalyst showing nearly 100 % selectivity towards 4e$^-$ mechanism and has already been commercialised (entry 1, Table 2.5).[61] At the same time, its prohibitively high cost galvanised the research effort towards the development of the core-shell structures and alloys (entries 2-4, Table 2.5).[62] Another approach is based on the development of the catalysts based only on the first-row transition metals.[6] This often includes the use of nitrogen-doped carbon nanotubes as a support for the metal atoms with the

catalytically active centres presumed to be MN_x (entries 5-6, Table 2.5). Interestingly, electrodes based on nitrogen-doped carbon showed almost exclusive formation of H_2O_2 and hence most of these materials are positioned as promising catalysts for the H_2O_2 synthesis (entry 7, Table 2.5). Compared to inorganic materials, some of the organometallics show the onset potentials close to that of Pt and similar or only slightly lower selectivities (entries 8-10, Table 2.5). Indeed, the Fe porphyrins have been found to be among the best ORR catalysts comparable to Pt in performance (entry 9, Table 2.5). Moreover, the stability tests showed their excellent durability and good resistance and methanol crossover which is highly relevant for the direct methanol fuel cell development.[63]

Table 2.5. Heterogeneous ORR catalysts operating in aqueous medium.

Entry	Catalyst	*Onset E (V vs NHE)*	*H_2O selectivity, %*	*Electrolyte*	*Ref.*
1	Pt/C[a]	1.00	~ 100	0.1 M $HClO_4$	[61]
2	Pt_3Co/C	1.05	~ 100	0.1 M $HClO_4$	[64]
3	Pd@$Pt_{o.7\text{-}4.3L}$/C[b]	1.00	~ 100	0.1 M $HClO_4$	[65]
4	Pt_3Y/C	1.00	~ 100	0.1 M $HClO_4$	[62]
5	Fe-N-carbon hybrid	0.81	~ 100	0.5 M H_2SO_4	[66]
6	Fe-N-carbon hybrid	0.25	~ 100	0.1 M KOH	[66]
7	N-doped carbon	0.55	< 10	0.5 M H_2SO_4	[52]
8	Co corrole/MWCNT[c]	0.75	95.6	0.5 M H_2SO_4	[67]
9	Fe porphyrin/CNTs	1.00	99	0.1 M $HClO_4$	[63]
10	Co porphyrin polymer	0.10	95	0.1M KOH	[68]

[a] *Pt/C corresponds to a composite consisting of Pt nanoparticles on the surface of carbon support.*

[b] *Pd@Pt_{xL} corresponds to Pd core with the X number of Pt layers on the surface.*

[c] *Multi-walled carbon nanotubes.*

In strong contrast to CO_2ERR and ORR, water oxidation always leads to the formation of oxygen only and hence the question of selectivity is usually not considered. Instead, the onset potential and the Tafel slope are the most important parameters. Examples of some good OER catalysts are illustrated in the Table 2.6. Clearly, the oxides of precious metals are by far the most active catalysts not only in terms of the reaction onset potential, but also because of extremely steep Tafel slope (entries 1-3, Table 2.6). However, as Ir and Ru are among the scarcest metals in the Earth crust, significant effort has been devoted to the development of more cost-effective alternatives. In this regard, the MnO_x derivatives exhibit good performance and stability while being widely accessible (entries 4-5, Table 2.6). Comparable performance could be achieved by the alternative inorganic materials comprising other first-row transition

metals such as Ni and Fe (entry 6, Table 2.6). However, the class of organometallics is poorly represented in the field of OER. Even though they show similar onset potentials, the characteristic Tafel plots are shallow which implies the lacklustre kinetics and need for high overpotential to drive the oxygen formation with reasonable rate (entry 9, Table 2.6). Also, organic ligands appear to be prone to degradation under positive potentials.[55]

Table 2.6. Heterogeneous OER catalysts operating in aqueous medium.

Entry	Catalyst	*Onset E (V vs NHE)*	*Tafel slope (mV/dec)*	*Electrolyte*	*Ref.*
1	IrO_x nanoparticles	~ 1.35	34.8	0.5 M H_2SO_4	[69]
2	Amorphous α-IrO_x	1.30	~ 30	1 M H_2SO_4	[70]
3	RuO_2 nanoparticles supported on carbon cloth	1.35	36.9	0.5 M H_2SO_4	[71]
4	Mn_3O_4 supported on Si_3N_4-Ag membrane	~ 0.83	- [c]	0.1 M KOH	[72]
5	β-MnO_2 nanofilm	0.76	90	0.1 M NaOH	[73]
6	Ag NWs@$Ni_{0.95}Fe_{0.05}$ LDH[a]	0.67	89	1 M KOH	[74]
7	Co corrole/MWCNT [b]	1.15	- [c]	0.1 M pH 7 phosphate buffer	[67]
8	Carbon-grafted Ir complex	~1.0	- [c]	0.1 M pH 5 acetate buffer	[75]
9	MnTPP grafted on carbon cloth	1.32	234-267	0.5 M H_2SO_4	[76]

[a] *Ag nanowires (NWs) coated (@) with a layered double hydroxide (LDH) containing 95 mol. % of $Ni(OH)_x$ and 5 % of $Fe(OH)_x$.*

[b] *Complex contains 2 pentafluorophenyl substituents to enhance its activity in the oxidation reaction.*

[c] *Not given.*

In conclusion, the molecular catalysts appear to be especially efficient for CO_2ERR under low overpotentials and their inherent tunability could be used to change both activity and selectivity to a much greater extent than in case of metals or metal oxides. Organometallics also perform well in ORR and could compete even with Pt in terms of activity while being significantly cheaper. However, the catalysis of OER requires very high positive potentials and the molecular catalysts may not last for long. Finally, it must be noted that the nature of catalytically active centres in inorganic and molecular catalysts is vastly different and a more detailed comparative literature survey of various types of catalysts with their pros and cons exceeds the scope of this dissertation by far.

2.4 Structure, redox behaviour and synthesis of porphyrins

As we noted above, the structural tunability is extremely beneficial for the development of efficient electrocatalysts as it allows to circumvent the restrictions imposed by scaling relationships and thus – to achieve the reaction rates and selectivities unattainable on conventional inorganic catalysts. In this regard organometallic complexes, especially those containing aromatic ligands may act as "reservoirs" for electrons due to extended molecular orbitals. Among numerous classes of complexes porphyrins and phthalocyanines are especially attractive due to their unique structural motif comprising a metal atom and a big conjugated ligand.

Structurally, porphyrins are flat macrocyclic compounds consisting of 4 pyrrole moieties interspaced by *meso*-carbons. Experimental evidence shows that the porphyrins exhibit clear aromatic behaviour due to $18e^-$ system which follows Hückel's ($4n + 2$) rule of aromaticity (Scheme 2.1a).[77] Furthermore, the porphyrin structure features four-dentate ligand which easily accommodates metal ions and metalloporphyrins also show aromatic character with all 26 π-electrons participating in delocalised electron system.[78] Oxidation state of the central atom depends on the metal involved. As such, with Fe and Mn porphyrins normally exist as $[Fe^{III}Por]X$ and $[Mn^{III}Por]X$ with the pentacoordinate metal centre where X is a monodentate ligand such as Cl or OAc. At the same time, Co, Ni and Cu analogues present as $M^{II}Por$ with four-coordinate central ion under normal conditions. It must be noted here that with the uptake of additional electrons Fe and Mn complexes tend to lose the axial ligand and form four-coordinate complexes as well.[25, 79] Also, the prominent Soret and Q-bands in UV/Vis spectra of porphyrins made them a unique subject for catalytic and coordination studies as any change in HOMO and LUMO leads to immediate change in adsorption.[80-82]

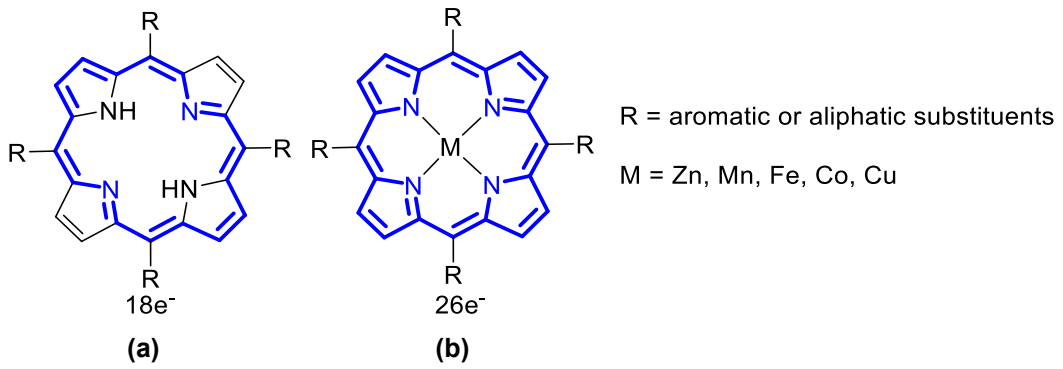

Scheme 2.1. (a) Electronic structure of free-base and (b) metalated porphyrin core.

Since the essential role of any electrocatalyst is to shuttle electrons between the electrode and a substrate, the organometallic catalysts must be able to participate in redox transformations. In this regard porphyrins feature a wide range of reversible single-electron transformations.[25] As such, upon reduction all these complexes exhibit two or three redox couples with the formation of products characterised by the formal oxidation states of metal atom $[M^{II}Por]$; $[M^{I}Por]^{-}$ and $[M^{0}Por]^{2-}$. However, the real distribution of electron density in these reduced species is far from the one implied by these simple formulas as the molecular orbitals extend across all conjugated π-system and involve both metal and ligand. Indeed, for a reduced porphyrin derivative $[M^{0}Por]^{2-}$ the resonance structures described by the equation 2.7 could be devised where $[M^{I}(Por\cdot)]^{2-}$ is a species with one electron located on the metal and the second – on the ligand while $[M^{II}(Por\mathbf{:})]^{2-}$ is the complex with both electrons centred on the macrocycle.[83-84]

$$[M^{0}TPP]^{2-} \leftrightarrow [M^{I}(TPP\cdot)]^{2-} \leftrightarrow [M^{II}(TPP\mathbf{:})]^{2-} \quad \textbf{(Equation 2.7)}$$

To elucidate the distribution of electron density within these unstable intermediates extensive research was performed by C. R melt et al. using Mössbauer and Raman spectroscopy supported by quantum calculations on the example of Fe tetraphenylporphyrin. It was established that the prevailing form is $[M^{II}(TPP\mathbf{:})]^{2-}$ while the formation of Fe^{I} and Fe^{0} structures incurs high energy penalty (Figure 2.5).[84-85] Similar conclusions were drawn for the Co derivatives. Indeed, the reduced form of porphyrin-like Cob(I)alamin features resonance of multiple electronic states with only 67 % contribution from the d^{8} Co(I) species while the rest is represented by the wide variety of open-shell structures.[86]

Based on large-scale involvement of ligand orbitals in redox transformations one would expect preferable irreversible transformations of porphyrin core under reductive conditions. However, this is clearly not the case as the build-up of charge on the macrocycle does not necessarily mean that any given reaction will completely avoid the metal centre. In this case plenty of data is available showing that reactivity of reduced porphyrins depends heavily on the nature of metal. For example, $[Fe^{II}(TPP\mathbf{:})]^{2-}$, though having 2 additional electrons on the aromatic molecular orbitals, does not participate in ligand reduction in the presence of proton donors and this feature makes it an excellent hydrogen evolution catalyst with no detectable hydrogenation of the macrocyclic ring.[87] Moreover, the reaction of this reduced complex with *n*-BuBr yielded exclusively Fe-alkylated product which additionally supports the theory of the ligand being rather an "electron reservoir" than a reactive centre.[88] At the same time,

Cu analogue shows opposite behaviour as during the reduction in the presence of Brønsted acids the complex undergoes $3H^+$, $3e^-$ reduction of the porphyrin ring.[87]

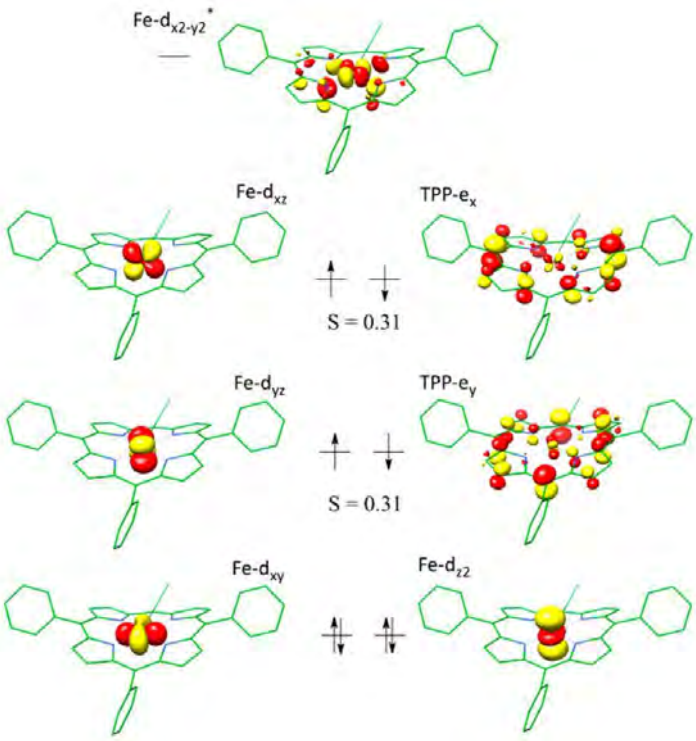

Figure 2.5. Molecular orbitals of $[Fe^{II}(TPP:)]^{2-}$.[84]

Further, the mechanisms of electrocatalysis vary significantly from one complex to another. Clear distinction could be made between porphyrins playing the role of pure redox catalysts (outer-sphere transfer of electron onto a substrate) and chemical catalysts (inner-sphere electron transfer). In a series of works on catalytic dehalogenation of *trans*-1,2-dibromocyclohexane a clear correlation between the nature of porphyrin complex and the catalytic mechanism was uncovered (Figure 2.6a).[89-90] It was found that Zn, Cu and free-base porphyrins behave as pure redox catalysts with exclusive outer-sphere electron transfer between the catalyst and the substrate (Figure 2.6b,c). In turn, Co, Fe and Ni complexes behave as chemical catalysts and outperform in terms of TOF by far the class of redox catalysts due to the formation of intermediates along the reaction coordinate (Figure 2.6b,c).[83, 89-90] Considering the dependence of Mn^{II} porphyrin catalysed ORR selectivity on the presence of proton donors, Mn complexes also play the role of chemical rather than redox catalysts.[79] Furthermore, this trend holds true for CO_2ERR as well where Fe porphyrins also show significant improvement of the reaction rate in the presence of proton donors in electrolyte.[91-92]

Thus, reduced porphyrins are excellent nucleophiles and readily transfer electrons onto O_2 and CO_2, however the exact oxidation state that is catalytically active depends on the substrate and the reaction conditions. For example, [M^{II}Por] is already reactive enough to interact with oxygen which was clearly presented for Fe and Mn porphyrins both in aqueous and nonaqueous media.[76, 79, 93] At the same time, the onset of CO_2ERR in nonaqueous medium usually happens only upon reduction of the porphyrin to the extremely reactive [M^0Por]$^{2-}$ state.[8, 25] At the same time, CO_2ERR in aqueous electrolyte catalysed by Co porphyrin takes place around the potential of Co^{II}/Co^{I} redox couple.[8, 43] At last, as the exact distribution of electrons in the reduced porphyrins is not always well-studied we will use widely accepted abbreviations [M^0(Por)]$^{2-}$, [M^I(Por)]$^-$, M^{II}(Por) for the reduced forms of complexes.

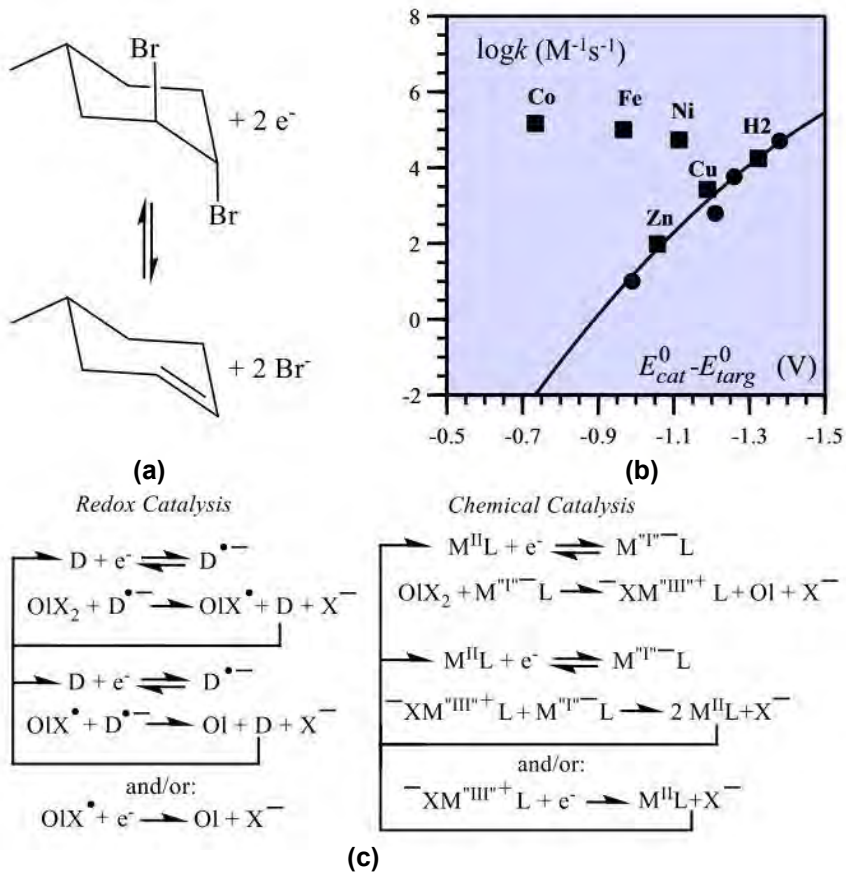

Figure 2.6. Distinction between chemical and pure redox catalysts studied on the example of porphyrin-catalysed dehalogenation of *trans*-1,2-dibromocyclohexane.[83]

Regarding the synthesis, construction of porphyrin core is generally based on acid-catalysed condensation of pyrroles and aldehydes (Scheme 2.2). Two sets of optimum conditions for this reaction have been established. A very convenient and cheap method developed by Adler and Longo is based on the reflux of pyrrole and aldehyde in propionic acid in the presence of air or oxygen.[94] This approach is generally used to prepare simple porphyrins and is extremely

versatile due to simplicity of porphyrin isolation from the reaction mixture as the target product is usually insoluble in propionic acid. However, the reaction mixture is kept at 141°C in the presence of oxidant and this might cause considerable degradation of heat- or oxygen-sensitive groups. Another method developed by Lindsey et al. is based on BF_3-catalysed condensation in CH_2Cl_2 at near room temperature with the following oxidation of porphyrinogen by chloranil or DDQ.[95] Thanks to the mild conditions employed, yields are generally higher than those in Adler-Longo procedure and the structures that could otherwise be damaged by prolonged exposure to O_2-saturated propionic acid also could be prepared. The only downside of this method is higher cost of quinone-based oxidants used in the sequence. The following insertion of the metal atom is a straightforward procedure and is usually achieved by the reflux of porphyrin solution with the excess of metal acetate in DMF or chloroform/methanol mixture.[96-97]

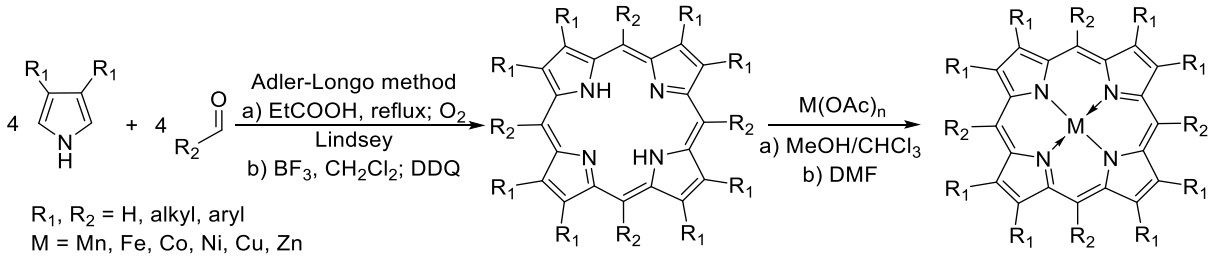

Scheme 2.2. General scheme of metalloporphyrin synthesis.

As one could clearly see form the Scheme 2.3, these methods yield a central porphyrin core with the symmetric configuration of the substituents while target uses might require more elaborate structures with more than one type of *meso*-substituent group present. In this scenario the synthesis becomes much more challenging as the molecule with D4h symmetry yields a complex mixture of products in any transformation involving peripheral positions. Hence, preparation of unsymmetrical porphyrins typically includes combination one-step statistical synthesis and derivatisation of more simple compounds such as tetraphenylporphyrin via a series of secondary transformations.[98] As an example, synthesis of free base pyrene-appended porphyrin **1** (Scheme 2.3a) was achieved through the statistical acid-catalysed synthesis from 2,6-dimethoxybenzaldehyde **2**, respective pyrene-derived aldehyde **3** and pyrrole.[46] In turn, preparation of nitroporphyrin **3** was achieved using the latter approach via mononitration of tetraphenylporphyrin **4** (Scheme 2.3b).[97, 99] Nevertheless, the exact choice of the synthetic pathway is always based on the availability of starting materials, scale and simplicity of product isolation.

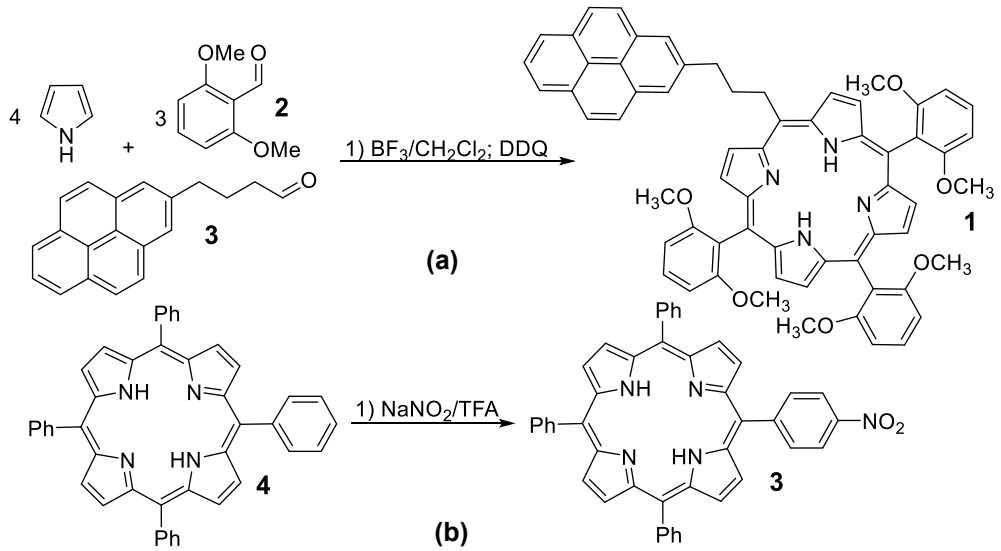

Scheme 2.3. Examples of unsymmetrical porphyrin syntheses: (a) assembly of macrocyclic core from the 1:3 mixture of aldehydes and (b) step-by step transformations starting with easily accessible tetraphenylporphyrin **4**.[46, 99]

2.5 Porphyrin-catalysed CO_2ERR

2.5.1 Homogeneous catalysts

Metalloporphyrins have been extensively studied as catalysts for electro- and photoreduction of carbon dioxide. Homogeneous systems have been widely utilised in mechanistic studies which allowed to elucidate factors affecting activity and selectivity of these complexes. Among all available non-noble metals, structures based on Fe received the most attention due to their unsurpassed activity in non-aqueous solutions. CO_2ERR activity of simple $[Fe^{III}TPP]Cl$ **5** (Scheme 2.4a) in DMF was studied in depth back in 1991.[100] The complex shows three successive single-electron reduction waves with the eventual formation of $[Fe^{0}TPP]^{2-}$ **6** (Scheme 2.4b). The first transformation was found to be accompanied by the loss of axial Cl^- ligand while the potential equal or greater than that of third redox couple is prerequisite for the appearance of catalytic current. Upon reaction with CO_2 intermediate undergoes loss of oxygen atom in the form of carbonate and $[Fe^{I}TPP\text{-}CO]$ releases the final product due to weak coordination of CO. Notably, in these conditions the complex quickly degrades, and only slight improvement of stability was achieved by introduction of various lateral substituents. In turn, significant enhancement of CO_2ERR rate in the presence of Mg^{2+} was discovered which acts as a Lewis acid that binds to CO_2 moiety in the $Fe^{II}\text{-}CO_2$ adduct. Thus, it became apparent that the presence of acids has a considerable stabilisation effect on the transition state of the catalytic reaction.[100] In further works it was found that the presence of weak Brønsted acids

such as trifluoroethanol, phenol or water has an even stronger effect compared to Mg^{2+} ions.[92]

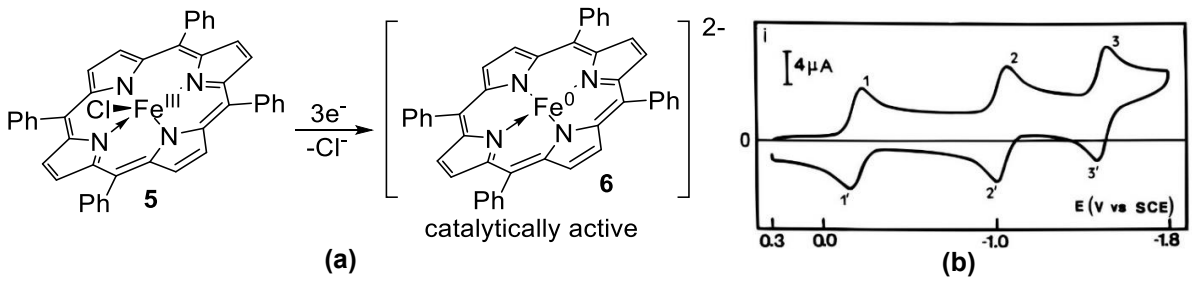

Scheme 2.4. (a) Formation of CO_2ERR-active form of catalyst $[Fe^0TPP]^{2-}$; (b) CV response observed for the sequential formation of $[Fe^{II}TPP]$ (1), $[Fe^{I}TPP]^-$ (2) and $[Fe^0TPP]^{2-}$ (3).[92]

The underlying reason of this rate enhancement in the presence of acids is binding of a proton donor to the oxygen atom in $[FeTPP\text{-}CO_2]^{2-}$ which in turn stabilises the transition state leading to this adduct and assists in C-O bond cleavage. This effect was further explored by incorporation of eight proximal -OH groups into the structure of Fe porphyrin **6** (Scheme 2.5a).[101] In this case, the local concentration of proton donors within the solvation shell around the catalytically active centre reaches as high as 150 M which is unattainable by any other method. As a result, stabilisation of $[Fe^{II}\text{-}CO_2]$ species **8** takes place via a net of hydrogen bonds (Scheme 2.5b). For this catalyst FE(CO) of 94 % and logTOF of 3.8 under an overpotential of 466 mV in the presence of 3 M PhOH was reported. What is more impressive, authors compared CO_2ERR performance of Fe octahydroxyporphyrin **7** with that of the well-known Ni(cyclam), $Mn(bipy)(CO)_3Br$ and two Ru(terpy) catalysts and the result clearly shows that this non-noble metal-based complex has considerably higher TOF values than even Ru derivatives.

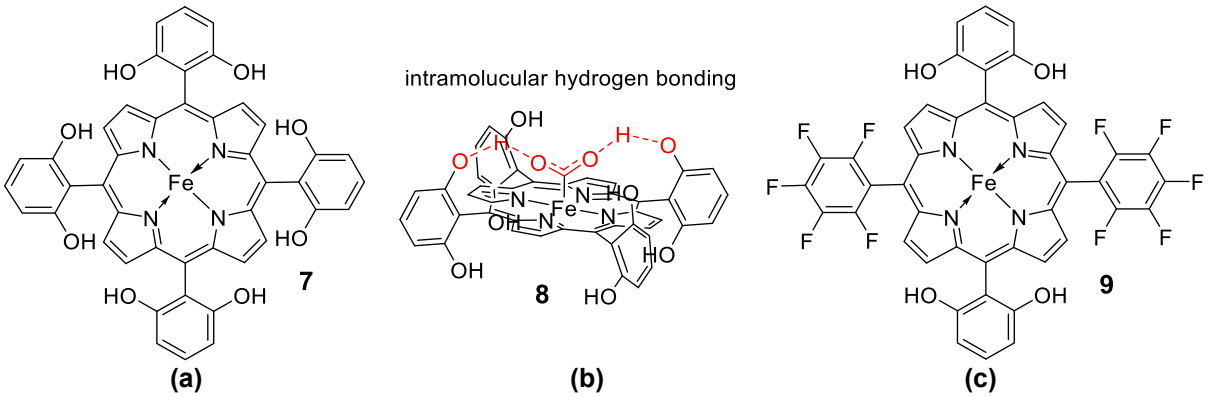

Scheme 2.5. (a) Structure of Fe octahydroxyporphyrin and (b) stabilisation of $Fe^{II}\text{-}CO_2$ by the network of intramolecular hydrogen bonds; (c) structure of a catalyst incorporating electronegative substituents and proton relays in one molecule.[101-102]

Further work showed that the activity could be improved even further by the introduction of electronegative substituents as in the case of Fe 5,15-di(2,3,4,5,6-pentafluorophenyl)-10,20-di(2,6-dihydroxphneyl)porphyrin **9** (Scheme 2.5c).[102] For this complex the effect of intermediate stabilisation by proximal proton relays is coupled with the reduction of the cathodic potential required to drive the Fe^{I}/Fe^{0} transformation. This strategy furnished an even more active catalyst compared to the porphyrin **7** with logTOF of 4.0 under similar conditions. Additionally, the introduction of a pentafluorophenyl substituent in the catalyst **9** increased the stability of the catalyst with maximum TON of 600 against 210 for the complex **6**. Finally, the strategy of intermediate stabilisation was employed to prepare the most active homogeneous CO_2ERR catalyst to date by the replacement of *ortho* -OH moieties with positively charged -NMe_3^+ groups in the complex **10** (Scheme 2.6a).[103] In this case the estimated TOF even at zero CO_2ERR overpotential is more than 300 s^{-1} with its maximum value as high as 10^6 s^{-1}. Fe porphyrin **9** bearing four positively charged -NMe_3^+ groups was tested as a homogeneous catalyst for CO_2ERR in aqueous media as well (Scheme 2.6b).[104] In this case the use of pendant charged moieties is required to solubilise the complexes in water. The mechanism of CO formation was found to be the same as in organic electrolytes and an impressive 72 h long electrolysis at -0.86 V vs NHE was performed with FE(CO) of 98-100 %. Notably, excellent selectivity of Fe porphyrins towards CO_2 in non-aqueous electrolytes was recently showcased in a report by Mondal et al. who proved that even in the presence of O_2 the CO_2ERR on Fe^0 centre is at least 500 times faster than ORR.[105]

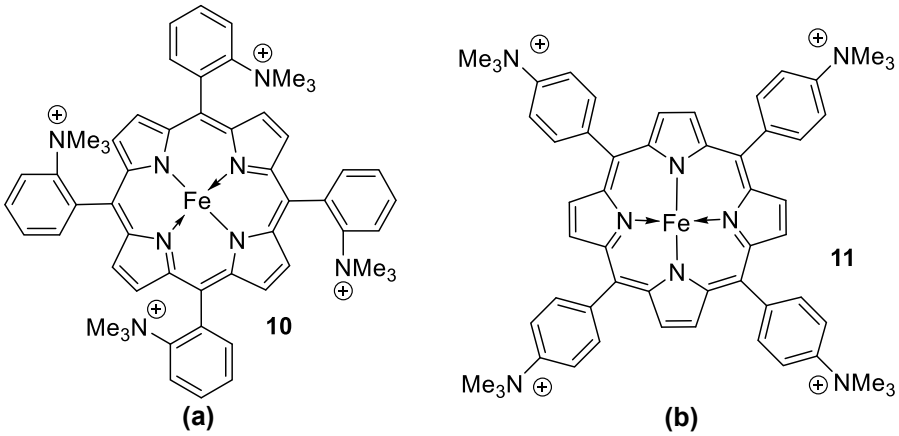

Scheme 2.6. Structures of (a) the most efficient homogeneous CO_2ERR electrocatalyst to date and (b) water-soluble Fe porphyrin-based catalyst.[103-104]

Homogeneous catalysis by CoTPP in non-aqueous electrolytes was reported as well.[81] As in case of Fe complexes, CO_2ERR is driven by Co^0 complex forming at the potentials as negative as -2.02 V vs SCE. The reaction was shown to proceed through a mechanism similar

to that exhibited by Fe complexes where $[Co^{0}TPP]^{2-}$ binds to CO_2 and the resulting intermediate $[Co^{II}TPP\text{-}CO_2]^{2-}$ after protonation releases H_2O, CO and starting CoTPP. However, in strong contrast to Fe counterparts the presence of electronegative substituents decreases the reaction rate despite the less negative potential of the Co^{I}/Co^{0} redox couple. Also, an extremely low stability of the complex was observed, however the exact nature of the deactivation products was not studied. CO_2ERR selectivity in DMF and the influence of proton donors on the reaction rate were also evaluated in a recent publication by Hu et al.[8] The reaction appears to be less selective compared to Fe analogues as $HCOO^-$ (4 %), CH_3COO^- (2 %) and oxalate (0.4 %) along with 2 % of H_2 were produced. Also, the rate of CO_2ERR catalysed by CoTPP in homogeneous solution does not depend on the presence and concentration of Brønsted acids. FE(CO) was found to be only 50 % as the rest of the current was wasted on severe decomposition of CoTPP. These observations clearly show that the Co porphyrins are inferior to their Fe counterparts in homogeneous CO_2ERR catalysis.

Zn complexes comprise an interesting and unusual phenomenon in the field of homogeneous CO_2 reduction catalysts where it is the metal rather than the ligand that acts as a "redox-innocent" centre. As such, a study on Zn bacteriochlorin-catalysed CO_2ERR was recently reported where authors attempted to improve the resistance of the Zn complex to reductive decomposition by the replacement of the porphyrin core with that of chlorine where one of the vulnerable C=C positions is fully saturated and thus could not participate in the reduction reaction.[106] This structure, though structurally similar to the porphyrin core, showed much higher resistance to reductive decomposition. Indeed, CO_2ERR with FE(CO) of 92 % and a current density of 2.3 mA/cm^2 was sustained for 5 h for chlorin (product of $2e^-$, 2 H^+ porphyrin reduction) while a fully aromatic porphyrin analogue completely bleached under the same conditions.

It is necessary to note that the stability and poisoning patterns of the molecular catalysts are undeniably one of the key aspects in the catalyst development, however they received surprisingly little attention. As such, it was shown that the Fe porphyrins, though being extremely active in CO_2ERR, could be poisoned by the evolving CO.[92] Also, electroreduction of the macrocyclic ligand could be responsible for the loss of activity and although the respective Zn chlorin showed excellent stability, in the control experiment with Zn porphyrin the reduction products were not detected.[106] The reductive demetallation could also occur under the reaction conditions, however these were detected only in case of Cu

porphyrins and phthalocyanines.[107-108] Moreover, the forming nanoparticles of Cu were found to be a true catalyst while the complex itself plays role of a precatalyst.[107]

Finally, an interesting comparative study on CO_2ERR activity of noble- and non-noble metal based molecular catalysts was performed.[101] Clearly, Mn(bipy)$(CO)_3$, Pd(biphos) and Re(bipy) complexes show excellent TOFs, however their activity clearly pales in comparison with that of macrocyclic derivatives such as porphyrins. Thus, considering their excellent activity and the well-developed theoretical understanding, it makes great sense to use porphyrins as benchmark structure for the development of heterogeneous catalysts for aqueous-based systems.

2.5.2 Heterogeneous catalysts

Compared to the activity of metalloporphyrins in homogeneous solutions, mechanisms of heterogeneous catalysis are comparatively less developed, mostly because such a study must consider the interference of the support and solid nature of the material both of which pose formidable challenges for spectral characterisation using NMR, UV/Vis and EPR. Additionally, aggregation and CO_2 diffusion problems make it difficult to standardise the surface concentrations of electrochemically active complexes.

Although a great number of studies deal with the activity of Fe porphyrins in homogeneous solutions, it appears that the transfer of their activity into aqueous electrolytes is extremely challenging due to highly negative potentials required to drive the formation of catalytically active Fe^0 species. Nevertheless, complex **9** (Scheme 2.5c) was immobilised in a Nafion layer on the surface of carbon powder and used as a heterogeneous electrocatalyst.[5] Superb activity of Fe hydroxyporphyrins developed in organic electrolytes was also successfully transferred to aqueous medium by immobilisation onto the surface of carbon nanotubes. Noncovalently immobilised complex showed FE(CO) of 97 % and TOF of 144 h^{-1} (0.04 s^{-1}) under potential of -1.03 V vs NHE.[46] Covalently grafted complex with a similar structure shows FE (CO) of 95 % and TOF of 178 h^{-1} (0.05 s^{-1}) at -1.06 V vs NHE.[10] However, one can see that the TOF values estimated from CV in DMF are by five orders of magnitude higher compared to those observed in long-run electrolysis in aqueous heterogeneous systems. Moreover, in two latter cases during CV study a gradual decrease of the peak current was observed upon repetitive scans which in case of noncovalent immobilisation was assigned to the catalyst leaching.[46]

In contrast to aprotic solvents, carbon-supported Co macrocyclic complexes perform considerably better in aqueous electrolytes. As such, a comparative study showed that although $[Co^0TPP]^{2-}$ is a catalytically active species in DMF, immobilisation on CNTs and use of aqueous electrolyte changes the reaction mechanism rendering $[Co^ITPP]^-$ to be catalytically active. This resulted in CO_2ERR proceeding with FE(CO) of 91 % on CoTPP/CNT hybrid material.[8] This feature allows to achieve the formation of catalytically active species without use of extremely negative potentials thus largely eliminating the problem of competing hydrogen evolution reaction. Additionally, comparison of CoTPP and FeTPP was performed and Fe analogue showed FE(CO) of only 64 % with 3.6 times lower current density. An additional advantage of Co porphyrins in heterogeneous systems is the exceptionally high stability, which again stems from lower reactivity of Co^I complexes compared to both Co^0 and Fe^0 counterparts. Indeed, heterogeneous Co complexes could survive as much as $3.0\text{-}3.9\cdot10^5$ turnovers which amounts to at least three orders of magnitude higher operational lifetime compared to the homogeneous system.[43, 45, 102]

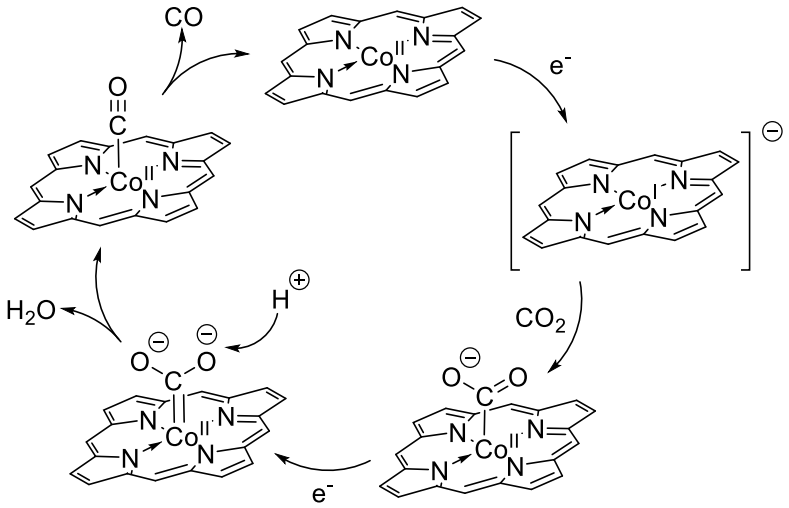

Scheme 2.7. Mechanism of CO_2ERR catalysed by Co porphyrins (meso-substituents are omitted for clarity).[91, 109-111]

Because of these mechanistic considerations, it is not surprising that Co macrocyclic complexes immobilised on the surface of carbon scaffolds are some of the most well studied CO_2ERR catalysts available to date, and the reaction mechanisms leading to this excellent activity have been a subject of rigorous scrutiny.[81, 110] It appears that the reaction follows the pathway shown in Scheme 2.7. However, some details are still debated such as the exact step where protonation takes place. For example, it was proposed that the formation of the protonated Co porphyrin ring may precede the nucleophilic attack on CO_2.[91] Also, the influence of

substituents on CO_2ERR activity of Co porphyrins was found to fall in line with that observed in homogeneous solutions, i.e. the electronegative groups decrease the activity of the catalysts.[112] Interestingly, Co protoporphyrin has been reported to be uniquely capable of CO_2 reduction to CH_4 in acidic electrolyte thus essentially overcoming the prohibitive scaling relationships discussed above.[109]

It should be noted here that CO_2ERR is often performed in an electrolyte containing 0.1 - 0.5 M $KHCO_3$ or $NaHCO_3$ and thus CO might arise from the reduction of both CO_2 and the supporting electrolyte itself. However, this question has been resolved in recent study of CO_2ERR catalysed by Co phthalocyanine where the influence of CO_2 partial pressure and HCO_3^- concentration was studied.[113] The reaction rate shows clear first-order dependence on [CO_2] and zero-order dependence on the concentration of supporting electrolyte. This observation unambiguously shows that it is CO_2 that is reduced to CO rather than HCO_3^- ions of the supporting electrolyte. However, even in the degassed bicarbonate solutions CO might be formed due to the equilibrium that produces a minor amount of free CO_2 in the solution.[114]

Finally, a heterogeneous catalyst based on Zn porphyrin was reported.[115] This remarkable example of redox innocent metal centre allows to produce CO in DMF/water mixture with excellent FE(CO) of 95 % and TOF of 14.4 s^{-1} at -1.7 V vs NHE. However, it appears the use of mixed electrolyte is unavoidable due to competing hydrogen evolution.

2.5.3 Concluding remarks

Porphyrins are excellent catalysts for homogeneous and heterogeneous CO_2ERR. Among different metals, Fe complexes exhibit excellent TOFs and FE(CO). However, their heterogenisation and transfer of CO_2ERR activity into aqueous medium proved to be quite difficult as the change of the reaction medium induces significant drop of TOF. In turn, Co derivatives show several orders of magnitude higher CO production rate and stability in water compared to Fe counterparts. Another interesting property of Co porphyrins is their increased stability in heterogeneous aqueous-based systems compared to what was observed in organic electrolytes. Several reports show isolated examples of either covalent and noncovalent immobilisation techniques, however until recently it was not clear which method is more advantageous in terms of activity and selectivity.

2.6 Porphyrin-catalysed ORR and OER

2.6.1 Homogeneous catalysts

As for CO_2ERR, Fe macrocyclic complexes are among the most studied molecular catalysts for ORR with well-established reaction mechanisms. Wasylenko et al. reported the study of [Fe^{III}TPP]Cl activity in ORR in DMF solution where the catalysis by Fe^{II}TPP complex forming upon single electron reduction was clearly observed. The electron transfer number (ETN) of 3.7 was measured using spectrochemical and electrochemical methods with excellent agreement between both methods.[116] The ORR activity was also studied in aqueous homogeneous solutions for porphyrins **12** and **13** soluble in dilute aqueous $HClO_4$ (Scheme 2.8a).[117] Similar to the activity of FeTPP, these complexes clearly promote $4e^-$ ORR with the 4-pyridil analogue **13** being more active and producing 15 % of H_2O_2 while the 2-pyridil analogue, though less efficient in terms of TOF, shows an ETN of 4.0. It is remarkable to compare the ORR selectivity of complex **13** and its methylated analogue **14** as the latter produces 95 % H_2O_2 which was assigned to the differences in proton delivery mechanism.[118] The authors suggested that the different proton delivery pathways play a crucial role in ORR as the 4-pyridil complex supports protonation of proximal O in the Fe^{III}-O-OH intermediate while the methylated pyridyl substituent does not support this pathway. Similar to the example of CO_2ERR, the O-O bond activation rate (and thus the contribution of the $4e^-$ pathway) could be significantly enhanced via introduction of groups that stabilise the reaction intermediates through the intramolecular hydrogen bonds. As such, catalytic activity in a series of hangman Fe porphyrin complexes **15-20** was studied for disproportionation of H_2O_2 (Scheme 2.8b).[119] Interestingly, higher pK_a values of pendant proton donors disfavour O-O bond cleavage, which was explained by deprotonation of strongly acidic groups (such as phosphonic acid) and hence their low stabilisation efficiency.

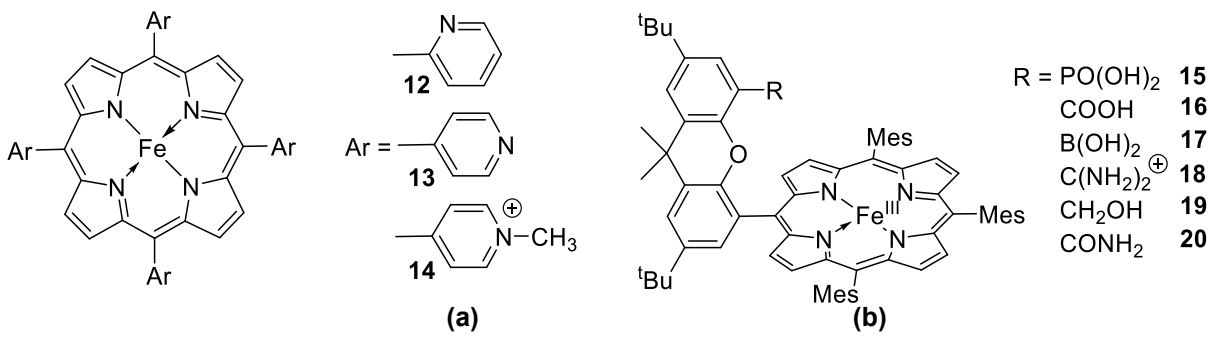

Scheme 2.8. Examples of Fe porphyrins used in homogeneous ORR catalysis.

The ORR activity of Mn macrocyclic complexes in homogeneous systems is still relatively underdeveloped compared to Fe and Co analogues though it is clear that their behaviour resembles the one of Fe analogues. The [Mn^{III}TPP]Cl ORR activity was studied by Passard et al. in acetonitrile solution with the detailed analysis of the relationship between ORR selectivity and pK_a of the acids involved in the catalysis. Much like with Fe complexes, it was shown that the Mn^{II} oxidation state is catalytically active. Also, the presence of acid in the reaction medium promoted a $4e^-$ reduction pathway with strong correlation between pK_a and ETN. In this study H_2O formation reached 98 % (ETN ≈ 4) in the presence of trifluoroacetic acid (TFA).[79] Interestingly, the porphyrin core is essential for $4e^-$ reduction as in a kinetic study of noncatalytic O_2 reduction Mn^{III} *tris*-pentafluorophenyl corrole in acetonitrile was shown to promote preferential formation of H_2O_2 via the Mn^{III}/Mn^{VI} redox cycle.[120]

Co porphyrins are also excellent catalysts for ORR, however, in strong contrast to Mn and Fe analogues, tend to catalyse ORR via the $2e^-$ reduction pathway in homogeneous systems. CoTPP-catalysed ORR in 1,2-dichloroethane was reported to proceed via the $2e^-$ pathway leading to the formation of H_2O_2 through the $HO_2\cdot$ radical. Remarkably, the kinetic constant drops considerably in the presence of water which acts as a ligand competing for coordination with the Co centre.[121] Also, Co^{II}TPP and its "picket fence" analogues were shown to be active ORR catalysts at the potential of Co^{III}/Co^{II} redox transformation and acidification of the solvent appears to increase the contribution of $4e^-$ reduction.[122]

Noteworthy, not only proton donors can decrease the activation barrier of O-O bond activation. As such, H_2O_2 activation by dimeric Mn complexes was studied and the rate of O-O bond splitting was found to be dependent on the Mn···Mn distance with TOF reaching a maximum around 4 Å.[123] This example illustrates the ability of a second metal atom to bind to the distal oxygen atom and thus to speed up the O-O cleavage as well. Cofacial macrocyclic Co complexes show the same pattern where both metal atoms bind to O_2 with the formation of μ-superoxo intermediates (Scheme 2.9). As such, the ORR activity of a series of dimeric Co porphyrins **21**-**24** (Scheme 2.9) were studied in acidic benzonitrile and their performance was compared to that of Co octaethylporphyrin.[124] It was discovered that the complex **23** with optimum Co···Co separation of 4.58 Å is capable of driving $4e^-$ ORR to H_2O. In contrast, if a mononuclear complex or the binuclear catalysts **21**, **22** and **24** with non-optimum Co···Co separation are used, $2e^-$ transformation to H_2O_2 becomes predominant.

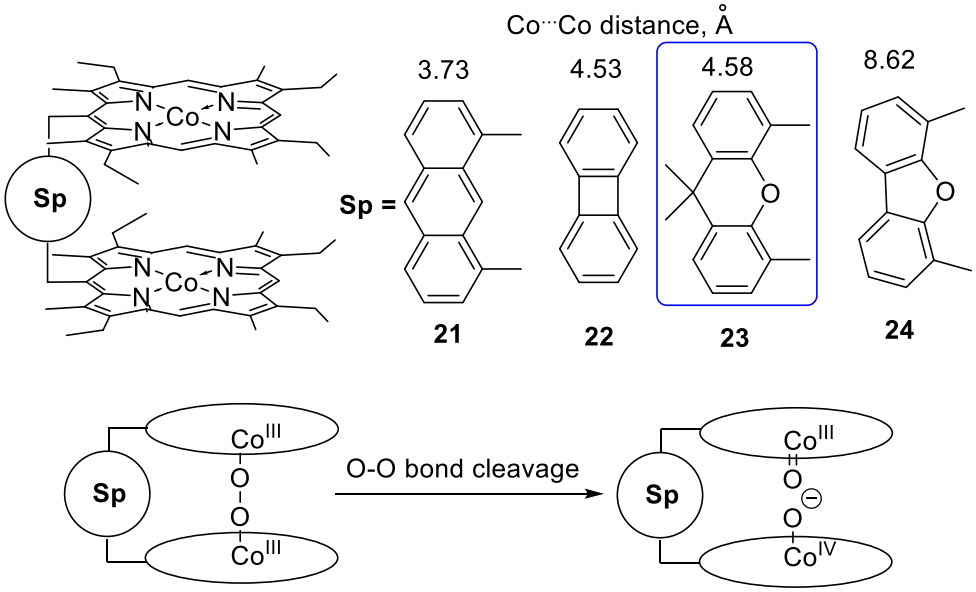

Scheme 2.9. Structures of Co cofacial binuclear porphyrin complexes.[124]

In turn, the OER catalysis by porphyrin complexes is relatively less studied compared to ORR due to the higher probability of their oxidative decomposition. Nevertheless, a water-soluble Mn tetrakis-(4-*N*-methylpyridil)-porphyrin **25** (Scheme 2.10) was shown to catalyse the OER at pH 7 and 10.[125] Catalysis of OER in neutral aqueous electrolyte was also achieved by a series of Co porphyrins **26-28** which were found to promote the reaction with the current onset at 1.41 V vs NHE (Scheme 2.10). The following study confirmed that the rate-determining step has chemical, rather than electrochemical nature and most probably corresponds to slow formation of the O-O bond.[126] Among the structures studied in this work, the diazole-substituted complex was found the most effective with the reaction rate constant of $1.4 \cdot 10^3$ s^{-1}. The role of buffer ions was assessed as well, and it was discovered that they can play two roles: as proton acceptors facilitating the reaction rate at low concentrations and as catalyst poisons in more concentrated solutions.

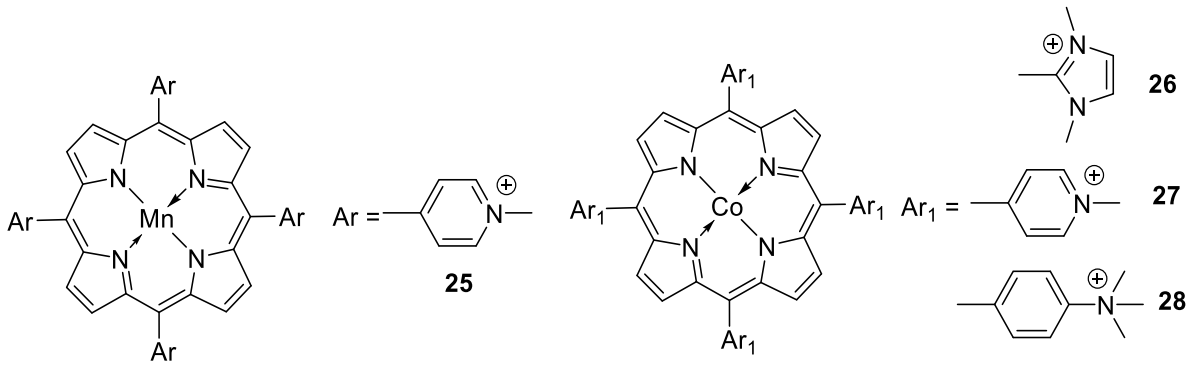

Scheme 2.10. Structures of water-soluble porphyrin-based OER catalysts.[125-126]

These observations show that the tuning of the complex structure can potentially be extremely beneficial for the reaction rate and selectivity due to favourable binding to the reaction intermediates. However, in case of homogeneous catalysis this can only be achieved by means of a tedious multistep synthesis. Also, inherent problems of homogeneous catalysts led to extensive research of heterogeneous molecular catalysts and potential benefits which this transition to the surface-based catalysis might offer.

2.6.2 Heterogeneous catalysts

The ORR and OER activity of porphyrin complexes was successfully extended to heterogenous systems as well. Moreover, even in homogeneous systems one cannot exclude participation of heterogeneous catalysis. This was shown in a brilliant report by Costentin et al. who found that even for a water-soluble Fe porphyrin in what appears to be a homogeneous system a microscopic amount of complex adsorbed on the surface of carbon electrode accounts for ~ 40 % of catalytic current as TOF on the surface is 780 s^{-1} which is 26 times higher than in the bulk solution (30 s^{-1}).[127]

As in case of the CO_2ERR discussed above, the activity of the complexes established in homogeneous solutions could be transferred into the aqueous heterogeneous systems as shown by in the study of asymmetric porphyrins immobilised on the surface of carbon electrodes. In this case unsymmetrical Fe porphyrins **29-31** were immobilised on the basal- and edge-plane graphite electrodes (Scheme 2.11).[128] The study of ORR in 1 M H_2SO_4 catalysed by these complexes showed that in the presence of 2-pyridine moiety the current density was the highest due to high pK_a of the lateral substituent (protonated pyridine moiety).

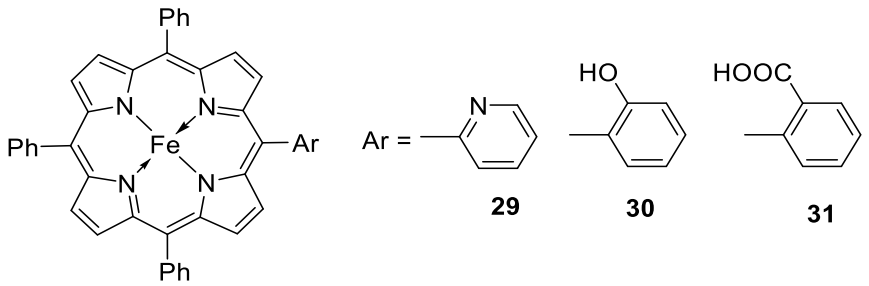

Scheme 2.11. Structures of unsymmetrical porphyrins used for the ORR catalysis in heterogeneous ORR.[128]

However, not only TOF values, but selectivity of molecular catalysts can be affected by the change of physical phase of the catalyst operation. One of the interesting examples is the study of the simplest Co porphin immobilised on the surface of a graphite electrode. In this work

authors reported unusual for Co complexes ORR selectivity for $4e^-$ reduction. This behaviour stems from the ability of the complex to form bridging structures Co-O-O-Co with metal atoms belonging to two different molecules due to the small size of the porphin core.[129] Similar behaviour was observed for Mn complexes covalently immobilised on the surface of carbon cloth electrodes. In this work it was shown that covalent immobilisation via a lateral phenyl substituent could be used to tune the average Mn-Mn distance and this change could trigger $4e^-$ ORR instead of predominant $2e^-$ pathway under low potentials.[76]

2.6.3 Concluding remarks

Porphyrins and related heterocycles such as corroles and phthalocyanines have been extensively studied as catalysts for ORR and, to the lesser extent, for OER. Examination of literature shows that the trends observed for CO_2ERR and other reactions described in the sections 2.3 and 2.4 are generally applicable to these processes as well. As such, Mn and Fe complexes show characteristic for inner-sphere electron transfer dependence of the reaction rate and selectivity on the presence of proton donors and poisoning experiments prove that the ORR takes place on the metal centre rather than on the ligand. It is noteworthy that the arrangement of ligands and proton donors around the metal centre are crucial for the catalytic activity of molecular complexes which brilliantly illustrates the principle of avoidance of high-energy intermediates. Moreover, another catalytically active centre located in close proximity could serve the same function as proton donor thus significantly improving the contribution of $4e^-$ mechanism.[130] Thus, for ORR the development of a method that would allow to tune the average M-M distance conveniently is of paramount importance. This method can allow to avoid tedious synthesis of porphyrins with intramolecular proton relays generally making a catalyst more cost-effective.

2.7 Immobilisation of molecular catalysts

As most molecular catalysts are not soluble in water they must be immobilised on an electrode in order to transfer their activity into the aqueous electrolyte. It should be noted that under no circumstances the electrocatalyst assembly can be considered as just a simple sum of a molecular catalyst and the conductive scaffold bearing it on the surface. The factors such as rate of interfacial charge transfer, stability of the bond, aggregation and diffusion of the reactant to the catalytically active sites must be considered. In general, the structure the electrocatalyst generally includes three parts: (i) a supporting electrode, (ii) an anchoring group connecting

the electrode and the catalyst molecule and (iii) a catalytically active centre itself. Heterogenisation of organometallics on the surface of conductive electrodes could be achieved by means of covalent and noncovalent immobilisation methods distinguished by the presence or absence of covalent bond with the surface.[10, 32]

Supports used for heterogenisation must be highly conductive to assure fast transfer of electrons between the organometallic catalyst and the external power supply of the electrolyser or the leads of the fuel cell and it must be non-reactive to survive the conditions of the electrocatalytic reaction. Also, if several reactions are thermodynamically possible, as in case of CO_2ERR or ORR in water, the supporting electrode must not promote the competing unwanted process. These requirements are satisfied by a range of materials such as carbon, metals and some of the metal oxides. Among them carbon in the form of fabric, paper, glassy carbon, pyrolytic graphite or carbon nanotubes are characterised by high overpotential for hydrogen discharge, excellent stability and competitive price. These properties make these forms of carbon a material of choice for supporting electrodes and thus further discussion will mostly focus on carbon-based hybrid structures.

Metals offer even better conductivity compared to carbon; however, they might also be reactive towards reactants and generally have lower hydrogen evolution overpotential except mercury. Oxides in the form of FTO glass are extremely useful for spectroscopic studies notwithstanding higher intrinsic resistance compared to metals and carbon. Also, a significant body of works has been published on organometallic complexes supported on semiconductors. However, they normally do not feature electronic conductivity in the dark due to lack of electrons in the conduction band and are mainly employed in photo- and photoelectrochemical processes as light harvesters. For this reason, semiconductor-based designs will not be considered in this thesis.

2.7.1 Noncovalent immobilisation

Noncovalent immobilisation is quite a popular choice as the procedure is usually quite straightforward. Also, the amount of the catalyst immobilised on the surface could be varied arbitrarily. However, noncovalently immobilised catalysts suffer from the aggregation issues, possible leaching and slow cross-interface charge transfer. Additionally, if the layer of a catalyst is too thick, the diffusion rate of a reactant to the catalytically active centre could be limited.

In general, noncovalent connection between the electrode surface and the catalyst is achieved solely by physisorption. Quite often no special measures are taken to assist the adsorption and the catalyst is simply drop-cast on the surface of electrode. In this case the stable electrode assembly is assured by extremely low solubility of the organometallic catalyst in the aqueous medium. As such, the CO_2ERR in aqueous medium was performed on Cu octahydroxyporphyrin with the formation of CO, CH_4 and C_2H_4.[131] To increase the electrochemically active surface of electrode, CNTs or carbon black are often mixed with the catalyst. As such, Fe porphyrin and Co phthalocyanine derivatives were immobilised on the surface of carbon powder and CNTs respectively both showing excellent activity in CO_2ERR.[5, 44] A comparative study was performed for Co porphyrin mixed with carbon black and CNTs and the latter material exhibited a superior CO_2ERR rate due to higher surface area of CNTs.[8]

Also, immobilisation of organometallics is readily achieved by embedding of the complexes into a layer of polymers that could simultaneously serve as a "glue" holding together a catalytically active layer and promote an electrochemical reaction. In this regard a prominent work has been performed by the group of McCrory who proved that the polypyridine surrounding Co phthalocyanine promotes proton transfer to CO_2ERR taking place on the Co centre.[132-133] Another polymer often used for heterogenisation of CO_2ERR and especially for ORR electrocatalysts is Nafion which is essentially a perfluorinated polyethylene backbone with a large number of acidic $-SO_3H$ groups. In this case, a Mn bipyridine complex encapsulated in the layer of Nafion showed good TON in CO_2 reduction to CO.[134] Furthermore, the absolute majority of heterogeneous ORR-active molecular electrocatalysts are also embedded into the layer of Nafion.[135-136]

It should be noted that the simple drop-casting offers little control over the diffusion of the reactants and aggregation. It is well known that the reaction rate exhibits characteristic volcano-shaped dependence on the loading where above a certain limit the reaction proceeds slower because of the increasing blocking effect of the organometallic layer.[8, 114] Thus, these problems received considerable attention and several approaches have been investigated. As such, Choi et al. employed long aliphatic chains attached to Co phtalocyanine that make the structure of the catalytically active layer more porous and thus more accessible to the small molecules of CO_2 during CO_2ERR.[137] Another method is based on the creation of a rigid mesoporous structure **32** with nano channels through which the reactants could easily diffuse to the catalytically active sites (Scheme 2.12a). COFs comprising Co and Fe porphyrins were

successfully utilised both in CO_2ERR and ORR.[45] As the linkers could bear donating or electronegative substituents, the activity of the COF-based catalyst could be additionally tuned to achieve better activity and selectivity which was explored on the example of CO_2ERR.[138-139] Various MOFs with organometallics incorporated into the structure were investigated for CO_2ERR and ORR as well.[93, 140-142] It must be noted here that COF- and MOF-based materials are classified in this discussion as noncovalently immobilised since there is no direct connection between the electrode and catalytically active material which is usually present in the form of powder or thin layer deposited on the surface of electrode.

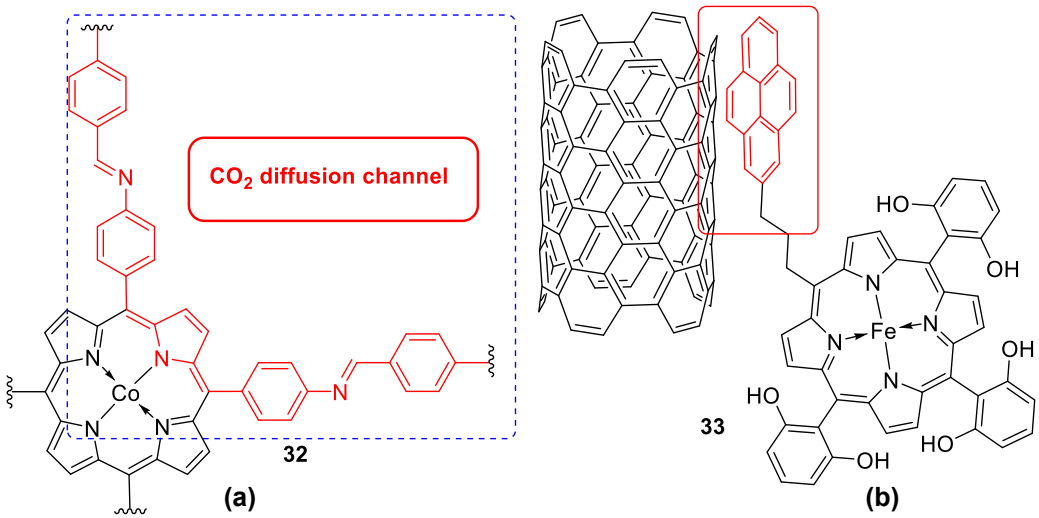

Scheme 2.12. (a) Co porphyrin -based COF structure[45] and (b) π-π interaction between CNTs and pyrene-appended Fe porphyrin.[46]

The problem of charge transfer and catalyst leaching could be solved using side groups that strongly interact with the surface of the supporting electrode. One of most effective approaches to noncovalent immobilisation is based upon creating strong π-π and hydrophobic interactions between organometallic catalysts and the surface of carbonaceous supports. This could be readily achieved by introducing conjugated substituents with an extended aromatic system. Among numerous possible groups the pyrene unit was found to be the most suitable for heterogenisation.[32] This approach was successfully utilised to transfer excellent CO_2ERR activity of Fe hydroxyporphyrin **33** (Scheme 2.12b) to the aqueous medium.[46] Pyrene-appended Co corrole immobilised on MWCNTs was employed for the catalysis of OER and ORR.[67] In ORR the current onset overpotential was only 330 mV in neutral electrolyte while in OER it showed exclusive $4e^-$ reduction at 0.75 V vs NHE in 0.5 M H_2SO_4. This approach was also employed for heterogenisation of non-macrocyclic complexes and as an example Co salophen OER catalyst was adsorbed on MWCNTs showing O_2 evolution with 330 mV overpotential as well.[49]

It should be noted that the elaboration of noncovalent heterogenisation techniques largely negates the advantage of its simplicity as more and more sophisticated syntheses must be performed to prepare COFs, MOFs or the catalysts with appended anchoring groups.

2.7.2 Covalent immobilisation

Covalent immobilisation of molecular catalysts provides excellent protection against leaching due to an extremely strong link with the electrode surface and at the same time assures fast electron transfer as the length of the chemical link is usually quite short. Compared to noncovalent technique this approach could be synthetically more challenging as pre-treatment of a support or preparation of the complexes bearing an anchoring group must be performed beforehand. Additionally, special attention must be paid to the compatibility of the resulting covalent link with the conditions of catalytic reaction. Hence, the choice of methods for grafting of organics to the conductive surfaces is quite limited due to the unreactive nature of carbon and quick hydrolysis of organometallic structures in case of metals and metal oxides.

Creation of a covalent bond with the carbon surface could be accomplished using several methods. One of the most widespread techniques relies on electroreduction of diazonium salts. It is believed that upon single-electron reduction the molecule loses N_2 with the formation of a transient radical that further attacks the sp^2 atom on the carbon plane in a mechanism resembling the Meerwein reaction.[143] This is an extremely useful technique that was employed for the grafting of aromatic groups to the surface of CNTs, carbon paper and graphite.[144-145] Importantly, this reaction furnishes C-C bond between the organic moiety and the carbon support which is one of the most stable anchors available. The method was developed initially on the example of various phenyl-substituted derivatives and later was extended to more complex molecules such as porphyrins and peptides.[143, 146] Interestingly, electroreduction of diazonium salts can be easily monitored using cyclic voltammetry as the curves show a very characteristic pattern where the current during the first cycle is considerably higher compared to that observed over the second and the following voltage sweeps due to formation of an insulating organic layer blocking the electrode.[146-147] 1,3-dipolar cycloaddition of azomethine ylides to C=C bonds within the carbon backbone is another approach that could be used to achieve immobilisation on carbon and at the same time introduce two new groups on the surface simultaneously.[32] However, this method requires preparation of specific secondary amines bearing an electron withdrawing group and thus is less popular compared to the diazonium chemistry.

In turn, covalent immobilisation on metal oxide surfaces requires different approaches as the stability of the M-O-R bonds in the presence of water becomes a major concern. It is well-known that the alkoxides readily hydrolyse in aqueous solutions and thus the methods suitable for grafting on carbon are not applicable to MO_x surfaces. Instead, carboxylate, phosphonate and siloxane bridges between the organic part and the support are to be used to preserve the structural integrity of the materials. Most of the methods rely on the presence of -OH moieties on the oxide surface which can bind to the anchoring group on the catalyst. As such, carbonates are believed to form an ester-like connection with the -OH group. Even stronger connection could be achieved using phosphonates as in this case three instead of one site could be involved in the formation of the chemical bonds. Also, chlorosilanes and siloxanes are extensively used for this purpose as the M-O-Si-R bridge is stable across a wide pH range.[7, 32]

Anchoring points within the structure of organometallic catalysts available for covalent ligation to the surface of electrode can be divided into two major groups: the central metal atoms and the lateral substituents. Clearly, the presence of a coordinating group on the electrode is required to connect a molecular catalyst via the metal centre. One of the earliest examples showcasing this strategy was reported as early as in 1991 where Co tetraphenylporphyrin was attached via 4-aminopyridine connected to glassy carbon via carboxy group (Scheme 2.13a). The resulting electrode showed excellent CO_2ERR activity with TON as high as 10^5.[148] A similar approach was used to immobilise Co phthalocyanine, but instead of a carboxy group, the pyridine moiety was immobilised via reduction of the corresponding diazonium salt (Scheme 2.13b). The catalyst was also used for CO_2ERR with TOF of 34.5 s^{-1} under the potential of -0.63 V vs RHE and outstanding total TON of $1.4 \cdot 10^6$.[113] A comparative study of pyridine- and imidazole-based bridges showed that the CO_2 reduction efficiency of the resulting material is similar regardless of the anchoring group, however in all cases both the FE(CO) and the current density were higher compared to simple drop-casting (Figure 2.13c).[149] A similar strategy was employed to immobilise Fe porphyrin on CNTs via a long imidazole bridge (Scheme 2.13d). The resulting material shows activity in ORR comparable to that of commercial Pt-based catalysts.[63] Furthermore, this immobilisation strategy is not restricted to heterocycles bearing pyridinic nitrogen as showcased by the example of a more simple approach not involving pre-grafting of anchoring groups where a covalent immobilisation of Co protoporphyrin IX on the surface of hydroxylated CNTs was achieved

(Scheme 2.13e). The resulting hybrid material was employed in CO_2ERR and exhibited TOF reaching 2.1 s^{-1} at -0.65 V vs RHE.[114]

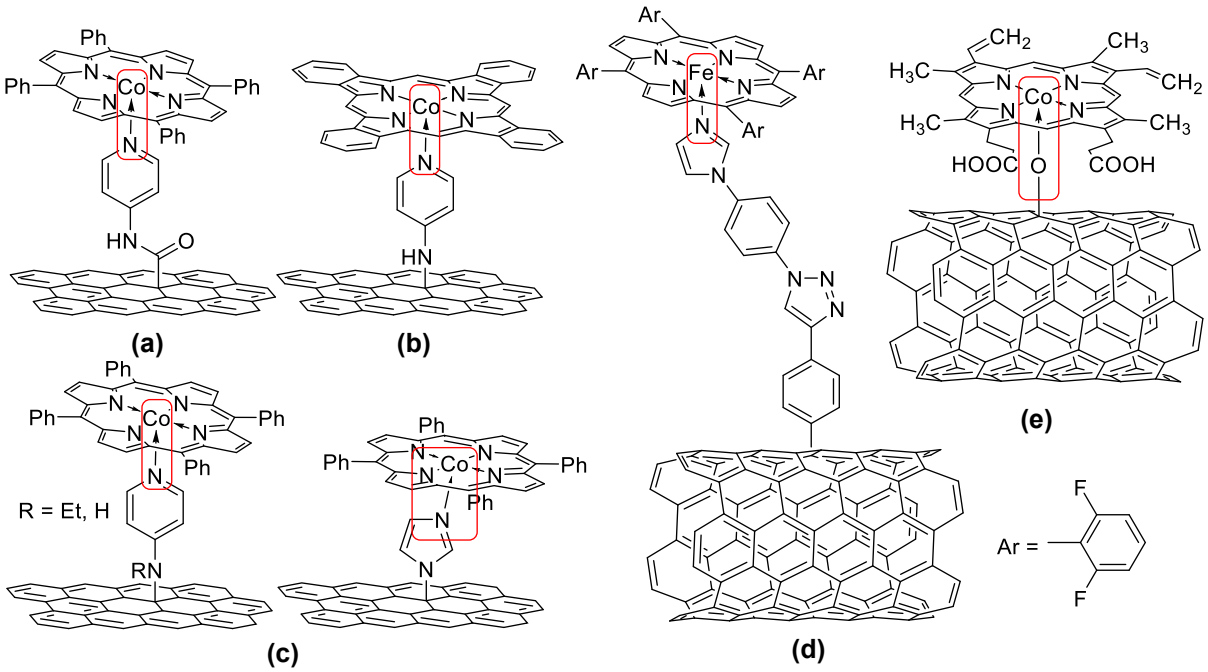

Scheme 2.13. Covalent immobilisation of macrocyclic electrocatalysts on the surface of carbon via metal centre: (a) – (c) – via pyridine anchoring group;[113, 148-149] (c) and (d) – via imidazole linker;[63, 149] and (e) binding to the hydroxylated CNTs.[114]

Covalent ligation of the complexes via a lateral moiety is another heterogenisation strategy which was successfully employed for the preparation of effective electrocatalysts. As such, it was used to immobilise Fe hydroxyporphyrin on the surface of carbon nanotubes (Scheme 2.14a).[10] Interestingly, the TOF achieved for this complex in CO_2ERR was very close to the one obtained for structurally similar complex in noncovalent immobilisation mode with pyrene anchoring moiety.[10, 46] Grafting of the porphyrin core via reduction of the corresponding diazonium salt was employed in another work (Scheme 2.14b) and the TOF in CO_2ERR achieved for covalently heterogenised complex was 8.3 s^{-1} under the potential of -1.05 V vs NHE and exceeded that of the noncovalent analogue by the factor of 1.9.[43] Apparently, the activity was bolstered by the rate of the charge transfer from the electrode onto the catalytically active centre. Further, the Co alkenyl porphyrin core was immobilised on the surface of conductive diamond via a long triazole-terminated alkyl chain (Scheme 2.14c). The activity and stability of this material in CO_2ERR were studied using CV, and the CO_2 reduction current was maintained over 10^3 scans, thus proving evidence of good catalyst durability.[150] Further, versatile grafting of the terpyridine Co complex on glassy carbon was reported, however the TON in CO_2ERR was only 70 (Scheme 2.14d).[151] The Mn porphyrin was

grafted on the surface of carbon cloth and the variation of the catalyst electrodeposition time was found to be a viable tool to control the ORR selectivity (Scheme 2.14e).[76]

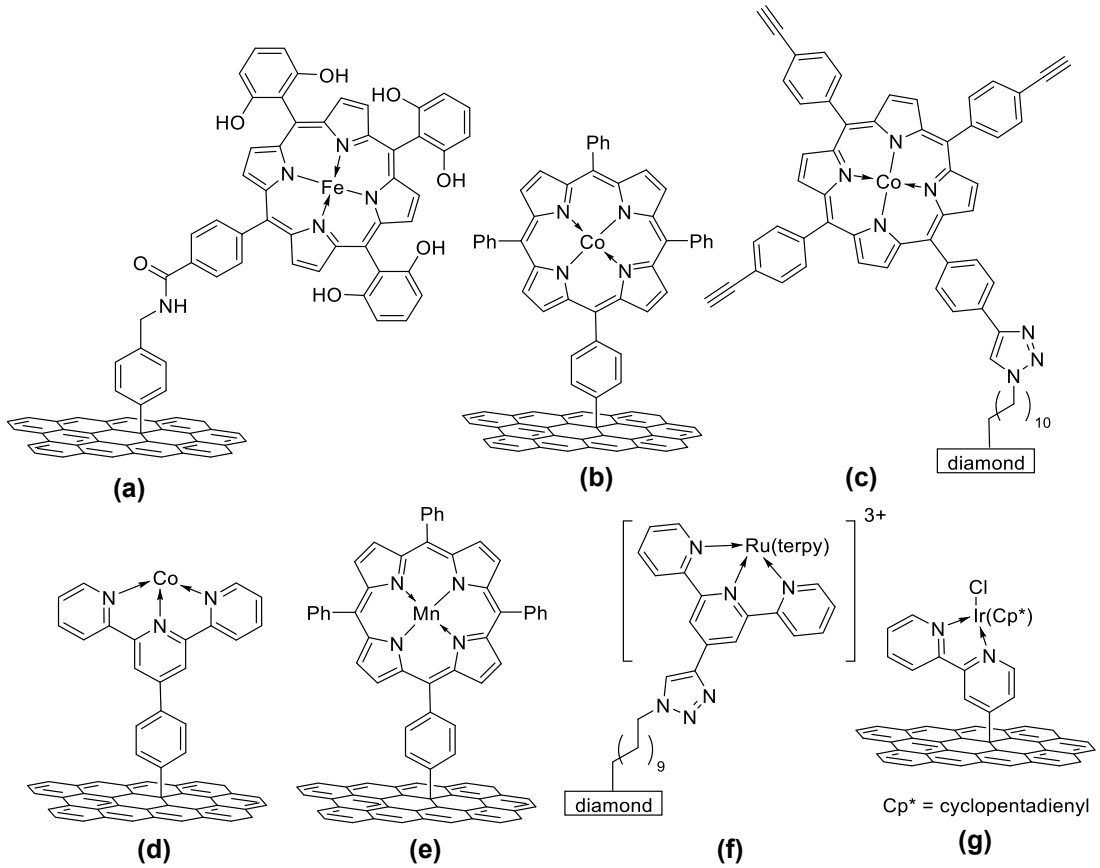

Scheme 2.14. Covalent ligation of molecular catalysts on the surface of carbon via a lateral substituent.[10, 43, 75-76, 150-152]

Grafting via a lateral substituent was employed for electrocatalysts operating under highly oxidative potentials as well. An interesting example showcasing stability that could be impaired by the ligation via a C-C bond was reported for $Re(terpy)_2^{3+}$ complex tethered to the conductive diamond (Scheme 2.14f). In this case the total number of redox cycles at the potential of up to 1.5 V vs NHE was as high as 10^6 without any noticeable changes in CV.[152] Similarly, the Ir(bipy) complex was grafted onto the carbon electrodes and efficient OER at 1.6 V vs NHE was achieved with TOF of 3.31 s^{-1} (Scheme 2.14g).[75]

Both strategies may be successfully used depending on the application of a material and the design of a catalyst. However, connection via a metal atom might be less preferable as one of the available reactant approach pathways is blocked by the ligand. Also, as the energy of the metal-ligand coordination is lower compared to that of the C-C bond, grafting through a lateral substituent might be able to preserve better the structural integrity of the material during continuous operation.

2.8 Summary

Molecular catalysts provide numerous advantages over purely inorganic materials in terms of activity and selectivity, and a significant progress has been made towards their development. Most of the research effort spanning the last four decades has been focused on homogeneous solutions with the aim of a comprehensive understanding of the reaction mechanisms. This approach is entirely justified as a wide variety of techniques is readily available for these studies including CV, NMR, FTIR, Raman spectroscopy, EPR and their combinations.

At the same time, heterogeneous catalysts provide significant advantages in terms of material reuse and employment of water as a reaction medium. Although one could assume that the heterogenisation of predeveloped electrocatalysts is just as simple as making sure the organometallics are not soluble in water, analysis of the literature shows that the transfer of their activity into the aqueous medium is not straightforward. Indeed, care must be taken as the choice of the supporting electrode, the complex itself and the anchoring strategy play a vital role in the overall performance of the electrochemical device. Possible issues include the rate of charge transfer, catalyst aggregation, reactant diffusion limitations and the stability of the hybrid electrode materials.

Among numerous classes of organometallic structures porphyrins immobilised on carbon supports are among the most active and selective catalysts for CO_2ERR. Their activity in ORR and OER has been shown to be comparable to some of the best commercial noble metal based electrocatalysts. Regarding the metals incorporated into the macrocyclic core, Co derivatives are excellent candidates for the catalysis of CO_2ERR and ORR. At the same time, the diversity of high oxidation states of Mn porphyrins and their propensity to participate in multicentred catalysis make them promising candidates for the catalysis of ORR and OER. Recent reports show that a wise choice of the immobilisation technique (either covalent or noncovalent) could pave the way to more active, selective, stable and affordable heterogeneous molecular catalysts which has essentially motivated the research described in this thesis.

2.8 References

[1] Bagotsky, V. S. In *Fundamentals of Electrochemistry*, **2005**; pp 33-50
[2] Barbir, F. In *PEM Fuel Cells (Second Edition)*, Barbir, F., Ed. Academic Press: Boston, **2013**; pp 17-32
[3] Franck, E. U., J. D. Cox, D. D. Wagman, V. A. Medvedev: CODATA — Key Values for Thermodynamics, aus der Reihe: CODATA, Series on Thermodynamic Properties. Hemisphere Publishing Corporation, New York, Washington, Philadelphia, London 1989. 271, *Berichte der Bunsengesellschaft für physikalische Chemie* **1990,** 94 (1), 93-93
[4] Nernst, W., Die elektromotorische Wirksamkeit der Jonen, *Z. Phys. Chem.* **1889,** 4U (1), 129
[5] Tatin, A.; Comminges, C.; Kokoh, B.; Costentin, C.; Robert, M.; Savéant, J.-M., Efficient electrolyzer for CO2 splitting in neutral water using earth-abundant materials, *Proc. Nat. Acad. Sci.* **2016**,
[6] Gewirth, A. A.; Varnell, J. A.; DiAscro, A. M., Nonprecious Metal Catalysts for Oxygen Reduction in Heterogeneous Aqueous Systems, *Chem. Rev.* **2018,** 118 (5), 2313-2339
[7] Corbin, N.; Zeng, J.; Williams, K.; Manthiram, K., Heterogeneous molecular catalysts for electrocatalytic CO2 reduction, *Nano Res.* **2019**,
[8] Hu, X.-M.; Rønne, M. H.; Pedersen, S. U.; Skrydstrup, T.; Daasbjerg, K., Enhanced Catalytic Activity of Cobalt Porphyrin in CO2 Electroreduction upon Immobilization on Carbon Materials, *Angew. Chem.* **2017,** 129 (23), 6568-6572
[9] Wu, J.; Yadav, R. M.; Liu, M.; Sharma, P. P.; Tiwary, C. S.; Ma, L.; Zou, X.; Zhou, X.-D.; Yakobson, B. I.; Lou, J.; Ajayan, P. M., Achieving Highly Efficient, Selective, and Stable CO2 Reduction on Nitrogen-Doped Carbon Nanotubes, *ACS Nano* **2015,** 9 (5), 5364-5371
[10] Maurin, A.; Robert, M., Catalytic CO2-to-CO conversion in water by covalently functionalized carbon nanotubes with a molecular iron catalyst, *Chem. Comm.* **2016,** 52 (81), 12084-12087
[11] Liu, Y.; Cheng, H.; Lyu, M.; Fan, S.; Liu, Q.; Zhang, W.; Zhi, Y.; Wang, C.; Xiao, C.; Wei, S.; Ye, B.; Xie, Y., Low Overpotential in Vacancy-Rich Ultrathin CoSe2 Nanosheets for Water Oxidation, *J. Am. Chem. Soc.* **2014,** 136 (44), 15670-15675
[12] Garrido-Barros, P.; Funes-Ardoiz, I.; Drouet, S.; Benet-Buchholz, J.; Maseras, F.; Llobet, A., Redox Non-innocent Ligand Controls Water Oxidation Overpotential in a New Family of Mononuclear Cu-Based Efficient Catalysts, *J. Am. Chem. Soc.* **2015,** 137 (21), 6758-6761
[13] Zitolo, A.; Goellner, V.; Armel, V.; Sougrati, M.-T.; Mineva, T.; Stievano, L.; Fonda, E.; Jaouen, F., Identification of catalytic sites for oxygen reduction in iron- and nitrogen-doped graphene materials, *Nature Mater.* **2015,** 14 (9), 937-942
[14] Rau, M. S.; Gennero de Chialvo, M. R.; Chialvo, A. C., Kinetic study of the hydrogen oxidation reaction on Pt over the complete overpotential range, *J. Power Sources* **2013,** 229, 210-215
[15] Weekes, D. M.; Salvatore, D. A.; Reyes, A.; Huang, A.; Berlinguette, C. P., Electrolytic CO2 Reduction in a Flow Cell, *Acc. Chem. Res.* **2018,** 51 (4), 910-918
[16] Oloman, C.; Li, H., Electrochemical Processing of Carbon Dioxide, *ChemSusChem* **2008,** 1 (5), 385-391
[17] Koper, M. T. M., Thermodynamic theory of multi-electron transfer reactions: Implications for electrocatalysis, *J. Electroanal. Chem.* **2011,** 660 (2), 254-260
[18] Seh, Z. W.; Kibsgaard, J.; Dickens, C. F.; Chorkendorff, I.; Nørskov, J. K.; Jaramillo, T. F., Combining theory and experiment in electrocatalysis: Insights into materials design, *Science* **2017,** 355 (6321), 4998
[19] Marcus, R. A., Theoretical relations among rate constants, barriers, and Broensted slopes of chemical reactions, *J. Phys. Chem.* **1968,** 72 (3), 891-899
[20] Marcus, R. A., On the Theory of Oxidation-Reduction Reactions Involving Electron Transfer. I, *J. Chem. Phys.* **1956,** 24 (5), 966-978
[21] Georgievskii, Y.; Hsu, C.-P.; Marcus, R. A., Linear response in theory of electron transfer reactions as an alternative to the molecular harmonic oscillator model, *J. Chem. Phys.* **1999,** 110 (11), 5307-5317
[22] Koper, M. T. M., Theory of multiple proton–electron transfer reactions and its implications for electrocatalysis, *Chem. Sci.* **2013,** 4 (7), 2710-2723
[23] Kulkarni, A.; Siahrostami, S.; Patel, A.; Nørskov, J. K., Understanding Catalytic Activity Trends in the Oxygen Reduction Reaction, *Chem. Rev.* **2018,** 118 (5), 2302-2312
[24] Xu, S.; Carter, E. A., Theoretical Insights into Heterogeneous (Photo)electrochemical CO2 Reduction, *Chem. Rev.* **2018**,
[25] Savéant, J.-M., Molecular Catalysis of Electrochemical Reactions. Mechanistic Aspects, *Chem. Rev.* **2008,** 108, 2348–2378
[26] Costentin, C.; Robert, M.; Saveant, J.-M., Catalysis of the electrochemical reduction of carbon dioxide, *Chem. Soc. Rev.* **2013,** 42 (6), 2423-2436
[27] Nørskov, J. K.; Rossmeisl, J.; Logadottir, A.; Lindqvist, L.; Kitchin, J. R.; Bligaard, T.; Jónsson, H., Origin of the Overpotential for Oxygen Reduction at a Fuel-Cell Cathode, *J. Phys. Chem. B* **2004,** 108 (46), 17886-17892

[28] Shi, C.; Hansen, H. A.; Lausche, A. C.; Nørskov, J. K., Trends in electrochemical CO2 reduction activity for open and close-packed metal surfaces, *Phys. Chem. Chem. Phys.* **2014,** 16 (10), 4720-4727
[29] Calle-Vallejo, F.; Martínez, J. I.; García-Lastra, J. M.; Rossmeisl, J.; Koper, M. T. M., Physical and Chemical Nature of the Scaling Relations between Adsorption Energies of Atoms on Metal Surfaces, *Phys. Rev. Lett.* **2012,** 108 (11), 116103
[30] Nørskov, J. K.; Abild-Pedersen, F.; Studt, F.; Bligaard, T., Density functional theory in surface chemistry and catalysis, *Proc. Nat. Acad. Sci.* **2011,** 108 (3), 937
[31] Nørskov, J. K.; Bligaard, T.; Rossmeisl, J.; Christensen, C. H., Towards the computational design of solid catalysts, *Nat. Chem.* **2009,** 1, 37
[32] Dalle, K. E.; Warnan, J.; Leung, J. J.; Reuillard, B.; Karmel, I. S.; Reisner, E., Electro- and Solar-Driven Fuel Synthesis with First Row Transition Metal Complexes, *Chem. Rev.* **2019,** 119 (4), 2752-2875
[33] Zhang, W.; Lai, W.; Cao, R., Energy-Related Small Molecule Activation Reactions: Oxygen Reduction and Hydrogen and Oxygen Evolution Reactions Catalyzed by Porphyrin- and Corrole-Based Systems, *Chem. Rev.* **2017,** 117 (4), 3717-3797
[34] Benson, E. E.; Kubiak, C. P.; Sathrum, A. J.; Smieja, J. M., Electrocatalytic and homogeneous approaches to conversion of CO2 to liquid fuels, *Chem. Soc. Rev.* **2009,** 38 (1), 89-99
[35] Costentin, C.; Robert, M.; Saveant, J.-M., Catalysis of the electrochemical reduction of carbon dioxide, *Chemical Society Reviews* **2013,** 42 (6), 2423-2436
[36] Benson, E. E.; Kubiak, C. P.; Sathrum, A. J.; Smieja, J. M., Electrocatalytic and homogeneous approaches to conversion of CO2 to liquid fuels, *Chemical Society Reviews* **2009,** 38 (1), 89-99
[37] Zhao, J.; Wang, X.; Xu, Z.; Loo, J. S. C., Hybrid catalysts for photoelectrochemical reduction of carbon dioxide: a prospective review on semiconductor/metal complex co-catalyst systems, *J. Mater. Chem. A* **2014,** 2 (37), 15228-15233
[38] Peterson, A. A.; Nørskov, J. K., Activity Descriptors for CO2 Electroreduction to Methane on Transition-Metal Catalysts, *J. Phys. Chem. Lett.* **2012,** 3 (2), 251-258
[39] Kuhl, K. P.; Hatsukade, T.; Cave, E. R.; Abram, D. N.; Kibsgaard, J.; Jaramillo, T. F., Electrocatalytic Conversion of Carbon Dioxide to Methane and Methanol on Transition Metal Surfaces, *J. Am. Chem. Soc.* **2014,** 136 (40), 14107-14113
[40] Matsubu, J. C.; Yang, V. N.; Christopher, P., Isolated Metal Active Site Concentration and Stability Control Catalytic CO2 Reduction Selectivity, *J. Am. Chem. Soc.* **2015,** 137 (8), 3076-3084
[41] De Luna, P.; Quintero-Bermudez, R.; Dinh, C.-T.; Ross, M. B.; Bushuyev, O. S.; Todorović, P.; Regier, T.; Kelley, S. O.; Yang, P.; Sargent, E. H., Catalyst electro-redeposition controls morphology and oxidation state for selective carbon dioxide reduction, *Nature Catal.* **2018,** 1 (2), 103-110
[42] Jiang, K.; Sandberg, R. B.; Akey, A. J.; Liu, X.; Bell, D. C.; Nørskov, J. K.; Chan, K.; Wang, H., Metal ion cycling of Cu foil for selective C–C coupling in electrochemical CO2 reduction, *Nature Catal.* **2018,** 1 (2), 111-119
[43] Marianov, A. N.; Jiang, Y., Covalent ligation of Co molecular catalyst to carbon cloth for efficient electroreduction of CO2 in water, *Appl. Catal. B* **2019,** 244, 881-888
[44] Zhang, X.; Wu, Z.; Zhang, X.; Li, L.; Li, Y.; Xu, H.; Li, X.; Yu, X.; Zhang, Z.; Liang, Y.; Wang, H., Highly selective and active CO2 reduction electrocatalysts based on cobalt phthalocyanine/carbon nanotube hybrid structures, *Nature Comm.* **2017,** 8, 14675
[45] Lin, S.; Diercks, C. S.; Zhang, Y.-B.; Kornienko, N.; Nichols, E. M.; Zhao, Y.; Paris, A. R.; Kim, D.; Yang, P.; Yaghi, O. M.; Chang, C. J., Covalent organic frameworks comprising cobalt porphyrins for catalytic CO2 reduction in water, *Science* **2015,** 349 (6253), 1208-1213
[46] Maurin, A.; Robert, M., Noncovalent Immobilization of a Molecular Iron-Based Electrocatalyst on Carbon Electrodes for Selective, Efficient CO2-to-CO Conversion in Water, *J. Am. Chem. Soc.* **2016,** 138 (8), 2492-2495
[47] J. Schneider, H. J., J.T. Muckermanl, E. Fujita, Thermodynamics and kinetics of CO2, CO, and H+ binding to the metal centre of CO2 reduction catalysts, *Chem. Soc. Rev.* **2012,** 41, 2036–2051
[48] Lee, C. H.; Kanan, M. W., Controlling H+ vs CO2 Reduction Selectivity on Pb Electrodes, *ACS Catal.* **2015,** 5 (1), 465-469
[49] Baranova, E. A.; Miles, N.; Mercier, P. H. J.; Le Page, Y.; Patarachao, B., Formic acid electro-oxidation on carbon supported PdxPt1−x (0≥x≥1) nanoparticles synthesized via modified polyol method, *Electrochimica Acta* **2010,** 55 (27), 8182-8188
[50] Frydendal, R.; Paoli, E. A.; Knudsen, B. P.; Wickman, B.; Malacrida, P.; Stephens, I. E. L.; Chorkendorff, I., Benchmarking the Stability of Oxygen Evolution Reaction Catalysts: The Importance of Monitoring Mass Losses, *ChemElectroChem* **2014,** 1 (12), 2075-2081
[51] Fukuzumi, S.; Lee, Y.-M.; Nam, W., Mechanisms of Two-Electron versus Four-Electron Reduction of Dioxygen Catalyzed by Earth-Abundant Metal Complexes, *ChemCatChem* **2017,** 10 (1), 9-28
[52] Park, J.; Nabae, Y.; Hayakawa, T.; Kakimoto, M.-a., Highly Selective Two-Electron Oxygen Reduction Catalyzed by Mesoporous Nitrogen-Doped Carbon, *ACS Catal.* **2014,** 4 (10), 3749-3754

[53] Man, I. C.; Su, H.-Y.; Calle-Vallejo, F.; Hansen, H. A.; Martínez, J. I.; Inoglu, N. G.; Kitchin, J.; Jaramillo, T. F.; Nørskov, J. K.; Rossmeisl, J., Universality in Oxygen Evolution Electrocatalysis on Oxide Surfaces, *ChemCatChem* **2011,** 3 (7), 1159-1165
[54] Calle-Vallejo, F.; Inoglu, N. G.; Su, H.-Y.; Martínez, J. I.; Man, I. C.; Koper, M. T. M.; Kitchin, J. R.; Rossmeisl, J., Number of outer electrons as descriptor for adsorption processes on transition metals and their oxides, *Chem. Sci.* **2013,** 4 (3), 1245-1249
[55] Daniel, Q.; Ambre, R. B.; Zhang, B.; Philippe, B.; Chen, H.; Li, F.; Fan, K.; Ahmadi, S.; Rensmo, H.; Sun, L., Re-Investigation of Cobalt Porphyrin for Electrochemical Water Oxidation on FTO Surface: Formation of CoOx as Active Species, *ACS Catal.* **2017,** 7 (2), 1143-1149
[56] Ren, S.; Joulié, D.; Salvatore, D.; Torbensen, K.; Wang, M.; Robert, M.; Berlinguette, C. P., Molecular electrocatalysts can mediate fast, selective CO2 reduction in a flow cell, *Science* **2019,** 365 (6451), 367
[57] Wu, Y.; Jiang, Z.; Lu, X.; Liang, Y.; Wang, H., Domino electroreduction of CO2 to methanol on a molecular catalyst, *Nature* **2019,** 575 (7784), 639-642
[58] Liu, S.; Wang, X.-Z.; Tao, H.; Li, T.; Liu, Q.; Xu, Z.; Fu, X.-Z.; Luo, J.-L., Ultrathin 5-fold twinned sub-25nm silver nanowires enable highly selective electroreduction of CO2 to CO, *Nano Energy* **2018,** 45, 456-462
[59] Ma, S.; Liu, J.; Sasaki, K.; Lyth, S. M.; Kenis, P. J. A., Carbon Foam Decorated with Silver Nanoparticles for Electrochemical CO2 Conversion, *Energy Technol.* **2017,** 5 (6), 861-863
[60] Liang, C.; Kim, B.; Yang, S.; Yang, L.; Francisco Woellner, C.; Li, Z.; Vajtai, R.; Yang, W.; Wu, J.; Kenis, P. J. A.; Ajayan, Pulickel M., High efficiency electrochemical reduction of CO2 beyond the two-electron transfer pathway on grain boundary rich ultra-small SnO2 nanoparticles, *J. Mater. Chem. A* **2018,** 6 (22), 10313-10319
[61] Shao, M.; Peles, A.; Shoemaker, K., Electrocatalysis on Platinum Nanoparticles: Particle Size Effect on Oxygen Reduction Reaction Activity, *Nano Lett.* **2011,** 11 (9), 3714-3719
[62] Greeley, J.; Stephens, I. E. L.; Bondarenko, A. S.; Johansson, T. P.; Hansen, H. A.; Jaramillo, T. F.; Rossmeisl, J.; Chorkendorff, I.; Nørskov, J. K., Alloys of platinum and early transition metals as oxygen reduction electrocatalysts, *Nature Chem.* **2009,** 1 (7), 552-556
[63] Wei, P.-J.; Yu, G.-Q.; Naruta, Y.; Liu, J.-G., Covalent Grafting of Carbon Nanotubes with a Biomimetic Heme Model Compound To Enhance Oxygen Reduction Reactions, *Angew. Chem. Int. Ed.* **2014,** 53 (26), 6659-6663
[64] Wang, D.; Xin, H. L.; Hovden, R.; Wang, H.; Yu, Y.; Muller, D. A.; DiSalvo, F. J.; Abruña, H. D., Structurally ordered intermetallic platinum–cobalt core–shell nanoparticles with enhanced activity and stability as oxygen reduction electrocatalysts, *Nature Mater.* **2013,** 12 (1), 81-87
[65] Wang, X.; Choi, S.-I.; Roling, L. T.; Luo, M.; Ma, C.; Zhang, L.; Chi, M.; Liu, J.; Xie, Z.; Herron, J. A.; Mavrikakis, M.; Xia, Y., Palladium–platinum core-shell icosahedra with substantially enhanced activity and durability towards oxygen reduction, *Nature Comm.* **2015,** 6 (1), 7594
[66] Pan, F.; Zhao, Q.; Wang, J.; Zhang, J., High-Performance Fe–N-Doped Graphene Electrocatalysts with pH-Dependent Active Sites for the Oxygen Reduction Reaction, *ChemElectroChem* **2015,** 2 (12), 2032-2040
[67] Lei, H.; Liu, C.; Wang, Z.; Zhang, Z.; Zhang, M.; Chang, X.; Zhang, W.; Cao, R., Noncovalent Immobilization of a Pyrene-Modified Cobalt Corrole on Carbon Supports for Enhanced Electrocatalytic Oxygen Reduction and Oxygen Evolution in Aqueous Solutions, *ACS Catal.* **2016,** 6 (10), 6429-6437
[68] Wu, Z.-S.; Chen, L.; Liu, J.; Parvez, K.; Liang, H.; Shu, J.; Sachdev, H.; Graf, R.; Feng, X.; Müllen, K., High-Performance Electrocatalysts for Oxygen Reduction Derived from Cobalt Porphyrin-Based Conjugated Mesoporous Polymers, *Advanced Mater.* **2014,** 26 (9), 1450-1455
[69] Minguzzi, A.; Locatelli, C.; Lugaresi, O.; Achilli, E.; Cappelletti, G.; Scavini, M.; Coduri, M.; Masala, P.; Sacchi, B.; Vertova, A.; Ghigna, P.; Rondinini, S., Easy Accommodation of Different Oxidation States in Iridium Oxide Nanoparticles with Different Hydration Degree as Water Oxidation Electrocatalysts, *ACS Catal.* **2015,** 5 (9), 5104-5115
[70] Smith, R. D. L.; Sporinova, B.; Fagan, R. D.; Trudel, S.; Berlinguette, C. P., Facile Photochemical Preparation of Amorphous Iridium Oxide Films for Water Oxidation Catalysis, *Chem. Mater.* **2014,** 26 (4), 1654-1659
[71] Ge, R.; Li, L.; Su, J.; Lin, Y.; Tian, Z.; Chen, L., Ultrafine Defective RuO2 Electrocatayst Integrated on Carbon Cloth for Robust Water Oxidation in Acidic Media, *Adv. Energy Mater.* **2019,** 9 (35), 1901313
[72] Gorlin, Y.; Lassalle-Kaiser, B.; Benck, J. D.; Gul, S.; Webb, S. M.; Yachandra, V. K.; Yano, J.; Jaramillo, T. F., In Situ X-ray Absorption Spectroscopy Investigation of a Bifunctional Manganese Oxide Catalyst with High Activity for Electrochemical Water Oxidation and Oxygen Reduction, *J. Am. Chem. Soc.* **2013,** 135 (23), 8525-8534
[73] Fekete, M.; Hocking, R. K.; Chang, S. L. Y.; Italiano, C.; Patti, A. F.; Arena, F.; Spiccia, L., Highly active screen-printed electrocatalysts for water oxidation based on β-manganese oxide, *Energy Environ. Sci.* **2013,** 6 (7), 2222-2232
[74] Zhang, X.; Marianov, A. N.; Jiang, Y.; Cazorla, C.; Chu, D., Hierarchically Constructed Silver Nanowire@Nickel–Iron Layered Double Hydroxide Nanostructures for Electrocatalytic Water Splitting, *ACS Appl. Nano Mater.* **2020,** 3 (1), 887-895

[75] deKrafft, K. E.; Wang, C.; Xie, Z.; Su, X.; Hinds, B. J.; Lin, W., Electrochemical Water Oxidation with Carbon-Grafted Iridium Complexes, *ACS Appl. Mater. Interfaces* **2012,** 4 (2), 608-613
[76] Marianov, A.; Jiang, Y., Effect of manganese porphyrin covalent immobilization on electrocatalytic water oxidation and oxygen reduction reactions, *ACS Sustainable Chem. Eng.* **2019,** 7, 3838-3848
[77] Lash, T. D., Origin of aromatic character in porphyrinoid systems, *J. Porphyrins Phthalocyanines* **2011,** 15 (11n12), 1093-1115
[78] Jusélius, J.; Sundholm, D., The Aromatic Character of Magnesium Porphyrins, *J. Org. Chem.* **2000,** 65 (17), 5233-5237
[79] Passard, G.; Dogutan, D. K.; Qiu, M.; Costentin, C.; Nocera, D. G., Oxygen Reduction Reaction Promoted by Manganese Porphyrins, *ACS Catal.* **2018,** 8 (9), 8671-8679
[80] Guo, H.; Jiang, J.; Shi, Y.; Wang, Y.; Liu, J.; Dong, S., UV−Vis Spectrophotometric Titrations and Vibrational Spectroscopic Characterization of meso-(p-Hydroxyphenyl)porphyrins, *J. Phys. Chem. B* **2004,** 108 (28), 10185-10191
[81] Behar, D.; Dhanasekaran, T.; Neta, P.; Hosten, C. M.; Ejeh, D.; Hambright, P.; Fujita, E., Cobalt Porphyrin Catalyzed Reduction of CO2. Radiation Chemical, Photochemical, and Electrochemical Studies, *J. Phys. Chem. A* **1998,** 102 (17), 2870-2877
[82] Wayland, B. B.; Minkiewicz, J. V.; Abd-Elmageed, M. E., Spectroscopic studies for tetraphenylporphyrincobalt(II) complexes of carbon monoxide, nitrogen oxide, molecular oxygen, methylisonitrile, and trimethyl phosphite, and a bonding model for complexes of carbon monoxide, nitrogen oxide, and molecular oxygen with cobalt(II) and iron(II) porphrins, *J. Am. Chem. Soc.* **1974,** 96 (9), 2795-2801
[83] Costentin, C.; Savéant, J.-M.; Tard, C., Ligand "noninnocence" in coordination complexes vs. kinetic, mechanistic, and selectivity issues in electrochemical catalysis, *Proc. Nat. Acad. Sci.* **2018,** 115 (37), 9104
[84] Römelt, C.; Song, J.; Tarrago, M.; Rees, J. A.; van Gastel, M.; Weyhermüller, T.; DeBeer, S.; Bill, E.; Neese, F.; Ye, S., Electronic Structure of a Formal Iron(0) Porphyrin Complex Relevant to CO2 Reduction, *Inorg. Chem.* **2017,** 56 (8), 4745-4750
[85] Römelt, C.; Ye, S.; Bill, E.; Weyhermüller, T.; van Gastel, M.; Neese, F., Electronic Structure and Spin Multiplicity of Iron Tetraphenylporphyrins in Their Reduced States as Determined by a Combination of Resonance Raman Spectroscopy and Quantum Chemistry, *Inorg. Chem.* **2018,** 57 (4), 2141-2148
[86] Jensen, K. P., Electronic Structure of Cob(I)alamin: The Story of an Unusual Nucleophile, *J. Phys. Chem. B* **2005,** 109 (20), 10505-10512
[87] Bhugun, I.; Lexa, D.; Savéant, J.-M., Homogeneous Catalysis of Electrochemical Hydrogen Evolution by Iron(0) Porphyrins, *J. Am. Chem. Soc.* **1996,** 118 (16), 3982-3983
[88] Lexa, D.; Saveant, J. M.; Wang, D. L., Electroreductive alkylation of iron porphyrins. Iron(III), iron(II) and iron(I) alkyl complexes from the reaction of doubly reduced iron(II) porphyrins with alkyl halides, *Organometallics* **1986,** 5 (7), 1428-1434
[89] Lexa, D.; Saveant, J. M.; Su, K. B.; Wang, D. L., Chemical vs. redox catalysis of electrochemical reactions. Reduction of trans-1,2-dibromocyclohexane by electrogenerated aromatic anion radicals and low oxidation state metalloporphyrins, *J. Am. Chem. Soc.* **1987,** 109 (21), 6464-6470
[90] Lexa, D.; Saveant, J. M.; Schaefer, H. J.; Su Khac, B.; Vering, B.; Wang, D. L., Outer-sphere and inner-sphere processes in reductive elimination. Direct and indirect electrochemical reduction of vicinal dibromoalkanes, *J. Am. Chem. Soc.* **1990,** 112 (17), 6162-6177
[91] Yao, C. L.; Li, J. C.; Gao, W.; Jiang, Q., Cobalt-porphine catalyzed CO2 electro-reduction: a novel protonation mechanism, *Phys. Chem. Chem. Phys.* **2017,** 19 (23), 15067-15072
[92] Bhugun, I.; Lexa, D.; Savéant, J.-M., Catalysis of the Electrochemical Reduction of Carbon Dioxide by Iron(0) Porphyrins: Synergystic Effect of Weak Br nsted Acids, *J. Am. Chem. Soc.* **1996,** 118 (7), 1769-1776
[93] Jahan, M.; Bao, Q.; Loh, K. P., Electrocatalytically Active Graphene–Porphyrin MOF Composite for Oxygen Reduction Reaction, *J. Am. Chem. Soc.* **2012,** 134 (15), 6707-6713
[94] Adler, A. D.; Longo, F. R.; Finarelli, J. D.; Goldmacher, J.; Assour, J.; Korsakoff, L., A simplified synthesis for meso-tetraphenylporphine, *J. Org. Chem.* **1967,** 32 (2), 476-476
[95] Lindsey, J. S.; Schreiman, I. C.; Hsu, H. C.; Kearney, P. C.; Marguerettaz, A. M., Rothemund and Adler-Longo reactions revisited: synthesis of tetraphenylporphyrins under equilibrium conditions, *J. Org. Chem.* **1987,** 52 (5), 827-836
[96] Funahashi, S.; Yamaguchi, Y.; Tanaka, M., High-pressure stopped-flow studies on the metalation of N-methyl-5,10,15,20-tetraphenylporphine in N,N-dimethylformamide, *Inorg. Chem.* **1984,** 23 (15), 2249-2251
[97] Konev, A. S.; Khlebnikov, A. F.; Levin, O. V.; Lukyanov, D. A.; Zorin, I. M., Photocurrent in Multilayered Assemblies of Porphyrin–Fullerene Covalent Dyads: Evidence for Channels for Charge Transport, *ChemSusChem* **2016,** 9 (7), 676-686
[98] Hiroto, S.; Miyake, Y.; Shinokubo, H., Synthesis and Functionalization of Porphyrins through Organometallic Methodologies, *Chem. Rev.* **2016**,

[99] Luguya, R.; Jaquinod, L.; Fronczek, F. R.; Vicente, M. G. H.; Smith, K. M., Synthesis and reactions of meso-(p-nitrophenyl)porphyrins, *Tetrahedron* **2004,** 60 (12), 2757-2763
[100] Hammouche, M.; Lexa, D.; Momenteau, M.; Saveant, J. M., Chemical catalysis of electrochemical reactions. Homogeneous catalysis of the electrochemical reduction of carbon dioxide by iron("0") porphyrins. Role of the addition of magnesium cations, *J. Am. Chem. Soc.* **1991,** 113 (22), 8455-8466
[101] Costentin, C.; Drouet, S.; Robert, M.; Savéant, J.-M., A Local Proton Source Enhances CO2 Electroreduction to CO by a Molecular Fe Catalyst, *Science* **2012,** 338 (6103), 90-94
[102] Costentin, C.; Passard, G.; Robert, M.; Savéant, J.-M., Ultraefficient homogeneous catalyst for the CO2-to-CO electrochemical conversion, *Proc. Nat. Acad. Sci.* **2014,** 111 (42), 14990
[103] Azcarate, I.; Costentin, C.; Robert, M.; Savéant, J.-M., Through-Space Charge Interaction Substituent Effects in Molecular Catalysis Leading to the Design of the Most Efficient Catalyst of CO2-to-CO Electrochemical Conversion, *J. Am. Chem. Soc.* **2016,** 138 (51), 16639-16644
[104] Costentin, C.; Robert, M.; Savéant, J.-M.; Tatin, A., Efficient and selective molecular catalyst for the CO2-to-CO electrochemical conversion in water, *Proc. Nat. Acad. Sci.* **2015,** 112 (22), 6882
[105] Mondal, B.; Sen, P.; Rana, A.; Saha, D.; Das, P.; Dey, A., Reduction of CO2 to CO by an Iron Porphyrin Catalyst in the Presence of Oxygen, *ACS Catal.* **2019,** 9 (5), 3895-3899
[106] Jiang, J.; Matula, A. J.; Swierk, J. R.; Romano, N.; Wu, Y.; Batista, V. S.; Crabtree, R. H.; Lindsey, J. S.; Wang, H.; Brudvig, G. W., Unusual Stability of a Bacteriochlorin Electrocatalyst under Reductive Conditions. A Case Study on CO2 Conversion to CO, *ACS Catalysis* **2018,** 8 (11), 10131-10136
[107] Weng, Z.; Wu, Y.; Wang, M.; Jiang, J.; Yang, K.; Huo, S.; Wang, X.-F.; Ma, Q.; Brudvig, G. W.; Batista, V. S.; Liang, Y.; Feng, Z.; Wang, H., Active sites of copper-complex catalytic materials for electrochemical carbon dioxide reduction, *Nature Comm.* **2018,** 9 (1), 415
[108] Kumar, M.; Neta, P.; Sutter, T. P. G.; Hambright, P., One-electron reduction and demetallation of copper porphyrins, *J. Phys. Chem.* **1992,** 96 (23), 9571-9575
[109] Shen, J.; Kortlever, R.; Kas, R.; Birdja, Y. Y.; Diaz-Morales, O.; Kwon, Y.; Ledezma-Yanez, I.; Schouten, K. J. P.; Mul, G.; Koper, M. T. M., Electrocatalytic reduction of carbon dioxide to carbon monoxide and methane at an immobilized cobalt protoporphyrin, *Nature Comm.* **2015,** 6, 8177
[110] Leung, K.; Nielsen, I. M. B.; Sai, N.; Medforth, C.; Shelnutt, J. A., Cobalt−Porphyrin Catalyzed Electrochemical Reduction of Carbon Dioxide in Water. 2. Mechanism from First Principles, *J. Phys. Chem. A* **2010,** 114 (37), 10174-10184
[111] Nielsen, I. M. B.; Leung, K., Cobalt−Porphyrin Catalyzed Electrochemical Reduction of Carbon Dioxide in Water. 1. A Density Functional Study of Intermediates, *J. Phys. Chem. A* **2010,** 114 (37), 10166-10173
[112] Zhu, M.; Yang, D.-T.; Ye, R.; Zeng, J.; Corbin, N.; Manthiram, K., Inductive and electrostatic effects on cobalt porphyrins for heterogeneous electrocatalytic carbon dioxide reduction, *Catal. Sci. Tech.* **2019,** 9 (4), 974-980
[113] Zhu, M.; Chen, J.; Guo, R.; Xu, J.; Fang, X.; Han, Y.-F., Cobalt phthalocyanine coordinated to pyridine-functionalized carbon nanotubes with enhanced CO2 electroreduction, *Appl. Catal. B* **2019,** 251, 112-118
[114] Zhu, M.; Chen, J.; Huang, L.; Ye, R.; Xu, J.; Han, Y.-F., Covalently Grafting Cobalt Porphyrin onto Carbon Nanotubes for Efficient CO2 Electroreduction, *Angew. Chem. Int. Ed.* **2019,** 0 (0),
[115] Wu, Y.; Jiang, J.; Weng, Z.; Wang, M.; Broere, D. L. J.; Zhong, Y.; Brudvig, G. W.; Feng, Z.; Wang, H., Electroreduction of CO2 Catalyzed by a Heterogenized Zn–Porphyrin Complex with a Redox-Innocent Metal Center, *ACS Central Sci.* **2017,** 3 (8), 847-852
[116] Wasylenko, D. J.; Rodríguez, C.; Pegis, M. L.; Mayer, J. M., Direct Comparison of Electrochemical and Spectrochemical Kinetics for Catalytic Oxygen Reduction, *J. Am. Chem. Soc.* **2014,** 136 (36), 12544-12547
[117] Matson, B. D.; Carver, C. T.; Von Ruden, A.; Yang, J. Y.; Raugei, S.; Mayer, J. M., Distant protonated pyridine groups in water-soluble iron porphyrin electrocatalysts promote selective oxygen reduction to water, *Chem. Comm.* **2012,** 48 (90), 11100-11102
[118] Bettelheim, A.; Kuwana, T., Rotating-ring-disk analysis of iron tetra(N-methylpyridyl)porphyrin in electrocatalysis of oxygen, *Anal. Chem.* **1979,** 51 (13), 2257-2260
[119] Chng, L. L.; Chang, C. J.; Nocera, D. G., Catalytic O−O Activation Chemistry Mediated by Iron Hangman Porphyrins with a Wide Range of Proton-Donating Abilities, *Org. Lett.* **2003,** 5 (14), 2421-2424
[120] Jung, J.; Liu, S.; Ohkubo, K.; Abu-Omar, M. M.; Fukuzumi, S., Catalytic Two-Electron Reduction of Dioxygen by Ferrocene Derivatives with Manganese(V) Corroles, *Inorg. Chem.* **2015,** 54 (9), 4285-4291
[121] Trojánek, A.; Langmaier, J.; Kvapilová, H.; Záliš, S.; Samec, Z., Inhibitory Effect of Water on the Oxygen Reduction Catalyzed by Cobalt(II) Tetraphenylporphyrin, *J. Phys. Chem. A* **2014,** 118 (11), 2018-2028
[122] Steiger, B.; Anson, F. C., Examination of Cobalt "Picket Fence" Porphyrin and Its Complex with 1-Methylimidazole as Catalysts for the Electroreduction of Dioxygen, *Inorg. Chem.* **2000,** 39 (20), 4579-4585
[123] Naruta, Y.; Sasayama, M.-A., Importance of Mn–Mn separation and their relative arrangement on the development of high catalase activity in manganese porphyrin dimer catalysts, *J. Chem. Soc., Chem. Comm.* **1994,** (23), 2667-2668

[124] Fukuzumi, S.; Okamoto, K.; Gros, C. P.; Guilard, R., Mechanism of Four-Electron Reduction of Dioxygen to Water by Ferrocene Derivatives in the Presence of Perchloric Acid in Benzonitrile, Catalyzed by Cofacial Dicobalt Porphyrins, *J. Am. Chem. Soc.* **2004,** 126 (33), 10441-10449
[125] Luna, M. A.; Moyano, F.; Sereno, L.; D'Eramo, F., Spectroscopic and electrochemical studies of high-valent water soluble manganese porphyrine. Electrocatalytic water oxidation, *Electrochim. Acta* **2014,** 135, 301-310
[126] Wang, D.; Groves, J. T., Efficient water oxidation catalyzed by homogeneous cationic cobalt porphyrins with critical roles for the buffer base, *Proc. Nat. Acad. Sci.* **2013,** 110 (39), 15579
[127] Costentin, C.; Dridi, H.; Savéant, J.-M., Molecular Catalysis of O2 Reduction by Iron Porphyrins in Water: Heterogeneous versus Homogeneous Pathways, *J. Am. Chem. Soc.* **2015,** 137 (42), 13535-13544
[128] Sinha, S.; Aaron, M. S.; Blagojevic, J.; Warren, J. J., Electrocatalytic Dioxygen Reduction by Carbon Electrodes Noncovalently Modified with Iron Porphyrin Complexes: Enhancements from a Single Proton Relay, *Chem. Eur. J.* **2015,** 21 (50), 18072-18075
[129] Shi, C.; Steiger, B.; Yuasa, M.; Anson, F. C., Electroreduction of O2 to H2O at Unusually Positive Potentials Catalyzed by the Simplest of the Cobalt Porphyrins, *Inorg. Chem.* **1997,** 36 (20), 4294-4295
[130] Baran, J. D.; Grönbeck, H.; Hellman, A., Analysis of Porphyrines as Catalysts for Electrochemical Reduction of O2 and Oxidation of H2O, *J. Am. Chem. Soc.* **2014,** 136 (4), 1320-1326
[131] Weng, Z.; Jiang, J.; Wu, Y.; Wu, Z.; Guo, X.; Materna, K. L.; Liu, W.; Batista, V. S.; Brudvig, G. W.; Wang, H., Electrochemical CO2 Reduction to Hydrocarbons on a Heterogeneous Molecular Cu Catalyst in Aqueous Solution, *J. Am. Chem. Soc.* **2016,** 138 (26), 8076-8079
[132] Liu, Y.; McCrory, C. C. L., Modulating the mechanism of electrocatalytic CO2 reduction by cobalt phthalocyanine through polymer coordination and encapsulation, *Nature Comm.* **2019,** 10 (1), 1683
[133] Kramer, W. W.; McCrory, C. C. L., Polymer coordination promotes selective CO2 reduction by cobalt phthalocyanine, *Chem. Sci.* **2016,** 7 (4), 2506-2515
[134] Walsh, J. J.; Neri, G.; Smith, C. L.; Cowan, A. J., Electrocatalytic CO2 reduction with a membrane supported manganese catalyst in aqueous solution, *Chem. Comm.* **2014,** 50 (84), 12698-12701
[135] Oldacre, A. N.; Crawley, M. R.; Friedman, A. E.; Cook, T. R., Tuning the Activity of Heterogeneous Cofacial Cobalt Porphyrins for Oxygen Reduction Electrocatalysis through Self-Assembly, *Chem.: Eur. J.* **2018,** 24 (43), 10984-10987
[136] Xiao, M.; Zhu, J.; Li, G.; Li, N.; Li, S.; Cano, Z. P.; Ma, L.; Cui, P.; Xu, P.; Jiang, G.; Jin, H.; Wang, S.; Wu, T.; Lu, J.; Yu, A.; Su, D.; Chen, Z., A Single-Atom Iridium Heterogeneous Catalyst in Oxygen Reduction Reaction, *Angew. Chem.* **2019,** 131 (28), 9742-9747
[137] Choi, J.; Wagner, P.; Gambhir, S.; Jalili, R.; MacFarlane, D. R.; Wallace, G. G.; Officer, D. L., Steric Modification of a Cobalt Phthalocyanine/Graphene Catalyst To Give Enhanced and Stable Electrochemical CO2 Reduction to CO, *ACS Energy Lett.* **2019**, 666-672
[138] Diercks, C. S.; Lin, S.; Kornienko, N.; Kapustin, E. A.; Nichols, E. M.; Zhu, C.; Zhao, Y.; Chang, C. J.; Yaghi, O. M., Reticular Electronic Tuning of Porphyrin Active Sites in Covalent Organic Frameworks for Electrocatalytic Carbon Dioxide Reduction, *J. Am. Chem. Soc.* **2018,** 140 (3), 1116-1122
[139] Diercks, C. S.; Liu, Y.; Cordova, K. E.; Yaghi, O. M., The role of reticular chemistry in the design of CO2 reduction catalysts, *Nature Mater.* **2018,** 17 (4), 301-307
[140] Kornienko, N.; Zhao, Y.; Kley, C. S.; Zhu, C.; Kim, D.; Lin, S.; Chang, C. J.; Yaghi, O. M.; Yang, P., Metal–Organic Frameworks for Electrocatalytic Reduction of Carbon Dioxide, *J. Am. Chem. Soc.* **2015,** 137 (44), 14129-14135
[141] Dong, B.-X.; Qian, S.-L.; Bu, F.-Y.; Wu, Y.-C.; Feng, L.-G.; Teng, Y.-L.; Liu, W.-L.; Li, Z.-W., Electrochemical Reduction of CO2 to CO by a Heterogeneous Catalyst of Fe–Porphyrin-Based Metal–Organic Framework, *ACS Appl. Energy Mater.* **2018,** 1 (9), 4662-4669
[142] Miner, E. M.; Gul, S.; Ricke, N. D.; Pastor, E.; Yano, J.; Yachandra, V. K.; Van Voorhis, T.; Dincă, M., Mechanistic Evidence for Ligand-Centered Electrocatalytic Oxygen Reduction with the Conductive MOF Ni3(hexaiminotriphenylene)2, *ACS Catal.* **2017,** 7 (11), 7726-7731
[143] Mahouche-Chergui, S.; Gam-Derouich, S.; Mangeney, C.; Chehimi, M. M., Aryl diazonium salts: a new class of coupling agents for bonding polymers, biomacromolecules and nanoparticles to surfaces, *Chem. Soc. Rev.* **2011,** 40 (7), 4143-4166
[144] Allongue, P.; Delamar, M.; Desbat, B.; Fagebaume, O.; Hitmi, R.; Pinson, J.; Savéant, J.-M., Covalent Modification of Carbon Surfaces by Aryl Radicals Generated from the Electrochemical Reduction of Diazonium Salts, *J. Am. Chem. Soc.* **1997,** 119 (1), 201-207
[145] Bahr, J. L.; Yang, J.; Kosynkin, D. V.; Bronikowski, M. J.; Smalley, R. E.; Tour, J. M., Functionalization of Carbon Nanotubes by Electrochemical Reduction of Aryl Diazonium Salts: A Bucky Paper Electrode, *J. Am. Chem. Soc.* **2001,** 123 (27), 6536-6542

[146] Gross, A. J.; Bucher, C.; Coche-Guerente, L.; Labbé, P.; Downard, A. J.; Moutet, J.-C., Nickel (II) tetraphenylporphyrin modified surfaces via electrografting of an aryldiazonium salt, *Electrochem. Comm.* **2011,** 13 (11), 1236-1239
[147] Wong, C. M.; Walker, D. B.; Soeriyadi, A. H.; Gooding, J. J.; Messerle, B. A., A versatile method for the preparation of carbon-rhodium hybrid catalysts on graphene and carbon black, *Chem. Sci.* **2016,** 7 (3), 1996-2004
[148] Atoguchi, T.; Aramata, A.; Kazusaka, A.; Enyo, M., Cobalt(II)-tetraphenylporphyrin-pyridine complex fixed on a glassy carbon electrode and its prominent catalytic activity for reduction of carbon dioxide, *J. Chem. Soc., Chem. Comm.* **1991,** (3), 156-157
[149] Tanaka, H.; Aramata, A., Aminopyridyl cation radical method for bridging between metal complex and glassy carbon: cobalt(II) tetraphenylporphyrin bonded on glassy carbon for enhancement of CO2 electroreduction, *J. Electroanal. Chem.* **1997,** 437 (1), 29-35
[150] Yao, S. A.; Ruther, R. E.; Zhang, L.; Franking, R. A.; Hamers, R. J.; Berry, J. F., Covalent Attachment of Catalyst Molecules to Conductive Diamond: CO2 Reduction Using "Smart" Electrodes, *J. Am. Chem. Soc.* **2012,** 134 (38), 15632-15635
[151] Elgrishi, N.; Griveau, S.; Chambers, M. B.; Bedioui, F.; Fontecave, M., Versatile functionalization of carbon electrodes with a polypyridine ligand: metallation and electrocatalytic H+ and CO2 reduction, *Chem. Comm.* **2015,** 51 (14), 2995-2998
[152] Ruther, R. E.; Rigsby, M. L.; Gerken, J. B.; Hogendoorn, S. R.; Landis, E. C.; Stahl, S. S.; Hamers, R. J., Highly Stable Redox-Active Molecular Layers by Covalent Grafting to Conductive Diamond, *J. Am. Chem. Soc.* **2011,** 133 (15), 5692-5694

CHAPTER 3. EXPERIMENTAL METHODS

3.1 Chemicals and materials

Chemicals were purchased from Sigma Aldrich and Alfa Aesar. Benzaldehyde and pyrrole were distilled under reduced pressure before use. Tetrabutylammonium hexafluorophosphate (TBAP) was recrystallized from ethanol and dried at 110 ºC. Anhydrous N,N-dimethylformamide (DMF) over molecular sieves was obtained from Ajax Finechem (purity > 99.9%; moisture content < 100 ppm). Carbon cloth was received from Fuel Cell Store. Flash column chromatography was performed on silica gel 70-230 mesh. Chloroform-*d* was stored over K_2CO_3 freshly dried at 300°C overnight. Other chemicals including cobalt (II) acetate $Co(OAc)_2$, manganese (II) acetate $Mn(OAc)_2$, propionic acid, dichloromethane (DCM), methanol, sodium nitrite $NaNO_2$, *n*-butanol, trifluoroacetic acid (TFA), tin (II) chloride $SnCl_2$, potassium bicarbonate $KHCO_3$, hydrochloric acid, ammonia solution, substituted benzaldehydes, boron trifluoride etherate $BF_3{\cdot}Et_2O$ and boron tribromide BBr_3 were used as received.

3.2 Syntheses of porphyrins

Meso-tetraphenylporphyrin (**TPP**)

Synthesis was based on the modified procedure reported by Adler et al.[1]

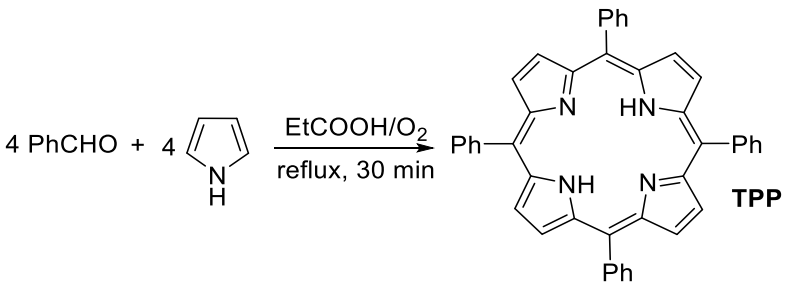

Scheme 3.1. Synthesis of *meso*-tetraphenylporphyrin

Benzaldehyde (3.184 g, 30 mmol) and pyrrole (2.013 g, 30 mmol) were dissolved in 300 mL of propionic acid. The solution was refluxed under mild flow of oxygen for 30 min. 250 mL of acid were distilled off and 80 mL of methanol were added after cooling to room temperature. The mixture was kept in the fridge overnight, the precipitate was filtered off, washed with ethanol and dried. Reflux of the product in *n*-BuOH for 1 h, filtration and drying furnished the pure, chlorin-free porphyrin in the form of violet crystalline substance (1.337 g, 29 %).

Note: purging the system with oxygen increased the yield from 21 % to 29 % and simultaneously allowed to eliminate the formation of undesirable chlorin.

^{1}H NMR (400 MHz, $CDCl_3$) δ 8.88 (s, 8H), 8.28 – 8.25 (m, 8H), 7.80 – 7.75 (m, 12H), -2.77 (s, 2H) ppm

^{13}C NMR (100 MHz, $CDCl_3$) δ 142.3, 140.0, 134.7, 131.2, 127.9, 126.8, 120.3 ppm

Spectral data are in accordance with reported literature values (Figures A1 and A2).[2]

5-(4-aminophenyl)-10,15,20-triphenylporphyrin (**TPP-NH$_2$**)

Synthesis was based on the modified procedure reported by Luguya et al.[3]

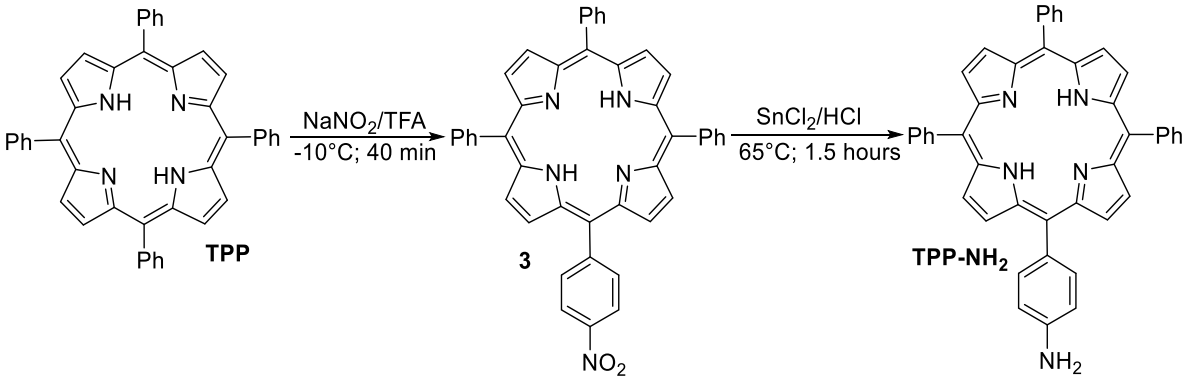

Scheme 3.2. Synthesis of 5-(4-aminophenyl)-10,15,20-triphenylporphyrin **TPP-NH$_2$**

a) Nitration.

Tetraphenylporphyrin **TPP** (615 mg; 1 mmol) was dissolved in 50 mL of trifluoroacetic acid. Dark green solution was cooled to -10 ºC on an ice-salt bath and sodium nitrite (104 mg; 1.5 mmol) was added in one portion. Solution quickly turned reddish-brown. Stirring was kept for 40 min, then the mixture was poured into 150 mL of water and carefully neutralized with K_2CO_3. Organic materials were extracted with dichloromethane (3 x 40 mL). Extracts were combined and dried over anhydrous Na_2SO_4. Solution was filtered, and its volume was reduced to ~ 10 mL on the rotary evaporator. Liquid was transferred onto the pad of silica and porphyrins were separated with flash column chromatography. A fraction, containing unreacted **TPP** and 5-(4-nitrophenyl)-10,15,20-triphenylporphyrin **3** was eluted with CH_2Cl_2:PE (1:2).

b) Reduction.

The mixture of compounds **TPP** and **3** produced in the previous step was placed into a 100 ml round-bottom flask with a gas inlet, mixed with 50 mL of concentrated HCl and stirred for 30 min under mild flow of argon. Then $SnCl_2 \cdot 2H_2O$ (814 mg, 3.6 mmol) was added in one portion

and the temperature was increased to 65 ºC. Heating and stirring were kept for 1.5 h. Then the reaction mixture was cooled down to room temperature and neutralized with NH_3 (30 % in water) until pH reached ~ 8. The resulting suspension was filtered under vacuum through a 0.5 cm pad of SiO_2. Organics were washed down from the filter with CH_2Cl_2 directly into separatory funnel until washings turned colorless. The organic phase was washed with brine, dried over anhydrous Na_2SO_4, filtered and the solvent was removed under reduced pressure. Individual components of the mixture were isolated using flash column chromatography (CH_2Cl_2:PE 1:3 → neat CH_2Cl_2). 124 mg of unreacted **TPP** was recovered along with aminoporphyrin **TPP-NH$_2$** (308 mg, 49 %).

Note 1: Nitration at low temperature significantly improved its selectivity compared with the published procedure.[3]

Note 2: isolation of aminoderivative **TPP-NH$_2$** at the end of sequence is more feasible than separation of porphyrins **TPP** and **3** due to bigger R_f difference.

Note 3: reduction of porphyrin **3** with $SnCl_2$ produces thick gunky precipitate of tin compounds floating at the interface of water and CH_2Cl_2 thus making simple extraction extremely cumbersome. Thus, filtration through a thin layer of silica or celite is recommended.

^{1}H NMR (400 MHz, $CDCl_3$) δ 8.98 (d, 2H), 8.88 – 8.87 (m, 6H), 8.28 – 8.24 (m, 6H), 8.03 – 8.00 (m, 2H), 7.82 – 7.74 (m, 9H), 7.05 – 7.01 (m, 2H), 3.95 (s, 2H), -2.69 (s, 2H) ppm

^{13}C NMR (100 MHz, $CDCl_3$) δ 146.2, 142.4, 142.4, 135.8, 134.7, 132.5, 127.8, 126.8, 126.8, 121.0, 120.1, 119.9, 113.6 ppm

Spectral data are in accordance with reported literature values (Figures A3, A4).[3]

5,10,15,20-tetrakis(2,3,4,5,6-pentafluorphenyl)porphyrin (**TPP-F$_{20}$**)

Synthesis was based on the general method reported by Lindsey et al.[4-5]

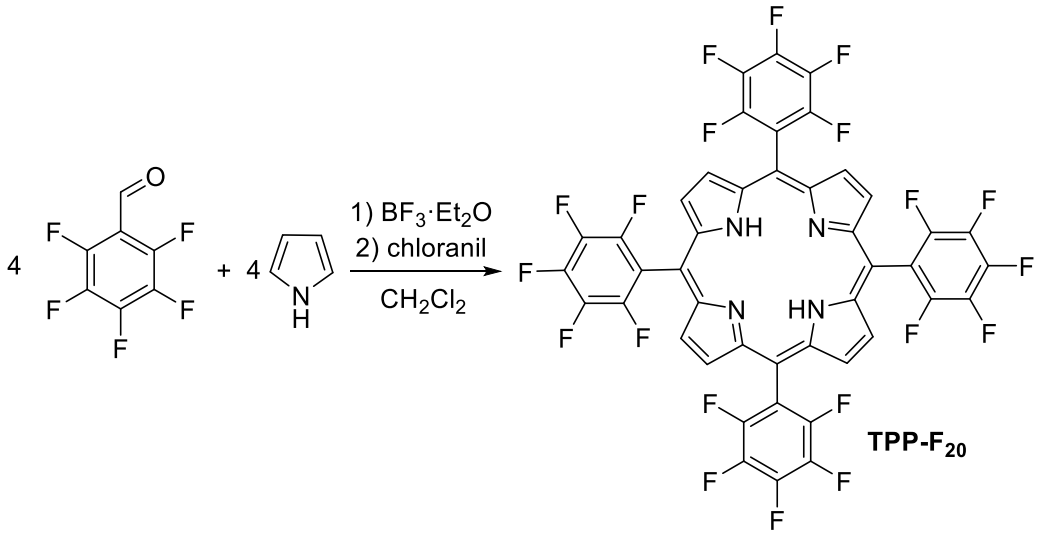

Scheme 3.3. Synthesis of 5,10,15,20-tetrakis(2,3,4,5,6-pentafluorphenyl)porphyrin

Pentafluorobenzaldehyde (598 mg, 3.05 mmol), pyrrole (212 µL, 3.05 mmol) and triethyl orthoacetate (183.3µL, 3.05 mmol) were dissolved in 300 mL of anhydrous CH_2Cl_2 and the solution was degassed by bubbling of nitrogen for at least 30 min. The vessel was wrapped in aluminium foil and $BF_3{\cdot}Et_2O$ (185 µL, 0.5 eqv) was injected in one portion. The reaction mixture was stirred for 24 hours at room temperature. Then, triethylamine (280 µL, 2 eqv relative to $BF_3{\cdot}Et_2O$) was added to quench the acidic catalyst and the mixture was stirred for additional 30 min. Chloranil (1.5 g, 6.1 mmol) was added into the reaction flask, the mixture was refluxed overnight and afterwards the solvent was removed under reduced pressure. Column chromatography on silica gel (CH_2Cl_2:PE 1:9) furnished 109 mg of porphyrin **TPP-F$_{20}$** as lustrous violet crystalline solid (yield 15%).

Note: the reaction mixture appears to be colorless after condensation in the presence of Lewis acid as the forming porphyrinogen is quite resistant to oxidation by oxygen. This might be confusing as the Lindsey procedure normally leads to quick formation of a dark solution.

^{1}H NMR (400.1 MHz, $CDCl_3$) δ 8.93 (s, 8H), -2.90 (s, 2H) ppm.

^{13}C NMR (100.6 MHz, $CDCl_3$) δ 146.8 (dm), 142.5 (dm), 137.7 (dm), 131.4 (s), 115.7 (td), 103.8 (s) ppm.

^{19}F NMR (376.5 MHz, $CDCl_3$) δ -136.5 (dd), -151.2 (t), -161.3 (td) ppm.

Spectral data are in agreement with the earlier reports (Figures A5 - A7).[6]

5,10,15,20-tetrakis(2,6-dimethoxyphenyl)porphyrin (**TPP-(OMe)$_8$**)

Synthesis was based on the general method reported by Lindsey et al.[4-5]

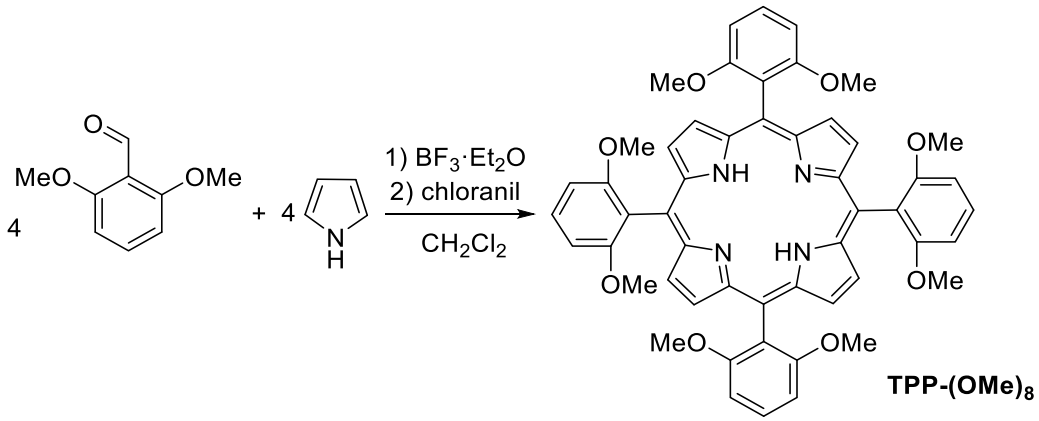

Scheme 3.4. Synthesis of 5,10,15,20-tetrakis(2,6-dimethoxyphenyl)porphyrin **TPP-(OMe)$_8$**

2,6-dimethoxybenzaldehyde (500 mg, 3 mmol) and pyrrole (208 µL, 3 mmol) were dissolved in 300 mL of anhydrous CH_2Cl_2 and the solution was degassed by bubbling of nitrogen for at least 30 min. The vessel was wrapped in foil and $BF_3{\cdot}Et_2O$ (38 µL, 0.1 eqv) was injected in one portion. The reaction mixture was stirred for 1.5 hours at room temperature. BF_3 was quenched with triethylamine (2 eqv relative to $BF_3{\cdot}Et_2O$) and the mixture was further stirred for 30 min. The flask was opened to air, chloranil (1.475 g, 6 mmol) was added and the mixture was refluxed for 2 h. Solvent was evaporated to the volume of 20 mL under reduced pressure and the dark reaction mixture was transferred onto a pad of silica gel. Column chromatography ($CH_2Cl_2 \rightarrow CH_2Cl_2$:$CH_3OH$ 50:1) furnished 109 mg of porphyrin **TPP-(OMe)$_8$** in the form of violet crystalline solid (yield 17%).

^{1}H NMR (400.1 MHz, $CDCl_3$) δ 8.66 (s, 8H), 7.67 (t, J = 8 Hz, 4H), 6.97 (d, J = 8 Hz, 8H), 3.49 (s, 24H) ppm.

^{13}C NMR (100.6 MHz, $CDCl_3$) δ 160.8, 129.9, 120.7, 110.9, 104.9, 56.3 ppm.

Spectral data are in agreement with the earlier reports (Figures A8, A9).[7]

5,10,15,20-tetrakis(2,6-dihydroxyphenyl)porphyrin (**TPP-(OH)8**)

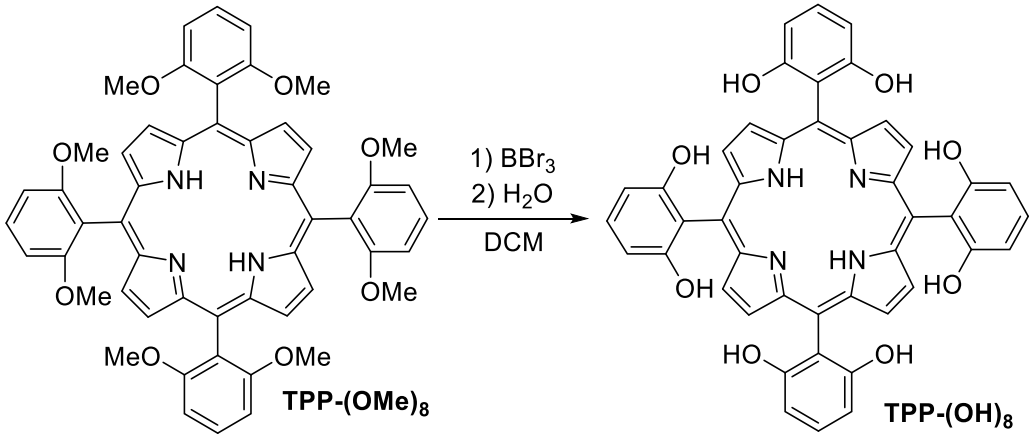

Scheme 3.5. Synthesis of 5,10,15,20-tetrakis(2,6-dihydroxyphenyl)porphyrin **TPP-(OH)8**

Porphyrin **TPP-(OMe)8** (40 mg, 0.047 mmol) was suspended in 5 mL of anhydrous CH_2Cl_2 and degassed with three freeze-pump-thaw cycles. The solution was cooled to -30 °C on a hexane-liquid nitrogen bath and BBr_3 (40 eqv) was injected via syringe. The addition of Lewis acid was accompanied by immediate change of colour from red to deep green. The reaction was let to warm up to room temperature and stirred for 24 h. 0.5 mL of H_2O followed by 10 mL of saturated $NaHCO_3$ solution under vigorous stirring were added to quench the acids present in the reaction mixture. CH_2Cl_2 was removed on a rotary evaporator and organics were extracted with ethyl acetate (3*50 mL). Extracts were combined, washed with brine, dried with anhydrous Na_2SO_4 and the solvent was removed under reduced pressure. Column chromatography (EtOAc:hexanes 1:3 → 1:1) yielded 24 mg of **TPP-(OH)8** as a violet solid (yield 64%).

Note: although literature procedures report complete dissolution of **TPP-(OMe)8**, an excess of solvent is detrimental for the progress of demethylation as we achieved removal of only 5 - CH_3 groups out of 8 when 50 mL of CH_2Cl_2 were used.

^{1}H NMR (400.1 MHz, CD_3OD) δ 8.90 (s, 8H), 7.48 (t, J = 8 Hz, 4H), 6.82 (d, J = 8 Hz, 8H), -2.74 (s, trace, suppressed by isotopic exchange with CD_3OD) ppm.

^{13}C NMR (100.6 MHz, CD_3OD) δ 159.5, 131.1, 118.1, 112.4, 108.0 ppm.

Spectral data are in agreement with the earlier reports (Figures A10, A11).[7]

Manganese(III) meso-tetraphenylporphyrin acetate (MnTPP)

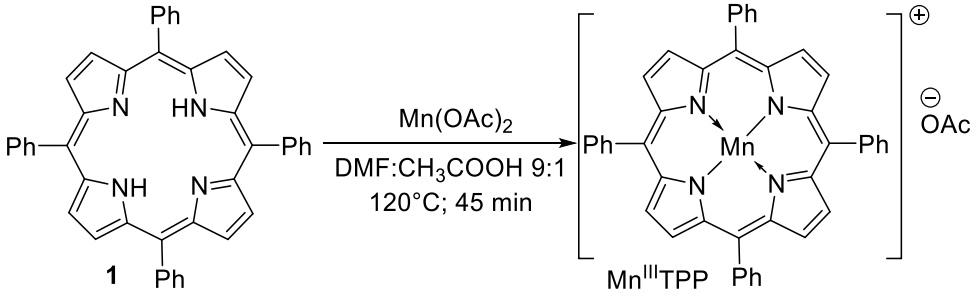

Scheme 3.6. Synthesis of manganese (III) tetraphenylporphyrin acetate (MnTPP)

Tetraphenylporphyrin **1** (615 mg, 1 mmol) was dissolved in 30 ml of DMF:CH_3COOH (9:1) mixture at 120 ºC and manganese acetate tetrahydrate (1.226 g, 5 mmol) was added in one portion. The reaction mixture was stirred for 45 min and cooled down to the room temperature. The complex was precipitated from the solution by dropwise addition of water (60 mL) over the course of 1 h, filtered off, washed with deionized water and dried at 80 ºC overnight. The crude product was purified by column chromatography on silica gel (neat CH_2Cl_2 → 1:19 MeOH:CH_2Cl_2). Recrystallization from CH_2Cl_2:heptane via slow evaporation of solvent yielded the complex MnTPP as greenish-black crystalline compound (311 mg, 43 %).

HRMS (ESI) calculated for $C_{44}H_{28}N_4Mn$ $[M]^+$: m/z 667.16890, found 667.16770.

UV-vis (DMF) λ (ε) 437 (63850), 465 (57800), 572 (9500), 611 (8550) 680 (2400)

IR (KBr) ν (cm^{-1}) 3053, 3022, 2918, 1597, 1570, 1487, 1441, 1342, 1074, 1011, 802, 754, 702.

Cobalt(II) porphyrins

Syntheses are based on the general method reported by Weng et al.[8]

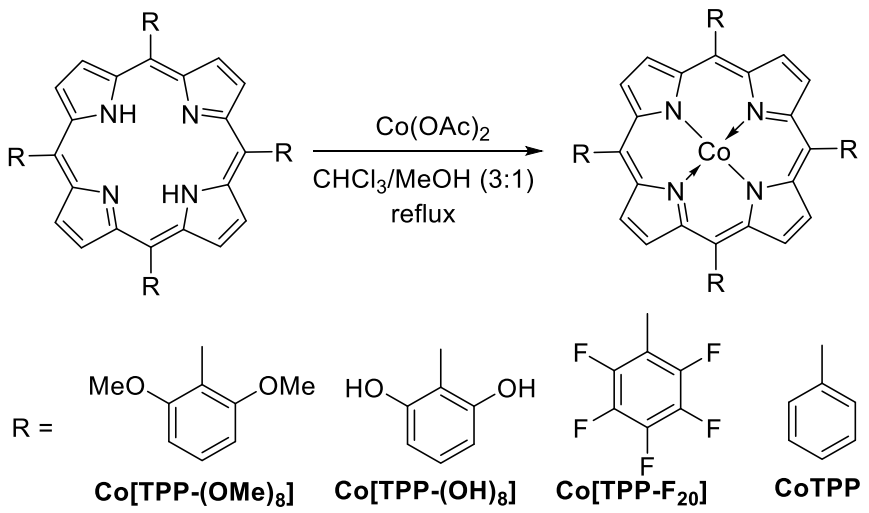

Scheme 3.7. Introduciton of Co into free-base porphyrins.

Porphyrins (0.1 mmol) were dispersed in 45 mL of chloroform and the solution was brought to a boil. After complete dissolution of a free-base porphyrin, 15 mL of methanol and 0.5 mmol of $Co(OAc)_2{\cdot}4H_2O$ were added and the solution was refluxed for 24 h. The reaction end point was detected by complete disappearance of bright red fluorescence under 365 nm UV light. If the fluorescence was present after 24 h, additional 0.1 mmol of $Co(OAc)_2{\cdot}4H_2O$ was added and the reflux was continued until the reaction was finished. Afterwards, the complex was extracted with 100 mL of CH_2Cl_2 and the extract was washed with 0.1 M aqueous solution of citric acid (2*50 mL). Then the organic phase was washed with deionised water and brine, dried over anhydrous Na_2SO_4, the solvent was removed on rotary evaporator and the reddish-brown crystalline precipitate was dried in vacuo for 24 h at room temperature. A typical yield is ~ 90%.

Note: metalation of porphyrins via prolonged reflux in DMF should be avoided as in this case a small amount (up to 5%) of free-base ligand remains unreacted even after repetitive additions of the cobalt salt.

CoTPP

^{1}H NMR (400 MHz, $CDCl_3$) δ 15.91 (s, 8H), 13.14 (s, 8H), 9.94 (s, 8H), 9.73 (s, 4H) ppm (Figure A12)

HRMS (ESI) calculated for $C_{44}H_{28}CoN_4$ $[M]^+$: m/z 671.16405, found 671.16284.

UV-vis (DMF) λ (ε) 429 (78200), 547 (10100)

Co[TPP-F_{20}]

HRMS (ESI) calculated for $C_{44}H_{28}CoN_4$ $[M]^+$: m/z 1030.9756, found 1030.9739.

UV-vis (DMF) λ (ε) 409 (147000), 527 (11000)

Co[TPP-$(OMe)_8$]

HRMS (ESI) calculated for $C_{52}H_{44}CoN_4O_8$ $[M]^+$: m/z 911.2486, found 911.2479.

UV-vis (DMF) λ (ε) 431 (116800), 544 (6000)

Co[TPP-$(OH)_8$]

HRMS (ESI) calculated for $C_{46}H_{29}CoN_5O_8$ $[(M-2H)+CH_3CN]^{2-}$ m/z 419.0680, found 419.0441.

UV-vis (DMF) λ (ε) 413 (41600), 430 (61200), 540 (4400)

3.3 Immobilisation of metalloporphyrins

Covalent immobilisation of Mn and Co porphyrins onto carbon electrodes

Carbon cloth was washed with concentrated dichloromethane and trifluoroacetic acid (TFA) in a Soxlet extractor for 24 h in each solvent, rinsed with concentrated HCl and water and dried. Then it was cut into 1*5 cm rectangular pieces, sewed with 0.5 mm silver wire through a narrow end the contact was sealed with melted polypropylene to leave another end free for use as a supporting electrode. The glassy carbon (GC) disk electrode was thoroughly polished with alumina slurry, washed with water and acetone and dried at 80 °C for 3 h.

Covalent immobilisation of Mn and Co tetraphenylporphyrin was performed in two steps, the first of which includes grafting of tetraphenylporphyrin ligand onto the carbon surface via electroreduction of the corresponding diazonium salt while the second stage is the introduction of the metal into the porphyrin core. 5-(4-aminophenyl)-10,15,20-triphenylporphyrin **TPP-NH_2** (15.1 mg, 0.024 mmol) was dissolved in 6 mL of H_2O:TFA (1:1) mixture and cooled down to -5°C in an ice-salt bath. 100 µL aliquot of $NaNO_2$ solution (1.5 eqv) was added into the reaction flask dropwise and the dark green mixture was stirred for 1 h. Septum with three electrodes was placed on top, electrodes were soaked in the solution for 30 min and the potential of 0.0 V vs Ag/AgCl (3M KCl) was applied for 1, 5 or 10 min. The working electrode

was removed, thoroughly washed with ethanol, DMF, water and dried at 80 °C for 3 h. Porphyrin-modified electrodes were soaked at 0.05 M solution of $Co(OAc)_2$ or $Mn(OAc)_2$ in DMF:CH_3COOH (9:1) at 120 °C for 45 min, then washed with DMF, water and dried. The resulting materials were denoted as **CoTPP-cov/1**, **CoTPP-cov/5** and **CoTPP-cov/10** (or **MnTPP-cov/1**, **MnTPP-cov/5**, **MnTPP-cov/10**) where 1, 5 and 10 corresponds to electrodeposition time in min. Immobilisation of Mn and Co porphyrin layers on the surface of the GC disk electrode was performed exactly in the same way as for carbon cloth. Description of conditions for optimisation and proof of diazonium salt formation are described in the Appendix.

Noncovalent immobilisation of CoTPP and MnTPP

Noncovalently immobilised CoTPP and MnTPP were prepared by dropping of 2 mM tetraphenylporphyrinate solution in DMF onto clean, dry carbon electrodes followed by drying at 80 °C for 3 h. The target surface coverages were $8\cdot10^{-8}$ mol/cm^2 for carbon cloth and $3.1\cdot10^{-8}$ mol/cm^2 for GC disk unless otherwise noted. Electrodes were washed with deionised water before catalytic experiments. The resulting materials were denoted as **CoTPP-noncov** and **MnTPP-noncov**. 5,10,15,20-tetrakis(2,3,4,5,6-pentafluorophenyl)porphyrin (**Co[TPP-F_{20}]**), 5,10,15,20-tetrakis(2,6-dimethoxyphenyl)porphyrin (**Co[TPP-$(OMe)_8$]**), 5,10,15,20-tetrakis(2,6-dihydroxyphenyl)porphyrin (**Co[TPP-$(OH)_8$]**) were immobilised on carbon cloth electrodes using the same drop-casting technique with the target surface concentration of $8\cdot10^{-8}$ mol/cm^2. The difference in the loading is based on the relative electrochemically active surface areas (S_{EA}) of the GC disk and carbon cloth.[9] Details on S_{EA} measurements are described in the Appendix.

3.4 Characterisation methods

Cyclic voltammetry in homogeneous nonaqueous systems

Electrochemical characterization of porphyrins dissolved in DMF was performed using a BioLogic SP-300 potentiostat. Cyclic voltammetry (CV) measurements were performed in a 25 mL round-bottom flask closed with a gas-tight septum bearing three electrodes inserted directly through the rubber. Degassed anhydrous DMF containing 0.1 M tetrabutylammonium hexafluorophosphate (TBAP) was used as supporting electrolyte. Degassing was attained using 3 freeze-pump-thaw cycles and the solutions were injected into a cell purged with nitrogen via syringe. An Ag wire immersed in DMF solution of 0.05 M $AgNO_3$ and 0.1 M TBAP was

employed as reference electrode and a Pt coil was used as auxiliary electrode. After each experiment ferrocene solution as an internal standard was injected into the electrochemical cell, values of $E^0(Fc^+/Fc)$ were measured and potentials were referenced and reported against this redox couple.[10] A freshly prepared Ag electrode had the potential of -0.018 V vs Fc^+/Fc. The typical concentration of porphyrins used in the procedures was 0.5 mM unless otherwise noted.

The amount of electrochemically active complex on the electrode surface (Γ_{EA}) was estimated using Equation 3.1:[11]

$$\Gamma_{EA} = \frac{Q_{CV}}{nFA} \quad \textbf{(Equation 3.1)}$$

Where Q_{CV} – the charge determined via integration of Co^{II}/Co^{I} or Mn^{III}/Mn^{II} reduction peak (C), n – the number of electrons transferred (1 in this case), F – Faraday's constant (96485 C/mol), A – the electrode area (cm^2).

A complimentary method of calculation was employed using Equation 3.2 to validate the Γ_{EA} estimation:[11]

$$\Gamma_{EA} = \frac{4 i_p RT}{F^2 A v} \quad \textbf{(Equation 3.2)}$$

Where i_p – the peak reoxidation current of Co^{II}/Co^{I} reduction wave (A), R – the universal gas constant (8.314 J/(mol·K), T – the electrolyte temperature (296 K), v – the potential scan rate (V/s).

As CoTPP and MnTPP are soluble in organic solvents, determination of Γ_{EA} for **CoTPP-noncov** and **MnTPP-noncov** was performed in the same cell using degassed aqueous 0.1 M KOH solution as electrolyte to minimise the influence of hydrogen discharge current. Pt wire was used as counter electrode. An Ag/AgCl (3M KCl) reference was employed and the potentials are reported against NHE. Conversion of potentials from Ag/AgCl (3M KCl) into NHE scale was performed using Equation 3.3.[12]

$$E_{NHE} = 0.210 + E_{Ag/AgCl} \quad \textbf{(Equation 3.3)}$$

Analysis of CoTPP deactivation products

To accumulate enough CoTPP deactivation products a custom-made 3.1 cm^2 carbon cloth electrode was employed. After a 4 h long CO_2ERR at the potential of -1.05 V vs NHE, the

organics were washed from the surface with DCM and the solvent was allowed to evaporate at room temperature to yield a reddish-brown gunky residue. For studies involving NMR spectroscopy and HRMS, the deactivation products were collected from three identical catalytic experiments and combined. For CV analysis, the quantity of organic products obtained after two runs was sufficient for experiments.

3.5 Electrocatalytic experiments

Cyclic and linear scan voltammetry

All electrocatalytic experiments were performed using a BioLogic SP-300 potentiostat at room temperature using an Ag/AgCl (3M KCl) reference electrode and a Pt coil auxiliary electrode. OER studies were performed in degassed 0.5 M H_2SO_4 electrolyte. ORR was studied in O_2-saturated 0.1 M KOH and 0.5 M H_2SO_4 solutions. For linear scan voltammetry (LCV) and cyclic voltammetry (CV) 25 mL round-bottom flask closed with gas-tight septum and equipped with Ag/AgCl (3M KCl) reference electrode and Pt coil counter electrode was used as a three-electrode electrochemical cell. Logarithms of currents were extracted from LCVs to build Tafel plots for ORR and OER. For OER the potential sweep rate was 1 mV/s while 10 V/s scan speed was employed for ORR studies. CVs relevant for CO_2ERR in aqueous electrolytes were obtained in N_2- or CO_2-saturated 0.5 M $KHCO_3$ solution using Ag/AgCl (3M KCl) reference electrode (0.21 V vs NHE). Potentials for aqueous systems are reported against NHE.

Rotating disk electrode (RDE) experiments

ORR selectivity was determined using polarisation curves obtained on a rotating disk electrode (RDE). The disk-only technique was chosen over the rotating ring-disk electrode (RRDE) because the immobilisation of the porphyrin layer involves the immersion of the electrode assembly into the solution of **TPP-N_2^+** in TFA/H_2O which would have damaged the platinum ring and hence significantly affect the measurements. Further, the analysis of recent literature shows that both RDE and RRDE methods show similar accuracy.[13]

For RDE measurements a 5 mm glassy carbon rotating disk electrode with digital control unit (Gamry) was used. The electrode was inserted into a three-electrode cell (Gamry) through a septum with a hole drilled at the centre. The electrolyte was saturated with O_2 by bubbling the gas through the solution for at least 20 min before experiment. Contact between stainless steel rod and rubber was greased to minimise friction and O_2 was continuously bubbled through the

solution. Ag/AgCl (3.5M KCl) was used as a reference electrode and platinum coil as a counter electrode. The LCV scan rate during RDE studies was 10 mV/s.

Experimental results were treated using the Koutecky-Levich Equation 3.4 to extract the Levich coefficient *B*:[14-15]

$$\frac{1}{j_m} = \frac{1}{j_k} + \frac{1}{B\sqrt{\omega}} \quad \textbf{(Equation 3.4)}$$

Where j_m is measured current density (mA/cm^2); j_k is kinetic current density (mA/cm^2); ω is the angular velocity of RDE (rad/s).

Formal electron transfer numbers (ETN) *n* in ORR were calculated from the slope *B* of the Koutecky-Levich plot using Equation 3.5:[15-16]

$$n = \frac{B\nu^{\frac{1}{6}}}{0.62FD^{\frac{2}{3}}C} \quad \textbf{(Equation 3.5)}$$

Where ν is the kinematic viscosity of the electrolyte (0.01 cm^2/s); *D* is the oxygen diffusion coefficient ($1.9\cdot10^{-5}$ cm^2/s), *C* is the oxygen concentration in saturated solution ($1.2\cdot10^{-6}$ mol/cm^3).

CO_2ERR controlled-potential electrolyses (CPE)

CPE experiments were performed in a gas-tight two-compartment electrochemical H-cell with a Ag/AgCl (3 M KCl) reference electrode. 0.5 M $KHCO_3$ saturated with CO_2 was employed as the electrolyte unless otherwise noted. Gaseous products from the cathodic headspace were analyzed on a GC 2014 (Shimadzu) equipped with packed Restek 6 ft column (molecular sieves 5 Å, i.d. 2 mm) and TCD detector. Ultra high purity helium was used as the carrier gas. Stability tests were performed as a series of three 4 h long CPE experiments at -1.05 V vs NHE (overpotential η = 500 mV). Between each run the electrochemical cell was purged with CO_2 for at least 30 min. To compare stability of different catalysts the recyclability parameter was calculated using equation 3.6:

$$Recyclability\ (\%) = \frac{n(CO)_{first\ run}}{n(CO)_{third\ run}}\ 100\% \quad \textbf{(Equation 3.6)}$$

Determination of TON, TOF and FE (CO) in CO_2ERR

Turnover numbers (TON) and turnover frequencies (TOF) in CO were determined using Equations 3.7 and 3.8, respectively:

$$TON = \frac{(CO)_i}{\Gamma_{EA}A} \ (\textbf{Equation 3.7}); \ TOF = \frac{(CO)_i}{\Gamma_{EA}A\tau} \ (\textbf{Equation 3.8})$$

Where $(CO)_i$ – the amount of CO measured with GC at a given time i (mol), τ – the reaction time (s).

Faradic efficiency [FE (CO)] values were calculated from the Equation 3.9:

$$FE_{CO} = 100\frac{[(CO)_i - (CO)_{i-1}]nF}{(Q_i - Q_{i-1})} \ (\textbf{Equation 3.9})$$

3.6 Spectral and morphological analyses

NMR spectroscopy

1D and 2D NMR spectroscopy was performed on a Bruker Avance III 400 MHz spectrometer. TOCSY (TOtal Correlation Spectroscopy), COSY (homonuclear COrrelation Spectroscopy), NOESY (Nuclear Overhauser Effect SpectroscopY), HSQC (Heteronuclear Single Quantum Coherence) and HMBC (Heteronuclear Multiple Bond Correlation) were performed with the sample spin rate of 19 Hz. 256 points were recorded to obtain the virtual axis f1 with accumulation of 8 scans for each spectrum along the f2 axis. DOSY (Diffusion Oriented Spectroscopy) spectra were recorded on a Bruker Avance III 500 MHz spectrometer using a field gradient between 5 and 95 % without rotation. Chemical shifts of ^{1}H and ^{13}C peaks were referenced against residual solvent peaks of $CDCl_3$ (δ = 7.26 and 77.16 ppm respectively).[17-18]

^{15}N HSQC and ^{2}D NMR experiments

For referencing of the ^{15}N HSQC spectrum chemical shift of nitromethane in $CDCl_3$ was used (δ = 380.5 ppm).[19] For ^{2}D NMR lock and shim were performed on the sample of neat $CDCl_3$ which was swapped for the sample dissolved in $CHCl_3$ immediately before the experiment.

Electrochemical impedance spectroscopy (EIS)

EIS measurements were performed using the same three-electrode setup and electrolytes as for electrocatalytic experiments at frequency range from 1.0 MHz to 0.1 Hz with perturbation amplitude of 10 mV.

Raman spectroscopy and SEM

A JEOL JSM 7100F FESEM microscope was used for scanning electron microscopy (SEM) imaging (5 kV acceleration potential). Raman spectra were recorded on Lab RAM HR Evolution spectrometer using a 473 nm laser. Top flat parts of carbon fibres were analysed to assure ~ 90° angle between the incident laser beam and the material.

UV-vis spectroscopy

UV-vis spectroscopy was performed on a single-beam HACH DR/4000 spectrometer (HACH) in a 10 mm quartz cuvette.

IR spectroscopy

FTIR spectroscopy was performed on the samples pressed into KBr pellets in the transmission mode.

3.7 References

[1] Adler, A. D.; Longo, F. R.; Finarelli, J. D.; Goldmacher, J.; Assour, J.; Korsakoff, L., A simplified synthesis for meso-tetraphenylporphine, *J. Org. Chem.* **1967,** 32 (2), 476-476
[2] Shi, B.; Boyle, R. W., Synthesis of unsymmetrically substituted meso-phenylporphyrins by Suzuki cross coupling reactions, *J. Chem. Soc., Perkin Trans. 1* **2002,** (11), 1397-1400
[3] Luguya, R.; Jaquinod, L.; Fronczek, F. R.; Vicente, M. G. H.; Smith, K. M., Synthesis and reactions of meso-(p-nitrophenyl)porphyrins, *Tetrahedron* **2004,** 60 (12), 2757-2763
[4] Lee, C.-H.; S. Lindsey, J., One-flask synthesis of meso-substituted dipyrromethanes and their application in the synthesis of trans-substituted porphyrin building blocks, *Tetrahedron* **1994,** 50 (39), 11427-11440
[5] Lindsey, J. S.; Schreiman, I. C.; Hsu, H. C.; Kearney, P. C.; Marguerettaz, A. M., Rothemund and Adler-Longo reactions revisited: synthesis of tetraphenylporphyrins under equilibrium conditions, *J. Org. Chem.* **1987,** 52 (5), 827-836
[6] Castro, K. A. D. F.; Silva, S.; Pereira, P. M. R.; Simões, M. M. Q.; Neves, M. d. G. P. M. S.; Cavaleiro, J. A. S.; Wypych, F.; Tomé, J. P. C.; Nakagaki, S., Galactodendritic Porphyrinic Conjugates as New Biomimetic Catalysts for Oxidation Reactions, *Inorg. Chem.* **2015,** 54 (9), 4382-4393
[7] Costentin, C.; Drouet, S.; Robert, M.; Savéant, J.-M., A Local Proton Source Enhances CO2 Electroreduction to CO by a Molecular Fe Catalyst, *Science* **2012,** 338 (6103), 90-94
[8] Weng, Z.; Jiang, J.; Wu, Y.; Wu, Z.; Guo, X.; Materna, K. L.; Liu, W.; Batista, V. S.; Brudvig, G. W.; Wang, H., Electrochemical CO2 Reduction to Hydrocarbons on a Heterogeneous Molecular Cu Catalyst in Aqueous Solution, *J. Am. Chem. Soc.* **2016,** 138 (26), 8076-8079
[9] McCrory, C. C. L.; Jung, S.; Peters, J. C.; Jaramillo, T. F., Benchmarking Heterogeneous Electrocatalysts for the Oxygen Evolution Reaction, *J. Am. Chem. Soc.* **2013,** 135 (45), 16977-16987
[10] Gritzner, G.; Kůta, J., Recommendations on reporting electrode potentials in nonaqueous solvents: IUPC commission on electrochemistry, *Electrochim. Acta* **1984,** 29 (6), 869-873
[11] Savéant, J.-M. In *Elements of Molecular and Biomolecular Electrochemistry*, John Wiley & Sons, Inc.: **2006**; pp 1-77
[12] Friis, E. P.; Andersen, J. E. T.; Madsen, L. L.; Bonander, N.; Møller, P.; Ulstrup, J., Dynamics of Pseudomonas aeruginosa azurin and its Cys3Ser mutant at single-crystal gold surfaces investigated by cyclic voltammetry and atomic force microscopy, *Electrochim. Acta* **1998,** 43 (9), 1114-1122
[13] Park, J.; Nabae, Y.; Hayakawa, T.; Kakimoto, M.-a., Highly Selective Two-Electron Oxygen Reduction Catalyzed by Mesoporous Nitrogen-Doped Carbon, *ACS Catal.* **2014,** 4 (10), 3749-3754
[14] Wiberg, G. K. H.; Zana, A., Levich Analysis and the Apparent Potential Dependency of the Levich B Factor, *Anal. Lett.* **2016,** 49 (15), 2397-2404
[15] Jahan, M.; Bao, Q.; Loh, K. P., Electrocatalytically Active Graphene–Porphyrin MOF Composite for Oxygen Reduction Reaction, *J. Am. Chem. Soc.* **2012,** 134 (15), 6707-6713
[16] Chen, W.; Chen, S., Oxygen Electroreduction Catalyzed by Gold Nanoclusters: Strong Core Size Effects, *Angew. Chem.* **2009,** 121 (24), 4450-4453
[17] Fulmer, G. R.; Miller, A. J. M.; Sherden, N. H.; Gottlieb, H. E.; Nudelman, A.; Stoltz, B. M.; Bercaw, J. E.; Goldberg, K. I., NMR Chemical Shifts of Trace Impurities: Common Laboratory Solvents, Organics, and Gases in Deuterated Solvents Relevant to the Organometallic Chemist, *Organometallics* **2010,** 29 (9), 2176-2179
[18] Marianov, A. N.; Jiang, Y., Effect of Manganese Porphyrin Covalent Immobilization on Electrocatalytic Water Oxidation and Oxygen Reduction Reactions, *ACS Sustainable Chem. Eng.* **2019,** 7 (4), 3838-3848
[19] Markley, J. L.; Bax, A.; Arata, Y.; Hilbers, C. W.; Kaptein, R.; Sykes, B. D.; Wright, P. E.; Wüthrich, K., Recommendations for the presentation of NMR structures of proteins and nucleic acids – IUPAC-IUBMB-IUPAB Inter-Union Task Group on the Standardization of Data Bases of Protein and Nucleic Acid Structures Determined by NMR Spectroscopy, *J. Biomol. NMR* **1998,** 12 (1), 1-23

CHAPTER 4. COVALENT IMMOBILISATION AND ELECTROCATALYTIC ACTIVITY OF MANGANESE PORPHYRIN

4.1 Introduction

Modern clean energy research is highly focused on the development of efficient electrochemical systems such as proton-exchange membrane fuel cells and electrolyzers where electrocatalysts are required to drive oxygen reduction (ORR), oxygen evolution (OER) and carbon dioxide reduction (CO_2ERR) reactions with reasonable rates at low overpotentials.[1-7] Among numerous examples of highly active and inexpensive electrode materials,[8] porphyrin-type complexes offer unsurpassed tunability of ligands by means of organic synthesis and simplicity of mechanistic studies.[7, 9-13] Several excellent reviews on porphyrin-catalysed ORR, OER and CO_2ERR are available.[12, 14]

Although a great number of molecular catalysts have been tested in these reactions, Mn porphyrins are remarkable for a wide range of metal oxidation states and affinity to O_2.[10, 15] As such, a work on the ORR activity of Mn porphyrinates with various substituents in alkaline medium was reported with strong emphasis on structure-activity relationships.[16] An in depth study of ORR mechanism catalysed by Mn tetraphenylporphyrin (MnTPP) was recently performed in acetonitrile and proton donors were found to greatly affect the H_2O yield which ranged from 75 to 97 %.[10] Moreover, it was established that dimeric Mn porphyrins offer optimum spatial arrangement for H_2O_2 binding and the separation between metal centres was found to play a key role with maximum catalytic O-O splitting TOF at around 4.0 Å Mn-Mn distance.[17] Regarding the OER, Mn biporphyrins were also found to be effective O_2 evolution catalysts in nonaqueous medium with Mn^V being catalytically active species.[17-19] In turn, the activity of MnTPP immobilised on a gas-diffusion electrode in CO_2ERR was reported to be extremely poor with no significant CO_2 reduction current under normal conditions and only a minor amount of hydrocarbons formed when the CO_2 pressure was increased to 20 bar.[20] Also, for a structurally similar Mn phthalocyanine a FE(CO) of 7 % accompanied by the formation of 2 % of CH_4 was reported. [21]

However, inherent drawback of molecular catalysts is that for real world applications they have to be deposited on the surface of an electrode.[22-23] In this regard, noncovalent immobilisation on carbon supports is a simple and efficient method based on physisorption of

organics on conductive hydrophobic solid materials.[24] Just to name a few, pyrene-modified Co corrole was found to be a good ORR and OER catalyst due to π-π interactions with multiwalled carbon nanotubes.[25] Immobilisation of Fe porphyrin bearing a proton relay substituent is another great example of this strategy.[24] Interestingly, catalytic activity could be significantly altered by simple physical adsorption on the electrode. Indeed, Costentin et al. showed that the small fraction of formally homogeneous Fe porphyrin catalyst adsorbed on the electrode surface accounts for at least half of the catalytic current in ORR in aqueous electrolyte.[26]

Another heterogenisation method is covalent ligation of complexes to the electrode surface. The great advantage of this methodology is that even normally soluble compounds could form heterogeneous systems with the structure of the catalytically active centre preserved intact. As such, Fe porphyrin linked to imidazole-modified carbon nanotubes is a good example of ORR catalyst heterogenisation via a coordination bond.[27] Similarly, Ir pincer complexes covalently immobilised on carbon or ITO furnished good OER catalysts.[28-29]

In this work we endeavoured to use the immobilisation mode of MnTPP as a tool to tune its electrocatalytic properties. The choice of MnTPP as a catalyst was motivated by an extremely wide range of oxidation states observed for Mn complexes in general and by the fact that highly efficient bi-centred catalytic activation of O-O bond was clearly observed on dimeric Mn porphyrins. Further, the ligand was chosen in such a way that at the end of synthetic sequence both covalently and non-covalently immobilised complexes would have identical structure. Porphyrin was covalently immobilised onto a carbon support using electroreduction of corresponding diazonium salt with the following metalation while noncovalent immobilisation is conveniently done via drop-casting. By variation of the electrodeposition time we aimed to optimize the porphyrin layer density and thus to tune the average Mn-Mn distance. It was assumed that in a series of materials with progressively closer situated active organometallic moieties it is possible to reach the point where at least two metal atoms would take part in electrocatalytic process. Hence, for covalently modified electrodes we anticipated to observe higher reaction rates and better selectivity to H_2O over H_2O_2 formation in ORR and improvement of the OER reaction rate.[30] Similar effects were anticipated to influence CO_2ERR where a higher density of the MnTPP layer on the surface of the electrode could steer the reaction selectivity towards CH_4 formation.

4.2 Results and discussion

4.2.1 Immobilisation of MnTPP on carbon cloth

A two-step procedure was implemented to ligate Mn porphyrin to the surface of electrodes. First, the tetraphenylporphyrin core was covalently linked to the carbon cloth via a phenylene linker (Scheme 4.1).[31-34] To achieve this, the diazonium salt generated in-situ from the aminoporphyrin **TPP-NH₂** in H_2O:TFA (1:1) mixture was electrochemically reduced at 0.0 V vs AgCl (3M KCl) on carbon fabric. The following treatment with hot DMF:AcOH (9:1) solution of $Mn(OAc)_2$ furnished covalently tethered Mn^{III} porphyrinate (**MnTPP-cov/1**, **MnTPP-cov/5** and **MnTPP-cov/10** where number is the electrodeposition time 1, 5 and 10 min).[35]

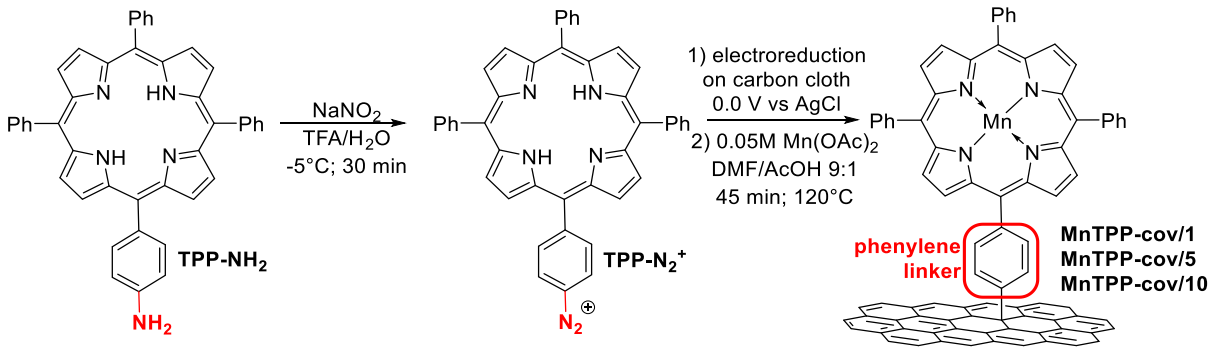

Scheme 4.1. Preparation of **MnTPP-cov/1**, **MnTPP-cov/5** and **MnTPP-cov/10**

For characterization of the resulting materials we employed cyclic voltammetry (CV), Raman spectroscopy and scanning electron microscopy (SEM). It should be noted here that CV and Raman provide the evidence of porphyrin formation on the surface, while the direct observation of covalent link with the support is rather impossible due to the extremely low concentration of the target C-C bond. In turn, with SEM one could either confirm or disprove the formation of crystallites and thick organic layers on the surface. Covalent ligation could be inferred from indirect evidence such as insolubility of a surface layer in organic solvents coupled with differences of electrochemical behaviour in comparison with noncovalent counterpart.

Cyclic voltammetry of **MnTPP-cov/1** in oxygen-free dry DMF electrolyte containing 0.1 M tetrabutylammonium hexafluorophosphate (TBAP) showed responses of Mn^{III}/Mn^{II} and Mn^{II}/Mn^{I} redox pairs at -0.69 and -1.81 V vs Fc^{+}/Fc that persisted after thorough washing with DMF (Figure 4.1a, red trace). Assignment of these waves to Mn redox transitions is evident from comparison with the CV of MnTPP in solution where Mn^{III}/Mn^{II} and Mn^{II}/Mn^{I} transitions

took place at -0.70 and -1.81 V, respectively (Figure A17, black trace). Distinction between covalent immobilisation and physical adsorption could be made based on the fact that MnTPP is easily soluble in organic solvents. As such, removal of the drop-cast complex from the electrode with DMF was straightforward and complete (Figure 4.1a, blue trace) while immobilisation via reduction of diazonium salt furnished a layer that could not be washed away by any means. Additionally, Mn^{III}/Mn^{II} cathodic and anodic peak currents showed a clear linear dependence on the potential scan rate rather than on its square root which supports our conclusion about very strong connection to the electrode surface (Figure 4.1b). This observation is especially significant considering that MnTPP is easily soluble in DMF and in case of purely Van-der-Waals interactions a nonlinear correlation would be evident.[36] Finally, peak separations of less than 59 mV at low scan rates are also characteristic for surface-bound species (Figure 4.1c).

Additional evidence of Mn porphyrin presence on the surface was obtained using Raman spectroscopy. As shown in Figure 4.1d, the spectrum of **MnTPP-cov/1** contains signature signals at 1007, 785 and 394 cm^{-1} which are extremely close to those found in the spectra of **MnTPP-noncov** and solid MnTPP. The difference in signal intensity comes from the lower amount of complex deposited on the surface upon electrodeposition. As retention of main spectral features upon immobilisation has been reported, it is a good indication of Mn porphyrin being formed on the surface.[37-38]

Next, we evaluated the amount of electrochemically active species on the carbon cloth surface as a function of immobilisation mode and electrodeposition time. As we sought a way to vary the average Mn-Mn distance, higher amounts of deposited complex would increase the possibility of two atoms to have an optimum distance for ORR or OER.[17] Estimation of Γ_{EA} for covalently modified materials was performed by integration of the Mn^{III}/Mn^{II} reduction wave in DMF. We found that Γ_{EA} increase slightly with longer electrodeposition time. As such, for **MnTPP-cov/1** Γ_{EA} is $0.80 \cdot 10^{-9}$ mol/cm^2 (as determined from CV presented in the Figure 4.1a, red trace), in **MnTPP-cov/5** this value rises to $0.91 \cdot 10^{-9}$ mol/cm^2 and reaches $0.99 \cdot 10^{-9}$ mol/cm^2 for **MnTPP-cov/10** (Figure 4.2a, violet and green traces, respectively). Clearly, a 10-fold increase of electrodeposition time led to only 1.24 times higher Γ_{EA} (Figure 4.2b) which agrees well with the results for covalent immobilisation of NiTPP on glassy carbon electrodes obtained by Gross et al.[33]

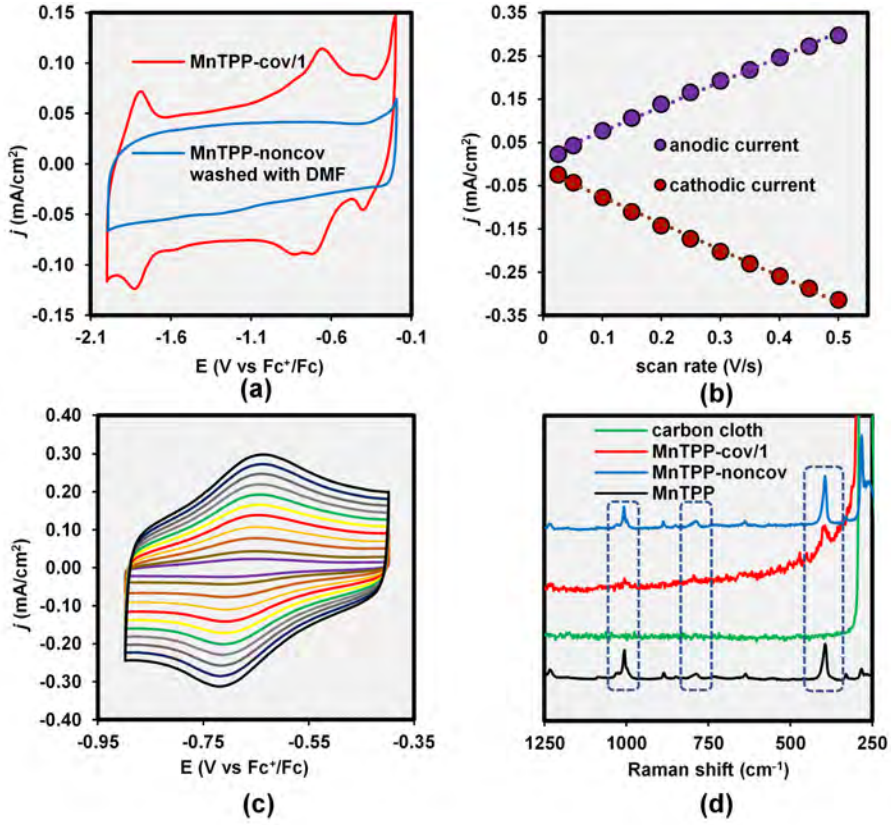

Figure 4.1. (a) Cyclic voltammetry of **MnTPP-cov/1** (red trace) and carbon cloth after MnTPP drop-casting and washing with DMF (blue trace); scan rate 100 mV/s. (b) Dependence of Mn^{III}/Mn^{II} peak current on the potential scan rate; (c) shape of Mn^{III}/Mn^{II} wave as a function of scan rate. Electrolyte: degassed DMF containing 0.1 M of TBAP in all cases; (d) Raman spectra of **MnTPP-noncov** (blue), **MnTPP-cov/1** (red), bare carbon cloth (green) and pure MnTPP (black).

However, with longer electrolysis time the shape of CV significantly changes. First, Mn^{II}/Mn^{I} reduction peak becomes more diffuse and for **MnTPP-cov/10** appears as a rather broad wave. Additionally, new reoxidation peaks appeared at -1.25 and -1.60 V. The nature of the signal at -1.25 V could be inferred form the study of homogeneous MnTPP in DMF (Figure 4.2c). We found analogous response to appear upon addition of H_2O in the system. Considering the propensity of Mn porphyrins to form dimeric complexes, we ascribed this feature to reoxidation of either μ-oxo dimeric species[17] or the agglomerates containing direct a Mn-Mn bond which is a general trend for Mn complexes in low oxidation states.[39] At the same time, a low-intensity redox wave centred at -1.60 V was ascribed to the presence of residual surface-bound free tetraphenylporphyrin based on comparison with its CV in the same electrolyte (Figure A17, red trace). This is possible considering prolonged porphyrin electrodeposition leads to the

formation of thick organic film which hinders penetration of $Mn(OAc)_2$ during the metalation step.[32] Thus, it appears that the thickness of the surface layer does progressively increase, most probably due to the formation of a multimolecular layer, although not all of the complex is accessible for electrochemical reaction. Interestingly, even after 10 min electrodeposition SEM did not show the formation of a uniform organic layer on the surface (Figure 4.2d). For drop cast **MnTPP-noncov**, the amount of electrochemically active complex was evaluated in aqueous alkaline electrolyte to avoid its dissolution. A characteristic response of Mn^{III}/Mn^{II} redox couple was recorded at -0.24 V vs NHE (inset in the Figure 4.2b) and Γ_{EA} estimated via integration of the reduction current peak is $1.6 \cdot 10^{-9}$ mol/cm^2.

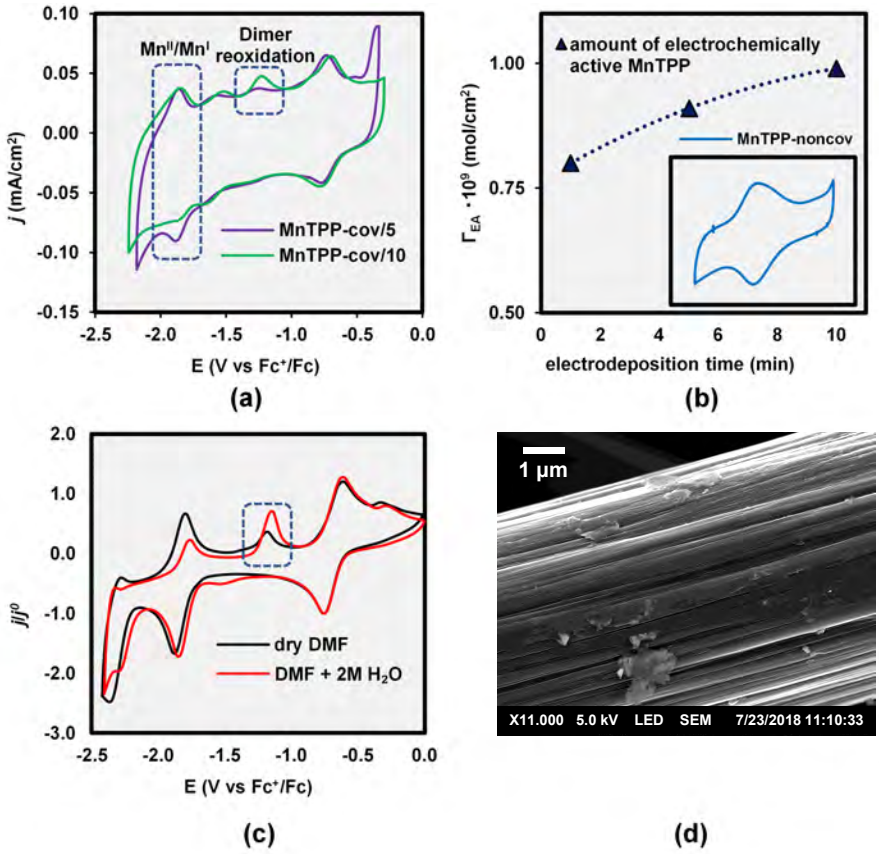

Figure 4.2. (a) CV of **MnTPP-cov/5** (violet trace) and **MnTPP-cov/10** (green trace) in DMF electrolyte. Signals ascribed to Mn^{II}/Mn^{I} redox couple and reoxidation of dimeric species are highlighted. (b) Correlation between electrodeposition time and Γ_{EA}. Estimation of Γ_{EA} for **MnTPP-noncov** was performed using CV in 0.1 M KOH (featured in inset); (c) Comparison of CVs for homogeneous MnTPP in dry DMF (black line) and after addition of 2M of H_2O (red line). Emerging reoxidation peak is highlighted. (d) SEM of **MnTPP-cov/10**. Scan rate 50 mV/s in all cases.

To sum up, we immobilised Mn porphyrin on the surface of carbon cloth electrodes in covalent and noncovalent modes. The amount of electrochemically active complex is the highest in case of **MnTPP-noncov**, while that in **MnTPP-cov/1** is the smallest. Covalent immobilisation led to progressive increase of the peak at -1.25 V vs Fc^{+}/Fc which we ascribed to reoxidation of dimeric Mn porphyrin species. Based on this, we speculated that for **MnTPP-cov/5** and **MnTPP-cov/10** the involvement of two Mn atoms into ORR or OER is possible. However, we were unable to make any conclusions regarding Mn-Mn interactions for **MnTPP-noncov** from characterization results only as the study is limited to aqueous electrolytes where the solvent stability window is narrow, and this information could be deduced from its catalytic properties.

4.2.2 Catalytic activity of MnTPP in OER

Encouraged by the results of characterization, we went on to study the performance of the prepared materials in electrocatalysis. First, we assessed the activity of MnTPP-derived electrodes in OER. CV provided good evidence that MnTPP does catalyse oxygen evolution (Figure 4.3a). The oxidation current has the onset at ~1.10 V vs NHE in all cases while carbon has no noticeable activity and the curve is almost flat. Interestingly, a well-defined peak current was found for **MnTPP-noncov** while for all covalently immobilised materials the CV curves have a broad maximum at 1.34 V vs NHE.

To gain insight into the kinetics of the electrode reaction, we performed LCV measurements and Tafel analysis. LCVs at slower scan rate (Figure 4.3b) confirmed the findings of CV study with characteristic peaks in case of **MnTPP-noncov** and **MnTPP-cov/1** while a more smooth increase of current density occurred on **MnTPP-cov/5** and **MnTPP-cov/10**. Analysis of corresponding Tafel plots (Figure 4.3c) clearly shows two regions. The first of them corresponds to the potentials less positive than 1.32 V vs NHE and shows slopes of 103-127 mV/dec for all covalently immobilised complexes and 169 mV/dec for **MnTPP-noncov**. These values are in good agreement with the rate limiting one-electron transfer from Mn complex to the electrode and most likely correspond to the formation of the Mn^{IV} species. Notably, the noncovalently immobilised catalyst appears to be less prone to oxidation as the deviation from the theoretically expected 120 mV/dec is much higher than that of the covalently immobilised complexes. The second region at higher potentials is characterised by a flatter line with the slope of 234-267 mV/dec for all materials regardless of the immobilisation mode. This change of the plot slope appears to correspond to the potentials where the reaction rate is limited by

either diffusion to the catalytically active centre or chemical steps such as O_2 loss rather than by electron transfer.[40-41]

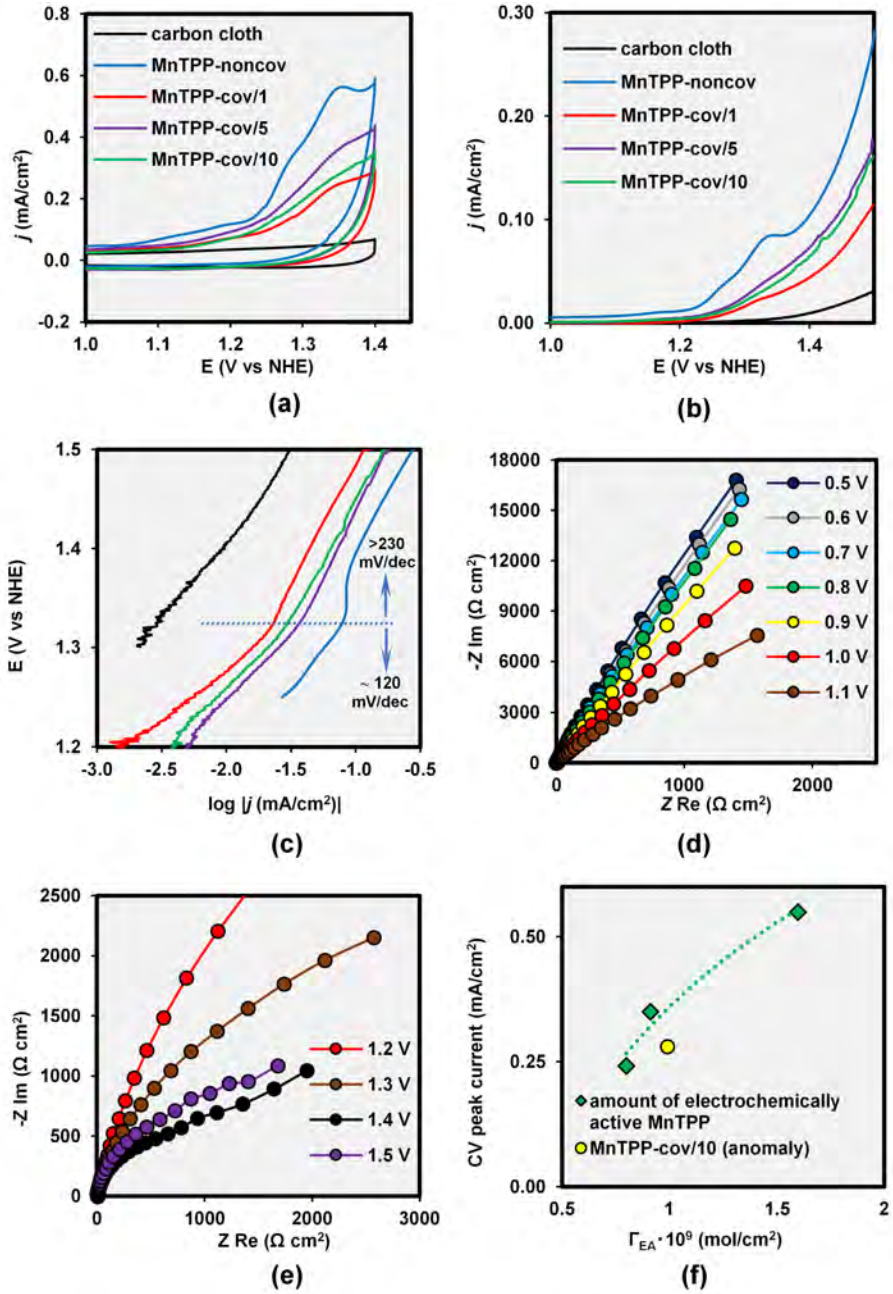

Figure 4.3. (a) CV study of carbon cloth (black), **MnTPP-noncov** (blue), **MnTPP-cov/1** (red), **MnTPP-cov/5** (violet) and **MnTPP-cov/10** (green) in OER. Scan rate: 50 mV/s. (b) LSVs of the same materials and (c) corresponding Tafel plots. (d) EIS of **MnTPP-noncov** under potentials from 0.5 to 1.1 V and (e) between 1.2 and 1.5 V. (f) Dependence of CV peak current on Γ_{EA}.

In order to confirm catalytic oxygen generation and test the stability of the resulting electrode materials, 4 h long controlled potential electrolyses (CPE) were performed on **MnTPP-noncov**, **MnTPP-cov/5** and bare carbon under a potential of 1.55 V vs NHE (Figure A18). Clearly, **MnTPP-noncov** is the most active catalyst in good agreement with LCV data. However, the water oxidation current on **MnTPP-noncov** deteriorates faster compared to **MnTPP-cov/5** and the corresponding curves merge after ~ 2.5 h of electrolysis. GC analysis of the gas from the anodic headspace after the experiment on **MnTPP-cov/5** shows O_2 to be the only gaseous reaction product (Figure A19). The average turnover frequencies (TOFs) were estimated to be 36 h^{-1} for **MnTPP-noncov** and 28 h^{-1} for **MnTPP-cov/5**.

To explore the factors limiting the reaction rate, we chose to perform EIS on **MnTPP-noncov** as the most active electrode material. As expected, at the potentials between 0.5 to 1.1 V (Figure 4.3d) the Nyquist plots appear as straight lines which corresponds to purely capacitive coating (see equivalent circuit in Figure A20a). However, at 1.2 and 1.3 V (Figure 4.3e) the lines show very broad semi-circles characteristic for slow reaction under kinetic control (refer to equivalent Randles circuit in Figure A20b) while a further increase of the potential leads to the appearance of characteristic diffusion polarisation at 1.4 and 1.5 V (equivalent circuit with Warburg impedance in Figure A20c). This sharp change between 1.3 and 1.4 V agrees well with the position of the peak in CVs and a critical point on Tafel plots at ~1.32 V. Thus, OER appears to be under kinetic control at the potentials below 1.32 V and under diffusion control above this point.

To sum up, although covalent immobilisation of MnTPP on the surface of carbon cloth gave a catalytically active material, the attachment mode has very small or no effect on its OER activity in terms of TOF. At the same time, **MnTPP-cov/5** shows superior stability compared to **MnTPP-noncov**. The reaction rate is largely proportional to the amount of the electrochemically active complex (Figure 4.3f) and at high overpotentials appears to be limited by the diffusion of H_2O molecules to the catalytically active centre. Interestingly, **MnTPP-cov/10** ($0.99 \cdot 10^{-9}$ mol/cm^2) has an activity even slightly lower than **MnTPP-cov/5** ($0.91 \cdot 10^{-9}$ mol/cm^2) though its Γ_{EA} is higher (Figure 4.3b,f). EIS results give grounds to believe that the diffusion limitations within the dense organic layer are responsible for this anomalous decline in TOF.

Finally, it is necessary to see how our results correlate to the earlier works on water oxidation catalysts immobilisation. As such, under 500 mV overpotential, the covalently grafted

derivative of Ru(dpc)(pic)$_3$ shows a TOF of 864 h^{-1} [42] while a similar noncovalently immobilised complex has a TOF of 49320 s^{-1} [43] which represents a 57-fold increase, which is huge difference. Though this might seem to contradict our data, the support employed in the first work is glassy carbon while in the second report authors used -COOH-modified carbon nanotubes and this change might play a crucial role in the reaction kinetics of Ru^{II}(pdc)(pic)$_3$-based catalysts. What is more, works concerning covalently immobilised (Cp*)-Ir(bipy)[28] and Ru(tpy)$_2$[44] water oxidation catalysts confirm retention of catalytic activity upon covalent immobilisation on the carbon surface and showed good catalyst stability in agreement with our observations.

4.2.3 Catalytic activity of MnTPP in ORR

Next, the activity was studied in the oxygen reduction reaction. Catalysis in ORR by MnTPP-modified electrodes was assessed both in acidic (0.5 M H_2SO_4) and alkaline (0.1 M KOH) media to simulate the performance of the materials in the respective types of fuel cells. LCV measurements were undertaken to evaluate the overall activity and Tafel analysis was used to obtain kinetic information. Rotating disk electrode experiments were used to estimate formal electron transfer numbers (ETNs).

In acidic medium LCV showed almost no ORR activity on bare carbon cloth with slow onset around 0.00 V vs NHE (Figure 4.4a, black trace). Covalent immobilisation of MnTPP led to a characteristic shift of current onset to more positive potentials. For **MnTPP-cov/5** and **MnTPP-cov/10** the reduction current sets off at ~0.30 V while **MnTPP-cov/1** showed even somewhat earlier onset at ~0.45 V. Notably, even though in case of **MnTPP-cov/1** the ORR has a more positive current onset potential, **MnTPP-cov/5** shows a higher reaction rate below 0 V. This shift is most probably due to higher degrees of polymerisation and branching in the organic layer of **MnTPP-cov/5** and **MnTPP-cov/10** which impacts the accessibility of the Mn centre by O_2 and H^+ (Figure A21).[32] Also, in case of **MnTPP-cov/5** and **MnTPP-cov/10** LCVs appear to have two broad waves (Figure 4.4a) which most probably correspond to two consecutive reduction reactions. Unfortunately, the study of noncovalently immobilised complex in acidic electrolyte was impossible as MnTPP dissolves upon reduction even though the starting MnTPP is completely insoluble in aqueous acids.

To gain insight into the reaction mechanism, corresponding Tafel plots were derived as shown in Figure 4.4c. In all cases we were able to identify a single well-defined linear region of purely electrochemical kinetics. As expected, bare carbon cloth has a slope of 219 mV/dec which is a

good indicator of very poor activity in ORR.[45] In turn, slopes between 110 and 125 mV/dec for **MnTPP-cov/1** – **MnTPP-cov/10** (Figure 4.4b) agree well with single electron transfer as the rate-limiting step at low potentials. EIS of **MnTPP-cov/5** shows semi-circles with Warburg resistance around at 0.1 V and 0 V (Figure A20a). As the potential becomes more negative, impedance rises, but then drops again and the diffusion component disappears leaving only charge transfer resistance impedance (Figure A20b).

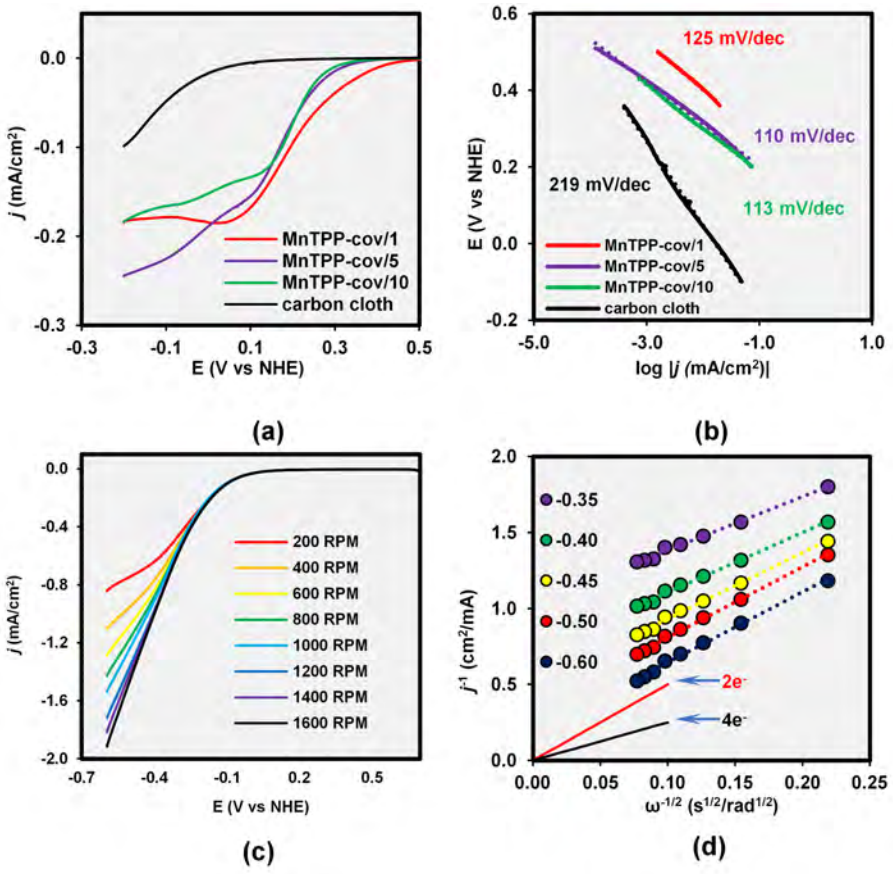

Figure 4.4. (a) LCVs of **MnTPP-cov/1** (red trace), **MnTPP-cov/5** (violet trace) and **MnTPP-cov/10** (green trace) and (b) corresponding Tafel plots. (c) LCVs obtained on RDE under various rotation rates for **MnTPP-cov/5**, and (d) Koutecky-Levich plots. Slopes corresponding to 2-electron (red) and 4-electron (black) reduction mechanisms are shown for reference. Electrolyte: O_2-saturated 0.5 M H_2SO_4.

As shown in the Figure 4.4d, oxygen reduction experiments were also performed on RDE to estimate catalyst selectivity to H_2O and H_2O_2. We chose **MnTPP-cov/5** as it showed the highest ORR current densities in LCV at the potentials more negative than 0 V. Catalyst selectivity appears to be highly dependent on the potential applied with ETN ranging from 2.1

at -0.60 V to 3.2 at -0.35 V vs NHE i.e. ORR selectivity to $4e^-$ reduction (to H_2O) is around 60 % at low overpotentials but drops to 5 % at more negative bias (Figure A22).

Based on these results, we concluded that the ORR proceeds via a series of one-electron reductions furnishing H_2O_2 and then H_2O. It appears that H_2O formation is slower than production of H_2O_2 and takes place mostly at low overpotentials.

In the next set of experiments, we studied the performance of the electrode materials in alkaline medium using LCV, RDE and ESI techniques as shown in Figure 4.5. In O_2-saturated 0.1 M KOH electrolyte bare carbon cloth showed an ORR current onset at -0.10 V (as measured at j = 0.05 mA/cm^2) with the peak at -0.19 vs NHE. **MnTPP-cov/1** and **MnTPP-noncov** shifted the ORR current by ~80 mV in the positive direction (Figure 4.5a). Both electrodes showed a single maximum similar to that observed in acidic electrolyte for **MnTPP-cov/1**. However, for **MnTPP-cov/5** and **MnTPP-cov/10** the O_2 reduction peak was less pronounced and appears to be rather a superposition of two poorly defined waves, thus showing the behaviour resembling the one observed in 0.5 M H_2SO_4. Though the current onsets are similar, overall currents for **MnTPP-cov/10** and **MnTPP-cov/5** at more negative potentials reach much higher values than on carbon and **MnTPP-noncov**, in particular **MnTPP-cov/5** is the most active.

Further, we studied corresponding Tafel plots (Figure 4.5b). In all cases we clearly identified linear regions of purely electrochemical kinetics. Carbon cloth showed a slope of 71 mV/dec which is rather close to the theoretically expected value of 60 mV/dec for $2e^-$ transfer and agrees well with earlier reports.[46-47] In turn, **MnTPP-cov/5** and **MnTPP-noncov** showed slopes of 133 and 109 mV/dec which could be interpreted as the result of one-electron reduction of Mn^{III} to Mn^{II} species.[10, 15] Interestingly, **MnTPP-cov/1** and **MnTPP-cov/10** showed Tafel slopes of 81 and 88 mV/dec, respectively. As these values are between $1e^-$ and $2e^-$ transfer, it appears that the reduction takes place both on carbon and Mn complex simultaneously.

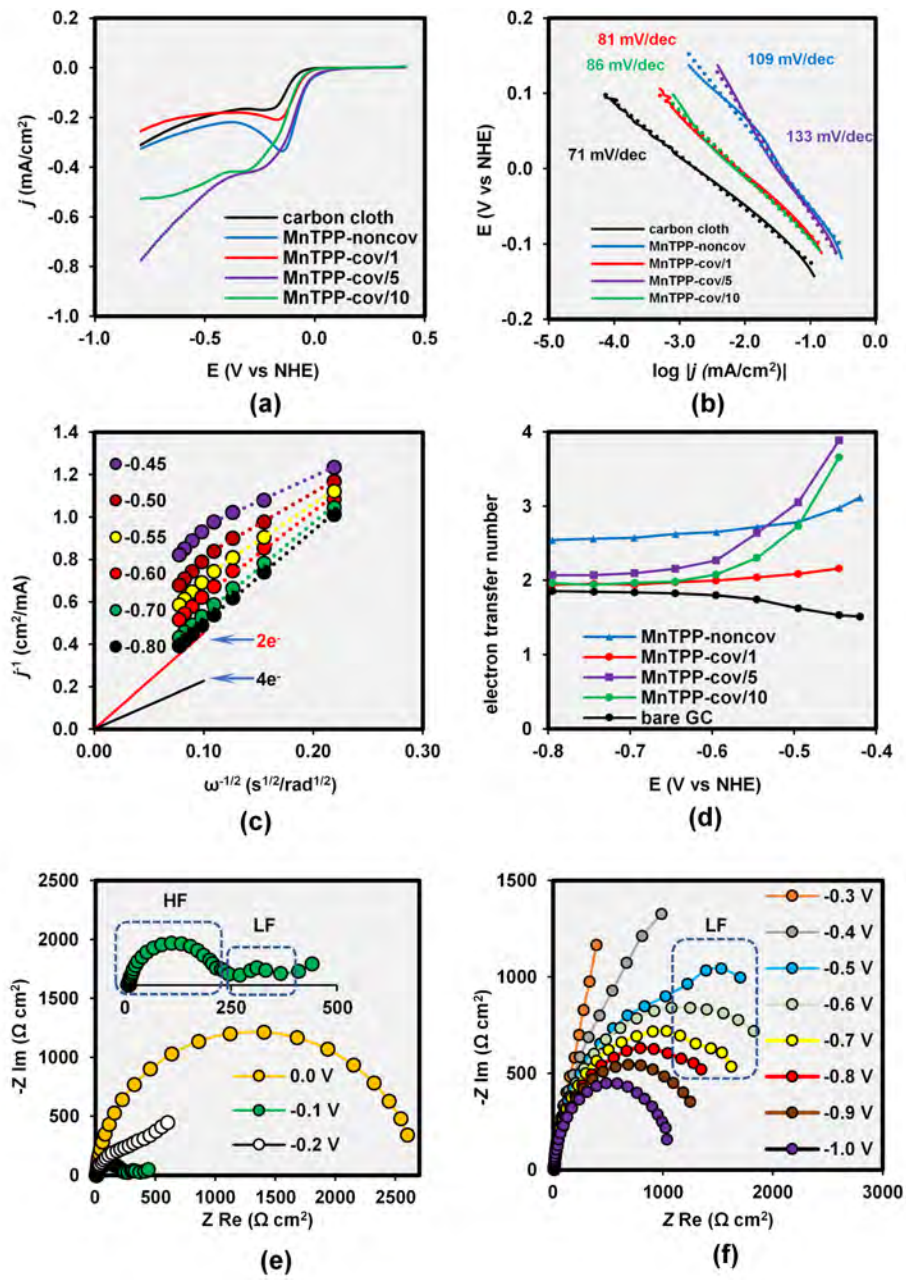

Figure 4.5. (a) LCVs of bare carbon cloth (black trace), **MnTPP-noncov** (blue trace), **MnTPP-cov/1** (red trace), **MnTPP-cov/5** (violet trace) and **MnTPP-cov/10** (green trace); (b) corresponding Tafel plots. (c) Koutecky-Levich plots obtained for **MnTPP-cov/5**. Slopes corresponding to 2-electron (red) and 4-electron (black) reduction mechanisms are shown for reference. (d) Formal electron transfer numbers obtained from the analysis of Koutecky-Levich plots. (e) EIS of **MnTPP-cov/5** at the potentials of from 0.0 to -0.2 V and (f) between -0.3 and -1.0 V. High-frequency (HF) and low-frequency (LF) time constants are marked with blue rectangles. Electrolyte: O_2-saturated 0.1 M KOH an all cases.

An RDE study of **MnTPP-noncov** in 0.1 M KOH electrolyte showed linear Koutecky-Levich plots with the ETN gradually decreasing from 2.9 to 2.5 with the increase of overpotential (Figure 4.5d). In turn, graphs obtained for **MnTPP-cov/5** under the same conditions showed the presence of two regions (Figures 4.5c, d). The first of them corresponds ~ $2e^-$ slope under rotation rates above 1000 RPM while the second one with slower angular velocities is quite close to that expected for $4e^-$ transfer. Notably, the $4e^-$ reduction appeared at the potentials more positive than -0.6 V. In case of **MnTPP-cov/10** the Koutecky-Levich plots (Figure A23) are similar and give ETNs very close to those calculated for **MnTPP-cov/5** (Figure 4.5d). The variation of slope could be interpreted as the two-step reaction taking place, most probably by stepwise reduction of O_2 to H_2O_2 and then to H_2O.[48] Impedance spectroscopy of **MnTPP-cov/5** showed two main features: a well-defined semi-circle at the frequencies above 1Hz (shown as HF in Figures 4.5e, f) and less pronounced, but clearly observable low-frequency constant in the mHz region (shown as LF in Figures 4.5e, f) under potentials below -0.1 V. This response could be understood as a circuit containing two capacitances which agrees well with the assumption of a two-step reduction with two separate charge carrier mechanisms and hence, two resistances. Finally, the stability of **MnTPP-cov/5** in the ORR was assessed via prolonged cycling in O_2-saturated alkaline electrolyte. We found that the activity was gradually decreasing, and after ~200 cycles the CV shape was quite similar to the one measured for bare carbon cloth (Figure A24).

Considering the results of RDE experiments, the presence of two waves on LCVs and two time constants in impedance spectra we believe that H_2O formation on the covalently immobilised complex takes place in a stepwise manner: first to H_2O_2 and then to H_2O. Reduction happens as a cascade of single electron transfers as evidenced by the slope of the Tafel plot, and the proposed reaction mechanism is featured in the Figure A25. Similar to the acidic medium, the fast step of H_2O_2 formation precedes its slower reduction to H_2O and completely takes over at high overpotentials. Considering that the Mn^{III}/Mn^{II} redox transformation is centred around -0.24 V, i.e. much earlier than ORR onset, we could conclude that the formation of active Mn^{II} species precedes the reaction of the catalyst with O_2. Also, the noncovalent heterogenization mode disfavours further reduction of H_2O_2 even at low overpotentials most probably due to its inability to accommodate two oxygen atoms on two Mn centres simultaneously and only massive excess of drop-cast catalyst allows it to achieve an ETN of 3.1.

In total, MnTPP-based catalysts showed lower current densities and required higher overpotentials than state of the art Pt/C (20%, E-TEK). The current density for the commercial

catalyst reaches ~ 6 mA/cm^2 [49-51] with the current onsets at +0.9 V in acidic medium[27, 49] and +0.1 V in alkaline electrolyte.[50-51] In both media Pt/C shows the preferable formation of H_2O across all the potential range. It is also interesting to compare the MnTPP catalysts with the performance of Ag/C materials which also have high ORR current densities, but ETNs show a variation between 4.0 and 3.8 with similarly increasing yield of H_2O_2 at more negative potentials.[50-51] However, for metal-based catalysts neither variation of metal loading nor particle size appear to provide such a great degree of control over the reaction rate and selectivity as for **MnTPP-cov**-based materials.[52]

4.2.4 Effect of immobilisation mode on the activity of MnTPP in CO_2ERR

Further, the activity of covalently immobilised MnTPP was assessed in CO_2ERR. Linear scan voltammetry in aqueous electrolyte revealed that the immobilised layer of Mn porphyrinate inhibits hydrogen discharge, however no significant current increase corresponding to high rate of CO_2 reduction was observed. Indeed, compared to bare carbon cloth, **MnTPP-cov/1** shifts the current onset from -0.77 V to -1.02 V vs NHE as measured at j = 0.1 mA/cm^2 (Figure 4.6a). At the same time, hydrogen evolution might mask the CO_2 reduction current if the reaction rate is comparatively small. To find out if the surface-bound complex is reactive toward CO_2, we performed a controlled potential electrolysis at -1.09 V vs NHE in CO_2-saturated 0.5 M $KHCO_3$ (η = 540 mV). The formation of CO as a sole product of CO_2 reduction along with H_2 evolution was detected and the reaction yielded 1.0 μmol/cm^2 of CO with the maximum FE(CO) of 13.3 % (Figures 4.6b, c, red curves). Unfortunately, a blank experiment with bare carbon cloth electrode led to the formation of H_2 and CO as well (Figure 4.6b, black trace). The amount of CO produced by carbon cloth electrode was 0.8 μmol/cm^2 which is only slightly smaller than what was obtained on **MnTPP-cov/1**. However, in full agreement with LSV data the maximum FE(CO) in blank experiment was only 1.7 % (Figure 4.6c, black trace).

To compare the catalytic performance of the heterogeneous complex in both immobilisation modes, the study of **MnTPP-noncov** with $6.7 \cdot 10^{-8}$ mol/cm^2 of the catalyst on the surface (100 times higher loading than on **MnTPP-cov/1**, the amount is typical for non-covalently modified electrodes) and **MnTPP-noncov(low)** bearing $6.7 \cdot 10^{-10}$ mol/cm^2 (equivalent to the loading on **MnTPP-cov/1**) was performed. Both electrodes were manufactured via drop-casting. As seen from linear scan voltammograms, regardless of the amount of drop-cast complex, noncovalently immobilised materials have similar electrochemical behavior (Figure 4.6a, blue and green traces) showing moderate inhibition of hydrogen evolution with the current density

reaching 0.1 mA/cm^2 at the potential of -0.87 V vs NHE. Electrolysis on **MnTPP-noncov(low)** at -1.09 V produced 0.2 μmol of CO in the course of a 2 h long experiment (Figure 4.6b, green trace). The faradic yield of CO reached a maximum of ~ 1.5% (Figure 4.6c, green trace). Interestingly, increase of the surface loading by two orders of magnitude led to a further drop of CO_2 reduction efficiency. Though the total amount of CO generated was the same 0.2 μmol, the FE(CO) decreased to 0.4 % (blue traces in the Figures 4.6b and 4.6c, respectively).

Thus, introduction of a covalent link between the immobilised complex and the electrode significantly suppressed the hydrogen evolution reaction and led to the increase of CO production rate. However, even in the case of **MnTPP-cov/1** the inherent low activity of MnTPP in CO_2ERR led to negligible amounts of CO produced in the reaction. Indeed, the Mn complex yielded much smaller amounts of CO compared to heterogeneous Fe and Co porphyrins.[53-55] Also, considering that the carbon cloth itself is capable of driving the CO_2ERR with low FE(CO), it is difficult to establish how much CO was produced on the support and on MnTPP itself.

To elucidate whether this low activity of MnTPP in the heterogeneous system is induced by the use of aqueous electrolyte or this is an inherent property of the complex, analysis of the CO_2ERR in the homogeneous system was performed as well. CV in dry DMF showed characteristic redox waves corresponding to the Mn^{III}/Mn^{II}, Mn^{II}/Mn^{I} and Mn^{I}/Mn^{0} (Figure 4.2c, black trace) the most negative of which becomes completely irreversible in the presence of CO_2 showing that $[Mn^0TPP]^{2-}$ quickly reacts with it (Figure 4.6d, violet trace). At the same time, the Mn^{II}/Mn^{I} wave has an intensity slightly higher than one electron meaning that the Mn^{I} complex has sufficient nucleophilicity to slowly react with CO_2 or traces of H_2O in the electrolyte. After addition of water to CO_2-saturated electrolyte the reversibility of this wave almost disappeared as well due to the reaction of $[Mn^{I}TPP]^-$ with H^+ and CO_2 though the peak cathodic current did not increase (Figure 4.6d, green trace). These observations gave grounds to believe that $[Mn^{I}TPP]^-$ and $[Mn^0TPP]^{2-}$ species may react with the species in the solution in two ways. First, they may act as weak electrocatalysts; however, the activity appears to be too low to induce a large reduction current as they are more prone to react with H^+ than CO_2 in good agreement with results obtained in heterogenous system. Another possibility is that MnTPP could irreversibly react with the substrate and the reduction current is wasted on complex decomposition instead.

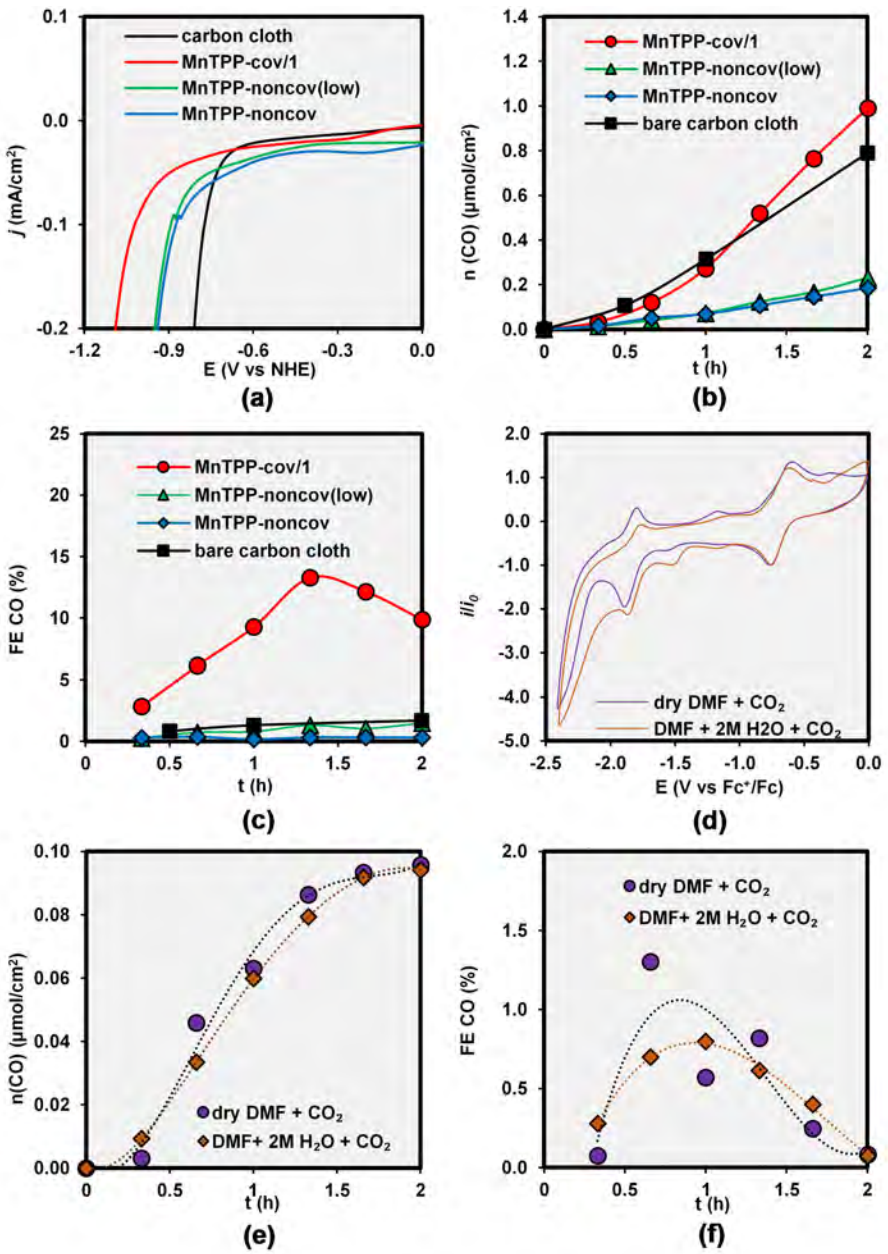

Figure 4.6. (a) LSVs obtained for bare carbon cloth (black trace), **MnTPP-cov/1** (red trace), **MnTPP-noncov** (blue trace) and **MnTPP-noncov(low)** (green trace); (b) amount of CO and (c) FE(CO) observed on the same materials during CPE under potential of - 1.09 V vs NHE. CO_2-saturated 0.5 M aqueous $KHCO_3$ was used as a supporting electrolyte in this heterogeneous system. (d) CVs of 2mM solution of MnTPP in CO_2-saturated DMF before (violet trace) and after (green trace) addition of 2 M H_2O. Scan rate 50 mV/s. (e) amount of CO and (d) FE(CO) measured during electrolysis of 2 mM MnTPP in CO_2-saturated DMF at -1.74 V vs Fc^+/Fc. Violet traces correspond to dry solvent and brown – to the one with 2 M of H_2O. 0.1 M TBAP was used as a supporting electrolyte in homogeneous system.

To elucidate the reaction mechanism, a prolonged electrolysis of homogeneous CO_2-saturated solution of MnTPP in DMF was performed at -1.74 V vs Fc^+/Fc (foot of the $[Mn^{II}TPP]/[Mn^{I}TPP]^-$ wave). A small amount of CO was detected as a sole CO_2 reduction as well with the cumulative production 2 times smaller than in an aqueous electrolyte with no noticeable MnTPP decomposition (Figures 4.6e-f, green curves). Interestingly, the CPE performed under the same potential in the presence of water shows a similar CO production rate and FE(CO) showing that the CO reduction rate most probably does not depend on the presence of proton donors. These experiments showed that $Mn^{I}TPP$ can react with CO_2, although it appears to be more selective towards hydrogen production rather than CO_2ERR. Moreover, even a small amount of CO present in the solution appears to be enough to coordinate to the metal centre and quench the CO_2ERR as evidenced by quick drop of FE(CO) by the end of 2 h long CPE. Catalysis by $[Mn^{0}TPP]^{2-}$ that might form via disproportionation of $[Mn^{I}TPP]^-$ or directly under potentials more negative than -2.0 V is highly unlikely due to instability of the Mn^0 complex. Indeed, CPE under -2.0 V vs Fc^+/Fc (foot of Mn^I/Mn^0 wave) was accompanied by severe catalyst decomposition which led to accumulation of a yellow precipitate on the surface of the carbon cloth and release of unmetalated ligand as evidenced by the isolation of free-base tetraphenylporphyrin from the reaction mixture (the structure was confirmed with ^{1}H NMR, Figure A26). Thus, the reductive current around Mn^I/Mn^0 redox transformation is based on the catalyst decomposition rather than on CO_2 reduction similar to the case of homogeneous CoTPP-catalysed CO_2ERR in DMF reported recently.[56]

4.3 Conclusions

To sum up, we immobilised covalently MnTPP onto carbon electrodes using electroreduction of the porphyrin diazonium salt with the following metalation of a surface-tethered ligand. Variation of electrodeposition time allows to conveniently tune the density of the organic layer on the surface and therefore to optimize the average Mn-Mn distance. After 5-min electrodeposition (**MnTPP-cov/5**) Γ_{EA} reaches the point where metal atoms are close enough to participate in multicentred electrochemical reactions to occur. This transition manifested itself in almost exclusive $4e^-$ ORR in alkaline solution at the potentials where the noncovalent analogue had a selectivity to H_2O formation of ~ 50 %. Also, as measured at -0.79 V vs NHE, the ORR current density on **MnTPP-cov/5** was 2.4 times higher than on **MnTPP-noncov**. Analysis of Tafel plots, impedance spectra and appearance of two diffuse reduction waves on LSVs and potential-dependant Koutecky-Levich plots suggest that the ORR on covalently

immobilised porphyrin most likely proceeds via a two-step reduction on Mn^{II} species where H_2O_2 is produced first and then reduced further to H_2O before it leaves the electrocatalyst layer. Meanwhile, the OER rate depends mainly on the amount of electrochemically active catalyst and heterogenisation method does not have a considerable effect on it. Finally, when tested in CO_2ERR, MnTPP shows generally poor activity both in homogeneous and heterogeneous systems. Indeed, even in non-aqueous electrolyte the amount of CO produced during prolonged CPE remains extremely low and if the potential is increased further to achieve Mn^{I}/Mn^{0} transformation, severe decomposition of the complex occurs.

Thus, activity and selectivity of Mn porphyrin-based catalysts in ORR could be conveniently tuned using different immobilisation methods providing a much greater degree of flexibility than the widely studied Pt/C and Ag/C catalysts. At the same time, the immobilisation mode appears to be irrelevant for OER and only the amount of the electrochemically active catalyst influences the reaction rate. At last, even though MnTPP has very low intrinsic activity in CO_2ERR, both the FE(CO) and the CO_2 reduction rate were noticeably higher when covalent link with the surface is introduced.

4.4 References

[1] Wang, C.-Y., Fundamental Models for Fuel Cell Engineering, *Chem. Rev.* **2004,** 104 (10), 4727-4766
[2] Subbaraman, R.; Tripkovic, D.; Chang, K.-C.; Strmcnik, D.; Paulikas, A. P.; Hirunsit, P.; Chan, M.; Greeley, J.; Stamenkovic, V.; Markovic, N. M., Trends in activity for the water electrolyser reactions on 3d M(Ni,Co,Fe,Mn) hydr(oxy)oxide catalysts, *Nat. Mater.* **2012,** 11, 550
[3] Leng, Y.; Chen, G.; Mendoza, A. J.; Tighe, T. B.; Hickner, M. A.; Wang, C.-Y., Solid-State Water Electrolysis with an Alkaline Membrane, *J. Am. Chem. Soc.* **2012,** 134 (22), 9054-9057
[4] Mo, J.; Kang, Z.; Retterer, S. T.; Cullen, D. A.; Toops, T. J.; Green, J. B.; Mench, M. M.; Zhang, F.-Y., Discovery of true electrochemical reactions for ultrahigh catalyst mass activity in water splitting, *Sci. Adv.* **2016,** 2 (11),
[5] Gasteiger, H. A.; Kocha, S. S.; Sompalli, B.; Wagner, F. T., Activity benchmarks and requirements for Pt, Pt-alloy, and non-Pt oxygen reduction catalysts for PEMFCs, *Appl. Catal. B* **2005,** 56 (1), 9-35
[6] Debe, M. K., Electrocatalyst approaches and challenges for automotive fuel cells, *Nature* **2012,** 486, 43
[7] Savéant, J.-M., Molecular Catalysis of Electrochemical Reactions. Mechanistic Aspects, *Chem. Rev.* **2008,** 108, 2348–2378
[8] Gewirth, A. A.; Varnell, J. A.; DiAscro, A. M., Nonprecious Metal Catalysts for Oxygen Reduction in Heterogeneous Aqueous Systems, *Chem. Rev.* **2018,** 118 (5), 2313-2339
[9] Fukuzumi, S.; Lee, Y.-M.; Nam, W., Mechanisms of Two-Electron versus Four-Electron Reduction of Dioxygen Catalyzed by Earth-Abundant Metal Complexes, *ChemCatChem* **2017,** 10 (1), 9-28
[10] Passard, G.; Dogutan, D. K.; Qiu, M.; Costentin, C.; Nocera, D. G., Oxygen Reduction Reaction Promoted by Manganese Porphyrins, *ACS Catal.* **2018,** 8 (9), 8671-8679
[11] Jung, J.; Liu, S.; Ohkubo, K.; Abu-Omar, M. M.; Fukuzumi, S., Catalytic Two-Electron Reduction of Dioxygen by Ferrocene Derivatives with Manganese(V) Corroles, *Inorg. Chem.* **2015,** 54 (9), 4285-4291
[12] Pegis, M. L.; Wise, C. F.; Martin, D. J.; Mayer, J. M., Oxygen Reduction by Homogeneous Molecular Catalysts and Electrocatalysts, *Chem. Rev.* **2018,** 118 (5), 2340-2391
[13] Meyer, T. J.; Sheridan, M. V.; Sherman, B. D., Mechanisms of molecular water oxidation in solution and on oxide surfaces, *Chem. Soc. Rev.* **2017,** 46 (20), 6148-6169
[14] Zhang, W.; Lai, W.; Cao, R., Energy-Related Small Molecule Activation Reactions: Oxygen Reduction and Hydrogen and Oxygen Evolution Reactions Catalyzed by Porphyrin- and Corrole-Based Systems, *Chem. Rev.* **2017,** 117 (4), 3717-3797
[15] den Boer, D.; Li, M.; Habets, T.; Iavicoli, P.; Rowan, A. E.; Nolte, R. J. M.; Speller, S.; Amabilino, D. B.; De Feyter, S.; Elemans, J. A. A. W., Detection of different oxidation states of individual manganese porphyrins during their reaction with oxygen at a solid/liquid interface, *Nat. Chem.* **2013,** 5, 621
[16] Masa, J.; Schuhmann, W., Systematic Selection of Metalloporphyrin-Based Catalysts for Oxygen Reduction by Modulation of the Donor–Acceptor Intermolecular Hardness, *Chem. Eur. J.* **2013,** 19 (29), 9644-9654
[17] Naruta, Y.; Sasayama, M.-A., Importance of Mn–Mn separation and their relative arrangement on the development of high catalase activity in manganese porphyrin dimer catalysts, *J. Chem. Soc., Chem. Comm.* **1994,** (23), 2667-2668
[18] Naruta, Y.; Sasayama, M.-a.; Sasaki, T., Oxygen Evolution by Oxidation of Water with Manganese Porphyrin Dimers, *Angew. Chem. Int. Ed.* **1994,** 33 (18), 1839-1841
[19] Shimazaki, Y.; Nagano, T.; Takesue, H.; Ye, B.-H.; Tani, F.; Naruta, Y., Characterization of a Dinuclear MnV=O Complex and Its Efficient Evolution of O2 in the Presence of Water, *Angew. Chem. Int. Ed.* **2004,** 43 (1), 98-100
[20] Sonoyama, N.; Kirii, M.; Sakata, T., Electrochemical reduction of CO2 at metal-porphyrin supported gas diffusion electrodes under high pressure CO2, *Electrochem. Comm.* **1999,** 1 (6), 213-216
[21] Furuya, N.; Koide, S., Electroreduction of carbon dioxide by metal phthalocyanines, *Electrochim. Acta* **1991,** 36 (8), 1309-1313
[22] Lu, G.-Q.; Wieckowski, A., Heterogeneous electrocatalysis: a core field of interfacial science, *Curr. Opin. Coll. Int.* **2000,** 5 (1), 95-100
[23] Costentin, C.; Robert, M.; Savéant, J.-M., Molecular catalysis of electrochemical reactions, *Curr. Opin. Electrochem.* **2017,** 2 (1), 26-31
[24] Sinha, S.; Aaron, M. S.; Blagojevic, J.; Warren, J. J., Electrocatalytic Dioxygen Reduction by Carbon Electrodes Noncovalently Modified with Iron Porphyrin Complexes: Enhancements from a Single Proton Relay, *Chem. Eur. J.* **2015,** 21 (50), 18072-18075
[25] Lei, H.; Liu, C.; Wang, Z.; Zhang, Z.; Zhang, M.; Chang, X.; Zhang, W.; Cao, R., Noncovalent Immobilization of a Pyrene-Modified Cobalt Corrole on Carbon Supports for Enhanced Electrocatalytic Oxygen Reduction and Oxygen Evolution in Aqueous Solutions, *ACS Catal.* **2016,** 6 (10), 6429-6437

[26] Costentin, C.; Dridi, H.; Savéant, J.-M., Molecular Catalysis of O2 Reduction by Iron Porphyrins in Water: Heterogeneous versus Homogeneous Pathways, *J. Am. Chem. Soc.* **2015,** 137 (42), 13535-13544
[27] Wei, P.-J.; Yu, G.-Q.; Naruta, Y.; Liu, J.-G., Covalent Grafting of Carbon Nanotubes with a Biomimetic Heme Model Compound To Enhance Oxygen Reduction Reactions, *Angew. Chem. Int. Ed.* **2014,** 53 (26), 6659-6663
[28] deKrafft, K. E.; Wang, C.; Xie, Z.; Su, X.; Hinds, B. J.; Lin, W., Electrochemical Water Oxidation with Carbon-Grafted Iridium Complexes, *ACS Appl. Mater. Interfaces* **2012,** 4 (2), 608-613
[29] Materna, K. L.; Rudshteyn, B.; Brennan, B. J.; Kane, M. H.; Bloomfield, A. J.; Huang, D. L.; Shopov, D. Y.; Batista, V. S.; Crabtree, R. H.; Brudvig, G. W., Heterogenized Iridium Water-Oxidation Catalyst from a Silatrane Precursor, *ACS Catal.* **2016,** 6 (8), 5371-5377
[30] Cheng, N.; Kemna, C.; Goubert-Renaudin, S.; Wieckowski, A., Reduction Reaction by Porphyrin-Based Catalysts for Fuel Cells, *Electrocatal.* **2012,** 3 (3), 238-251
[31] Baranton, S.; Bélanger, D., Electrochemical Derivatization of Carbon Surface by Reduction of in Situ Generated Diazonium Cations, *J. Phys. Chem. B* **2005,** 109 (51), 24401-24410
[32] Mahouche-Chergui, S.; Gam-Derouich, S.; Mangeney, C.; Chehimi, M. M., Aryl diazonium salts: a new class of coupling agents for bonding polymers, biomacromolecules and nanoparticles to surfaces, *Chem. Soc. Rev.* **2011,** 40 (7), 4143-4166
[33] Gross, A. J.; Bucher, C.; Coche-Guerente, L.; Labbé, P.; Downard, A. J.; Moutet, J.-C., Nickel (II) tetraphenylporphyrin modified surfaces via electrografting of an aryldiazonium salt, *Electrochem. Comm.* **2011,** 13 (11), 1236-1239
[34] Picot, M.; Nicolas, I.; Poriel, C.; Rault-Berthelot, J.; Barrière, F., On the nature of the electrode surface modification by cathodic reduction of tetraarylporphyrin diazonium salts in aqueous media, *Electrochem. Comm.* **2012,** 20, 167-170
[35] Rocklin, R. D.; Murray, R. W., Chemically modified carbon electrodes: Part XVII. Metallation of immobilized tetra(aminophenyl)porphyrin with manganese, iron, cobalt, nickel, copper and zinc, and electrochemistry of diprotonated tetraphenylporphyrin, *J. Electroanal. Chem. Interfacial Electrochem.* **1979,** 100 (1), 271-282
[36] Savéant, J.-M. In *Elements of Molecular and Biomolecular Electrochemistry*, John Wiley & Sons, Inc.: **2006**; pp 1-77
[37] Anariba, F.; Viswanathan, U.; Bocian, D. F.; McCreery, R. L., Determination of the Structure and Orientation of Organic Molecules Tethered to Flat Graphitic Carbon by ATR-FT-IR and Raman Spectroscopy, *Anal. Chem.* **2006,** 78 (9), 3104-3112
[38] Zhang, X.; Wu, Z.; Zhang, X.; Li, L.; Li, Y.; Xu, H.; Li, X.; Yu, X.; Zhang, Z.; Liang, Y.; Wang, H., Highly selective and active CO2 reduction electrocatalysts based on cobalt phthalocyanine/carbon nanotube hybrid structures, *Nature Comm.* **2017,** 8, 14675
[39] Bourrez, M.; Orio, M.; Molton, F.; Vezin, H.; Duboc, C.; Deronzier, A.; Chardon-Noblat, S., Pulsed-EPR Evidence of a Manganese(II) Hydroxycarbonyl Intermediate in the Electrocatalytic Reduction of Carbon Dioxide by a Manganese Bipyridyl Derivative, *Angew. Chem. Int. Ed.* **2014,** 53 (1), 240-243
[40] Gojković, S. L.; Gupta, S.; Savinell, R. F., Heat-treated iron(III) tetramethoxyphenyl porphyrin chloride supported on high-area carbon as an electrocatalyst for oxygen reduction: Part II. Kinetics of oxygen reduction, *J. Electroanal. Chem. Interfacial Electrochem.* **1999,** 462 (1), 63-72
[41] Baglia, R. A.; Zaragoza, J. P. T.; Goldberg, D. P., Biomimetic Reactivity of Oxygen-Derived Manganese and Iron Porphyrinoid Complexes, *Chem. Rev.* **2017,** 117 (21), 13320-13352
[42] Tong, L.; Göthelid, M.; Sun, L., Oxygen evolution at functionalized carbon surfaces: a strategy for immobilization of molecular water oxidation catalysts, *Chem. Comm.* **2012,** 48 (80), 10025-10027
[43] Li, F.; Li, L.; Tong, L.; Daniel, Q.; Göthelid, M.; Sun, L., Immobilization of a molecular catalyst on carbon nanotubes for highly efficient electro-catalytic water oxidation, *Chem. Comm.* **2014,** 50 (90), 13948-13951
[44] Ruther, R. E.; Rigsby, M. L.; Gerken, J. B.; Hogendoorn, S. R.; Landis, E. C.; Stahl, S. S.; Hamers, R. J., Highly Stable Redox-Active Molecular Layers by Covalent Grafting to Conductive Diamond, *J. Am. Chem. Soc.* **2011,** 133 (15), 5692-5694
[45] Chen, Z.; Higgins, D.; Chen, Z., Nitrogen doped carbon nanotubes and their impact on the oxygen reduction reaction in fuel cells, *Carbon* **2010,** 48 (11), 3057-3065
[46] Chai, G.-L.; Hou, Z.; Ikeda, T.; Terakura, K., Two-Electron Oxygen Reduction on Carbon Materials Catalysts: Mechanisms and Active Sites, *J. Phys. Chem. C* **2017,** 121 (27), 14524-14533
[47] Park, J.; Nabae, Y.; Hayakawa, T.; Kakimoto, M.-a., Highly Selective Two-Electron Oxygen Reduction Catalyzed by Mesoporous Nitrogen-Doped Carbon, *ACS Catal.* **2014,** 4 (10), 3749-3754
[48] Stephen, T.; Andrew, T.; C., J. D., A Consideration of the Application of Koutecký-Levich Plots in the Diagnoses of Charge-Transfer Mechanisms at Rotated Disk Electrodes, *Electroanal.* **2002,** 14 (3), 165-171
[49] Lim, B.; Jiang, M.; Camargo, P. H. C.; Cho, E. C.; Tao, J.; Lu, X.; Zhu, Y.; Xia, Y., Pd-Pt Bimetallic Nanodendrites with High Activity for Oxygen Reduction, *Science* **2009,** 324 (5932), 1302

[50] Demarconnay, L.; Coutanceau, C.; Léger, J. M., Electroreduction of dioxygen (ORR) in alkaline medium on Ag/C and Pt/C nanostructured catalysts—effect of the presence of methanol, *Electrochim. Acta* **2004,** 49 (25), 4513-4521
[51] Guo, J.; Hsu, A.; Chu, D.; Chen, R., Improving Oxygen Reduction Reaction Activities on Carbon-Supported Ag Nanoparticles in Alkaline Solutions, *J. Phys. Chem. C* **2010,** 114 (10), 4324-4330
[52] Lim, E. J.; Choi, S. M.; Seo, M. H.; Kim, Y.; Lee, S.; Kim, W. B., Highly dispersed Ag nanoparticles on nanosheets of reduced graphene oxide for oxygen reduction reaction in alkaline media, *Electrochem. Comm.* **2013,** 28, 100-103
[53] Maurin, A.; Robert, M., Noncovalent Immobilization of a Molecular Iron-Based Electrocatalyst on Carbon Electrodes for Selective, Efficient CO2-to-CO Conversion in Water, *J. Am. Chem. Soc.* **2016,** 138 (8), 2492-2495
[54] Maurin, A.; Robert, M., Catalytic CO2-to-CO conversion in water by covalently functionalized carbon nanotubes with a molecular iron catalyst, *Chem. Comm.* **2016,** 52 (81), 12084-12087
[55] Marianov, A. N.; Jiang, Y., Covalent ligation of Co molecular catalyst to carbon cloth for efficient electroreduction of CO2 in water, *Appl. Catal. B* **2019,** 244, 881-888
[56] Hu, X.-M.; Rønne, M. H.; Pedersen, S. U.; Skrydstrup, T.; Daasbjerg, K., Enhanced Catalytic Activity of Cobalt Porphyrin in CO2 Electroreduction upon Immobilization on Carbon Materials, *Angew. Chem.* **2017,** 129 (23), 6568-6572

CHAPTER 5. COVALENT IMMOBILISATION AND ELECTROCATLYTIC ACTIVITY OF COBALT PORPHYRIN IN CO_2ERR AND ORR

5.1 Introduction

As we noted in the Chapter 2 the activity of Co porphyrins is remarkable both in CO_2ERR and ORR. Interestingly, Co^I is a catalytically active form of complex in case of CO_2ERR only in aqueous medium where these complexes are not readily soluble. This is in strong contrast to homogeneous systems where the formation of highly reactive Co^0 species is required to drive CO formation.[1] In case of ORR the activity of Co binuclear porphyrin complexes was found to be dependent on the Co···Co separation and the interatomic distance could be tuned using various bridges between porphyrin cores, but a similar effect could be achieved by the creating of a dense layer of the complex on the surface.[2-4] Hence, the development of an effective heterogenisation technique is paramount for this class of catalysts.

Noncovalent electrode modification via drop-casting has been widely used for heterogenisation of Co macrocyclic complexes. As such, high activity of Co tetraphenylporphyrin (CoTPP) and Co phtalocyanine composites with carbon nanotubes (CNT) rely on high surface area of the CNT to maximize CO_2 reduction activity.[1, 5] Pyrene-appended Fe porphyrin makes use of π-π interactions between the CNT carbon plane and its pyrene unit.[6] Approaches based on incorporation of the porphyrin core into metal-organic frameworks (MOFs) [7-8] and covalent organic frameworks (COFs) [9-10] produced good catalysts with the latter yielding TON of up to $2.9 \cdot 10^5$ with an overpotential of 550 mV. Notwithstanding their utility, noncovalently immobilised catalysts may suffer from slow electron transfer and leaching due to weak connection to the electrode.[6, 11] Noncovalent immobilisation of the simplest Co porphin complex was found to trigger $4e^-$ ORR, most probably due to its small size, which positions the flat molecules in the face-to-face position.[4] However, for readily available CoTPP this effect was not observed.[2]

In turn, covalent attachment is a rather appealing option since a catalyst could be tethered to the electrode via a stable chemical bond assuring fast electron transfer onto the catalytically active centre and protecting material against physical damage in the conditions of severe effervescence. However, reports of covalently immobilised CO_2ERR catalysts are much scarcer due to more sophisticated preparation and so far, TONs/TOFs reported for covalently

tethered complexes have been quite low. As such, Fe hexahydroxyporphyrin was grafted to carbon nanotubes via an amide linker accumulating TON of 532 over 3 h in aqueous electrolyte at -1.06 V vs NHE.[12] In another example, Co porphyrin was attached to conductive diamond via a long 1,2,3-triazolyl-terminated alkyl chain. This hybrid electrode maintained a CO_2 reduction current after 103 cycles between -0.5 and -1.8 V vs Ag/Ag^+ in acetonitrile.[13] CO formation was unambiguously detected by FTIR; however, no TON was experimentally measured. The third example is covalent grafting of Co terpyridine onto glassy carbon with the following study of its activity in hydrogen evolution reaction and CO_2ERR in DMF.[14] Although in the presence of CO_2 the faradic current dropped to baseline levels within 30 min, the catalyst showed a TON in CO of 70. Notably, potentially explosive pure diazoniums salts have often been used as grafting agents.[12, 14-15] For ORR, covalent immobilisation of Co porphyrin incorporated into a COF-like structure based on graphene oxide, showed excellent $4e^-$ selectivity, however as there was no noncovalently immobilised analogue in this study, it is difficult to determine the exact cause of the dramatic shift in the reaction selectivity.[16]

In the present work, we endeavoured to attach covalently CoTPP to the surface of carbon cloth via a phenylene linker using electroreduction of the corresponding diazonium salt safely generated in situ. We assumed such a short conductive linker would enhance the rate of electron transfer onto the Co centre, impart higher stability to the resulting material and increase the surface concentration of the electrochemically active complex.[17] Furthermore, as on the example of Mn porphyrins we showed that it is possible to increase the contribution of $4e^-$ ORR pathway in the reaction mechanism, we sought to determine if a similar effect could be observed for Co analogues which normally behave as $2e^-$ ORR catalysts.[3] CoTPP was chosen as a catalyst since its great stability in CO_2ERR is well known (the cumulative TON of up to $2.9 \cdot 10^5$ was reported)[10] and compared to the Fe analogues CoTPP is more active in the aqueous medium as discussed in the section 2.5. It is also notable that the CoTPP is an excellent catalyst for the ORR as well, but the reaction proceeds predominantly via $2e^-$ mechanism and hence it would be highly desirable to trigger the $4e^-$ reduction pathway without any losses in terms of activity. As in the case of study on Mn porphyrinates, the choice of tetraphenylporphyrin core as a ligand was largely dictated by the fact that the synthetic procedure would furnish a covalently immobilised material with the catalyst structure identical to the one found in noncovalently heterogenised analogue.

5.2 Results and discussion

5.2.1 Immobilisation of CoTPP on carbon cloth

Covalently immobilised Co tetraphenylporphyrin (**CoTPP-cov/1**) was prepared using the multistep procedure as described in the Scheme 5.1. Diazotation of **TPP-NH₂** in aqueous trifluoroacetic acid (1:1) at -5°C generates **TPP-N₂⁺** and the following electroreduction at 0.0 V vs Ag/AgCl (3M KCl) in potentiostatic mode on a carbon cloth electrode furnishes a layer of covalently grafted porphyrin.[18-21] Introduction of the cobalt atom into surface-tethered porphyrin core was attained via treatment with 0.05 M solution of $Co(OAc)_2$ in DMF/CH_3COOH (9:1) at 120 °C with the formation of hybrid material **CoTPP-cov/1**.[22] A scanning electron microscopy (SEM) study revealed the lack of visible crystalline deposits and scattered thin patches of polymerized material (Figure 5.1a). Energy dispersive X-ray spectroscopy (EDS) mapping shows uniform distribution of nitrogen and Co throughout the surface of carbon fibres confirming good coverage with Co porphyrinate (Figure 5.1b). Also, we believe that the rather positive potential used for grafting allowed to mitigate overreduction of transient radicals and achieve their connection with the carbon surface.[15, 21]

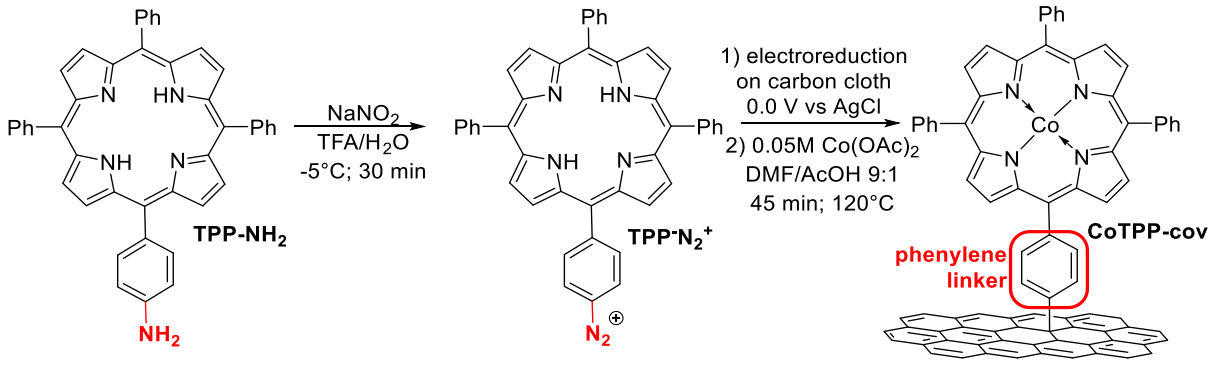

Scheme 5.1. Preparation of covalently immobilised Co tetraphenylporphyrin (**CoTPP-cov/1**).

To compare properties of the same catalyst in noncovalent immobilisation mode we prepared electrodes via drop-casting of CoTPP solution in DMF onto the carbon cloth (denoted as **CoTPP-noncov**). The total amount of the deposited complex was $8 \cdot 10^{-8}$ mol/cm^2 unless otherwise noted.

Raman spectroscopy and electrochemical studies were performed to confirm the formation of the covalently immobilised porphyrin layer. Cyclic voltammetry (CV) in dry oxygen-free DMF containing 0.1 M of tetrabutylammonium hexafluorophosphate (TBAP) as supporting electrolyte (Figure 5.1c, red trace) showed typical responses of Co^{II}/Co^{I} and Co^{I}/Co^{0} redox

pairs at -1.30 V and -2.39 V vs Fc^+/Fc respectively. These values are close to the formal redox potentials of $[Co^{II}TPP]/[Co^{I}TPP]^-$ and $[Co^{I}TPP]^-/[Co^{0}TPP]^{2-}$ in homogeneous solution (-1.31 and -2.42 V vs Fc^+/Fc, Figure 5.1c, blue trace). The covalent nature of the complex immobilisation could be inferred from the fact that the **CoTPP-noncov** is easily washed away from the electrode with DMF leaving pristine carbon fabric without any characteristic redox behavior. In turn, removal of electrodeposited complex could not be attained by any means without destruction of the electrode. CV measurements in degassed aqueous 0.5 M KOH gave a surface loading of the electrochemically active complex (Γ_{EA}) of ~ $6.9 \cdot 10^{-10}$ mol/cm^2 with clear linear correlation between peak current and potential scan rate (Figure 5.1d-e). Values of Γ_{EA} found by integration of the reduction wave using Equation 3.1 and from the reoxidation peak currents through Equation 3.2 are in good agreement.

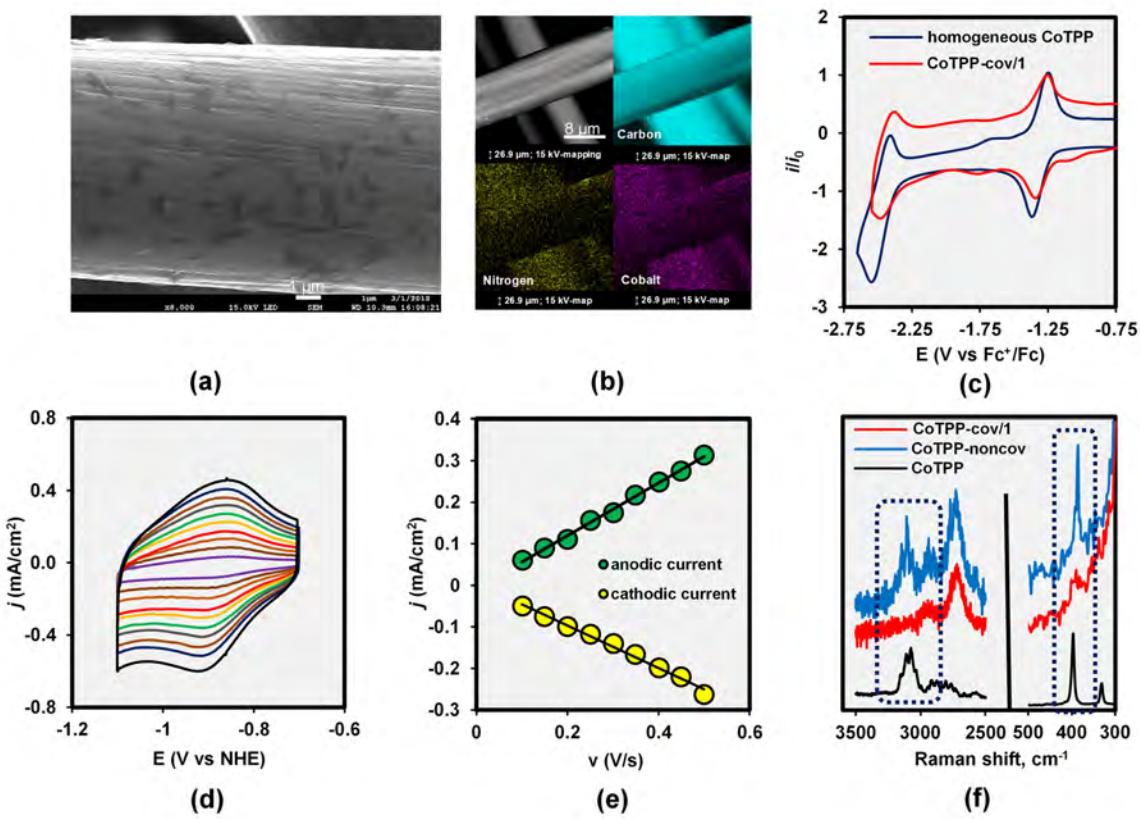

Figure 5.1. (a) SEM imaging and (b) EDS mapping of **CoTPP-cov/1**; elements shown are: C (cyan), N (yellow) and Co (violet). (c) CV of CoTPP and **CoTPP-cov/1** in DMF containing 0.1 M of TBAP as a supporting electrolyte, scan rate 100 mV/sec, currents are normalized to the Co^{II}/Co^{I} reoxidation peak; (d) dependence of CV shape and (e) peak current density on the potential scan rate in degassed 0.5 M aqueous KOH electrolyte; (f) Raman spectra of **CoTPP-cov/1**, **CoTPP-noncov** and solid CoTPP. TBAP: tetrabutylammonium hexafluorophosphate.

Raman spectra provided additional evidence of CoTPP formation on the surface (Figure 5.1f). Since retention of signature signals is expected upon immobilisation, a band at 385 cm^{-1} found in the spectra of **CoTPP-cov/1** and **CoTPP-noncov** could be identified as the strongest peak of the CoTPP spectrum.[5, 23] Notably, both for **CoTPP-noncov** and **CoTPP-cov/1** the peak is shifted compared to the unsupported complex by 9 cm^{-1} and in the latter case it is more diffuse. Also, a group of bands corresponding to C-H vibrations between 3000 and 3200 cm^{-1} is clearly visible in the spectra of **CoTPP-noncov** and free CoTPP does not appear in the case of **CoTPP-cov/1** (Figure 5.1f). Overall, changes in CoTPP Raman spectra upon attachment to the carbon support could be interpreted as a result of strong electronic interactions with its surface.[5] [24]

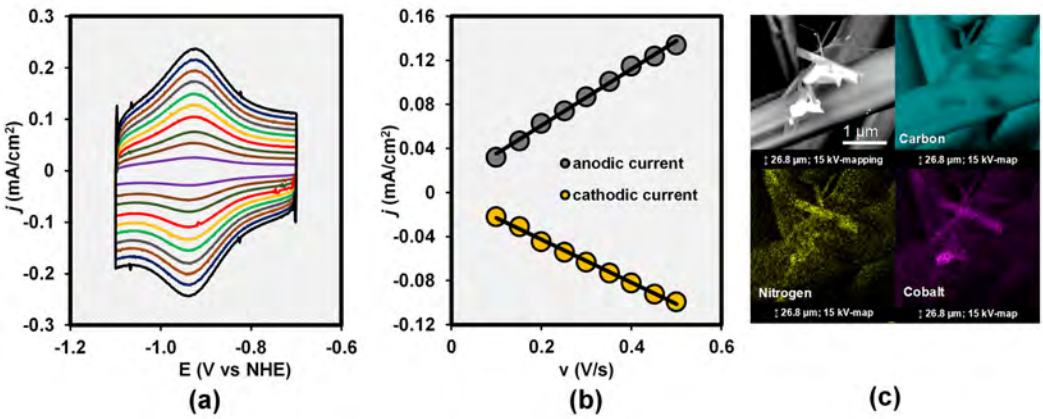

Figure 5.2. (a) CV of CoTPP-noncov on a carbon cloth electrode and (b) anodic and cathodic peak currents of Co^{I}/Co^{II} redox pair in 0.5 M degassed KOH at various scan rates; (c) SEM image and EDS mapping of **CoTPP-noncov**.

Regarding **CoTPP-noncov**, the CV response of the reversible redox couple $[Co^{II}TPP]/[Co^{I}TPP]^{-}$ in degassed 0.5 KOH was also used to calculate Γ_{EA}. Clearly, only $2.9 \cdot 10^{-10}$ mol/cm^2 or 0.36 % of all deposited complex is electrochemically active (Figure 5.2a). Typical for heterogeneous systems, a linear dependence of peak current on the potential scan rate is clearly seen and Γ_{EA} calculated by integration of the reduction wave correlates with the value obtained from the peak reoxidation current (Figure 5.2b). Representative SEM imaging of the resulting material revealed formation of flaky crystals greatly segregated on the edges of carbon cloth (Figures 5.2c, A27). EDS mapping showed high concentrations of cobalt and nitrogen in these aggregates with uniform distribution of these elements across other parts of the surface (Figure 5.2c). Clearly, most of the area bears uniformly adsorbed layer of CoTPP while crystals are formed by the material left after surface saturation.

We also estimated the average surface area occupied by a single porphyrin unit. The ratio of the electrochemically active surface area (S_{EA}) to the geometric area (SG) for carbon cloth was found to be 2.6 using double layer capacitance (DLC) measurements as shown in the Figure A29. Considering Γ_{EA} of $6.9 \cdot 10^{-10}$ mol/cm^2, each porphyrin moiety in **CoTPP-cov/1** on average takes 0.4 nm^2 while this value for **CoTPP-noncov** is 0.9 nm^2. These values give grounds to believe that we deal with a thin multilayer rather than with a monolayer on the surface of **CoTPP-cov/1** and **CoTPP-noncov** as well.

Additionally, the immobilisation mode considerably affects the double layer capacitance. As measured in 0.1 M KOH electrolyte, carbon cloth and **CoTPP-noncov** have a DLC of ~ 289 and 219 μF/cm^2, respectively (Figures A16 and A29 respectively). We believe the organic film in noncovalent immobilisation mode is quite permeable and it is possible for electrolyte to reach the electrode surface under the layer of complex while a 70 μF/cm^2 drop is rather caused by the presence of microcrystals isolating the carbon from the electrolyte. In turn, the DLC of **CoTPP-cov/1** is 391 μF/cm^2 (Figure A29) which is 102 μF/cm^2 higher than that of the bare carbon fabric showing that the electrodeposited layer of hydrophobic porphyrin is quite dense as the capacitance increase comes from the diffusion limitations imposed on solvated ions by organometallic moieties. [25]

To sum up, we immobilised Co porphyrin on the surface of carbon cloth in covalent and noncovalent modes. Carbon fibers are uniformly covered with the redox active layer of Co porphyrinate in both cases as clearly evidenced by electrochemical studies and Raman spectra. Covalent ligation of the porphyrin core to the surface of carbon cloth could be inferred from the facts that the immobilised complex in **CoTPP-cov/1** is not soluble in organic solvents and appear to closer interact with carbon fibers than in **CoTPP-noncov** which results in higher a DLC capacitance.[25] In the following study we consider values of Γ_{EA} as the active amount of complex taking part in CO_2ERR (Figures 5.1c and 5.2a).

5.2.2 Catalytic activity of CoTPP in CO_2ERR

CV was used to assess the overall activity of CoTPP in both immobilisation modes. Voltammograms showed poorly defined irreversible reduction peaks heavily overlapped with H^+ discharge (Figures 5.3a-b). A characteristic increase of the reduction current and shift of its onset towards more positive potentials upon saturation of the electrolyte with CO_2 were clearly observed as well.[10] As such, for **CoTPP-noncov** in degassed electrolyte the reduction current of 1 mA/cm^2 was attained at -0.99 V vs NHE while in the presence of CO_2 the same

value was reached at -0.92 V (Figure 5.3a). Comparison of **CoTPP-noncov** and **CoTPP-cov/1** shows that the overall activity of the latter is considerably higher. As measured at -1.0 V, the faradic current in CO_2-saturated electrolyte rose from 1.7 to 4.7 mA/cm^2 with the introduction of the covalent link (Figure 5.3a, red trace and Figure 5.3b, blue trace). Interestingly, CV of an electrode bearing $8\cdot10^{-10}$ mol/cm^2 of CoTPP (the amount is similar to Γ_{EA} of **CoTPP-cov/1**) was close to the one recorded for bare carbon cloth (Figure 5.3b, violet trace). An increase of surface loading to $1.6\cdot10^{-7}$ and $2.4\cdot10^{-7}$ mol/cm^2 did not improve the catalytic activity thus additionally proving saturation of the carbon surface with CoTPP (Figure 5.3b, green and brown traces, respectively). To confirm the results obtained from the analysis of CV curves, 4 h long electrolyses at -1.10 V (η = 550 mV) were undertaken. **CoTPP-cov/1** exhibited a much higher CO production rate of 82 μmol/cm^2 with the FE(CO) of 71 % and a current density of ~ 1.5 mA/cm^2 while **CoTPP-noncov** produced only 40 μmol/cm^2 of CO with FE(CO) of 52 % and a current density of ~ 1 mA/cm^2 (Figure 5.3c-e, red and blue traces, respectively). In good agreement with CV data, a decrease of the complex loading to $8\cdot10^{-10}$ mol/cm^2 led to a sharp drop of CO_2 reduction efficiency to 1.9 μmol/cm^2 with FE(CO) of 5 % only (Figures 5.3c-e, violet traces). Bare carbon cloth also produces 1.7 μmol of CO with FE(CO) of 1.7 %, but immobilisation of the porphyrin layer almost completely suppresses its activity (Figure A30a). Also, the NMR analysis of the electrolytes after 4 h long electrolyses failed to detect the formation of any liquid products such and methanol or formate in good agreement with the earlier reports.

Encouraged by the results of the preliminary evaluation, we performed a series of 30 min electrolyses at potentials between -1.00 and -1.20 V vs NHE. The aim of this electrokinetic study was to optimize the electrode potential in CO_2ERR, gain insight into the influence of the covalent bond with the electrode on the reaction mechanism and clarify the nature of active sites responsible for concurrent hydrogen evolution. As clearly seen from Figure 5.4a, the total amount of CO produced by **CoTPP-cov/1** is much higher at all potentials reaching 16.1 μmol/cm^2 at -1.20 V as opposed to **CoTPP-noncov** which yields 7.1 μmol/cm^2 under the same conditions.

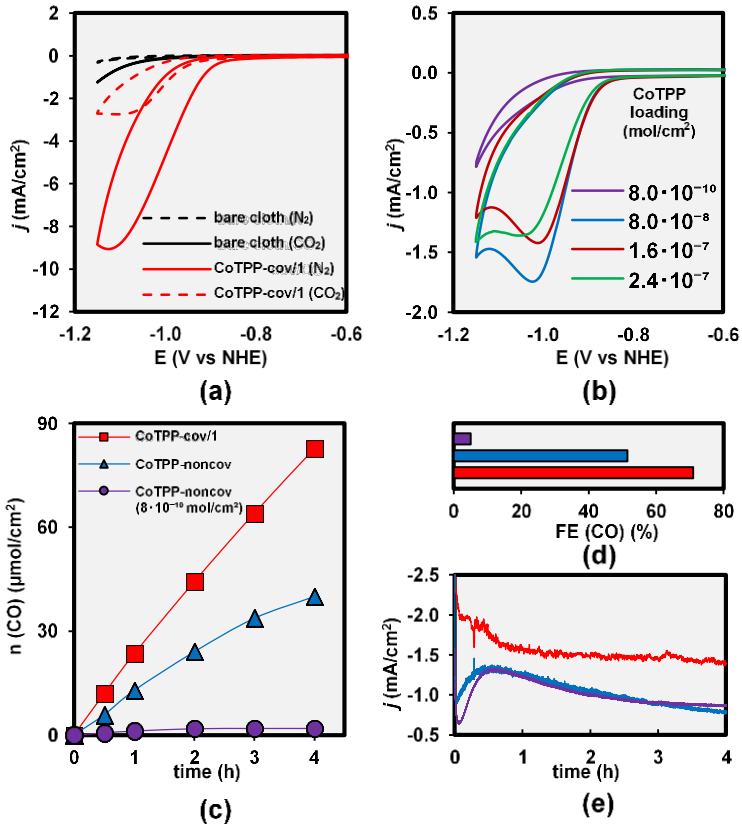

Figure 5.3. (a) CVs of **CoTPP-cov/1** in N_2- and CO_2-purged aqueous electrolyte, CVs of bare carbon cloth are shown for clarity; (b) CV traces of **CoTPP-noncov** with the variable amount of noncovalently immobilised CoTPP in CO_2-saturated electrolyte; (c) total amount of CO, (d) FE(CO) and (e) current densities observed during 4 h long controlled potential electrolyses (CPE) at -1.10 V vs NHE in CO_2-saturated electrolyte. Electrolyte: 0.5 M $KHCO_3$ in all cases, potential scan rate is 100 mV/s.

Although the better overall CO evolution rate is not surprising considering the higher amount of electrochemically active complex in **CoTPP-cov/1**, a striking difference between immobilisation modes becomes apparent from the comparison of TOF values (Figure 5.4a). At the lowest studied potential of -1.00 V **CoTPP-cov/1** has TOF of 4.8 s^{-1} which is 2.4 times higher than that of **CoTPP-noncov**. However, at the potentials more negative than -1.10 V the difference in per site activity is less pronounced and TOF reaches 13 s^{-1} at -1.20 V in both cases. Clearly, the covalent ligation of the catalyst to the carbon surface markedly increases the CO_2ERR rate at low potentials.

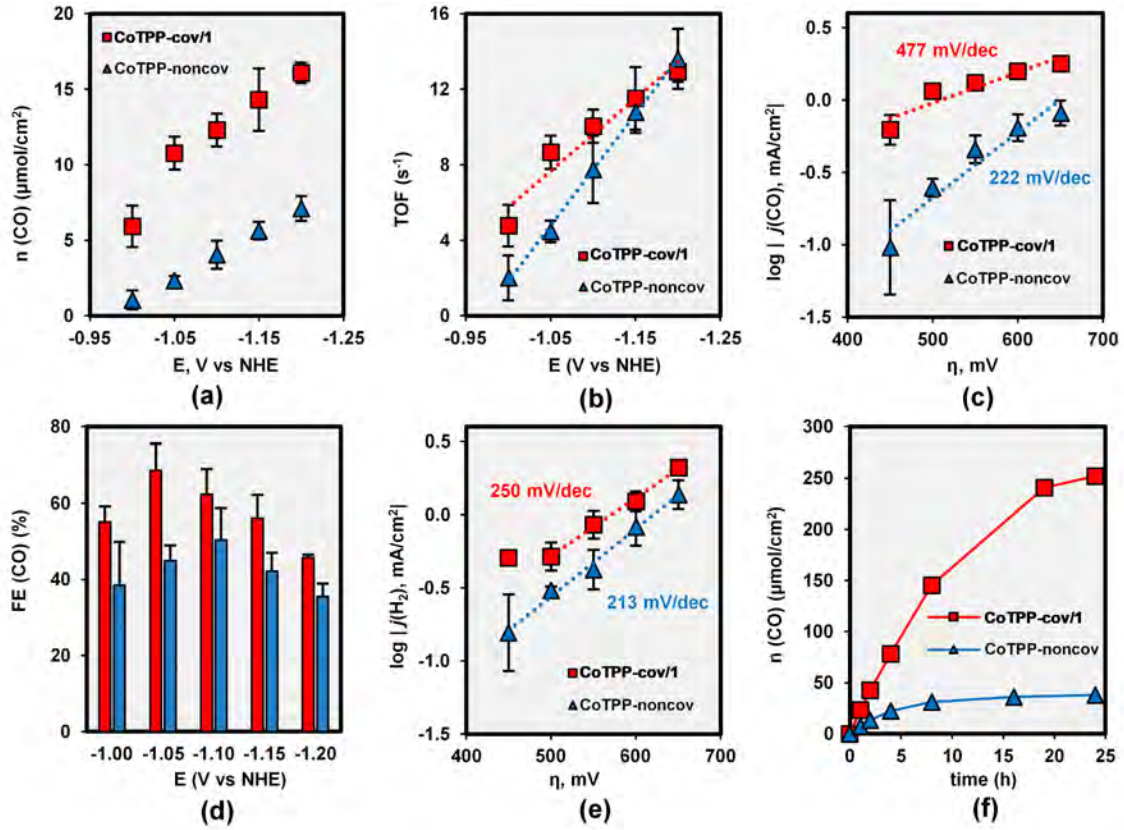

Figure 5.4. (a) total amount of CO produced and (b) TOF observed for CoTPP in both immobilisation modes as a function of the applied potential; (c) Tafel plot of CO_2ERR; (d) FE(CO); (e) Tafel plot of H_2 evolution. Experiments were performed as 30 min runs in CO_2-saturated 0.5 M aqueous $KHCO_3$; measured values and standard deviation bars represent average of three measurements; (d) total amount of CO obtained during 24 h long electrolysis at -1.05 V vs NHE.

To elucidate factors affecting the reaction speed, we plotted the logarithm of the average CO_2 reduction current density against overpotential (Figure 5.4c). For **CoTPP-noncov**, the Tafel plot has the slope of 222 mV/dec. This value is generally consistent with 255 mV/dec reported by Hu et al for the CoTPP-CNT composite,[1] but considerably higher than 165 mV/dec found for Co porphyrin embedded in MOF.[7] In strong contrast to **CoTPP-noncov**, for **CoTPP-cov/1** the slope is 477 mV/dec that is close to 470 mV/dec reported by Lin et al for CoTPP-based COF.[10] Also, the current-overpotential relationship follows Ohm's law rather than the Tafel's and analysis of earlier works shows similar behaviour for other macrocyclic catalysts containing a Co atom.

One could clearly see that the kinetic behaviour of **CoTPP-cov/1** and **CoTPP-noncov** are distinctively different. Although CO_2ERR is a complex multistep process,[26-27] the

following observations provide important clues: (i) the Tafel plot steepness drops with the introduction of a conjugated linker between porphyrin and electrode; (ii) the TOF at the potentials close to that of the reversible Co^{I}/Co^{II} redox couple substantially increases upon introduction of a conductive linker (iii) CO evolution kinetics shows apparent deviation from logarithmic behaviour coupled with the absence of curve flattening at high overpotentials. Clearly, the diffusion polarization could not be a limiting factor as otherwise the line flattening would be evident while purely electrochemical kinetics should lead to an exponential rise of the CO_2ERR curve.[28] Thus, we conclude that the CO formation reaction is fast compared to the speed of the Co^{I}TPP species regeneration and the electron transfer onto the complex is a primary rate-limiting step at the potentials more positive than -1.10 V vs NHE. It appears that this process is responsible for the observed resistance polarization and the π-system of the phenylene anchoring group significantly improves the Co^{II} to Co^{I} transformation. Meanwhile, more negative bias renders the electron transfer from the electrode to the catalyst fast enough regardless of the immobilisation mode and either CO extrusion or nucleophilic attack on CO_2 becomes the slowest process of the catalytic cycle which manifests itself in merging of TOF curves (Figure 5.4b).

FE(CO) is also dependent on the applied potential (Figure 5.4d). The highest average FE(CO) of 67 % for **CoTPP-cov/1** was achieved at -1.05 V. However, this value for **CoTPP-noncov** was only 50 % at -1.10 V, i.e. at 50 mV more negative electrode bias. Regarding the dependence of FE(CO) on the electrode potential, two distinctively different mechanisms could lead to simultaneous formation of gases: both are produced solely on CoTPP or CO forms on the catalyst and H_2 on the support. Analysis of water discharge kinetics on **CoTPP-cov/1** and **CoTPP-noncov** reveals a clear logarithmic dependence of the hydrogen evolution current on the potential (Figure A32). Tafel plots derived from these curves are rather parallel having slopes of 213 mV/dec for **CoTPP-cov/1** and 250 mV/dec for **CoTPP-noncov** (Figure 5.4e)**.** Although H^+ reduction measured on the bare carbon cloth has a slope of 105 mV/dec (Figure A31), this difference is expected considering that around half of the current is spent on CO_2ERR. Based on this, the carbon fabric is responsible for concurrent H_2 production while CoTPP itself has selectivity to CO_2 of not less than 91 % as measured by Hu et al.[1] Thus, FE(CO) is defined by the superposition of H_2 evolution kinetics which is governed by the exponential law and that of CO_2ERR that is rather a function of the amount of accessible catalyst, its nature and the rate of electron transfer from the electrode surface onto the

catalytically active centre. Hence, the point of the highest FE(CO) corresponds to the balance where the CO_2ERR is already fast and water discharge is still slow.

Finally, we studied the long-term performance of CoTPP-modified electrodes under a potential of -1.05 V vs NHE where **CoTPP-cov/1** showed the highest FE(CO). By the end of 24 h long electrolysis **CoTPP-cov/1** produced 252 μmol/cm^2 of CO as opposed to **CoTPP-noncov** with the overall CO production of 38 μmol/cm^2 (Figure 5.4d). The cumulative TON of **CoTPP-cov/1** was calculated to be $3.9 \cdot 10^5$ while that of **CoTPP-noncov** was $1.3 \cdot 10^5$ only (Figure A33a). The FE(CO) for **CoTPP-cov/1** reached 81 % and the catalyst maintained a high FE(CO) for at least 8 h (Figure A33b). Clearly, the TON observed for **CoTPP-cov/1** was 3 times higher with better FE(CO) which means that covalent immobilisation does improve the overall stability of the electrode material. However, by the end of electrolysis the FE(CO) and TOF dropped in both cases due to changes in porphyrin structure.[1] Based on these observations, we concluded that more than one mechanism is responsible for the catalyst deactivation. Strong bond with the electrode surface does prevent such phenomena as leaching and recrystallisation while the stability of the complex itself is largely unaffected by the heterogenization mode.

Table 5.1. **Comparison of heterogeneous metalloporphyrin catalysts operating in aqueous medium.**

Entry	Catalyst	V vs NHE	Electrolyte	FE(CO), %	TOF, s^{-1}	Ref.
1	**CoTPP-cov/1**	-1.05	0.5 M $KHCO_3$	67	8.3	This work
2	**CoTPP-noncov**	-1.05	0.5M $KHCO_3$	45	4.4	This work
3	CoTPP/CNT	-1.10	0.5M $KHCO_3$	91	2.75	[1]
4	COF-367-Co	-1.09	0.5M $KHCO_3$	91	0.56	[10]
5	COF-367-Co	-1.09	0.5M $KHCO_3$	40	2.6	[10]
6	CAT_{Pyr}/CNT	-1.03	0.5M $NaHCO_3$	93	0.04	[6]
7	CAT_{CO2H}	-1.06	0.5M $NaHCO_3$	86	0.05	[12]

Compared with earlier reports concerning CoTPP-based catalysts, TOF values obtained in our work both for **CoTPP-cov/1** and **CoTPP-noncov** (Table 1, entries 1 and 2) are clearly higher. As not all noncovalently deposited complex is electrochemically active, in case of CoTPP/CNT hybrid this difference is most likely due to the fact that we used Γ_{EA} values instead of total catalyst loading (Table 1, entry 3).[1] In case of COFs the resulting TOF most probably is affected by CO_2 diffusion limitations within porous framework structure.[10] At the same time, an estimation of surface loading for Fe counterparts was performed in the same manner and the catalytic activity of our **CoTPP-cov/1** is ~ 200 and ~160 times higher than that of CAT_{Pyr} and CAT_{CO2H} respectively (Table 1, entries 6 and 7).[6, 12] Although the average

FE(CO) that we measured in our work is somewhat lower than that described in previous reports, it is the result of the carbon fabric being used as a support instead of CNTs.

5.2.3 Catalytic activity of CoTPP in ORR

Next, the activity of Co porphyrin was studied in the oxygen reduction reaction. In the first step of our investigation we endeavoured to assess the catalytic activity and stability of CoTPP in acidic (0.5 M H_2SO_4), neutral (0.1 M $KClO_4$) and alkaline (0.1 M KOH) media. CV and LCV measurements were performed to evaluate the overall activity while Tafel analysis of linear scans was employed to obtain kinetic information. It should be noted that for the initial screening of the reaction conditions we employed **CoTPP-noncov** and based on these results the activity of covalently immobilised electrodes was studied. Also, we intentionally avoided the use of Nafion resin for immobilisation in order to observe the intrinsic activity of the complex as otherwise slow diffusion of H_2O_2 through the layer of polymer might have interfered with the kinetic measurements.

The general activity of CoTPP in ORR was assessed using CV. The CV study of **CoTPP-noncov** in alkaline medium (Figure 5.5a, black trace) showed well-defined quasi-reversible redox couple at 0.02 V vs NHE. A similar behaviour was observed in a neutral electrolyte, however the intensity of reoxidation wave significantly decreased and the $E^{1/2}$ shifted to 0.07 V bs NHE and a further increase of pH led to a complete disappearance of the reoxidation peak. This behaviour could be explained by the formation of the HO_2^- anion that could be transformed back to O_2 upon reversed scan. Importantly, the variation of the CV scan rate showed a linear dependence of the peak current on the square root of the scan rate which is typical for homogeneous systems (Figure A34). Thus, this is indeed O_2 transformation that is responsible for this redox couple as extremely low solubility of CoTPP would furnish a typical heterogeneous system with nonlinear line shape.[29]

A further study of the ORR using LSV showed that indeed the onset of the reduction current (as measured at 0.1 mA/cm^2) shifted from 0.05 V at pH = 13 to 0.13 V at pH = 7 and further to 0.53 V at pH = 0 (Figure 5.5b). This drift of the current onset corresponds to 13 mV shift per unit of pH in alkaline medium which quickly increases to 67 mV/pH in neutral and acidic electrolytes. This observation gives grounds to believe that the reaction furnishes molecular H_2O_2 in acidic medium as for normal H_2O_2 or H_2O formation the theoretically expected value would be 59 mV/pH which is quite close to the experimentally recorded value. At the same time, in alkaline solutions the ORR shows an anomalously low dependence on pH. Indeed,

even considering the participation of one H^+ in the reaction mechanism would furnish the slope of 30 mV/dec. Thus, this deviation from the thermodynamically expected value most probably could be interpreted as a result of a mixed mechanism of ORR furnishing the HO_2^- anion and either the $\cdot O_2^-$ anion radical or the $HO_2\cdot$ radical that can diffuse into the solution and quickly react with O_2 thus giving rise to a mechanism resembling homogeneous redox catalysis described by Savéant et al.[30]

Further investigation of the reaction mechanism using Tafel analysis (Figure 5.5c) shows a quick increase of the slope with the increase of pH. As such, in acidic medium the slope is 105 mV/dec which correlates well with the expected 118 mV/dec value for a first single electron transfer being the rate-determining step. Further, in neutral electrolyte the plot slope changes to 58 mV/dec which is close to the value expected for the $2e^-$ electron transfer as a rate-determining step. This could be the result of proton-coupled electron transfer with the catalyst going through the Co^{II}/Co^{IV} redox cycle. Finally, the slope reaches 45 mV/dec in alkaline medium. This value correlates well with the mechanism where the transfer of the second electron is a rate-determining step.[31] Our conclusions agree well with the theory of multielectron transfer described by Koper which implies the highest probability of proton-coupled electron transfers to the systems with pH close to the pK_a of reactants and products.[32]

To evaluate the viability of the reaction pH, we performed an express study of the catalyst stability under various pH values (Figure 5.5d-f). In this series of experiments the **CoTPP-noncov** electrode was subject to 500 cycles in O_2-saturated electrolyte under various pH. Clearly, in case of an acidic medium the current onset gradually shifts towards more negative potentials and the appearance of new peaks was recorded which might stem from oxidation of CoTPP or carbon cloth support (Figure 5.5d). In neutral medium, the stability appears to be higher, however, a similar effect of reduction current onset drift was observed. Interestingly, the intensity of the reoxidation peak also quickly decreased in this case which is most probably the result of CoTPP decomposing to new products (Figure 5.5e). Finally, only in alkaline medium CoTPP showed good stability without any significant drift of the peak potentials both for reduction and oxidation waves (Figure 5.5f). Based on these observations, the following studies were performed in 0.1 M KOH to assure stability of the electrocatalyst.

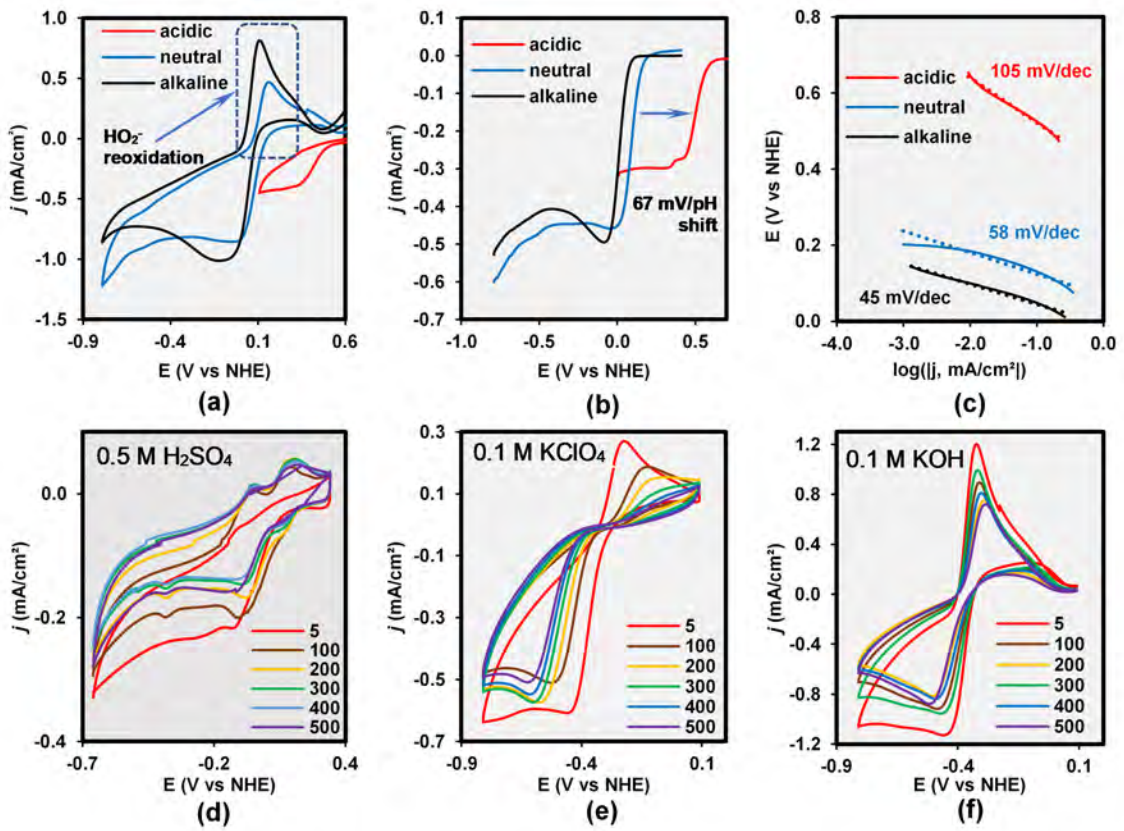

Figure 5.5. (a) CVs, (b) LSVs and (c) corresponding Tafel plots of **CoTPP-noncov** in O_2-saturated 0.5 M H_2SO_4 (red trace), 0.1 M $KClO_4$ (blue trace) and 0.1 M KOH (black trace). CV and LSV scan rates 50 mV/s and 10 mV/s respectively. (d) – (f) stability study of **CoTPP-noncov** as a function of the solution pH.

Next, we investigated the influence of covalent immobilisation of CoTPP activity and selectivity of ORR in alkaline medium. LSV study confirmed that the immobilisation mode had little effect on the reduction current onset and the difference between prolonged TPP electrodeposition times appears to minor (Figure 5.6a). However, the current onset is largely defined by the nature of the catalyst rather than by its heterogenisation mode and thus the experimental evidence falls in line with the theoretically expected results. At the same time, we found that the diffusion-limited current was increasing steadily. Indeed, as measured at -0.6 V vs NHE ORR current for **CoTPP-cov/1** was 0.41 mA/cm^2 which increased to 0.52 mA/cm^2 for **CoTPP-cov/5** and to 0.63 mA/cm^2 on **CoTPP-cov/10**. The latter observation is of high importance as this may signify that the reaction transfers more electrons while consuming the same amount of substrate.

Further, a dramatic difference between covalently and noncovalently immobilised complexes is evident from the CV study. Indeed, even though the **CoTPP-cov/x** electrodes exhibit similar

onset of the reduction current compared to **CoTPP-noncov** around 0.00 V vs NHE (Figure 5.6b), they show significantly reduced intensity of HO_2^- reoxidation peak that could possibly mean a higher contribution of the $4e^-$ reduction pathway as more of the peroxide is consumed during reductive stage of the experiment. Further, the heterogenisation mode drastically changed the slope of Tafel slope (Figure 5.6c). Indeed, while **CoTPP-noncov** showed 45 mV/dec slope, the steepness for **CoTPP-cov/x** decreased to 82 mV/dec for **CoTPP-cov/10**, 86 mV/dec for **CoTPP-cov/1** and 102 mV/dec for **CoTPP-cov/5**. This change falls in line with the change of the reaction mechanism from $1e^-$ transfer to $2e^-$ transfer being a predominant mechanism. However, the deviation from expected 59 mV/dec most probably stem from the fact that the $1e^-$ transfer is still present and thus interferes with the reaction mechanism.

Further, to confirm that the covalent immobilisation of the complex could increase the rate of H_2O_2 reduction forming in the course of ORR, we performed a series of CV experiments in 0.05 M alkaline solution of H_2O_2 (Figure 5.6d). Indeed, the peak reduction current for **CoTPP-noncov** was 1.4 mA/cm^2 which increased to 3.1 mA/cm^2 for **CoTPP-cov/1** and rose further to 3.4 mA/cm **for CoTPP-cov/5** and **CoTPP-cov/10**. Thus, with longer electrodeposition time the activity of covalently immobilised CoTPP in H_2O_2 dramatically increases and amounted to increase by the factor of 2.4. Moreover, we noted that under more negative potentials this difference becomes even more significant, especially for **CoTPP-cov/5** and **CoTPP-cov/10** for which the H_2O_2 reduction current reached 11.1 and 12.0 mA/cm^2 that is 2.9 times higher than for **CoTPP-noncov**. Thus, these observations gave grounds to believe that it is possible to enhance the contribution of $4e^-$ reduction mechanism using prolonged electrodeposition time. Interestingly, H_2O_2 reduction appears to be quasireversible on all the electrodes in question and agrees well with the $E^{1/2}$ obtained for ORR thus additionally confirming that the assignment of the reoxidation peak to HO_2^- to O_2 was correct.

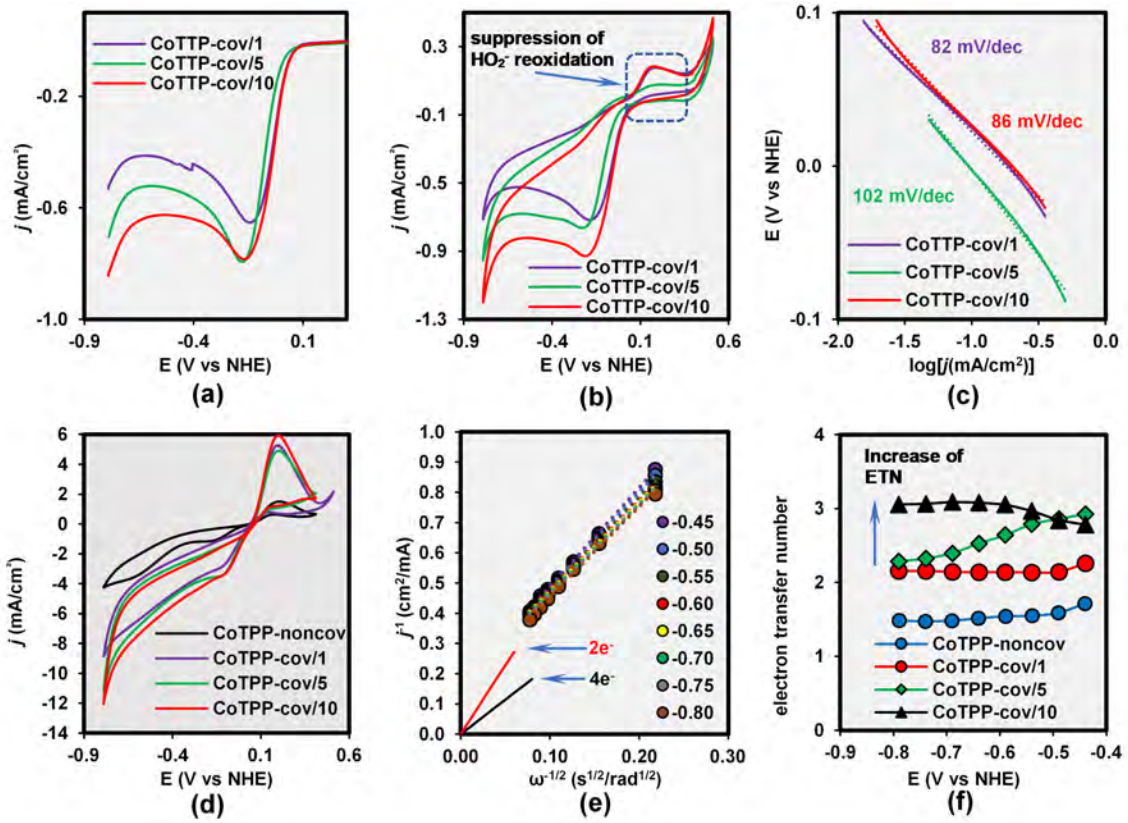

Figure 5.6. (a) LSVs, (b) CVs and (c) corresponding Tafel plots of **CoTPP-cov/1** (red trace), **CoTPP-cov/5** (violet trace) and **CoTPP-cov/10** (green trace). Electrolyte: O_2-saturated 0.1 M KOH an all cases. CV and LSV scan rates 50 mV/s and 10 mV/s respectively. (d) CV study of **CoTPP-cov/x** and **CoTPP-noncov** in H_2O_2 reduction. Electrolyte: N_2-purged 0.1 M KOH containing 0.05 M of H_2O_2. (e) Koutecky-Levich plots obtained for **CoTPP-cov/10**. Slopes corresponding to 2-electron (red) and 4-electron (black) reduction mechanisms are shown for reference. (f) Formal electron transfer numbers obtained from the analysis of Koutecky-Levich plots as a function of electrode potential.

Finally, we performed RDE studies of all electrode designs in order to estimate the formal electron transfer numbers using Koutecky-Levich analysis. In this case we expected to observe a gradual increase of electron transfer number as a function of electrodeposition time. Indeed, we were able to obtain linear plots across the potentials corresponding to diffusion-limited currents and the example of this for **CoTPP-cov/10** is shown on the Figure 5.6e. Comparison of ETNs observed for all electrodes is shown in the Figure 5.6d. One could clearly see that the ETN corresponding to **CoTPP-noncov** is even below 2 which could be a direct consequence of mixed catalysis of ORR by heterogeneous CoTPP and reduced $\cdot O_2^-$ or $HO_2\cdot$ radicals in the bulk solution. At the same time, **CoTPP-cov/1** showed the line corresponding to almost excusive H_2O_2 with ETN of 2.1-2.2 across all the potentials. However, accumulation of a more

dense catalyst layer on the surface of the carbon electrode led to a significant increase of the ETN which reached as high as 2.9 for **CoTPP-cov/5** and 3.1 for **CoTPP-cov/10**, especially under potentials around -0.7 V vs NHE. This change corresponds to an increase of the H_2O formation contribution to ORR from ~ 0 % to 55 % even though H_2O_2 is a kinetically preferable pathway.[33]

Thus, we were able to experimentally observe the enhancement of ORR selectivity towards $4e^-$ reduction on CoTPP similar to the one we reported for Mn-based systems.[3] It appears that this change of the reaction mechanism upon covalent immobilisation is a general phenomenon and not restricted to the class on Mn-based macrocycles. As the macrocyclic moieties are forced to form a dense layer of catalytically active centres during potentiostatic electrodeposition of the ligand, this most probably triggers multicentred catalysis described in multiple reports concerning binuclear Co porphyrin – based catalysts.[2] At the same time, our method obviates the need for lengthy preparation of complex bridged structures thus providing a cost effective access to the complexes with high selectivity to $4e^-$ ORR pathway. It is worth to note that our study was focused on a system without a layer of Nafion which could further increase the catalyst selectivity, however a detailed analysis of the proton delivery mechanisms was far outside of the scope for the current research.[16, 34]

Compared to the results reported for purely inorganic ORR catalysts, covalently immobilised CoTPP shows a current onset potential of 0.0 V vs NHE (as measured at 0.1 mA/cm^2) in alkaline electrolyte which translates into η = 460 mV (Figure 5.6a). Clearly, this is comparable to the state-of-the-art ORR catalysts such as Pt/C (20% E_TEK) and Ag/C catalysts which show current onset around + 0.1 V in alkaline electrolyte.[35-36] At the same time, organometallic counterparts are not based on the precious metals and provide an unsurpassed degree of control over the reaction rate and selectivity. Moreover, our study clearly shows that depending on the application (either fuel cell design or synthesis of H_2O_2 from O_2), the reaction direction could be chosen at will by simple change of the heterogenisation method.

5.3 Conclusions

In summary, we studied the effect of covalent ligation to carbon cloth on electrocatalytic activity of CoTPP in CO_2ERR in aqueous medium. Due to the presence of π-conjugated linker between the carbon electrode and CoTPP, the TOF at overpotentials below 550 mV rose by the factor of ~ 2 compared to **CoTPP-noncov**. Moreover, the surface density of electrochemically active species significantly increased and FE (CO) also reached the highest value at a 50 mV

less negative potential. As a result of simultaneous improvement in TOF and Γ_{EA}, **CoTPP-cov/1** produced 6.6 times more CO than noncovalently deposited counterpart in a 24 h long catalytic experiment with FE (CO) reaching 81 %. The cumulative TON of $3.9 \cdot 10^5$ is one of the highest reported to date. Electrokinetic data show that the phenylene linker enhances the electron transfer rate from the electrode to porphyrin core functioning virtually as a conductive molecular wire while H_2 is produced on the carbon support. Thus, covalent immobilisation is a key element in the overall design of efficient heterogeneous electrocatalysts for CO_2ERR. A more detailed study of the reaction mechanism and catalyst deactivation pathways will be reported in due course.

In turn, the ORR selectivity of Co porphyrin-based catalysts could be conveniently tuned using either a covalent or noncovalent heterogenisation technique. Indeed, while noncovalently immobilised CoTPP shows ETN of less than 2.0 (100 % H_2O_2), this number was as high as 3.1 (45 % H_2O_2) for the same catalyst deposited by 10 min electrodeposition. Thus, by a simple change of the synthetic procedure one could avoid tedious synthesis of multinuclear complexes while still observing good selectivity towards H_2O formation. Future research directed into the influence of proton conductive polymers is required to elucidate the proton delivery mechanisms and to achieve a complete change of the reaction direction upon covalent immobilisation of organometallic catalysts.

5.4 References

[1] Hu, X.-M.; Rønne, M. H.; Pedersen, S. U.; Skrydstrup, T.; Daasbjerg, K., Enhanced Catalytic Activity of Cobalt Porphyrin in CO2 Electroreduction upon Immobilization on Carbon Materials, *Angew. Chem.* **2017,** 129 (23), 6568-6572
[2] Dalle, K. E.; Warnan, J.; Leung, J. J.; Reuillard, B.; Karmel, I. S.; Reisner, E., Electro- and Solar-Driven Fuel Synthesis with First Row Transition Metal Complexes, *Chem. Rev.* **2019,** 119 (4), 2752-2875
[3] Marianov, A.; Jiang, Y., Effect of manganese porphyrin covalent immobilization on electrocatalytic water oxidation and oxygen reduction reactions, *ACS Sustainable Chem. Eng.* **2019,** 7, 3838-3848
[4] Shi, C.; Steiger, B.; Yuasa, M.; Anson, F. C., Electroreduction of O2 to H2O at Unusually Positive Potentials Catalyzed by the Simplest of the Cobalt Porphyrins, *Inorg. Chem.* **1997,** 36 (20), 4294-4295
[5] Zhang, X.; Wu, Z.; Zhang, X.; Li, L.; Li, Y.; Xu, H.; Li, X.; Yu, X.; Zhang, Z.; Liang, Y.; Wang, H., Highly selective and active CO2 reduction electrocatalysts based on cobalt phthalocyanine/carbon nanotube hybrid structures, *Nature Comm.* **2017,** 8, 14675
[6] Maurin, A.; Robert, M., Noncovalent Immobilization of a Molecular Iron-Based Electrocatalyst on Carbon Electrodes for Selective, Efficient CO2-to-CO Conversion in Water, *J. Am. Chem. Soc.* **2016,** 138 (8), 2492-2495
[7] Kornienko, N.; Zhao, Y.; Kley, C. S.; Zhu, C.; Kim, D.; Lin, S.; Chang, C. J.; Yaghi, O. M.; Yang, P., Metal–Organic Frameworks for Electrocatalytic Reduction of Carbon Dioxide, *J. Am. Chem. Soc.* **2015,** 137 (44), 14129-14135
[8] Hod, I.; Sampson, M. D.; Deria, P.; Kubiak, C. P.; Farha, O. K.; Hupp, J. T., Fe-Porphyrin-Based Metal–Organic Framework Films as High-Surface Concentration, Heterogeneous Catalysts for Electrochemical Reduction of CO2, *ACS Catalysis* **2015,** 5 (11), 6302-6309
[9] Diercks, C. S.; Lin, S.; Kornienko, N.; Kapustin, E. A.; Nichols, E. M.; Zhu, C.; Zhao, Y.; Chang, C. J.; Yaghi, O. M., Reticular Electronic Tuning of Porphyrin Active Sites in Covalent Organic Frameworks for Electrocatalytic Carbon Dioxide Reduction, *J. Am. Chem. Soc.* **2018,** 140 (3), 1116-1122
[10] Lin, S.; Diercks, C. S.; Zhang, Y.-B.; Kornienko, N.; Nichols, E. M.; Zhao, Y.; Paris, A. R.; Kim, D.; Yang, P.; Yaghi, O. M.; Chang, C. J., Covalent organic frameworks comprising cobalt porphyrins for catalytic CO2 reduction in water, *Science* **2015,** 349 (6253), 1208-1213
[11] Hu, X.-M.; Salmi, Z.; Lillethorup, M.; Pedersen, E. B.; Robert, M.; Pedersen, S. U.; Skrydstrup, T.; Daasbjerg, K., Controlled electropolymerisation of a carbazole-functionalised iron porphyrin electrocatalyst for CO2 reduction, *Chem. Comm.* **2016,** 52 (34), 5864-5867
[12] Maurin, A.; Robert, M., Catalytic CO2-to-CO conversion in water by covalently functionalized carbon nanotubes with a molecular iron catalyst, *Chem. Comm.* **2016,** 52 (81), 12084-12087
[13] Yao, S. A.; Ruther, R. E.; Zhang, L.; Franking, R. A.; Hamers, R. J.; Berry, J. F., Covalent Attachment of Catalyst Molecules to Conductive Diamond: CO2 Reduction Using "Smart" Electrodes, *J. Am. Chem. Soc.* **2012,** 134 (38), 15632-15635
[14] Elgrishi, N.; Griveau, S.; Chambers, M. B.; Bedioui, F.; Fontecave, M., Versatile functionalization of carbon electrodes with a polypyridine ligand: metallation and electrocatalytic H+ and CO2 reduction, *Chem. Comm.* **2015,** 51 (14), 2995-2998
[15] Allongue, P.; Delamar, M.; Desbat, B.; Fagebaume, O.; Hitmi, R.; Pinson, J.; Savéant, J.-M., Covalent Modification of Carbon Surfaces by Aryl Radicals Generated from the Electrochemical Reduction of Diazonium Salts, *J. Am. Chem. Soc.* **1997,** 119 (1), 201-207
[16] Tang, H.; Yin, H.; Wang, J.; Yang, N.; Wang, D.; Tang, Z., Molecular Architecture of Cobalt Porphyrin Multilayers on Reduced Graphene Oxide Sheets for High-Performance Oxygen Reduction Reaction, *Angew. Chem. Int. Ed.* **2013,** 52 (21), 5585-5589
[17] Savéant, J.-M. In *Elements of Molecular and Biomolecular Electrochemistry*, John Wiley & Sons, Inc.: **2006**; pp 1-77
[18] Baranton, S.; Bélanger, D., Electrochemical Derivatization of Carbon Surface by Reduction of in Situ Generated Diazonium Cations, *J. Phys. Chem. B* **2005,** 109 (51), 24401-24410
[19] Mahouche-Chergui, S.; Gam-Derouich, S.; Mangeney, C.; Chehimi, M. M., Aryl diazonium salts: a new class of coupling agents for bonding polymers, biomacromolecules and nanoparticles to surfaces, *Chem. Soc. Rev.* **2011,** 40 (7), 4143-4166
[20] Gross, A. J.; Bucher, C.; Coche-Guerente, L.; Labbé, P.; Downard, A. J.; Moutet, J.-C., Nickel (II) tetraphenylporphyrin modified surfaces via electrografting of an aryldiazonium salt, *Electrochem. Comm.* **2011,** 13 (11), 1236-1239
[21] Picot, M.; Nicolas, I.; Poriel, C.; Rault-Berthelot, J.; Barrière, F., On the nature of the electrode surface modification by cathodic reduction of tetraarylporphyrin diazonium salts in aqueous media, *Electrochem. Comm.* **2012,** 20, 167-170

[22] Rocklin, R. D.; Murray, R. W., Chemically modified carbon electrodes: Part XVII. Metallation of immobilized tetra(aminophenyl)porphyrin with manganese, iron, cobalt, nickel, copper and zinc, and electrochemistry of diprotonated tetraphenylporphyrin, *J. Electroanal. Chem. Interfacial Electrochem.* **1979,** 100 (1), 271-282
[23] Liu, Y.-C.; McCreery, R. L., Reactions of Organic Monolayers on Carbon Surfaces Observed with Unenhanced Raman Spectroscopy, *J. Am. Chem. Soc.* **1995,** 117 (45), 11254-11259
[24] Anariba, F.; Viswanathan, U.; Bocian, D. F.; McCreery, R. L., Determination of the Structure and Orientation of Organic Molecules Tethered to Flat Graphitic Carbon by ATR-FT-IR and Raman Spectroscopy, *Anal. Chem.* **2006,** 78 (9), 3104-3112
[25] Saby, C.; Ortiz, B.; Champagne, G. Y.; Bélanger, D., Electrochemical Modification of Glassy Carbon Electrode Using Aromatic Diazonium Salts. 1. Blocking Effect of 4-Nitrophenyl and 4-Carboxyphenyl Groups, *Langmuir* **1997,** 13 (25), 6805-6813
[26] Nielsen, I. M. B.; Leung, K., Cobalt−Porphyrin Catalyzed Electrochemical Reduction of Carbon Dioxide in Water. 1. A Density Functional Study of Intermediates, *J. Phys. Chem. A* **2010,** 114 (37), 10166-10173
[27] Leung, K.; Nielsen, I. M. B.; Sai, N.; Medforth, C.; Shelnutt, J. A., Cobalt−Porphyrin Catalyzed Electrochemical Reduction of Carbon Dioxide in Water. 2. Mechanism from First Principles, *J. Phys. Chem. A* **2010,** 114 (37), 10174-10184
[28] Stern, M.; Geary, A. L., Electrochemical Polarization I. A Theoretical Analysis of the Shape of Polarization Curves, *J. Electrochem. Soc.* **1957,** 104 (1), 56-63
[29] Marianov, A. N.; Jiang, Y., Covalent ligation of Co molecular catalyst to carbon cloth for efficient electroreduction of CO2 in water, *Appl. Catal. B* **2019,** 244, 881-888
[30] Savéant, J.-M., Molecular Catalysis of Electrochemical Reactions. Mechanistic Aspects, *Chem. Rev.* **2008,** 108, 2348–2378
[31] Corbin, N.; Zeng, J.; Williams, K.; Manthiram, K., Heterogeneous molecular catalysts for electrocatalytic CO2 reduction, *Nano Res.* **2019**,
[32] Koper, M. T. M., Theory of multiple proton–electron transfer reactions and its implications for electrocatalysis, *Chem. Sci.* **2013,** 4 (7), 2710-2723
[33] Seh, Z. W.; Kibsgaard, J.; Dickens, C. F.; Chorkendorff, I.; Nørskov, J. K.; Jaramillo, T. F., Combining theory and experiment in electrocatalysis: Insights into materials design, *Science* **2017,** 355 (6321), 4998
[34] Wu, Z.-S.; Chen, L.; Liu, J.; Parvez, K.; Liang, H.; Shu, J.; Sachdev, H.; Graf, R.; Feng, X.; Müllen, K., High-Performance Electrocatalysts for Oxygen Reduction Derived from Cobalt Porphyrin-Based Conjugated Mesoporous Polymers, *Advanced Mater.* **2014,** 26 (9), 1450-1455
[35] Demarconnay, L.; Coutanceau, C.; Léger, J. M., Electroreduction of dioxygen (ORR) in alkaline medium on Ag/C and Pt/C nanostructured catalysts—effect of the presence of methanol, *Electrochim. Acta* **2004,** 49 (25), 4513-4521
[36] Guo, J.; Hsu, A.; Chu, D.; Chen, R., Improving Oxygen Reduction Reaction Activities on Carbon-Supported Ag Nanoparticles in Alkaline Solutions, *J. Phys. Chem. C* **2010,** 114 (10), 4324-4330

CHAPTER 6. RATIONAL DESIGN OF STABLE COBALT PORPHYRIN-BASED CATALYSTS FOR CO_2ERR

6.1 Introduction

The electroreduction of CO_2 (CO_2ERR) in aqueous medium is an excellent strategy to facilitate the widespread utilization of this cheap and abundant feedstock.[1-2] However, because of the notoriously high overpotential required to drive single-electron CO_2 reduction, the cathodic processes must follow an electrocatalytic multielectron proton-assisted pathway.[3-4] The development of highly active organometallic CO_2ERR electrocatalysts has been a long-standing goal and a number of efficient molecular catalysts been discovered as described in a series of excellent reviews.[5-7] Although significant progress has been made in the direction of catalyst activity improvement, catalyst stability has largely been neglected, and the discovery of durable materials has been quite serendipitous rather than based on a detailed understanding of decomposition pathways.[5, 7]

Only a small number of studies that elucidate deactivation mechanisms and subsequently design catalysts capable of withstanding negative potentials have been reported.[8-9] For example, in the case of Re(bipy)$(CO)_3$, one of the first CO_2ERR catalysts, the formation of dimeric species was found to be the main degradation mechanism.[8] In another example, Jiang et al. proposed to utilize Zn bacteriochlorin as a CO_2ERR catalyst[9] as it is already reduced and thus less prone to further reductive decomposition compared to porphyrins (pathway (a) in Scheme 6.1).[10-11] Notably, in this work authors also performed a control CO_2ERR experiment on a Zn porphyrin and HRMS analysis of the reaction mixture failed to detect the expected formation of reduced macrocyclic species.[9] Though not discussed in the report, that is an important finding which provides evidence that the protonation might ultimately be not responsible for the activity loss.

Fe porphyrins are among the most active CO_2ERR catalysts but there is limited information regarding their deactivation. In some cases, CO evolving during the reaction can poison the catalyst since it has a considerably higher affinity to the metal centre than CO_2 (pathway (b) in the Scheme 6.1).[12] The most active catalyst of this class, tetrakis-(2-trimethylamminophenyl)porphyrin, was found to show minor, yet unexplained, changes in the UV/Vis spectrum and cyclic voltammograms (CV) after a 4 h long CO_2ERR experiment.[13] For a number of other Fe porphyrins the maximum TONs were reported between 210 and 600

depending on the structure of the catalyst, however no mechanistic information was reported as well.[14-15] Grodkowski et al. in their insightful work also proposed that chlorin might be a decay product of Fe porphyrin.[16]

The complexes described above are active in non-aqueous medium while use of aqueous electrolytes and heterogenized catalysts provides additional challenges due to competition from the hydrogen evolution reaction (HER). In this regard, Maurin and Robert successfully transferred activity of Fe hydroxyporphyrins into aqueous-based medium using pyrene-appended derivative immobilised carbon nanotubes and in this case reported gradual activity loss over a 12 h-long controlled potential electrolysis (CPE) which was assigned to leaching and chemical degradation of the complex.[17] Loss of metal upon one-electron reduction reported for Cu porphyrins and phthalocyanines is one of the few examples where the decomposition products were actually studied (pathway (c) in the Scheme 6.1).[18-19] At the same time, carbon-supported Co porphyrins are among the best macrocyclic catalysts which exhibit excellent activity and FE to CO with cumulative TONs in neutral aqueous electrolyte as high as $3.0 \cdot 10^5$ for COF[20] and $3.9 \cdot 10^5$ for covalently immobilised complexes.[21] Although initial TOFs are impressive, activity drops in the course of prolonged electrolysis.[20-22] Moreover, minor changes in the UV/Vis spectrum were reported after CO_2ERR catalysed by CoTPP immobilised on carbon nanotubes though the exact nature of transformation was not studied.[22]

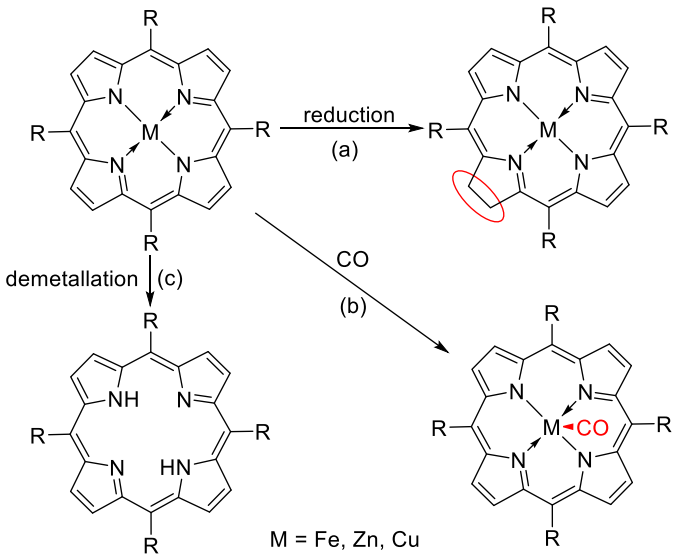

Scheme 6.1 Metalloporphyrin decomposition pathways.

Herein, we report a systematic study shedding light on the mechanism of Co porphyrin deactivation mechanism during CO_2ERR in aqueous electrolyte and establishing a viable strategy to overcome this unfortunate impediment. First, we evaluated the influence of leaching

and possible catalyst poisoning by the evolving CO. Subsequently, a combination of high-resolution mass spectrometry (HRMS), NMR spectroscopy and cyclic voltammetry (CV) was employed to study organometallic products formed from CoTPP. Then, based on our understanding of the deactivation mechanism, we attempted to improve catalyst longevity using thermodynamic stabilization of the reactive $[Co^{I}]^{-}$ intermediate through axial coordination of pyridine and introduction of electronegative substituents. Finally, approaches based on kinetic suppression of deactivation process were devised and evaluated. Our results show that understanding of degradation mechanisms is a crucial step in the catalyst design and provides a solid framework for systematic development of stable and potentially commercially viable electrocatalysts.

6.2 Results and discussion

6.2.1 Deactivation pathway of CoTPP

The loss of activity by a heterogeneous molecular catalyst during prolonged CO_2ERR might be caused by a number of factors such as leaching, poisoning, chemical decomposition or a combination of these factors.[23-24] To determine the contribution of each pathway, we systematically investigated all of these possibilities.

First, to clarify if leaching is a major cause of deactivation, we compared long-term performance of covalently and noncovalently immobilised complexes i.e. **CoTPP-cov/1** and **CoTPP-noncov**, respectively, in Figure 6.1a. It was expected that if the activity decay takes place only due to detachment of the catalyst from the electrode surface, stability would significantly improve upon introduction of a covalent bond with the carbon cloth in **CoTPP-cov/1** compared to the noncovalently heterogenized counterpart **CoTPP-noncov**.[25] To test this hypothesis, we performed a series of three 4 h long CO_2ERR on **CoTPP-cov/1** and **CoTPP-noncov** at -1.05 V vs NHE purging the cell with CO_2 between each CPE (Figure 6.1b). Clearly, CO production on **CoTPP-cov/1** dropped from 37.2 μmol/cm^2 in the first run to 11.0 μmol/cm^2 in the third experiment which represents a 70 % decline in catalytic activity (recyclability 30 %). At the same time, **CoTPP-noncov** produced 14.8 μmol/cm^2 of CO at the beginning of the sequence and only 5.9 μmol/cm^2 in the last electrolysis amounting to 60 % activity loss over three catalytic runs (recyclability 40 %). To sum up, even though **CoTPP-noncov** showed marginally better stability, both covalently and noncovalently immobilised catalysts lose activity in a similar fashion.

Next, we attempted to establish the nature of any potential organometallic decomposition products formed on the electrodes and in the electrolyte after catalysis. The CV of **CoTPP-cov/1** after one 4 h CO_2ERR run (Figure 6.1c) was recorded in DMF to determine the nature of residual surface species. A single faint redox response was found at -1.34 V vs Fc^+/Fc which is close to -1.30 V reported for Co^{II}TPP/[Co^{I}TPP]$^-$ couple measured in homogeneous solution in DMF.[21] At more negative potentials only non-specific reduction current was recorded. Further, organic material recovered from **CoTPP-noncov** after identical long run CO_2ERR was also studied using CV in non-aqueous electrolyte (Figure 6.1d). In this case, we identified two reversible redox pairs. First wave at -1.31 V clearly corresponds to Co^{II}TPP/[Co^{I}TPP]$^-$ transformation while second redox pair at -1.47 V represents a response of some new, yet unknown product. Finally, we extracted organic products from electrolyte with DCM and no CoTPP was found using ^{1}H NMR spectroscopy in both cases (Figure A36), however traces of unknown organics were detected.

These results lead to two important conclusions. First, the catalyst degrades regardless of the heterogenization method. Covalent immobilisation of CoTPP on the surface of carbon cloth electrode[21] or carbon nanotubes[26] does improve its activity but has no considerable effect on stability and recyclability. Second, CoTPP survives electrolysis at least partially and was detected only on the electrode surface but is absent in the bulk solution. Hence, complex leaching is not responsible for the deactivation process as otherwise covalently immobilised **CoTPP-cov/1** would be more stable[25] than **CoTPP-noncov** and for the latter electrode the complex would have been found in the extract from aqueous electrolyte after CO_2ERR assuming no chemical side-reactions take place. To the best of our knowledge, this is the first work confirming that even noncovalent immobilisation of an insoluble catalyst is sufficient to keep the structural integrity of electrocatalyst/carbon hybrid intact during CO_2ERR. It is also worth comparing our results with those obtained for pyridine-appended Fe hexahydroxyporphyrin immobilised on carbon nanotubes where there was a decrease in catalytic current after multiple scans and decline in the rate of CO production during CPE notwithstanding strong π-π interaction with the carbon plane of the electrode.[17] These changes were explained by leaching and deactivation, however no additional details were provided which makes it difficult to confirm if the immobilisation mode had a direct effect on the catalyst stability.

As inhibition by the reaction product is known for Fe porphyrin electrocatalysts,[12] our next step was to evaluate the influence of CO on Co derivatives. To estimate if CO coordination to

Co could interfere with the reaction, we performed CV of CoTPP dissolved in DMF under CO and N_2 atmospheres (Figure 6.1e). We chose to use nonaqueous electrolyte for this experiment because CoTPP is not soluble in water and HER is the dominant electrode process at the potentials of Co^{II}/Co^{I} redox transformation. Clearly, no significant changes occurred upon introduction of CO in the cell as the potentials of Co^{II}/Co^{I} and Co^{I}/Co^{0} redox pairs exactly matched those obtained in N_2-saturated electrolyte and no significant changes in current density took place. Further, FTIR was employed to detect the presence of CO bound to the Co centre in the products after electrolysis (Figure A35). Normally, strong CO bands are expected to appear between 1750 and 2100 cm^{-1},[27-29] however no new signals were found in this region thus excluding the possibility of CO significantly impeding the catalytic process, especially in aqueous electrolyte where CO solubility is 2.6 times lower compared with DMF.[30-31]

The observations described above indicate that CO poisoning is also an unlikely mechanism of the catalyst deactivation. It was reported that CO forms a 1:1 adduct with Co porphyrins,[32-33] however it seems that the affinity of CO to the metal centre is too weak to give any response in CV and affect the catalytic process. Furthermore, one could assume from Figure 6.1d that the new peak might correspond to the [CoTPP-CO] redox pair, but this is clearly not the case. Thus, it appears that the Co complex suffers significant chemical changes which render it unreactive towards CO_2 and at least one product formed in the process is characterised by distinctive redox couple at -1.47 V vs Fc^{+}/Fc.

To confirm the chemical nature of CoTPP deactivation, we performed ^{1}H NMR analysis of the complex recovered from **CoTPP-noncov** after CO_2ERR. First, we performed ^{1}H NMR spectroscopy of CoTPP after 4 h long reduction in the presence of CO_2 in 0.5 M $KHCO_3$ (Figure 6.1f). The resulting spectrum shows a striking difference with that of the pure complex.[21] Broad singlets consistent with the presence of CoTPP were observed at 15.87, 13.13, 9.93 and 9.73 ppm, however a large number of new peaks appeared after prolonged electrolysis. The aromatic region features a signal at 9.0 ppm which resembles the signal of the β-protons in the porphyrin core and multiplets at 8.20-8.19 and 7.77-7.75 ppm most likely corresponding to a monosubstituted Ph group. A compound or a mixture of isomers giving rise to these signals was denoted as **component X** for the future discussion. Next, there is an alkenyl-like multiplet at 5.36-5.33 ppm overlapping with a wide peak, probably from -OH or -NH groups. Finally, the most prominent feature of the spectrum is a group of multiplets between 0.5 and 2.5 ppm corresponding to aliphatic protons, possibly overlapped with amine and hydroxyl signals which typically appear in this region as well. Notably, from the position of signals in the aromatic

region one could assume that it is nonmetalated tetraphenylporphyrin (TPP) that gives rise to these peaks, however, the lack of the characteristic singlet corresponding to shielded pyrrolic NH protons at -2.71 ppm rules out this hypothesis. A ^{1}H NMR spiking experiment also confirmed the lack of free-base TPP after the catalytic reaction (Figure A37).

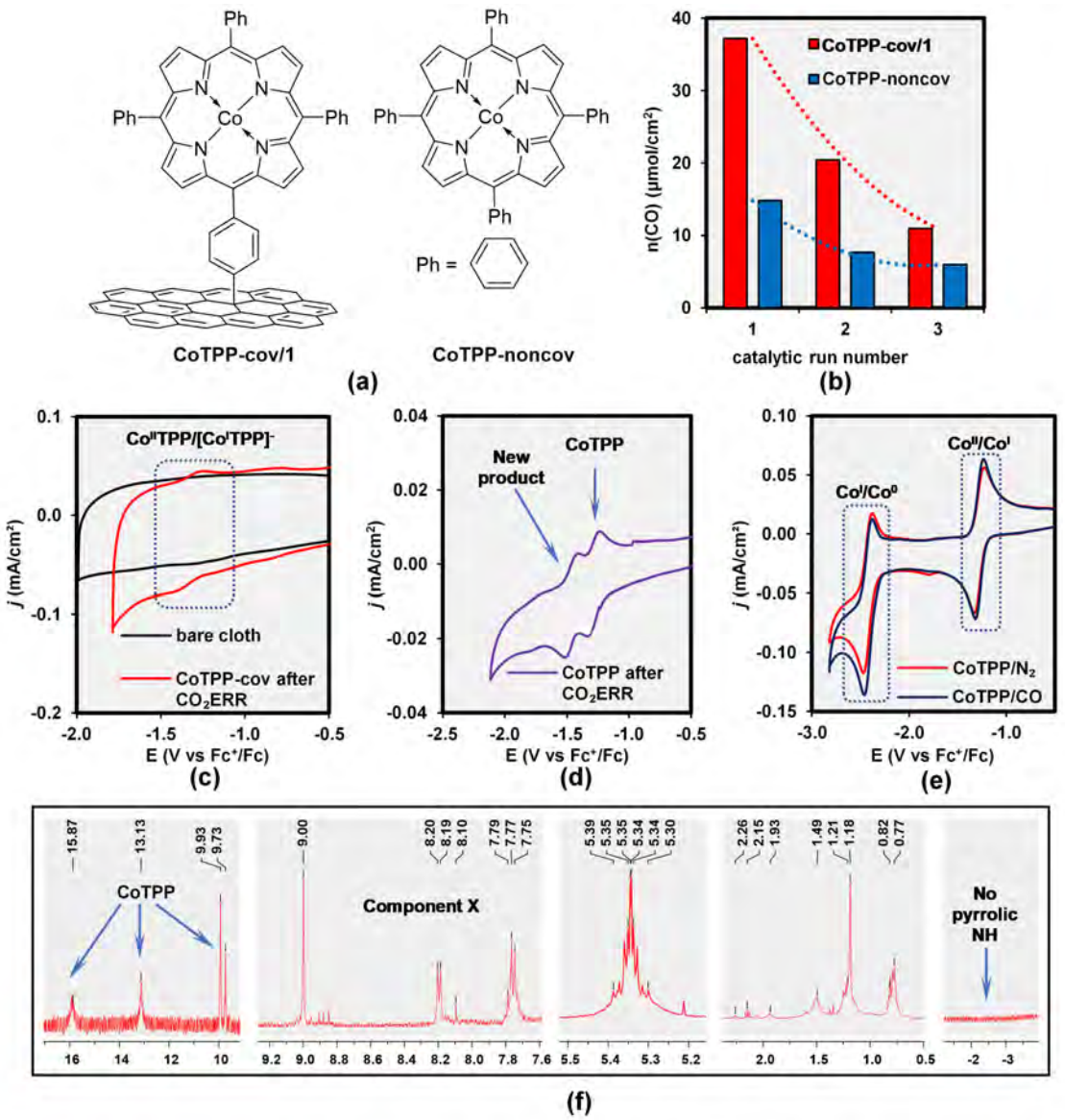

Figure 6.1 (a) schematic representation of **CoTPP-cov/1** and **CoTPP-noncov**; (b) CO evolution on **CoTPP-cov/1** and **CoTPP-noncov** during three catalytic runs at -1.05 V vs NHE in CO_2-saturated 0.5 M $KHCO_3$; (c) CV in dry degassed DMF of **CoTPP-cov/1** recovered after 4 h long CO_2ERR (red trace) and bare carbon cloth electrode (black trace); (d) CV in DMF of the catalyst recovered from **CoTPP-noncov** after 4 h long CO_2ERR; (e) CV of CoTPP in the N_2-purged (red trace) and CO-saturated (blue trace) DMF electrolyte; (f) ^{1}H NMR spectrum of CoTPP-derived products recovered from **CoTPP-noncov** after CO_2ERR in aqueous medium. CV scan rate 100 mV/s in all cases.

Thus, NMR results clearly show that the deactivation stems from chemical degradation of the electrocatalyst and the next step of investigation was directed towards identification of the new products. First, in a control experiment a 4 h long electrolysis at -1.05 V on a bare carbon cloth electrode was performed in the absence of a catalyst and ^{1}H NMR spectroscopy was used to detect organics formed from the carbon support itself. The aliphatic and alkenyl signals observed earlier correspond to the products of the reduction of carbonaceous support rather than the complex itself (Figure A38). Moreover, the same NMR pattern was observed for the organic products extracted from the electrolytes after CPE on **CoTPP-cov/1** and **CoTPP-noncov** (Figure A36). Further, running CO_2ERR in a fully deuterated system containing CO_2-saturated 0.5 M $KDCO_3$ in D_2O gave almost the same result only with a signal at 0.9 ppm losing around half of its intensity. This experiment pinpoints a spectral footprint of protons introduced from the electrolyte and indicates that the protonation of the porphyrin core is not responsible for the formation of **component X** (Figure A41). Interestingly, ^{2}D NMR recorded in $CHCl_3$ showed no signals except natural abundance deuterium in the solvent (Figure A42), however it is possible considering deuterium's quadrupolar nucleus with I = 1 renders it insensitive especially in the presence of paramagnetic CoTPP. These observations show that the **component X** is the only product formed from CoTPP and no protons are taken up from the aqueous electrolyte.

The next important question is whether the **component X** is formed due to CoTPP participation in CO_2ERR or simply because of its reaction with water. To investigate how saturation of electrolyte with CO_2 affects structural changes of the catalyst under negative potentials, we performed identical experiment in N_2-sparged 0.1 M $KClO_4$ to exclude the presence of CO_2, both directly or from equilibrium with HCO_3^-. The resulting spectrum (Figure A40) also shows unreacted CoTPP and reduction products of carbon, however, the peaks in the aromatic region are extremely weak compared to the sample extracted from the reaction in CO_2-saturated electrolyte. As expected, no CO was formed during the electrolysis in CO_2-free electrolyte. Considering this, it is CO_2 that induces the formation of deactivation product rather than water.

To gain a better insight into the structure of the resulting product, we used a range of 2D NMR experiments performed on the residue recovered from **CoTPP-noncov**. First, to separate overlapped signals we employed a range of homonuclear correlation methods. The TOCSY pulse sequence allowed us to establish chemical shifts of components in each spin system of the product. As shown in (Figures 6.2a), **component X** clearly contains two spin systems, the first of which corresponds to the groups resembling β-CH porphyrin protons while phenyl

substituents constitute the second system of *J*-coupled protons. However, as there are two *J*-coupled *β*-CH signals, the porphyrin core is asymmetric and most likely has some proton-free substituents. The COSY spectrum (Figure A43) was also recorded and the resulting ^{1}H-^{1}H correlations are in good agreement with TOCSY. A NOESY experiment was employed to identify through-space interactions and indicates that the protons of the macrocycle and the *ortho*-protons of the phenyl group are located in close proximity (Figure A44).

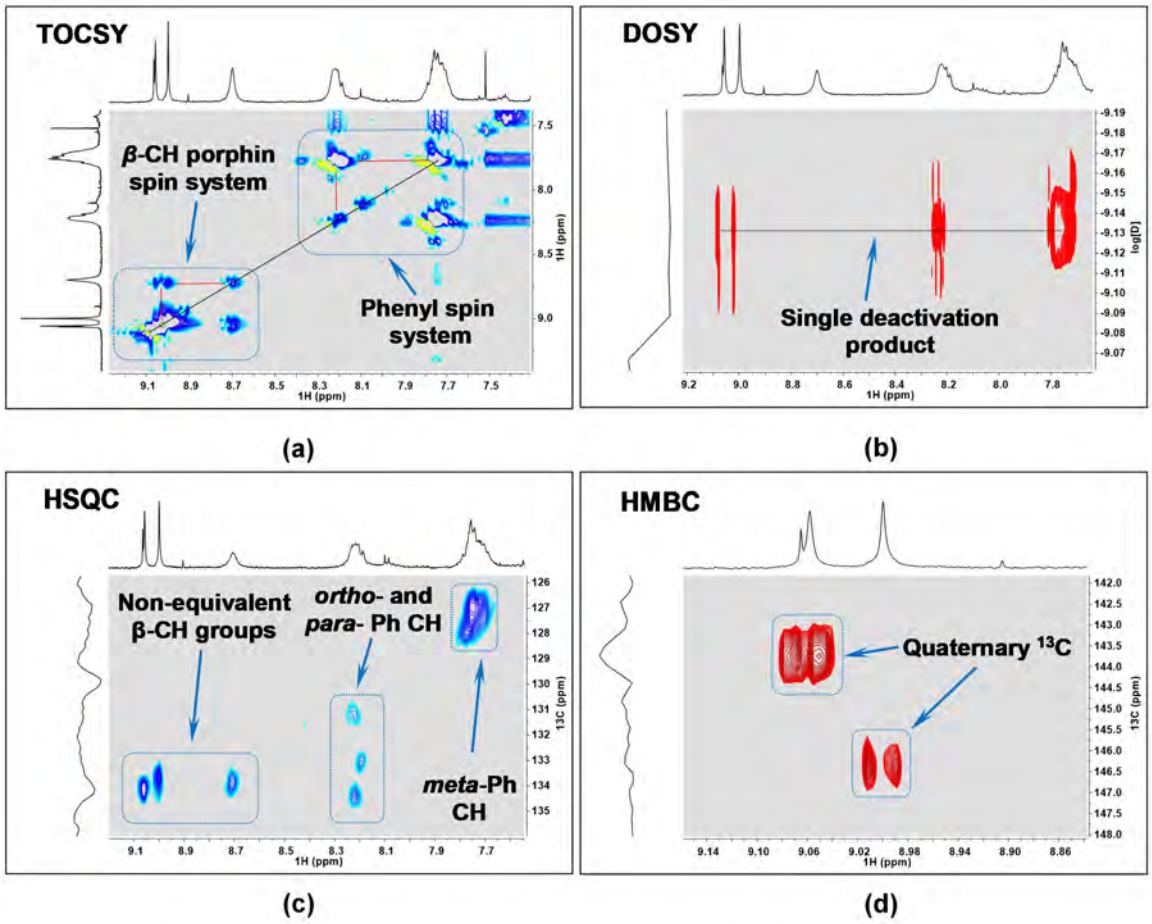

Figure 6.2. 2D NMR spectra of CoTPP deactivation products extracted from **CoTPP-noncov** after 4 h long CO_2ERR at -1.05 V vs NHE. (a) TOCSY; (b) DOSY; (c) HSQC and (d) HMBC. Only aromatic region is shown for clarity.

Next, we used DOSY NMR to measure chemical shifts of the components against their diffusion coefficients (Figure 6.2b). As one could clearly see, all aromatic signals at 9.06 – 7.67 ppm correspond to one derivative or a group of structural isomers with D = $7.4 \cdot 10^{-10}$ m^2/s which means that **component X** is a single product rather than a mixture. Further, ^{15}N HSQC was performed to study ^{1}J (^{15}N-^{1}H) correlations which give evidence of N-H bond formation during CO_2ERR (Figure A39). Results clearly indicate that there are three types of N-H groups

represented by ^{15}N signals at 325.1, 102.0 and -23.0 ppm, however all of them correspnd to the products of carbon cloth reductive decomposition. At the same time, there is no free-base porphyrin formed during CO_2ERR which means that Co is not lost in the process. Finally, ^{13}C HSQC was employed to study ^{1}J (^{13}C-^{1}H) correlations (Figure 6.2c) and ^{13}C HMBC was used to detect long-range (^{13}C-^{1}H) couplings (Figure 6.2d). From these experiements we found that **component X** contains 4 inequivalent phenyl groups with overalapped proton signals (*meta-, ortho-* and *para-* protons). Also, porphyrin-like *β*-CH signals correlate to quaternary carbons which give peaks at 144.0 and 146.4 ppm thus providing additional evidence of connection between phenyl group and the rest of the molecule.

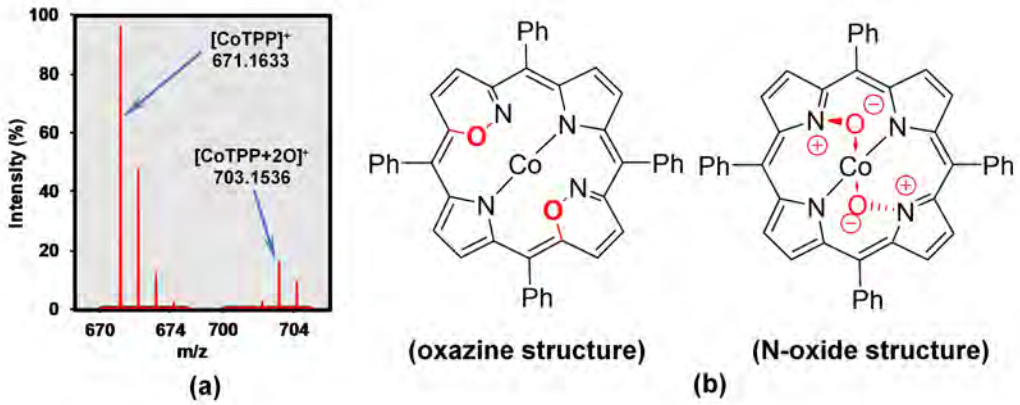

Figure 6.3. (a) positive mode HRMS spectrum of CoTPP deactivation product and (b) proposed structures of deactivation products.

To finalize this structural study, we performed a positive-mode HRMS analysis of the reaction mixture which allowed us to identify molecular masses of two major constituents in the mixture (Figure 6.3a). First, the biggest peak with m/z 671.1633 in HRMS clearly corresponds to CoTPP ($[M]^+$, Δ = -1.0 ppm). Surprisingly, the next major signal with m/z 703.1536 corresponds to the product of addition of two oxygen atoms to the complex ($[M]^+$ Δ = -0.43 ppm). As this is the only product corresponding to the structure similar to the starting complex, that ion most probably corresponds to the sought-after **component X**. One could assume that this might be simply a coordination complex with atmospheric O_2, but this is not the case as HRMS of fresh CoTPP does not show this peak and its NMR has no non-paramagnetic aromatic signals.[21] Moreover, oxidation of CoTPP with H_2O_2 in an attempt to simulate the presence of adventitious oxidizers also did not produce the expected product. Analysis of separately prepared [Co^{III}TPP]Cl also shows that $[Co^{III}]^+$ complex could not be responsible for

the observed signals as the respective NMR ^{1}H and the electrochemical behaviour both are different to those of **component X** (Figures A45 and A46, respectively). Based on the findings described above we proposed structures of deactivation products described in the Figure 6.3b. So far, our efforts to clarify the structure further using single crystal X-ray diffraction were not successful due to formation of carbon reduction products which are difficult to separate and prevent growth of high-quality crystals.

Based on the observations described above, we deduced the deactivation mechanism shown in Scheme 6.2. As in CO_2-free reaction this product is not formed, oxygen is transferred during CO_2ERR from CO_2, most likely within the [CoTPP-CO_2]$^-$ intermediate. Since the aromaticity of the macrocycle is retained, the oxygen is inserted into C-N bond of the pyrrolic moiety with the formation of an oxazine structure or into the N-Co bond forming an N-oxide product. In a normal catalytic cycle, [CoTPP-CO_2]$^-$ is protonated by the solvent, loses a water molecule and the resulting [CoTPP-CO] yields CO and starting CoTPP with the latter entering the catalytic cycle again.[34-35] In turn, adjacent bonds in [CoTPP-CO_2]$^-$ might fulfil the same role as protons and form oxygenated adducts through a minor, but apparently irreversible side reaction. These oxygenates distort the structure of the reactive porphyrin complex thus rendering the catalyst inactive in catalysis. We must admit here that the actual mechanism might be much more complex, but the Scheme 6.2 provides enough understanding of the deactivation pathway to devise a strategic framework for a rational design of durable catalysts.

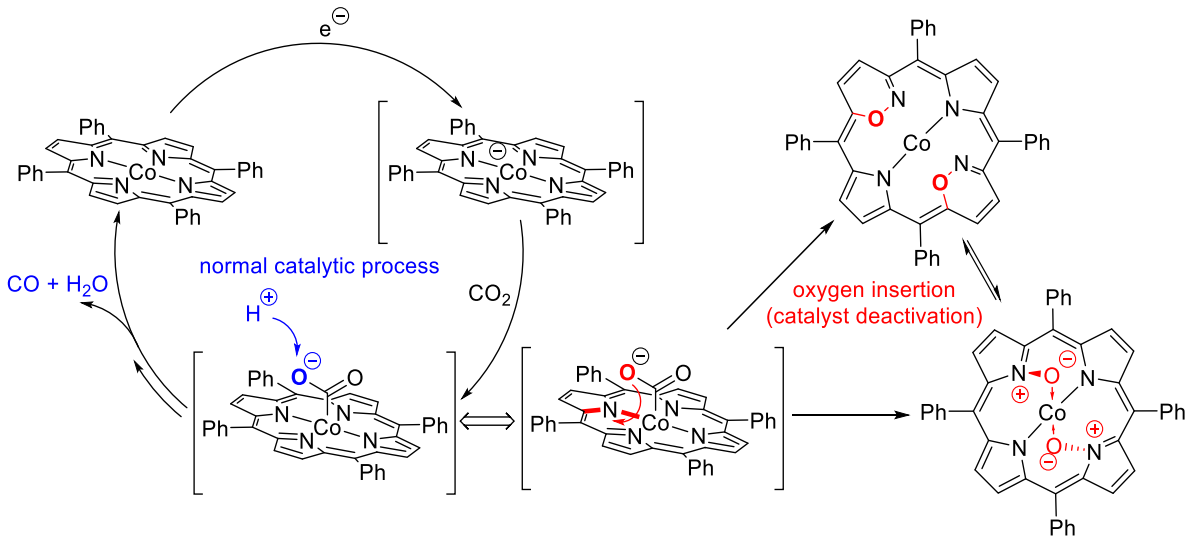

Scheme 6.2. Proposed CoTPP decomposition mechanism.

6.2.2 Rational design of a stable CO_2ERR catalyst

The observed decomposition product suggests that the development of stable catalysts requires inhibition of oxygen migration from CO_2. To solve this problem, the thermodynamic and kinetic stabilization of $[CoTPP\text{-}CO_2]^-$ intermediate could be utilized. Thermodynamic stabilization is directed towards lowering of the Co^{II}/Co^{I} redox potential through axial coordination of the metal centre or introduction of electronegative substituents. Generally, the purpose of these changes is to make intermediate less reactive towards its own ligand.[14, 36] Meanwhile, the kinetic approach is based on the use of bulky substituents around the metal centre which restricts access to the vulnerable internal aromatic ring and introduction of proton donors around the metal atom to speed up protonation of $[CoTPP\text{-}CO_2]^-$ and thus reduce the probability of oxygen insertion into the porphyrin itself.[37]

From a thermodynamic point of view, the simplest method of complex stabilization is its coordination with δ-donors such as pyridine (Py) (Figure 6.4a).[36, 38-39] CV recorded for CoTPP in DMF in the presence of 1 M Py shows the appearance of new redox wave at -0.65 V vs Fc^+/Fc which had the same shape both in degassed and CO_2-saturated electrolyte and most probably corresponds to the electron transfer onto the coordinated Py ligand (Figure 6.4b). Interestingly, a second redox wave corresponding to electron transfer onto the porphyrin itself shifted to the more negative potential of -1.42 V compared to pure CoTPP (-1.30 V). These observations agree well with the reports showing that Py forms an adduct with Co porphyrins.[33, 39] Interestingly, the second redox wave becomes irreversible and splits into two in the presence of CO_2, most probably because the complex quickly reacts with it. However, this is an undesirable process as the complex undergoes irreversible changes even on the CV timescale.

Next, we studied the performance of **CoTPP-cov/1** in CO_2ERR in the presence of 1 M pyridine in aqueous electrolyte. During prolonged electrolysis FE (CO) was as low as 1.6 % at the beginning of the reaction and dropped to 0.2 % by the end of the process (Figure 6.4c). The reaction quickly slowed down as well, and the total amount of CO produced in the experiment dropping by the factor of 20 compared to the pyridine-free electrolyte which means that the ligands competing with CO_2 are in fact catalytic poisons. Moreover, considering that $[CoTPP\text{-}Py]^-$ reacts with CO_2 irreversibly, this result agrees well with CV data (Figure 6.4b). Instead, H_2 was mostly produced in good agreement with pyridine-catalysed HER in CO_2-saturated electrolytes studied by Dirdi et al.[40]

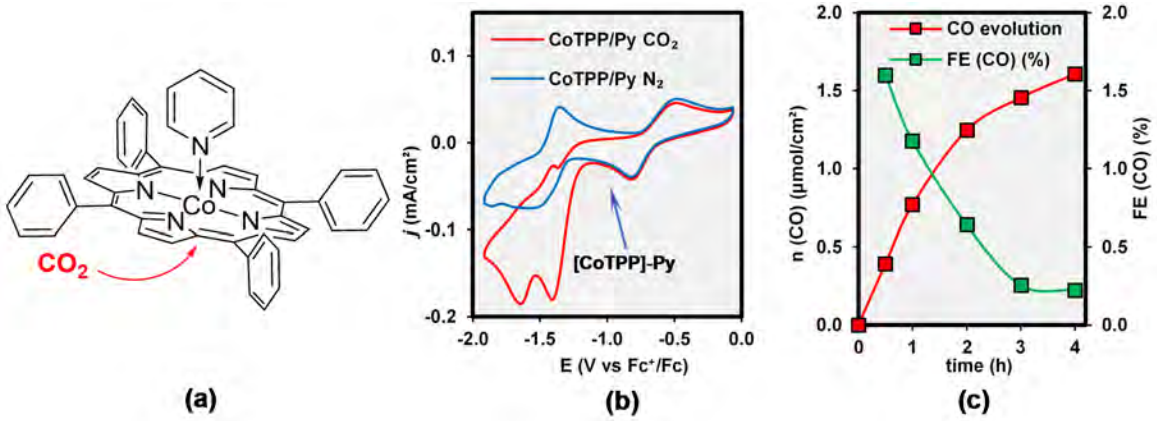

Figure 6.4. (a) coordination of pyridine with CoTPP; (b) CV of CoTPP in DMF/1M pyridine electrolyte saturated with N_2 (blue trace) and CO_2 (red trace); (c) CO evolution (red curve) and FE (CO) (green curve) during CO_2ERR in CO_2-saturated 0.5 M $KHCO_3$ containing 1 M of pyridine.

As the coordination approach was unsuccessful, we turned our attention to the design of the macrocyclic ligand itself. A significant body of works is available on the improvement of catalyst activity via introduction of electron-deficient substituents[14, 41] and proton relays.[17, 31, 42-43] Interestingly, the concept of using bulky moieties to protect vulnerable parts of the molecule is well-known in purely organometallic chemistry,[37] but underrepresented in the field of electrocatalysis.[44] Also, the influence of substituents on Co porphyrin activity has been studied only recently and electron withdrawing substituents were shown to have a detrimental effect on CO_2 reduction rate, however, stability aspects have not been discussed.[45] In this regard we synthesized porphyrins **Co[TPP-F$_{20}$]**, **Co[TPP-(OH)$_8$]** and **Co[TPP-(OMe)$_8$]** with the structures shown in Figure 5a-c (synthetic procedures are described in the Chapter 3). **Co[TPP-F$_{20}$]** is an example of purely thermodynamic stabilization of Co^I centre due to the lower redox Co^{II}/Co^I potential compared to CoTPP.[13, 41] The next derivative **Co[TPP-(OH)$_8$]** was chosen as we expected that introduction of a proton donor into the reactive intermediate directly would enhance the local concentration of H^+ around Co in the [Co([TPP-(OH)$_8$])-CO_2] intermediate and thus lower the probability of oxygen migration from -CO_2 during CO_2ERR.[31, 43] The third complex **Co[TPP-(OMe)$_8$]** was synthesised to test a kinetic-only stabilization approach as this complex contains eight bulky -OCH_3 groups around the porphyrin ring thus denying the oxygen atom the direct access to the macrocycle.

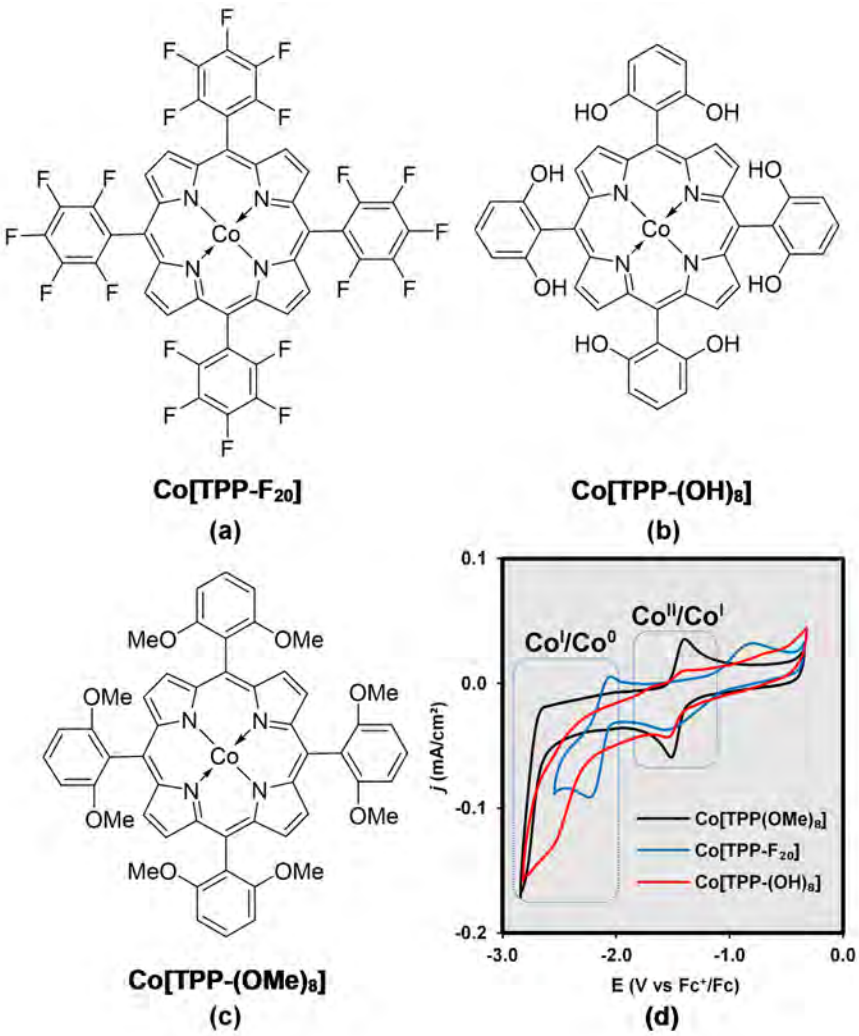

Figure 6.5. Structure of (a) 5,10,15,20-tetrakis(2,3,4,5,6-pentafluorophenyl)porphyrin (**Co[TPP-F$_{20}$]**); (b) 5,10,15,20-tetrakis(2,6-dihydroxyphenyl)porphyrin (**Co[TPP-(OH)$_8$]**); (c) 5,10,15,20-tetrakis(2,6-dimethoxyphenyl)porphyrin (**Co[TPP-(OMe)$_8$]**); (d) CV study of three complexes in degassed DMF/0.1 M TBAP electrolyte.

To gain insight into the electrochemical behaviour of these complexes, CVs of solutions in degassed DMF were recorded (Figure 6.5d). All curves show well-defined Co^I/Co^{II} transitions. Interestingly, for the **Co[TPP-F$_{20}$]** redox couple $[Co^{II}TPP\text{-}F_{20}]/[Co^{I}TPP\text{-}F_{20}]^-$ is quasireversible which is most probably due to high electronegativity of fluorine atoms pulling electron density from the porphyrin moiety onto the pentafluorophenyl substituent. In turn, the first redox couple of **Co[TPP-(OH)$_8$]** and **Co[TPP-(OMe)$_8$]** is reversible. However, one could clearly see that the reversibility of this wave is nearly perfect only for **Co[TPP-(OMe)$_8$]** while **Co[TPP-(OH)$_8$]** shows a clear intensity drop of the reoxidation peak, likely because of -OH deprotonation. Further, the Co^I/Co^0 couple is partially reversible for **Co[TPP-F$_{20}$]** and

completely irreversible for two other derivatives. We believe that this loss of reversibility takes place due to the extrusion of F^-, MeO^- and OH^- groups from dianions.

More information about the electron density distribution in the synthesized complexes could be drawn from comparison of the redox potentials summarised in Table 6.1. The introduction of strong electron withdrawing and donating groups has a limited influence on the potential of the Co^{II}/Co^{I} redox couple as the difference with CoTPP is only 0.13 - 0.16 V after introduction of $-C_6F_5$ and $-C_6H_3(OH)_2$ groups. In turn, the substituent effect reaches 0.27 V for Co^{I}/Co^{0} transformation both for electron donating and withdrawing groups. These results indicate that the first reduction is mostly macrocycle-centred while the second electron is accepted onto yet uncharged phenyl ring. Our conclusions fall in line with earlier the reports which showed that the electrons accepted by porphyrins are indeed located on the ligand rather than on the metal.[46-47] Hence, strong electron withdrawing substituents could significantly draw electron density onto lateral moieties even for the first redox transformation. Also, it shows that simple shift of Co^{II}/Co^{I} to more positive potentials is hardly a viable strategy for stability improvement due to unfavourable redistribution of electron density in the active form of the catalyst. This is an important finding as keeping the negative charge on the porphyrin moiety instead of letting it delocalize on the lateral substituents would boost the catalysis and prevent destruction of the phenyl aromatic system.

Table 6.1 Summary of Co^{II}/Co^{I} and Co^{I}/Co^{0} redox potentials.

complex	E^0 (Co^{II}/Co^{I})	ΔE^0 (Co^{II}/Co^{I})	E (Co^{I}/Co^{0})	ΔE^0 (Co^{I}/Co^{0})[a]
CoTPP	-1.30	-	-2.43	-
Co[TPP-F_{20}]	-1.17	0.13	-2.16	0.27
Co[TPP-$(OH)_8$]	-1.46	-0.16	-2.36[b]	0.07
Co[TPP-$(OMe)_8$]	-1.45	-0.15	-2.70	-0.27

[a] *potentials for Co^{I}/Co^{0} were measured and compared at 80 μA/cm² because the redox waves for* ***Co[TPP-$(OH)_8$]*** *and* ***Co[TPP-$(OMe)_8$]*** *were irreversible even at the scan rate of 10 V/s.*
[b] *current is most probably defined by the reduction of protons derived form -OH groups in the molecule*

To validate our theory all three complexes were immobilised on carbon cloth electrodes and studied using CV in aqueous medium to evaluate their activity (Figure 6a-c) while three consecutive 4 h long CPE experiments were performed to assess their stability and recyclability in long-run electrolyses under a potential of -1.05 V (Figure 6.6d-f). CVs of all three complexes show an increase of the reduction current in the presence of CO_2, which however might arise from CO_2 reduction itself as well as from an enhanced HER rate due to slightly higher acidity in the presence of CO_2. Notably, the potentials of current onsets in all cases match well with the redox behaviour observed in nonaqueous electrolyte. However, we note that **Co[TPP-F_{20}]**

shows almost no distinctive wave corresponding to the Co^{II}/Co^{I} pair most likely because the complex undergoes chemical transformations even without CO_2. In turn, **Co[TPP-(OH)8]** shows a distinctive Co^{II}/Co^{I} wave in the degassed electrolyte which does not disappear even in the presence of CO_2. This behaviour is most probably the result of reduction-first pathway due to the presence of proton donors around the Co centre.[48] Finally, **Co[TPP-(OMe)8]** shows a very distinctive quasi-reversible redox wave in the degassed solution which immediately disappears in the presence of CO_2.

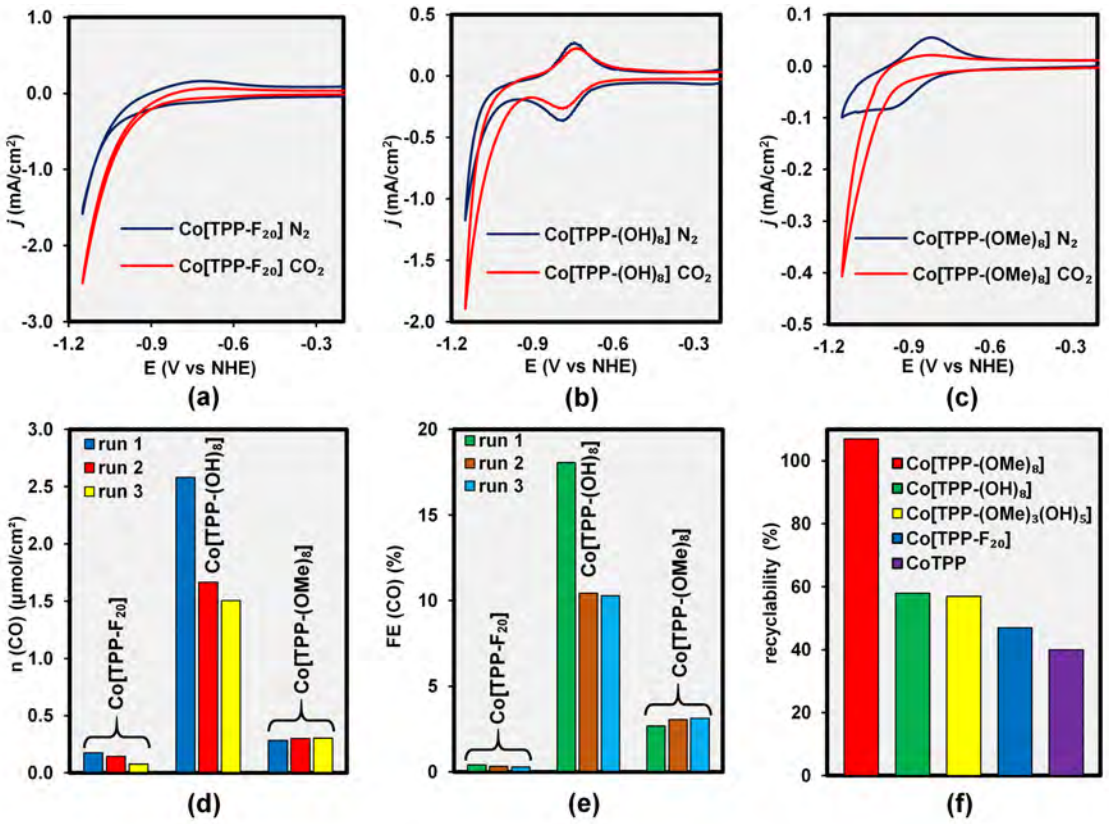

Figure 6.6. CV of carbon-supported (a) **Co[TPP-F20]**, (b) **Co[TPP-(OH)8]** and (c) **Co[TPP-(OMe)8]** in degassed (blue trace) and CO_2-saturated (red) electrolyte; (d) amount of CO evolved and (e) FE (CO) observed on all porphyrins in three consecutive electrolyses; (f) recyclability of all noncovalently immobilised catalysts described in this Chapter under the potential of -1.05 V vs NHE in CO_2-saturated 0.5 M $KHCO_3$ and with surface loading of $8 \cdot 10^{-8}$ mol/cm^2.

Next, we evaluated the stability of each catalyst using repetitive CPE experiments. As expected, **Co[TPP-F20]** shows the worst result out of three catalysts both in terms of stability and activity with the amount of CO produced steadily decreasing from 0.17 μmol/cm^2 in the first run to 0.08 μmol/cm^2 in the third experiment thus representing 53 % decline in activity

(47 % recyclability, Figures 6.6d, f). The FE (CO) is not only extremely small but also drops from 0.41 % to 0.28 % (Figure 6.6e).

At the same time, **Co[TPP-(OH)$_8$]** shows much better CO_2ERR rate even though the Co^{II}/Co^{I} redox couple required more negative potential to drive the reaction. This catalyst produced 2.58 μmol/cm^2 of CO with FE (CO) of 18.1 % in the first catalytic run. However, the reaction slowed down after repetitive catalyst reuse by 42 % as only 1.51 μmol/cm^2 of CO was produced in the last run (58 % recyclability) and FE (CO) dropped to 10.3 %. Interestingly, both FE (CO) and CO evolution rate levelled off after first significant drop as the activity decay between the second and the third electrolysis was as little as 9 %. Clearly, introduction of proton donors into the complex does improve its lifespan compared to **CoTPP-noncov** and **Co[TPP-F$_{20}$]** (Figure 6.6f), however the deactivation still takes place.

In turn, the activity of **Co[TPP-(OMe)$_8$]** was found to be between that of **Co[TPP-F$_{20}$]** and **Co[TPP-(OH)$_8$]** with 0.28 μmol/cm^2 of CO detected after the first experiment and FE (CO) of 2.7 % while its recyclability proved to be exceptionally high as no noticeable decay was detected if the overpotential is kept at 500 mV (for the performance of **Co[TPP-(OMe)$_8$]** under more negative potentials see Figure A47). Moreover, a 7 % increase of CO_2ERR current density by the third electrolysis was observed, most probably due to the system gradually reaching a steady state. We also attempted to combine the positive influence of bulky groups and proton donors using a catalyst with a partially demethylated TPP-(OMe)$_3$(OH)$_5$ ligand, however the resulting catalyst **Co[TPP-(OMe)$_3$(OH)$_5$]** had lower activity compared to **Co[TPP-(OH)$_8$]** while showing almost the same recyclability of 57 % over the course of three catalytic runs (Figures 6.6f and A48).

The stability study is summarised in the Figure 6.6f. Clearly, CoTPP is the least stable catalyst followed by **Co[TPP-F$_{20}$]**, **Co[TPP-(OH)$_8$]** and **Co[TPP-(OMe)$_8$]**. These results show that the presence of bulky groups around the catalytically active site provides the biggest boost in terms of recyclability (from 40 % for CoTPP to ~ 100 % for **Co[TPP-(OMe)$_8$]**) due to steric protection of the reactive centre. Proton donors also prolong the lifetime of the complex, though to lesser extent. Conversely, thermodynamic stabilization of the Co(I) oxidation state only marginally improves the operational life of the catalyst (to 47 % for **Co[TPP-F$_{20}$]**) while its activity is 87 times lower than that of CoTPP. It should be pointed out here that the ability of a catalyst to be reused might be even more important than its absolute activity as an electrode featuring moderate reaction rate indefinitely would be economically more viable than a more

active one with the lifespan of mere several hours. Thus, our observations firmly establish the kinetic inhibition of decomposition reactions as the most promising method for the development of stable electrocatalysts for CO_2ERR.

6.3 Conclusions

In this work we studied the deactivation pathway of a heterogeneous CoTPP catalyst in CO_2ERR in aqueous electrolyte. Migration of oxygen from the adsorbed CO_2 onto the porphyrin ligand was found to be the main process responsible for the loss of catalytic activity while leaching, demetallation and poisoning by CO make little to no contribution to the deactivation process. The study of substituted porphyrins led us to the conclusion that the most efficient method of the catalyst stabilization is steric protection of the macrocyclic core via introduction of bulky lateral groups as this approach yielded 100 % recyclable catalyst. Proton donors around the porphyrin core promote protonation of CO_2 and thus also improve the catalyst lifetime. In turn, electron withdrawing substituents pull the electron density away from the reaction centre and essentially quench the catalysis while not giving any advantages in terms of the catalyst longevity. Furthermore, our attempt to stabilize the catalyst by coordination of an additional pyridine ligand to the Co centre led the formation of a complex which is unable to reduce CO_2. Generally, kinetic suppression of catalyst decomposition was found to be the most successful strategy for the development of highly stable electrocatalysts and this result could be used as a general guidance in the search of economically viable electrocatalysts.

6.4 References

[1] Jensen, M. T.; Rønne, M. H.; Ravn, A. K.; Juhl, R. W.; Nielsen, D. U.; Hu, X.-M.; Pedersen, S. U.; Daasbjerg, K.; Skrydstrup, T., Scalable carbon dioxide electroreduction coupled to carbonylation chemistry, *Nat. Comm.* **2017,** 8 (1), 489
[2] Weekes, D. M.; Salvatore, D. A.; Reyes, A.; Huang, A.; Berlinguette, C. P., Electrolytic CO2 Reduction in a Flow Cell, *Acc. Chem. Res.* **2018,** 51 (4), 910-918
[3] Benson, E. E.; Kubiak, C. P.; Sathrum, A. J.; Smieja, J. M., Electrocatalytic and homogeneous approaches to conversion of CO2 to liquid fuels, *Chem. Soc. Rev.* **2009,** 38 (1), 89-99
[4] Costentin, C.; Robert, M.; Saveant, J.-M., Catalysis of the electrochemical reduction of carbon dioxide, *Chem. Soc. Rev.* **2013,** 42 (6), 2423-2436
[5] Francke, R.; Schille, B.; Roemelt, M., Homogeneously Catalyzed Electroreduction of Carbon Dioxide—Methods, Mechanisms, and Catalysts, *Chem. Rev.* **2018,** 118 (9), 4631-4701
[6] Fukuzumi, S.; Lee, Y.-M.; Ahn, H. S.; Nam, W., Mechanisms of catalytic reduction of CO2 with heme and nonheme metal complexes, *Chem. Sci.* **2018,** 9 (28), 6017-6034
[7] Dalle, K. E.; Warnan, J.; Leung, J. J.; Reuillard, B.; Karmel, I. S.; Reisner, E., Electro- and Solar-Driven Fuel Synthesis with First Row Transition Metal Complexes, *Chem. Rev.* **2019,** 119 (4), 2752-2875
[8] Benson, E. E.; Kubiak, C. P., Structural investigations into the deactivation pathway of the CO2 reduction electrocatalyst Re(bpy)(CO)3Cl, *Chem. Comm.* **2012,** 48 (59), 7374-7376
[9] Jiang, J.; Matula, A. J.; Swierk, J. R.; Romano, N.; Wu, Y.; Batista, V. S.; Crabtree, R. H.; Lindsey, J. S.; Wang, H.; Brudvig, G. W., Unusual Stability of a Bacteriochlorin Electrocatalyst under Reductive Conditions. A Case Study on CO2 Conversion to CO, *ACS Catal.* **2018,** 8 (11), 10131-10136
[10] Jiang, J.; Materna, K. L.; Hedström, S.; Yang, K. R.; Crabtree, R. H.; Batista, V. S.; Brudvig, G. W., Antimony Complexes for Electrocatalysis: Activity of a Main-Group Element in Proton Reduction, *Angew. Chem.* **2017,** 129 (31), 9239-9243
[11] Windle, C. D.; George, M. W.; Perutz, R. N.; Summers, P. A.; Sun, X. Z.; Whitwood, A. C., Comparison of rhenium–porphyrin dyads for CO2 photoreduction: photocatalytic studies and charge separation dynamics studied by time-resolved IR spectroscopy, *Chem. Sci.* **2015,** 6 (12), 6847-6864
[12] Bhugun, I.; Lexa, D.; Savéant, J.-M., Catalysis of the Electrochemical Reduction of Carbon Dioxide by Iron(0) Porphyrins: Synergystic Effect of Weak Br nsted Acids, *J. Am. Chem. Soc.* **1996,** 118 (7), 1769-1776
[13] Azcarate, I.; Costentin, C.; Robert, M.; Savéant, J.-M., Through-Space Charge Interaction Substituent Effects in Molecular Catalysis Leading to the Design of the Most Efficient Catalyst of CO2-to-CO Electrochemical Conversion, *J. Am. Chem. Soc.* **2016,** 138 (51), 16639-16644
[14] Costentin, C.; Passard, G.; Robert, M.; Savéant, J.-M., Ultraefficient homogeneous catalyst for the CO2-to-CO electrochemical conversion, *Proc. Nat. Acad. Sci.* **2014,** 111 (42), 14990
[15] Costentin, C.; Robert, M.; Savéant, J.-M., Current Issues in Molecular Catalysis Illustrated by Iron Porphyrins as Catalysts of the CO2-to-CO Electrochemical Conversion, *Acc. Chem. Res.* **2015,** 48 (12), 2996-3006
[16] Grodkowski, J.; Behar, D.; Neta, P.; Hambright, P., Iron Porphyrin-Catalyzed Reduction of CO2. Photochemical and Radiation Chemical Studies, *J. Phys. Chem. A* **1997,** 101 (3), 248-254
[17] Maurin, A.; Robert, M., Noncovalent Immobilization of a Molecular Iron-Based Electrocatalyst on Carbon Electrodes for Selective, Efficient CO2-to-CO Conversion in Water, *J. Am. Chem. Soc.* **2016,** 138 (8), 2492-2495
[18] Weng, Z.; Wu, Y.; Wang, M.; Jiang, J.; Yang, K.; Huo, S.; Wang, X.-F.; Ma, Q.; Brudvig, G. W.; Batista, V. S.; Liang, Y.; Feng, Z.; Wang, H., Active sites of copper-complex catalytic materials for electrochemical carbon dioxide reduction, *Nature Comm.* **2018,** 9 (1), 415
[19] Kumar, M.; Neta, P.; Sutter, T. P. G.; Hambright, P., One-electron reduction and demetallation of copper porphyrins, *J. Phys. Chem.* **1992,** 96 (23), 9571-9575
[20] Lin, S.; Diercks, C. S.; Zhang, Y.-B.; Kornienko, N.; Nichols, E. M.; Zhao, Y.; Paris, A. R.; Kim, D.; Yang, P.; Yaghi, O. M.; Chang, C. J., Covalent organic frameworks comprising cobalt porphyrins for catalytic CO2 reduction in water, *Science* **2015,** 349 (6253), 1208-1213
[21] Marianov, A. N.; Jiang, Y., Covalent ligation of Co molecular catalyst to carbon cloth for efficient electroreduction of CO2 in water, *Appl. Catal. B* **2019,** 244, 881-888
[22] Hu, X.-M.; Rønne, M. H.; Pedersen, S. U.; Skrydstrup, T.; Daasbjerg, K., Enhanced Catalytic Activity of Cobalt Porphyrin in CO2 Electroreduction upon Immobilization on Carbon Materials, *Angew. Chem.* **2017,** 129 (23), 6568-6572
[23] Ananikov, V. P.; Beletskaya, I. P., Toward the Ideal Catalyst: From Atomic Centers to a "Cocktail" of Catalysts, *Organometallics* **2012,** 31 (5), 1595-1604
[24] Bartholomew, C. H., Mechanisms of catalyst deactivation, *Appl. Catal. A.* **2001,** 212 (1), 17-60

[25] Ruther, R. E.; Rigsby, M. L.; Gerken, J. B.; Hogendoorn, S. R.; Landis, E. C.; Stahl, S. S.; Hamers, R. J., Highly Stable Redox-Active Molecular Layers by Covalent Grafting to Conductive Diamond, *J. Am. Chem. Soc.* **2011,** 133 (15), 5692-5694
[26] Zhu, M.; Chen, J.; Huang, L.; Ye, R.; Xu, J.; Han, Y.-F., Covalently Grafting Cobalt Porphyrin onto Carbon Nanotubes for Efficient CO2 Electroreduction, *Angew. Chem. Int. Ed.* **2019,** 0 (0),
[27] Machan, C. W.; Sampson, M. D.; Chabolla, S. A.; Dang, T.; Kubiak, C. P., Developing a Mechanistic Understanding of Molecular Electrocatalysts for CO2 Reduction using Infrared Spectroelectrochemistry, *Organometallics* **2014,** 33 (18), 4550-4559
[28] Smieja, J. M.; Sampson, M. D.; Grice, K. A.; Benson, E. E.; Froehlich, J. D.; Kubiak, C. P., Manganese as a Substitute for Rhenium in CO2 Reduction Catalysts: The Importance of Acids, *Inorg. Chem.* **2013,** 52 (5), 2484-2491
[29] Smieja, J. M.; Kubiak, C. P., Re(bipy-tBu)(CO)3Cl−improved Catalytic Activity for Reduction of Carbon Dioxide: IR-Spectroelectrochemical and Mechanistic Studies, *Inorg. Chem.* **2010,** 49 (20), 9283-9289
[30] Kutal, C.; Weber, M. A.; Ferraudi, G.; Geiger, D., A mechanistic investigation of the photoinduced reduction of carbon dioxide mediated by tricarbonylbromo(2,2'-bipyridine)rhenium(I), *Organometallics* **1985,** 4 (12), 2161-2166
[31] Costentin, C.; Drouet, S.; Robert, M.; Savéant, J.-M., A Local Proton Source Enhances CO2 Electroreduction to CO by a Molecular Fe Catalyst, *Science* **2012,** 338 (6103), 90-94
[32] Wayland, B. B.; Abd-Elmageed, M. E.; Mehne, L. F., Low-spin cobalt(II)-Schiff base and -porphyrin complexes of carbon monoxide, isocyanomethane, trimethyl arsine, and phosphines. Electron paramagnetic resonance studies, *Inorg. Chem.* **1975,** 14 (7), 1456-1460
[33] Kadish, K. M.; Ou, Z.; Shao, J.; Gros, C. P.; Barbe, J.-M.; Jérôme, F.; Bolze, F.; Burdet, F.; Guilard, R., Alkyl and Aryl Substituted Corroles. 3. Reactions of Cofacial Cobalt Biscorroles and Porphyrin-Corroles with Pyridine and Carbon Monoxide, *Inorg. Chem.* **2002,** 41 (15), 3990-4005
[34] Nielsen, I. M. B.; Leung, K., Cobalt−Porphyrin Catalyzed Electrochemical Reduction of Carbon Dioxide in Water. 1. A Density Functional Study of Intermediates, *The Journal of Physical Chemistry A* **2010,** 114 (37), 10166-10173
[35] Leung, K.; Nielsen, I. M. B.; Sai, N.; Medforth, C.; Shelnutt, J. A., Cobalt−Porphyrin Catalyzed Electrochemical Reduction of Carbon Dioxide in Water. 2. Mechanism from First Principles, *The Journal of Physical Chemistry A* **2010,** 114 (37), 10174-10184
[36] Kramer, W. W.; McCrory, C. C. L., Polymer coordination promotes selective CO2 reduction by cobalt phthalocyanine, *Chem. Sci.* **2016,** 7 (4), 2506-2515
[37] Strieter, E. R.; Blackmond, D. G.; Buchwald, S. L., Insights into the Origin of High Activity and Stability of Catalysts Derived from Bulky, Electron-Rich Monophosphinobiaryl Ligands in the Pd-Catalyzed C−N Bond Formation, *J. Am. Chem. Soc.* **2003,** 125 (46), 13978-13980
[38] Lin, X. Q.; Boisselier-Cocolios, B.; Kadish, K. M., Electrochemistry, spectroelectrochemistry, and ligand addition reactions of an easily reducible cobalt porphyrin. Reactions of (Tetracyanotetraphenylporphinato)cobalt(II) (((CN)4TPF)Co(II)) in pyridine and in pyridine/methylene chloride mixtures, *Inorg. Chem.* **1986,** 25 (18), 3242-3248
[39] Shirazi, A.; Goff, H. M., Carbon-13 and proton NMR spectroscopy of four- and five-coordinate cobalt(II) porphyrins: analysis of NMR isotropic shifts, *Inorg. Chem.* **1982,** 21 (9), 3420-3425
[40] Dridi, H.; Comminges, C.; Morais, C.; Meledje, J.-C.; Kokoh, K. B.; Costentin, C.; Savéant, J.-M., Catalysis and Inhibition in the Electrochemical Reduction of CO2 on Platinum in the Presence of Protonated Pyridine. New Insights into Mechanisms and Products, *J. Am. Chem. Soc.* **2017,** 139 (39), 13922-13928
[41] Zhang, X.; Wu, Z.; Zhang, X.; Li, L.; Li, Y.; Xu, H.; Li, X.; Yu, X.; Zhang, Z.; Liang, Y.; Wang, H., Highly selective and active CO2 reduction electrocatalysts based on cobalt phthalocyanine/carbon nanotube hybrid structures, *Nature Comm.* **2017,** 8, 14675
[42] Maurin, A.; Robert, M., Catalytic CO2-to-CO conversion in water by covalently functionalized carbon nanotubes with a molecular iron catalyst, *Chem. Comm.* **2016,** 52 (81), 12084-12087
[43] Nichols, E.; Derrick, J. S.; Nistanaki, S. K.; Smith, P. T.; Chang, C. J., Positional effects of second-sphere amide pendants on electrochemical CO2 reduction catalyzed by iron porphyrins, *Chem. Sci.* **2018**,
[44] Choi, J.; Wagner, P.; Gambhir, S.; Jalili, R.; MacFarlane, D. R.; Wallace, G. G.; Officer, D. L., Steric Modification of a Cobalt Phthalocyanine/Graphene Catalyst To Give Enhanced and Stable Electrochemical CO2 Reduction to CO, *ACS Energy Letters* **2019**, 666-672
[45] Zhu, M.; Yang, D.-T.; Ye, R.; Zeng, J.; Corbin, N.; Manthiram, K., Inductive and electrostatic effects on cobalt porphyrins for heterogeneous electrocatalytic carbon dioxide reduction, *Catal. Sci. Tech.* **2019,** 9 (4), 974-980
[46] Römelt, C.; Song, J.; Tarrago, M.; Rees, J. A.; van Gastel, M.; Weyhermüller, T.; DeBeer, S.; Bill, E.; Neese, F.; Ye, S., Electronic Structure of a Formal Iron(0) Porphyrin Complex Relevant to CO2 Reduction, *Inorg. Chem.* **2017,** 56 (8), 4745-4750

[47] Gurinovich, G. P.; Gurinovich, I. F.; Ivashin, N. V.; Sinyakov, G. N.; Shulga, A. M.; Terekhov, S. N.; Filatov, I. V.; Dzilinski, K., Electronic structure of metalloporphyrin π-anions, *J. Mol. Structure* **1988,** 172, 317-343
[48] Ngo, K. T.; McKinnon, M.; Mahanti, B.; Narayanan, R.; Grills, D. C.; Ertem, M. Z.; Rochford, J., Turning on the Protonation-First Pathway for Electrocatalytic CO2 Reduction by Manganese Bipyridyl Tricarbonyl Complexes, *J. Am. Chem. Soc.* **2017,** 139 (7), 2604-2618

CHAPTER 7. CONCLUSIONS AND OUTLOOK

7.1 Conclusions

This thesis describes the influence of heterogenisation modes on the performance of porphyrin-based heterogeneous electrocatalysts designed for energy applications operating in aqueous medium. Covalent immobilisation of the complexes onto the carbon surface was conveniently achieved via potentiostatic electroreduction of the corresponding diazonium salt with the following introduction of a metal atom. Noncovalently immobilised catalysts were prepared using the conventional drop-casting technique. Following successful preparation of the desired materials, their structure and electrocatalytic performance in CO_2 electroreduction (CO_2ERR), oxygen reduction (ORR) and oxygen evolution (OER) were evaluated.

First, a reliable procedure for covalent immobilisation of Mn porphyrin on the surface of carbon cloth electrodes was developed. Electroreduction of porphyrin diazonium salt safely generated *in situ* with the following treatment of the electrode with hot solution of $Co(OAc)_2$ in DMF/CH_3COOH was found to be a reliable tool for covalent ligation of the macrocyclic complex. The resulting layer of Mn tetraphenylporphyrin retained spectral and electrochemical features characteristic for noncovalently immobilised complex as evidenced by the results of Raman spectroscopy and CV analysis. Electrodeposition duration was found to be a convenient tool to control the amount of electrochemically active catalyst on the electrode. Analysis of electrochemical data suggests that the increase of porphyrin surface concentration upon prolonged electrodeposition shortens the average Mn···Mn distance and proportionally enhances the probability of at least two metal atoms simultaneously participating in a catalytic process.

With the established synthetic procedure in hands the influence of covalent immobilisation on the performance of Mn tetraphenylporphyrin in ORR, OER and CO_2ERR reactions was evaluated. Optimisation of the organic layer density was found to have a profound effect on the catalyst performance in ORR in alkaline medium. 5 min electrodeposition furnishes the best catalyst which features predominantly a 4-electron pathway at low overpotentials where noncovalent counterpart shows selectivity to H_2O of ~50 %. What is more, the overall catalytic current at -0.79 V vs NHE was 2.4 times higher for covalently immobilised porphyrinate. Electrokinetic measurements and impedance spectroscopy suggest that the reaction proceeds via formation of an Mn^{II} intermediate with stepwise O_2 reduction to H_2O_2 and then to H_2O.

Similar effects were observed in an acidic electrolyte. The OER rate was found to be less sensitive to the immobilisation mode and mainly dependant on the amount of electrochemically active catalyst only. The study of Mn porphyrins in CO_2ERR showed that the complex is largely inactive in aqueous medium and significant portion of CO evolution takes place on the supporting carbon cloth electrode instead. Nevertheless, the competing hydrogen evolution was largely suppressed when covalent immobilisation was used, most probably due much better coverage of the carbon surface compared to drop-casting. Analysis of homogeneous CO_2ERR in the presence of MnTPP shows that CO coordinates strongly to the metal centre effectively quenching the reaction catalysed by $[Mn^{I}TPP]^{-}$ species. In turn, $[Mn^{0}TPP]^{2-}$ species generated under more negative potentials does not support catalysis and react irreversibly with CO_2 which leads to rapid irreversible decomposition of the complex accompanied by liberation of the free ligand due to demetallation.

Based on the encouraging results obtained for MnTPP-based catalysts the strategy of covalent immobilisation was expanded to encompass CoTPP analogues which are known for their excellent activity both in CO_2ERR and ORR. Synthesis of covalently immobilised Co porphyrin using a two-step procedure was successfully undertaken thus proving high reliability of this technique. Compared to the noncovalent mode, covalent ligation leads to a 2.4 times higher surface density of electrochemically active species with retention of signature Raman and CV features. Furthermore, ligation of CoTPP via the resulting phenylene group had a profound effect on the electrocatalytic performance in CO_2ERR. Indeed, the formation of CO in neutral aqueous electrolyte at –1.05 V vs NHE (η = 500 mV) occurs with a TOF of 8.3 s^{-1} while noncovalent counterpart exhibits TOF of 4.5 s^{-1} only and a maximum FE(CO) of 67 % is achieved at 50 mV less negative potential. The catalyst accumulated an impressive TON of $3.9 \cdot 10^{5}$ in a 24 h long electrolysis surpassing performance of the drop-cast analogue by a factor of 3 and showed FE(CO) of up to 81 %. Notably, the TON and TOF values achieved in our study are among of the highest reported to date surpassing those measured for Fe hydroxyporphyrins and Co porphyrin-based covalent organic frameworks. Electrokinetic analysis demonstrated that the electron transfer from the electrode onto porphyrin moiety plays an important role in overall reaction kinetics, especially at minimal overpotentials. Thus, the short covalent link with the support is a key element of heterogeneous catalyst design for CO_2ERR.

The performance of CoTPP-modified carbon cloth electrodes was further evaluated in ORR. Screening of the reaction conditions revealed that the complex is stabile only in alkaline

electrolyte and noncovalently immobilised porphyrin shows an ETN of less than 2 which corresponds to 100 % selectivity to H_2O_2 formation. The following study of covalently modified electrodes shows that the effect of multicentred catalysis also manifests itself upon increase of immobilisation time similar to the case of Mn porphyrin-catalysed reaction. Indeed, we achieved an ETN of 3.1 on CoTPP-cov/10 (10 min long electrodeposition) which corresponds to 55 % selectivity towards H_2O formation. However, the current onset overpotential is independent of the complex immobilisation mode. These observations fall in line with H_2O_2 reduction activity of the electrocatalysts which has current onset close to that of the ORR and at the same time shows a significant increase of the reaction rate upon covalent immobilisation of CoTPP. Thus, the effect of covalent ligation on the ORR is not limited to Mn complexes and is a rather general phenomenon.

Finally, the problem of stability of molecular electrocatalysts under long-term operation was studied. Co porphyrin was chosen as an example of a highly active catalyst and its decomposition pattern in CO_2ERR was investigated. In contrast to earlier reports, the experimental evidence described in this dissertation shows that it is uptake of oxygen from CO_2 by the macrocyclic core that leads to the loss of activity while leaching, demetallation, poisoning by CO and reduction to chlorins play no significant role in the deactivation process. Interestingly, the immobilisation mode has little to no effect on reusability of heterogeneous CoTPP-based catalysts. This insight into the reaction mechanism made it possible to establish a strategy for the development of more stable porphyrin-based catalysts. Indeed, introduction of steric protection into the porphyrin core in the form of eight bulky -OCH_3 groups furnishes 100 % recyclable heterogeneous molecular catalyst **Co[TPP-(OMe)$_8$]**, though with lower overall activity compared to CoTPP. Lateral proton donors also significantly improve catalyst lifetime due to favourable protonation of $[CoTPP\text{-}CO_2]^-$ intermediate. In turn, thermodynamic stabilisation of the Co^I active form by electronegative substituents or additional axial ligands does not give any advantage in terms of stability while significantly decreasing the CO_2ERR rate. This work shows that the careful analysis of catalyst deactivation mechanism and its following kinetic inhibition are crucial tools in the quest for industrially viable electrocatalysts.

7.2 Future work

This thesis is focused on the influence of immobilisation modes on the performance of heterogeneous porphyrin-based catalysts for CO_2ERR, ORR and OER. It was demonstrated that the introduction of covalent link between the catalyst and the supporting electrode could

bring about increased TOFs and significantly affect ORR selectivity. Also, a framework for the development of more durable macrocyclic complexes was proposed and validated. Despite enormous advances in the field, the development of molecular electrocatalysts still requires significant breakthroughs in several areas.

One of the biggest problems is their low stability in prolonged electrolyses. Indeed, even though numerous examples of extremely active catalysts have been reported, decomposition under operation conditions largely negates advantages of high TOFs. Though this issue is well known, the mechanistic studies of decomposition processes are severely underrepresented in the current literature. Moreover, scrutiny shows that the deactivation pathways are mostly assumed rather than studied. At the same time, this is understandable as the challenges implied by the work of this type are truly formidable due to tedious separations of minute quantities of final products. More than that, the resulting organometallics may have unexpected structures requiring elaborate spectral and crystallographic characterisations. However, this is the challenge to answer as unstable catalysts cannot be economically viable. Hence, additional in-depth studies of decomposition pathways are necessary to build a solid theoretical background for the development of durable materials. Only then, combined with the current knowledge regarding structure-activity relationships, it will be possible to achieve effective long-term operation required for industrial applications. As an example, the reduction of macrocyclic core could be counteracted by the introduction of electronegative substituents. Similarly, the reductive demetallation may be suppressed by the addition of the pendant coordinating groups such as pyridine that would stabilise the metal centre. More radical solutions include the use of novel complexes with an extremely rigid structure (such as phthalocyanines) and lateral proton donors (such as the -OH or $-NH_2$ groups) lowering the energy of the transition complex.

Closely connected to the direction mentioned above would be the studies on the influence of catalytic poisons on the performance of electrocatalysts in CO_2ERR utilisation of the effluent gases with minimum purification can significantly decrease the feedstock costs. A first step has already been done as one recent study showed that the porphyrin-based catalysts can reduce CO_2 in the presence of appreciable amounts of O_2. At the same time, the raw products of natural fuel combustion could also contain trace amounts of SO_2, NO and other catalytic poisons which may affect the catalytic activity. Similarly, the use of ambient air with possible pollutants may have significant detrimental effects on the performance of fuel cells and more work on the molecular interactions of ORR catalysts with such compounds as H_2S and NH_3 should be performed.

Further, as it was clearly demonstrated on the examples of Co and Fe porphyrin catalysed CO_2ERR, the transition to the aqueous medium often changes the reaction pathways rendering some of the complexes much less active. At the same time, the mechanistic understanding of this change has not been elucidated yet. Considering the wide range of available information on the reaction mechanisms obtained in homogeneous non-aqueous systems it would be highly desirable to generalise the results accumulated to date and extend them to heterogeneous systems. Hence, detailed studies of the solvent effects in electrocatalytic reactions are required. This would allow to unify the research framework and close the gap between homogeneous and heterogeneous catalysts.

A fourth direction can be described as the development of new catalysts and reaction conditions with improved selectivity to multielectron reductions and one-pot syntheses. Indeed, for CO_2ERR it would be desirable to produce the products such as ethylene right in the cell. Also, CO_2ERR coupled with other reactions such as carbonylations within a single system would allow to synthesise high-value products from the feedstocks of zero or negative cost. A similar approach could be applied to ORR and OER where mild *in-situ* oxidations could replace currently used oxidants such as H_2O_2. Moreover, it is highly beneficial to find ways to tune selectivity without lengthy de novo syntheses, for example using novel supporting electrodes. Clearly, it is possible to achieve using immobilisation effects at least on the example of ORR and further development in this direction for CO_2ERR is necessary.

Finally, more attention is to be devoted to the development of the efficient continuous flow-type reactors. This is especially important for such reactions as CO_2ERR since the solubility of CO_2 in aqueous electrolytes is low and the elimination of diffusion limitations by running the electroreduction on gas-diffusion electrodes could potentially eliminate this problem. Also, departure from a classic H-cell design implied use of ion-exchange polymers that may either improve or hamper the proton and electron delivery mechanisms. Hence, running CO_2ERR in the presence of ionomers normally is yet to be described in detail.

APPENDIX

A1. NMR spectra of porphyrins

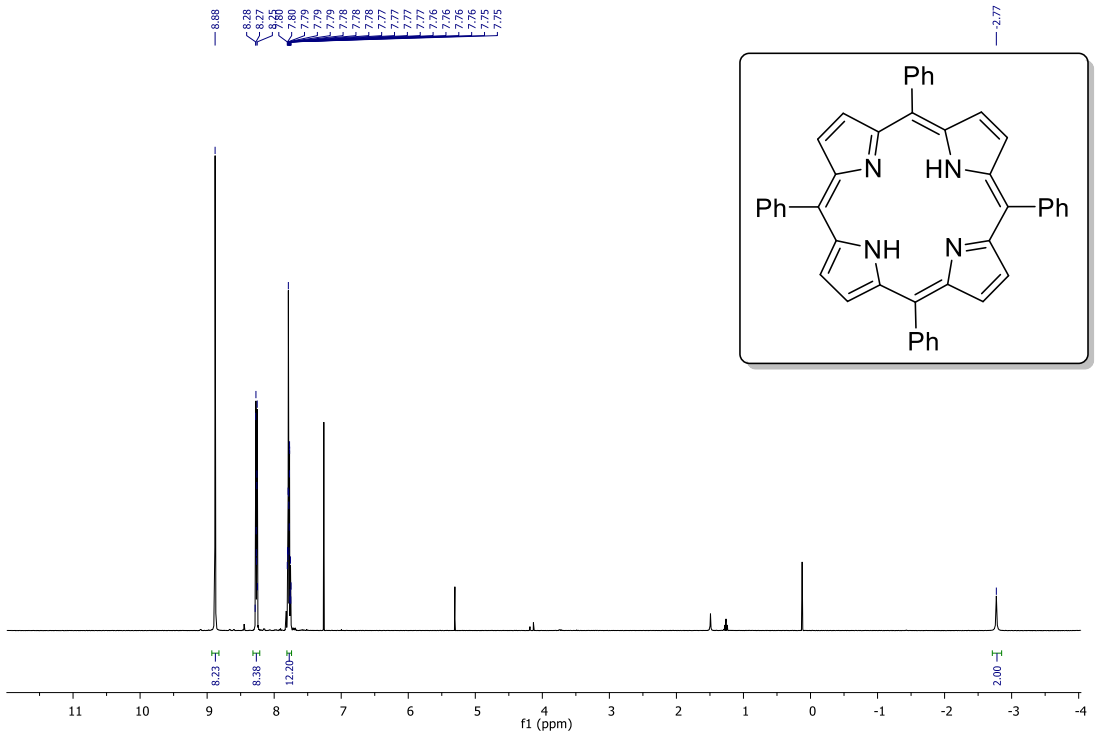

Figure A1. ^{1}H NMR spectrum of *5,10,15,20-tetraphenylporphyrin* **1** ($CDCl_3$, 400 MHz).

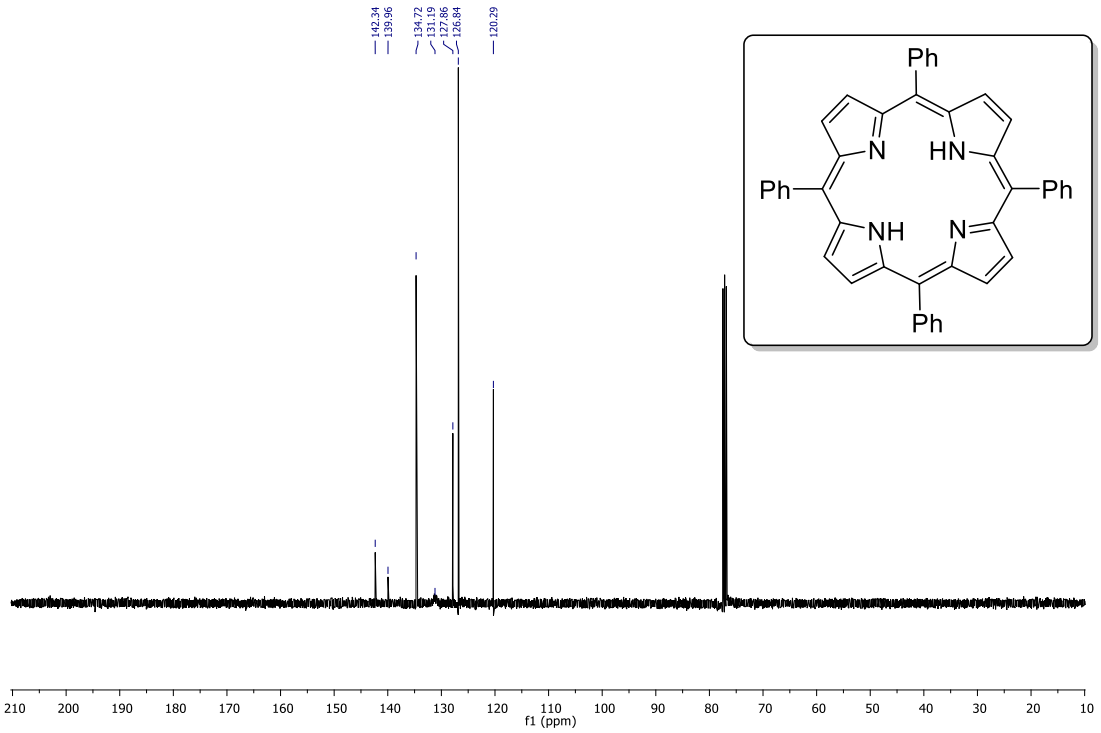

Figure A2. ^{13}C NMR spectrum of *5,10,15,20-tetraphenylporphyrin* **1** ($CDCl_3$, 100 MHz).

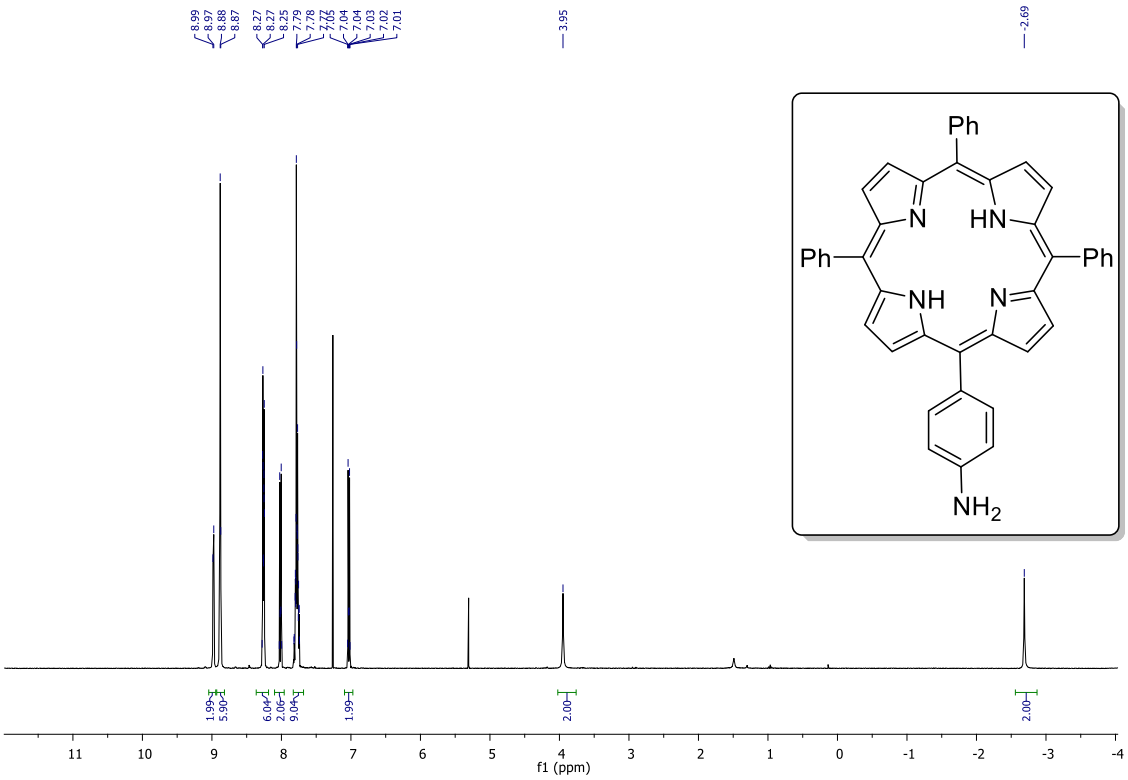

Figure A3. ^{1}H NMR spectrum of 5-(4-aminophnenyl)-10,15,20-triphenylporphyrin **TPP-NH₂** ($CDCl_3$, 400 MHz).

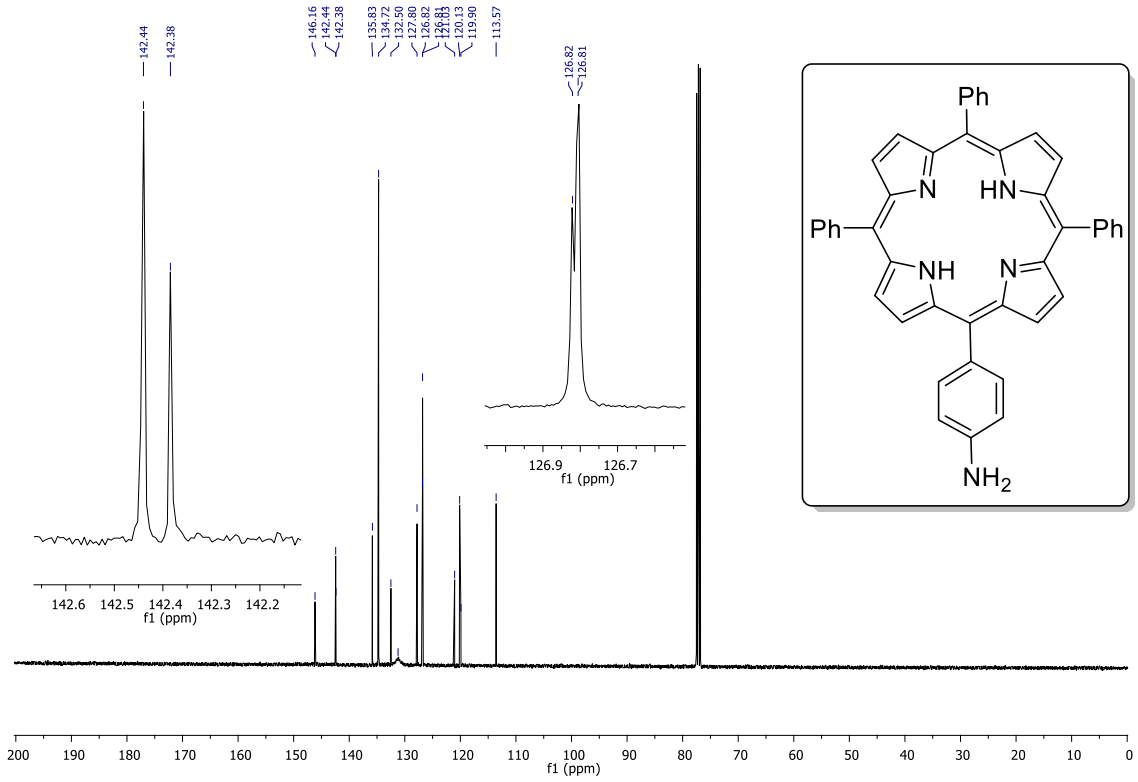

Figure A4. ^{13}C NMR spectrum of 5-(4-aminophnenyl)-10,15,20-triphenylporphyrin **TPP-NH₂** ($CDCl_3$, 100 MHz).

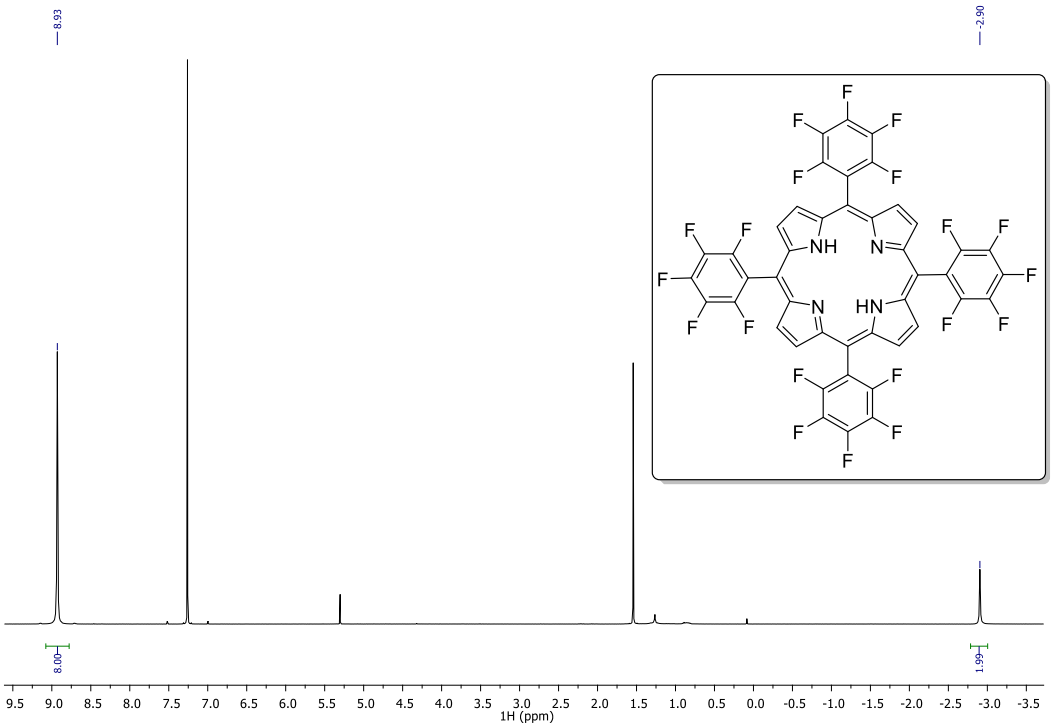

Figure A5. ^{1}H NMR spectrum of 5,10,15,20-tetrakis(2,3,4,5,6-pentafluorphenyl)porphyrin **TPP-F$_{20}$** ($CDCl_3$, 400.1 MHz).

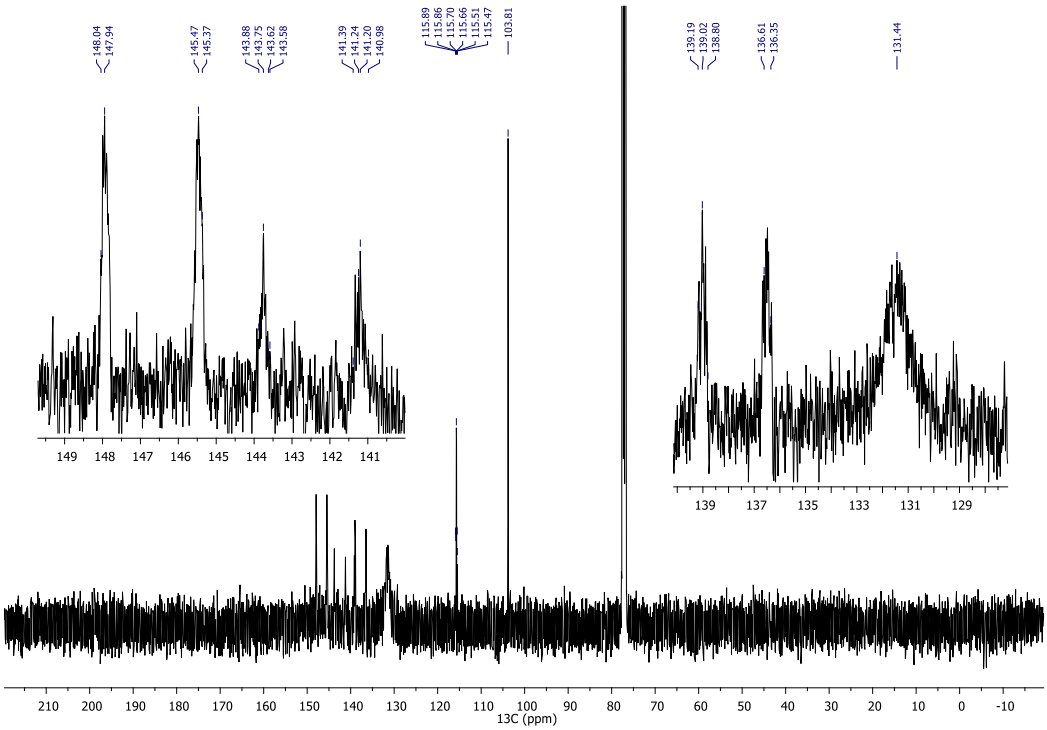

Figure A6. ^{13}C NMR spectrum of 5,10,15,20-tetrakis(2,3,4,5,6-pentafluorphenyl)porphyrin **TPP-F$_{20}$** ($CDCl_3$, 100.6 MHz).

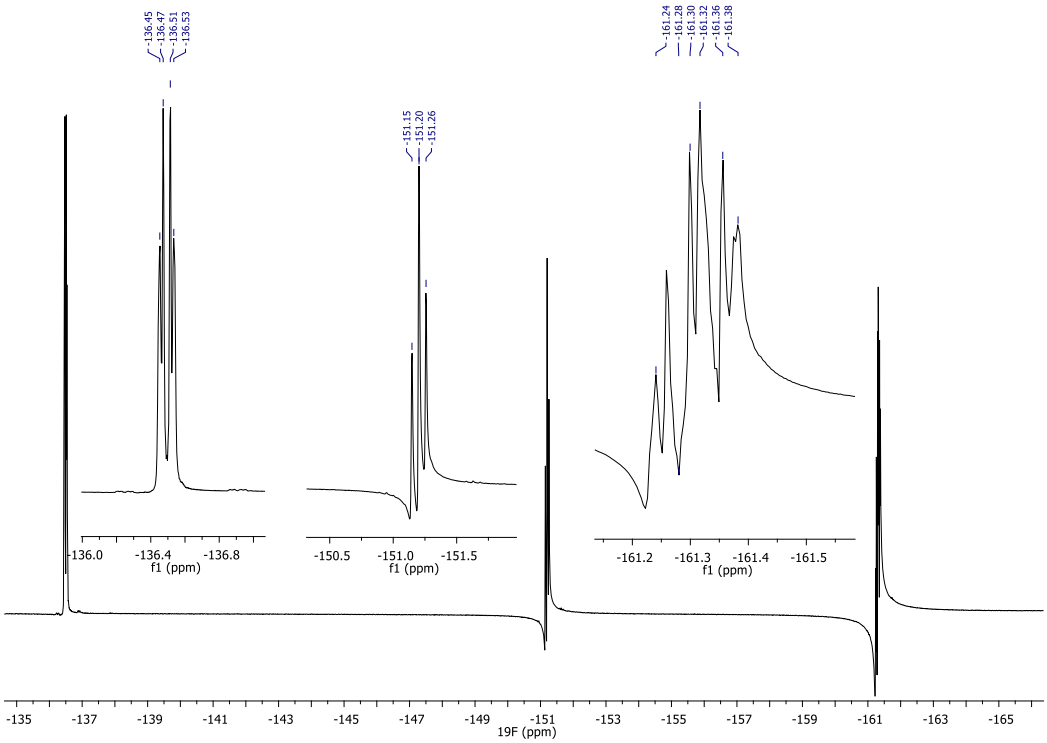

Figure A7. ^{19}F NMR spectrum of 5,10,15,20-tetrakis(2,3,4,5,6-pentafluorphenyl)porphyrin **TPP-F$_{20}$** ($CDCl_3$, 376.5 MHz).

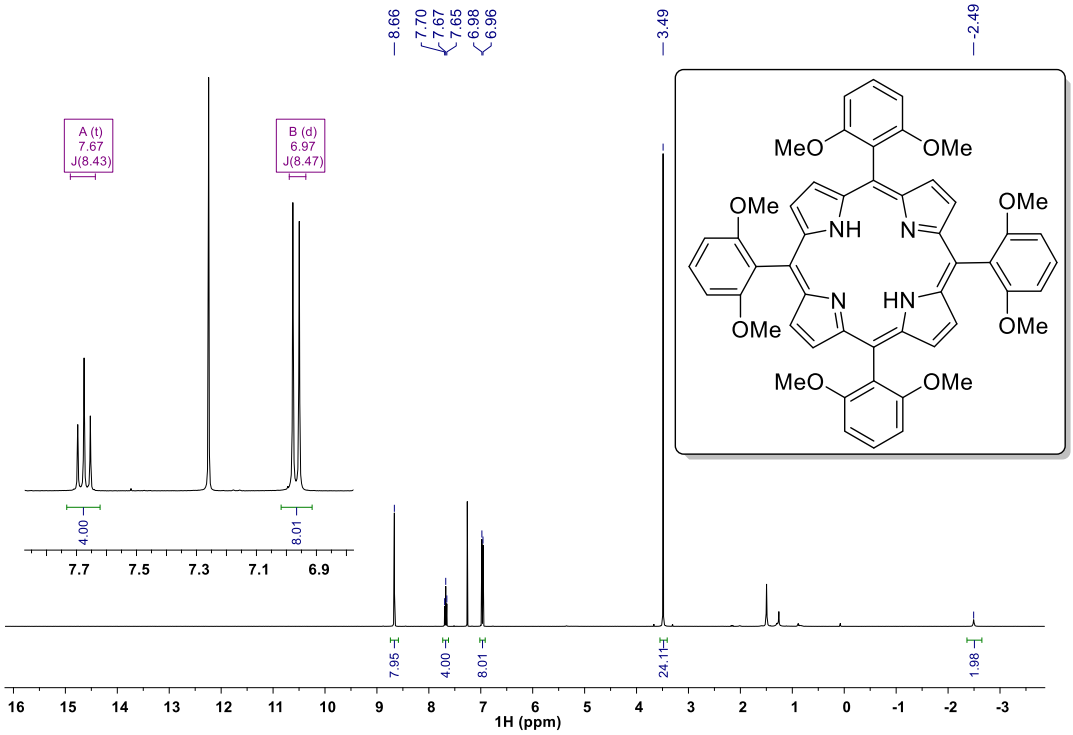

Figure A8. ^{1}H NMR spectrum of 5,10,15,20-tetrakis(2,6-dimethoxyphenyl)porphyrin **TPP-(OMe)$_8$** ($CDCl_3$, 400.1 MHz).

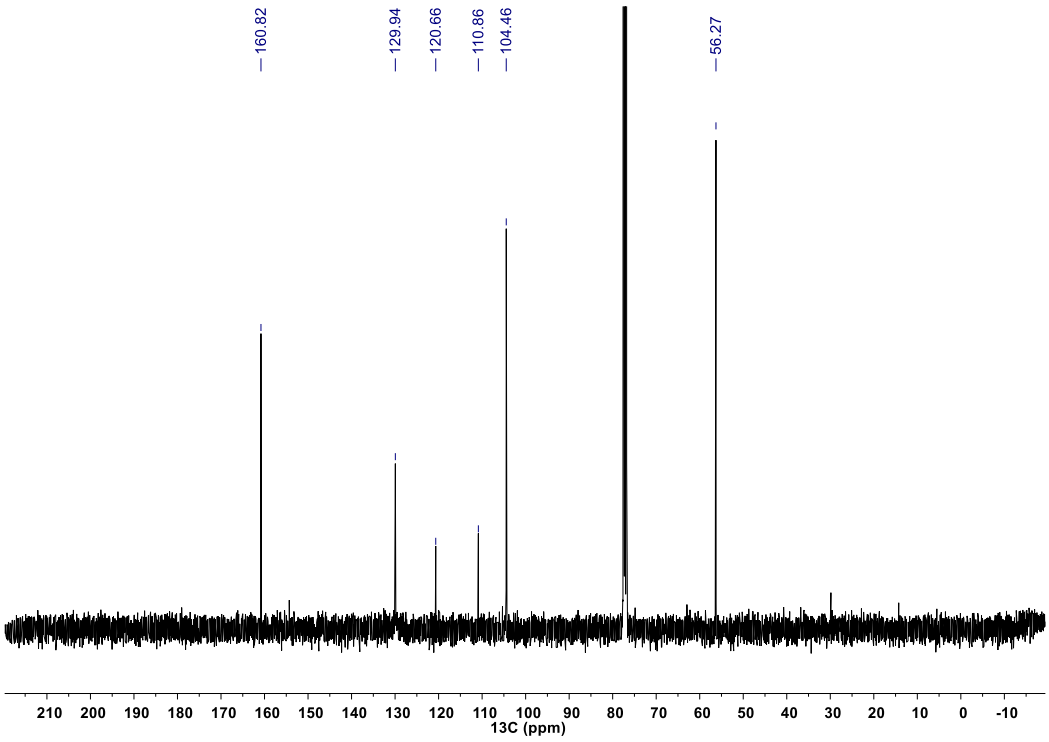

Figure A9. ^{13}C NMR spectrum of 5,10,15,20-tetrakis(2,6-dimethoxyphenyl)porphyrin **TPP-(OMe)8** ($CDCl_3$, 100.6 MHz).

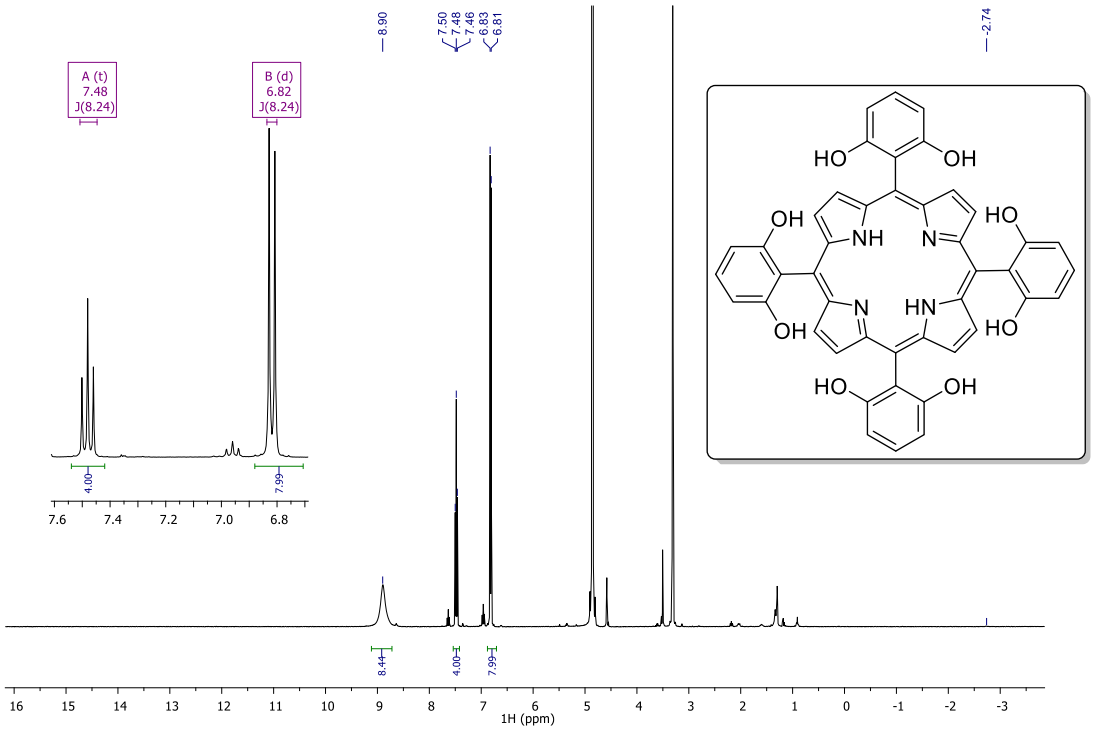

Figure A10. ^{1}H NMR spectrum of *5,10,15,20-tetrakis(2,6-dihydroxyphenyl)porphyrin* **TPP-(OH)8** (CD_3OD, 400.1 MHz).

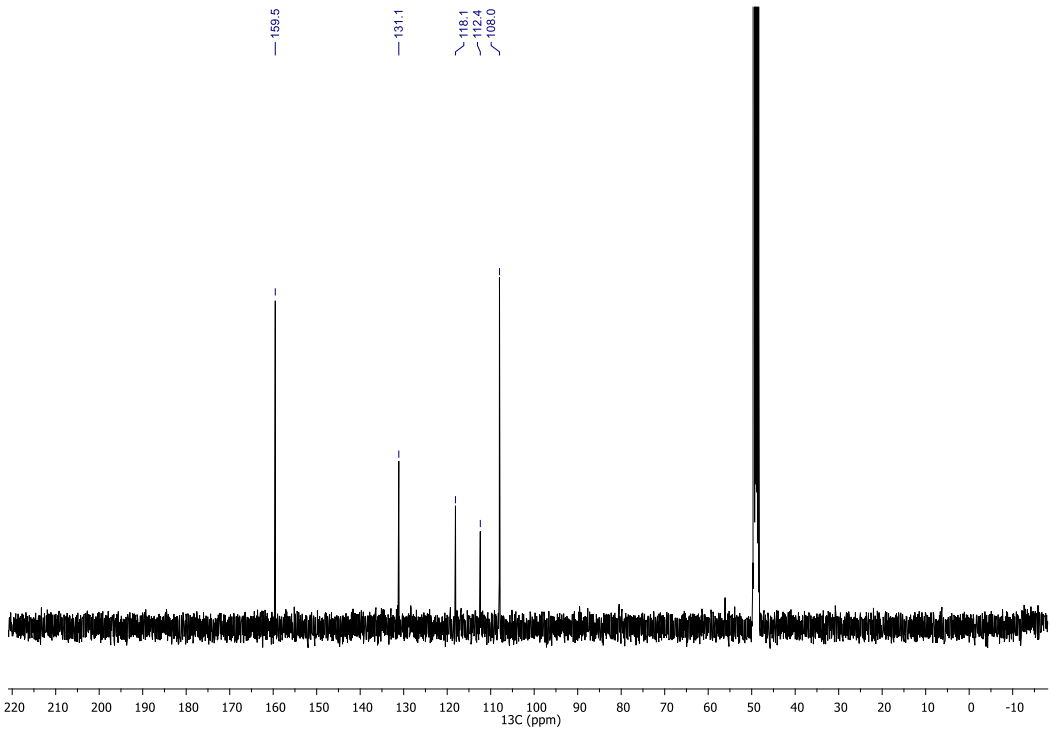

Figure A11. ^{13}C NMR spectrum of *5,10,15,20-tetrakis(2,6-dihydroxyphenyl)porphyrin* **TPP-(OH)8** (CD_3OD, 100.6 MHz).

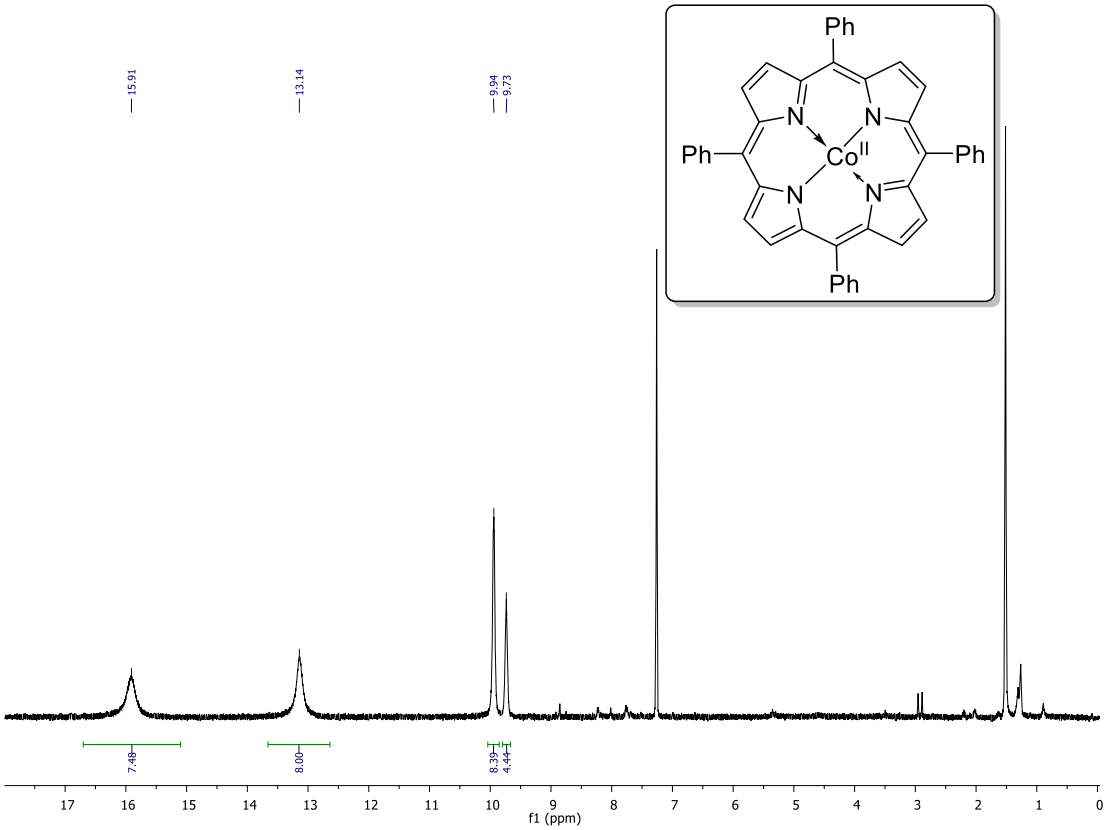

Figure A12. ^{1}H NMR spectrum of cobalt (II) 5,10,15,20-tetraphenylporphyrin CoTPP ($CDCl_3$, 100 MHz).

A2. Determination of the potential for carbon cloth covalent modification

Aminoporphyrin **TPP-NH2** (12.6 mg, 0.02 mmol) was dissolved in 20 mL of TFA:H_2O (1:1) mixture in a 50 mL round-bottom flask and cooled down to -5 ºC. $NaNO_2$ (66.4 mg) was dissolved in 10 mL of deionized water and 250 µL aliquot (1.2 eqv) was added into the flask under stirring. Reaction mixture was stirred for 30 min at -10 ºC, then the septum with three electrodes was placed on top and cyclic voltammograms were recorded. Blank experiment without addition of $NaNO_2$ was performed under the same conditions. The appearance of irreversible reduction peak around -0.05 V vs AgCl (3M KCl) after addition of $NaNO_2$ corresponds to the reduction of $-N_2^+$ group and the formation of transient aromatic radicals attacking carbon surface (Figure A13a). Notably, during the first scan insulating organic layer was formed as evidenced by the lack of significant redox responses during the second cycle (Figure S6A) in strong contrast to the blank acidic solution of **TPP-NH2** (Figure A14b). Since overreduction of aromatic radicals upon cycling to -0.4 V vs SCE was reported by Picot et al.,[1] we opted to use more positive potential of 0.0 V vs AgCl in the potentiostatic mode.

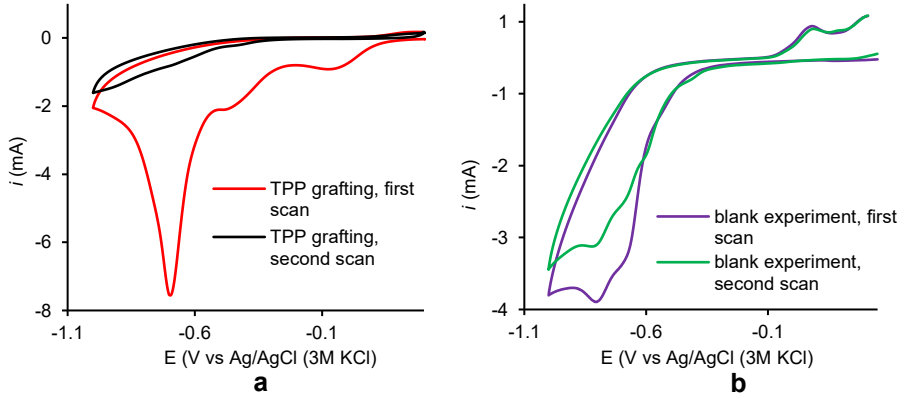

Figure A13. CV of (a) **TPP-N2+** formed via diazotation of **TPP-NH2**; (b) CV of **TPP-NH2** without $NaNO_2$ in TFA/H_2O (1:1).

A3. Evidence of TPP-N_2^+ formation in the grafting solution

Although **TPP-N2+** was not isolated form the reaction mixture during carbon cloth modification, its formation is evidenced by the formation of a corresponding 5-(4-hydroxyphenyl)-10,15,20-trihenylporphyrin **TPP-OH** as depicted in the Scheme A1.

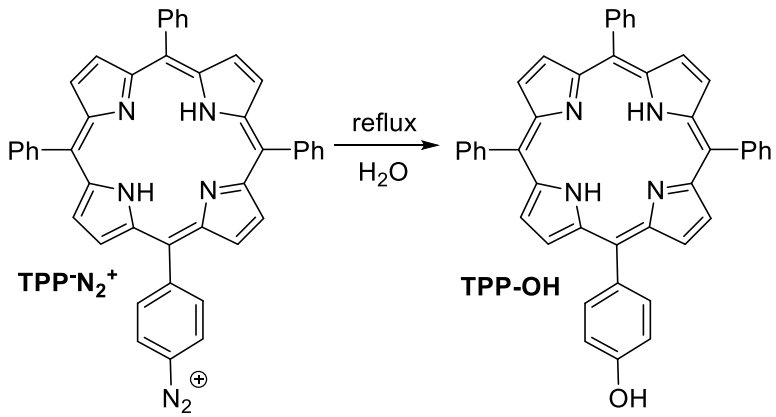

Scheme A1. Formation of 5-(4-hydroxyphenyl)-10,15,20-triphenylporphyrin (**TPP-OH**).

Solution left after 5 grafting experiments was brought to a boil and solvent (TFA + H_2O) was distilled off. The gunky residue was neutralised with saturated aqueous solution of $NaHCO_3$, organics were extracted with CH_2Cl_2. Extract was dried with anhydrous Na_2SO_4 and solvent was removed under reduced pressure. The main product of the reaction was isolated by column chromatography (CH_2Cl_2:PE 1:4 → neat CH_2Cl_2) (13.4 mg; 18 %). No aminoporphyrin was found in the mixture confirming 100 % consumption of **TPP-NH₂** in diazotation.

^{1}H NMR (400 MHz, $CDCl_3$) δ 8.89 – 8.85 (m, 8H), 8.24 – 8.22 (m, 6H), 8.07 – 8.05 (m, 2H), 8.03 – 8.00 (m, 2H), 7.79 – 7.74 (m, 9H), 7.16 – 7.14 (m, 2H), 5.13 (s, 1H), -2.75 (s, 2H) ppm

^{13}C NMR (100 MHz, $CDCl_3$) δ 155.6, 142.4, 142.3, 135.8, 134.9, 134.7, 131.2, 127.9, 126.8, 120.3, 120.2, 120.0, 113.8 ppm

HRMS (ESI) calculated for $C_{44}H_{31}N_4O$ $[M+H]^+$: m/z 631.24924, found 631.24845.

Spectral data are in accordance with reported literature values (Figures A14, A15).[2]

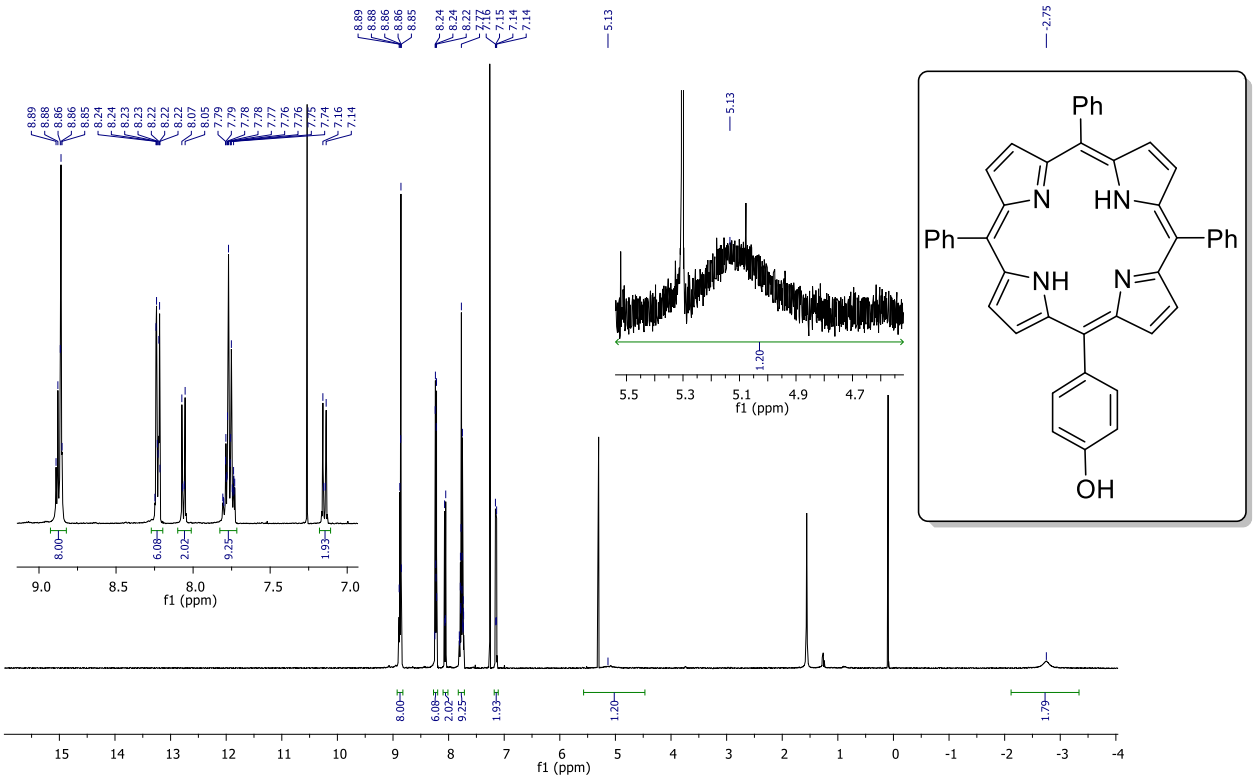

Figure A14. ^{1}H NMR spectrum of 5-(4-hydroxyphnenyl)-10,15,20-triphenylporphyrin **TPP-OH** ($CDCl_3$, 400 MHz).

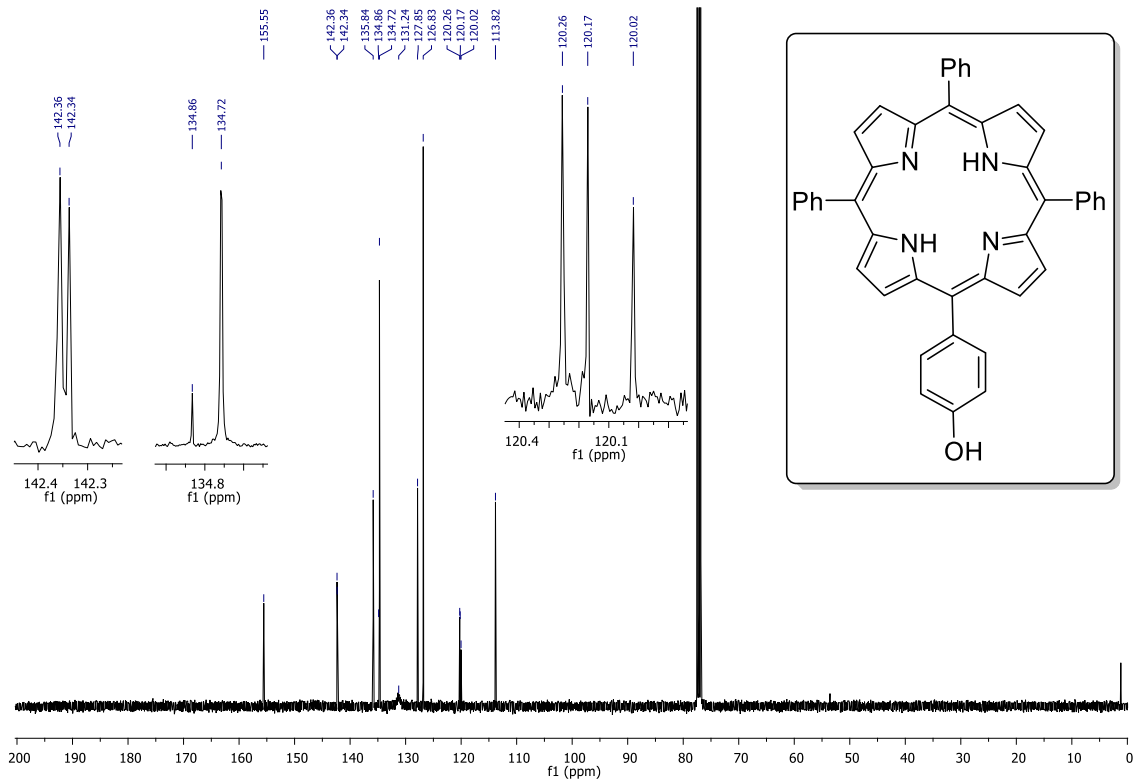

Figure A15. ^{13}C NMR spectrum of 5-(4-hydroxyphnenyl)-10,15,20-triphenylporphyrin **TPP-OH** ($CDCl_3$, 100 MHz).

A4. Determination of carbon cloth relative electrochemically active surface area

Electrochemically active surface area of carbon cloth was determined via measurements of double layer (DL) capacitance in aqueous 0.1 $KClO_4$ at – 0.39 V vs NHE where no faradic current was observed.[3] 5 mm polished glassy carbon disk electrode was used as a standard. CVs were recorded at scan rates from 0.05 to 0.5 V/s and linear correlation of capacitance current on sweep rate was observed. Slopes of the graphs indicate DL capacitance values (Figure A16)

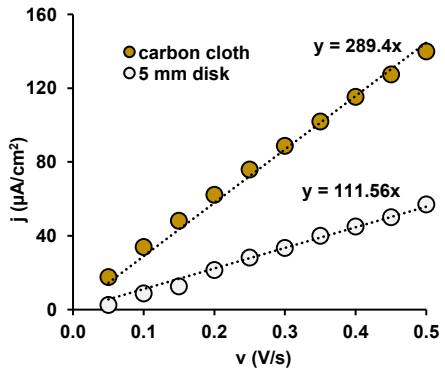

Figure A16. Anodic capacitive current densities obtained for carbon cloth and polished 5 mm glassy carbon disc electrodes.

Ratio of electrochemically active surface area (S_{EA}) to geometric area (S_G) of carbon cloth was found using Equation A1:

$$S_{EA}/S_G = \frac{C_{carbon\ cloth}}{C_{glassy\ carbon}} = 2.6\ (\textbf{Equation A1})$$

Where $C_{carbon\ cloth}$ is DL capacitance of carbon cloth (μF/cm^2) and $C_{glassy\ carbon}$ is DL capacitance of polished glassy carbon (μF/cm^2).

A5. Electrochemical behaviour of MnTPP and tetraphenylporphyrin in DMF

To determine the nature of complex electrodeposited on carbon, Mn^{III}/Mn^{II} (-0.70 V) and Mn^{II}/Mn^{I} (-1.81 V) redox waves of MnTPP were recorded (Figure A17, black trace). Additionally, CV study of free-base ligand was performed to confirm the identity of weak redox response centred around -1.60 V (Figure A17, red trace).

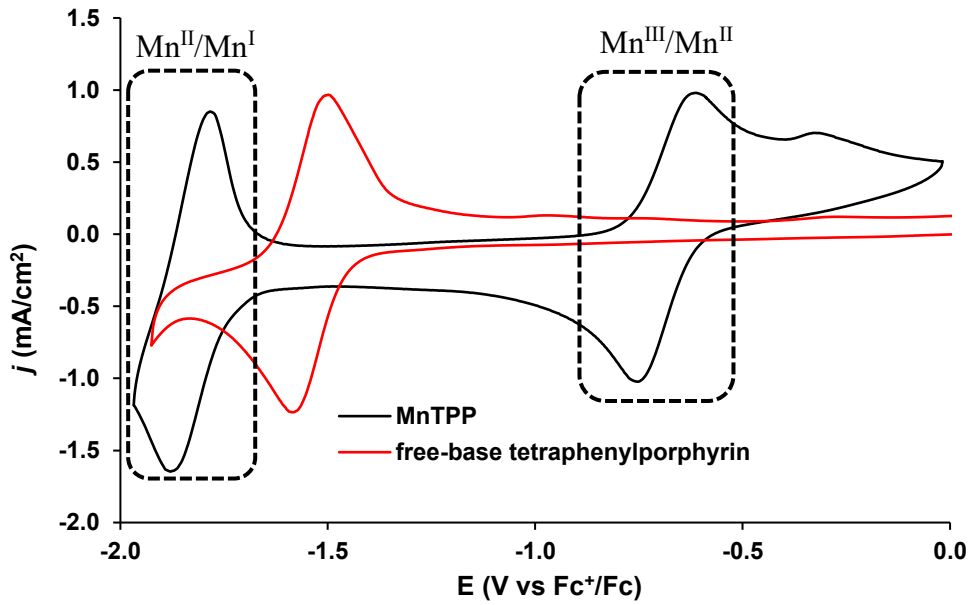

Figure A17. CVs of manganese porphyrinate (MnTPP) (black trace) and free-base tetraphenylporphyrin (red trace) recorded in dry degassed DMF electrolyte. Scan rate: 50 mV/s; TBAP concentration: 0.1 M; concentration of analytes: 2 mM.

A6. Long-run OER experiments on MnTPP-cov/5 and MnTPP-noncov

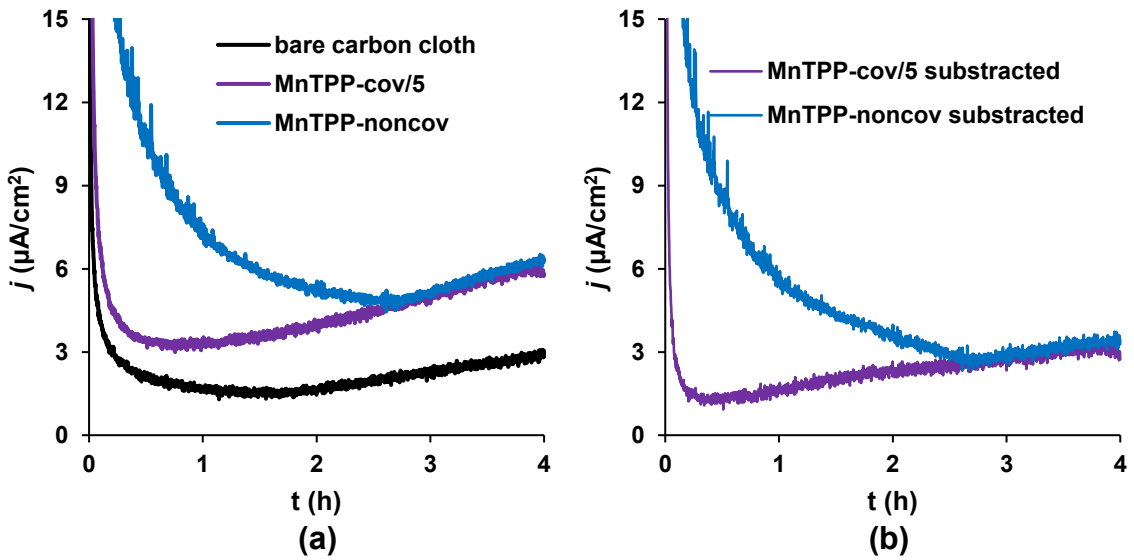

Figure A18. (a) CPE curves for **MnTPP-noncov** (blue trace), **MnTPP-cov/5** (violet trace) and bare carbon cloth (black trace) under 1.55 V vs NHE; (b) CPE curves of **MnTPP-noncov** and **MnTPP-cov/5** with background subtracted. Electrolyte: degassed 0.5 M H_2SO_4.

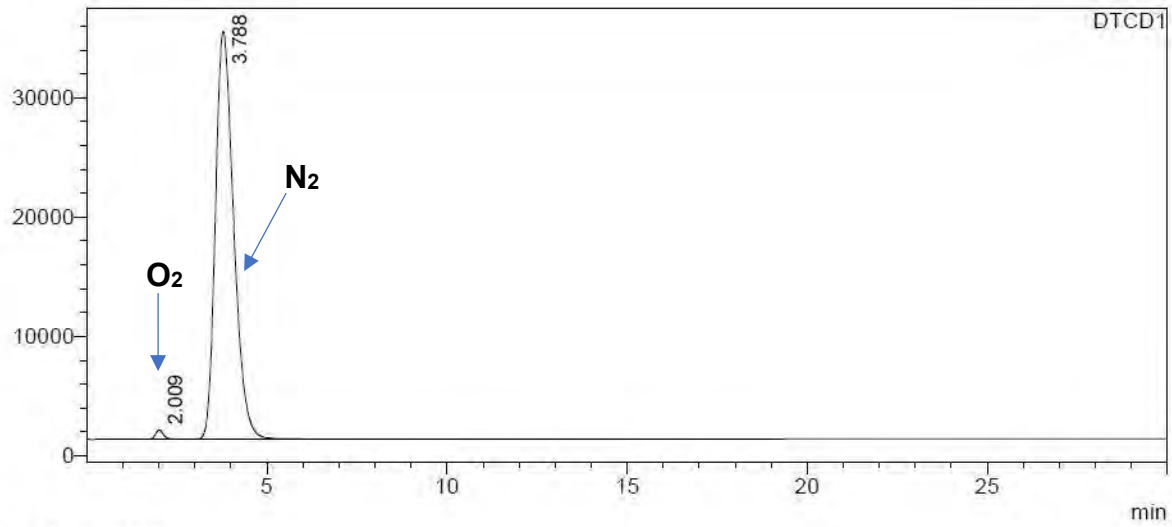

<Peak Table>

DTCD1

Peak#	Ret. Time	Area	Height	Conc.	Unit	Mark	Name
1	2.009	11910	777	0.980		M	
2	3.788	1203805	34173	99.020		M	
Total		1215715	34950				

Figure A19. GC analysis of anodic headspace gases after CPE on **MnTPP-cov/5**.

A7. Equivalent circuits for EIS analysis

Equivalent circuits simulating EIS characteristics are presented in Figures A20a-c.

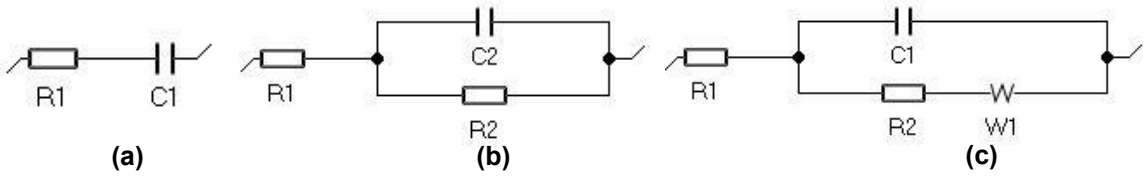

Figure A20. Schematic representation of equivalent circuits: (a) purely capacitive coating; (b) Randles circuit; (c) circuit containing Warburg impedance. Abbreviations: R1 - solution resistance, R2 charge transfer impedance (resistance due to limited rate of electrochemical reaction), C2 – capacitance of electric double layer, W1 – Warburg impedance (arising from diffusion limitations).

A8. Structure of MnTPP-cov/5 and MnTPP-cov/10

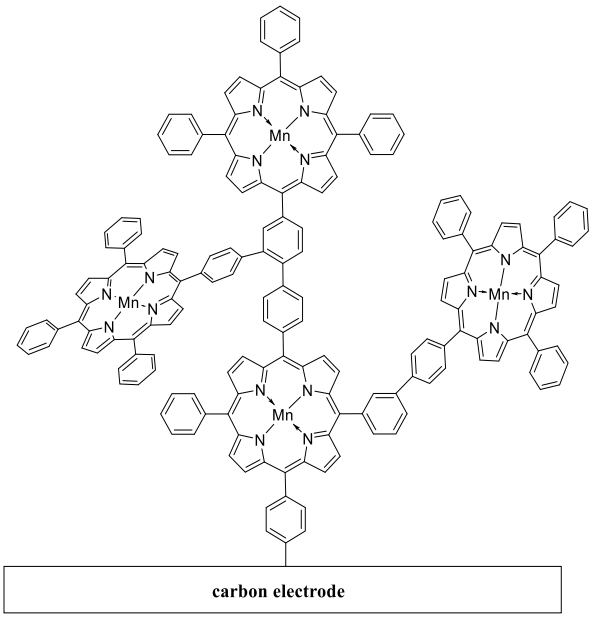

Figure A21. Schematic representation of **MnTPP-cov/5** and **MnTPP-cov/10** structures. Polymerization and more extensive branching of organometallic moieties is thought to affect current onset compared to **MnTPP-cov/1**.

A9. ETNs observed MnTPP-cov/5 in acidic electrolyte

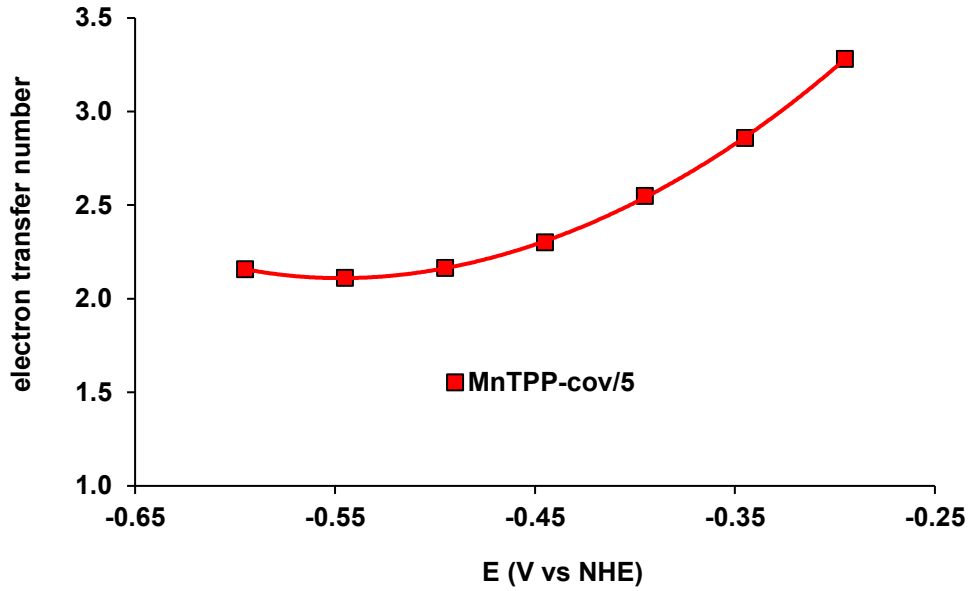

Figure A22. Electron transfer number observed in ORR on **MnTPP-cov/5** in acidic medium. Electrolyte: O_2-saturated 0.5 M H_2SO_4.

A10. Koutecky-Levich plots of MnTPP-cov/10 in alkaline medium

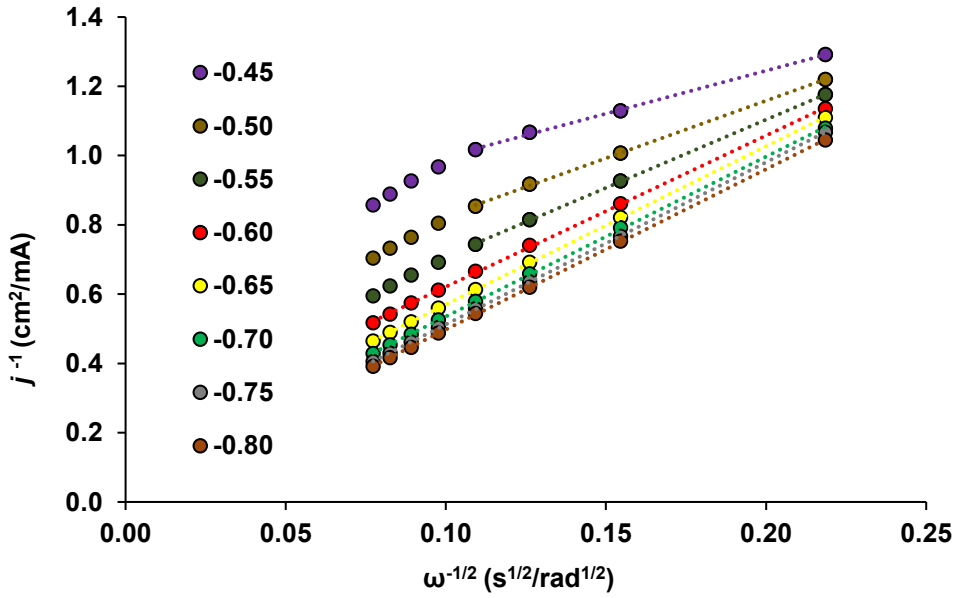

Figure A23. Koutecky-Levich plots obtained for **MnTPP-cov/10** during RDE experiments in O_2-saturated 0.1 M KOH.

A11. Stability study of MnTPP-cov/5 in ORR

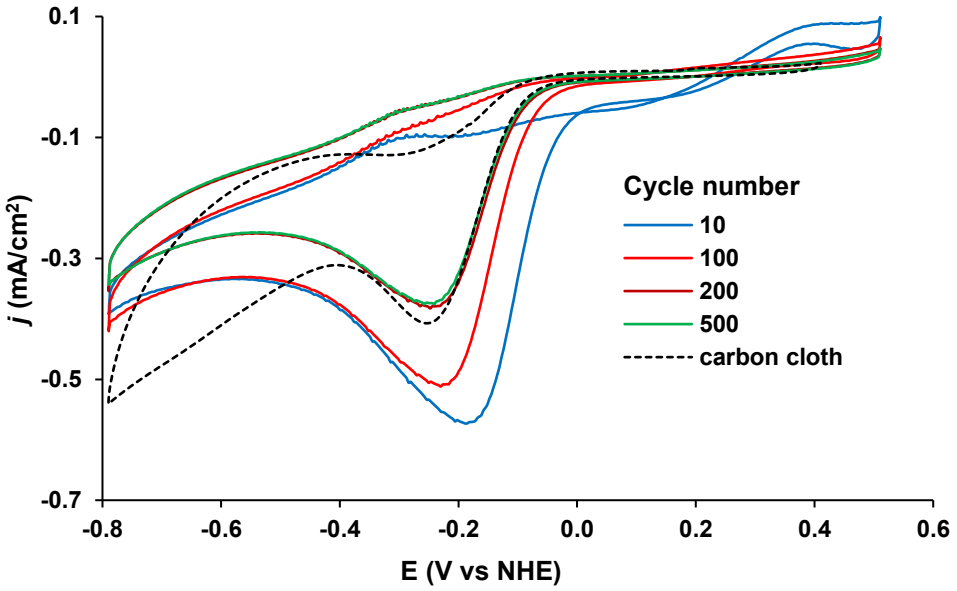

Figure A24. Changes in CV of **MnTPP-cov/5** upon prolonged cycling in the conditions of ORR. CV of bare carbon cloth is shown for clarity (black dotted line). Electrolyte: O_2-saturated 0.1 M KOH; scan rate: 50 mV/s.

A12. Proposed mechanism of MnTPP-cov/5-catalysed ORR

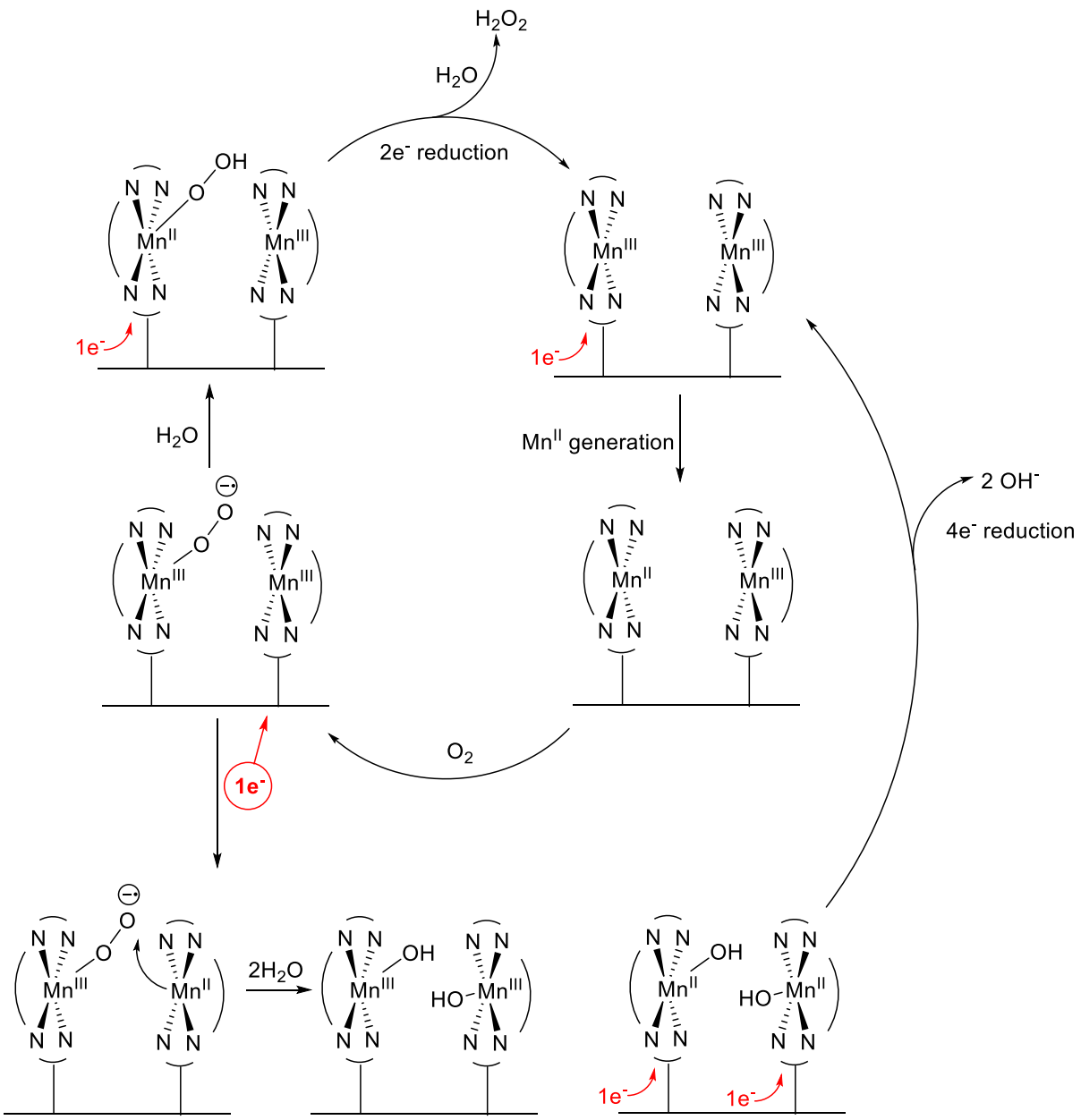

Figure A25. Proposed mechanism of ORR catalysed by **MnTPP-cov/5** in alkaline medium.

A13. NMR study of MnTPP reductive decomposition products

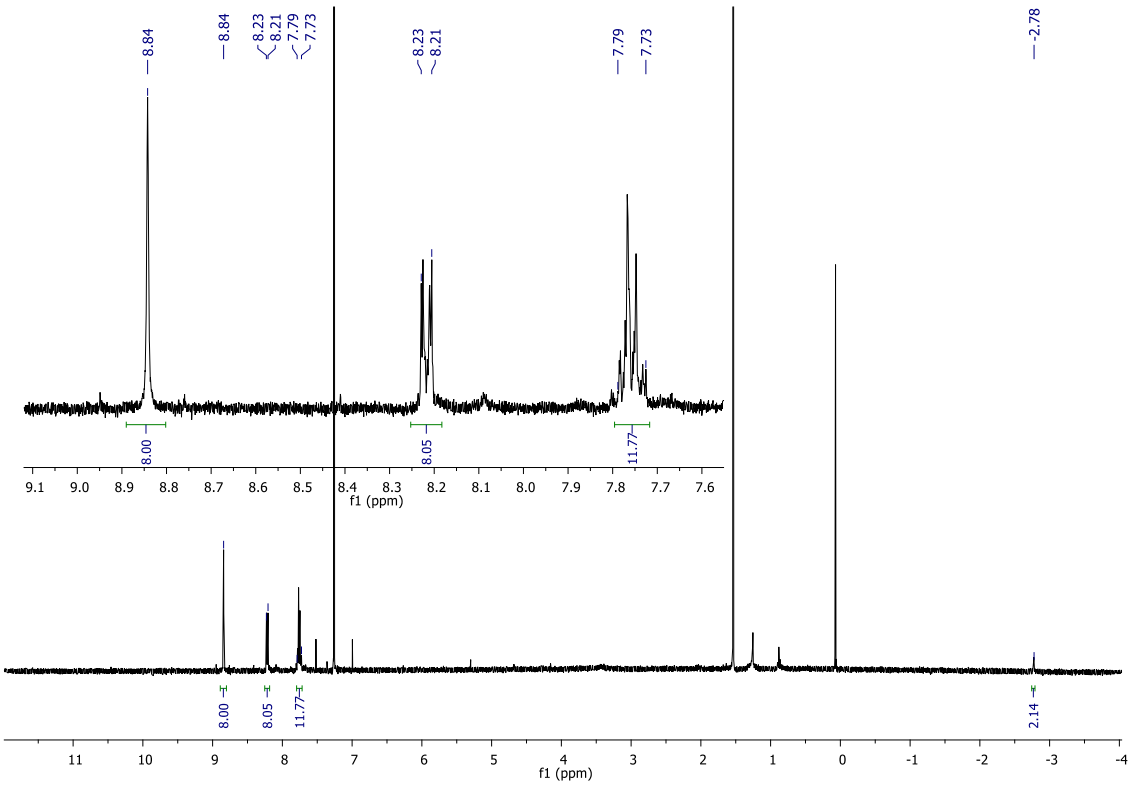

Figure A26. ^{1}H NMR spectrum of *meso*-tetraphenylporphyrin isolated after electrolysis of $Mn^{III}TPP$ at -2.0 V vs Fc^{+}/Fc ($CDCl_3$, 400 MHz).

A14. Morphology of CoTPP-noncov

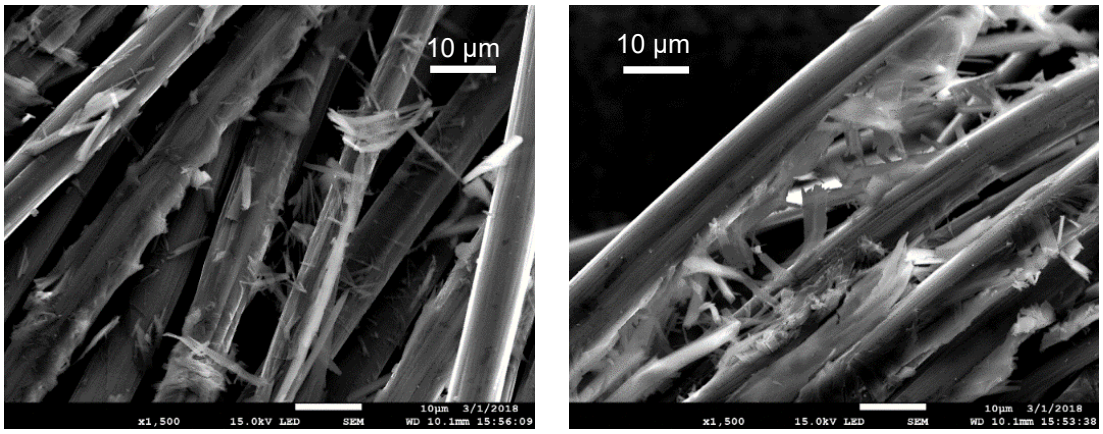

Figure A27. Representative SEM images of **CoTPP-noncov**. Flaky and needle-shaped crystals of CoTPP are clearly seen.

XRD of pulverized carbon cloth and **CoTPP-noncov** showed that carbon cloth is essentially a fiber-like graphite (Figure A28).[4] Although formation of microcrystals is evident from SEM, the amount of complex is well below the threshold of XRD sensitivity and hence, both materials have identical diffraction pattern.

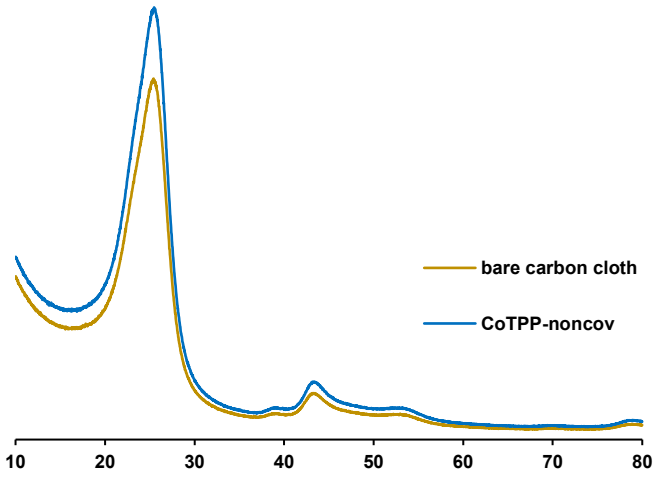

Figure A28. XRD patterns of carbon cloth and **CoTPP-noncov**.

A15. CoTPP-cov/1 and CoTPP-noncov double layer capacitance

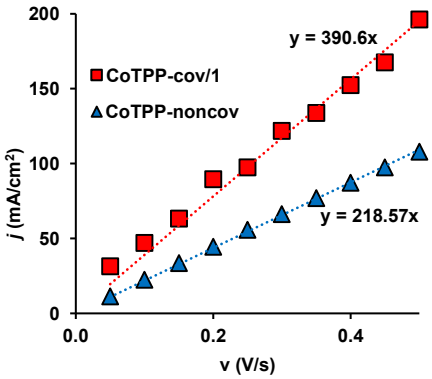

Figure A29. Anodic capacitive current as a function of CV scan rate measured for **CoTPP-cov/1** and **CoTPP-noncov** in degassed 0.1 M KOH electrolyte.

A16. CO_2ERR blank experiments

4 h long electrolysis on carbon cloth working electrode at -1.10 V vs NHE showed evolution of 1.7 µmol/cm^2. Deposition of $8 \cdot 10^{-8}$ mol/cm^2 of catalytically inactive zinc tetraphenylporphyrin (ZnTPP) further decreased the amount of CO to 0.5 µmol/cm^2 (Figure A30a).

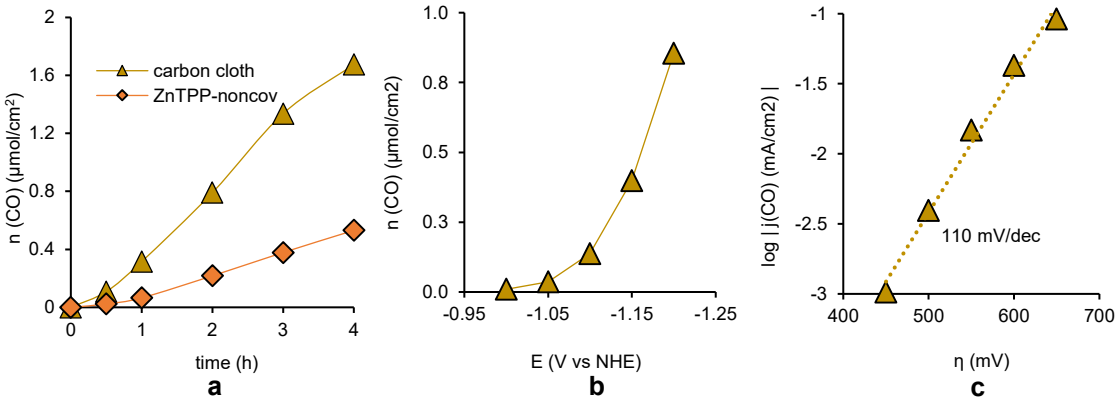

Figure A30. (a) CO evolution on bare carbon cloth and on a carbon cloth electrode loaded with $8 \cdot 10^{-8}$ mol/cm^2 of zinc (II) tetraphenylporphyrin (ZnTPP) during 4 h long electrolysis at -1.10 V vs NHE; (a) CO evolution on carbon cloth treated with $Co(OAc)_2$ and (b) Tafel plot of CO reduction current.

Also, a series of 30 min electrolyses at various potentials was performed on the carbon cloth treated with hot solution of $Co(OAc)_2$ in DMF/CH_3COOH and washed with DMF and water (Figure A30b). 0.9 µmol of CO was produced at -1.20 V vs NHE and Tafel plot slope was 110 mV/dec (Figure A30c) which is close to theoretically expected 118 mV/dec for an uncatalysed process with the single-electron reduction being a rate-limiting step. FE (CO) did not exceed 4% at any potential.

Experiments described above clearly evidence that almost all CO_2 reduction current comes from CoTPP. Moreover, deposition of porphyrinate further decreases activity of carbon cloth to negligible levels. Based on these, we neglected activity of the support since it is well within the experimental error.

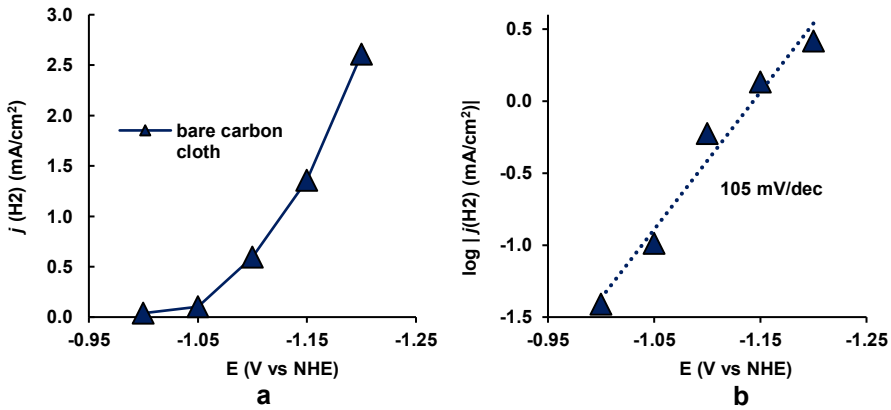

Figure A31. (a) H_2 evolution current on bare carbon cloth and (b) corresponding Tafel plot.

A17. H_2 evolution currents on CoTPP-cov/1 and CoTPP-noncov

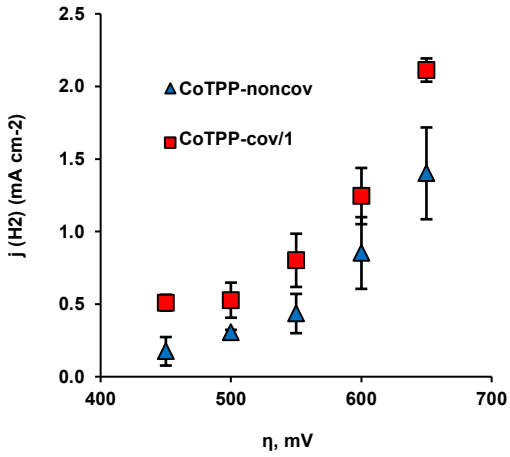

Figure A32. Water discharge currents observed during electrokinetic studies of **CoTPP-cov/1** and **CoTPP-noncov**.

A18. 24 h-long CO_2ERR on CoTPP-cov/1 and CoTPP-noncov

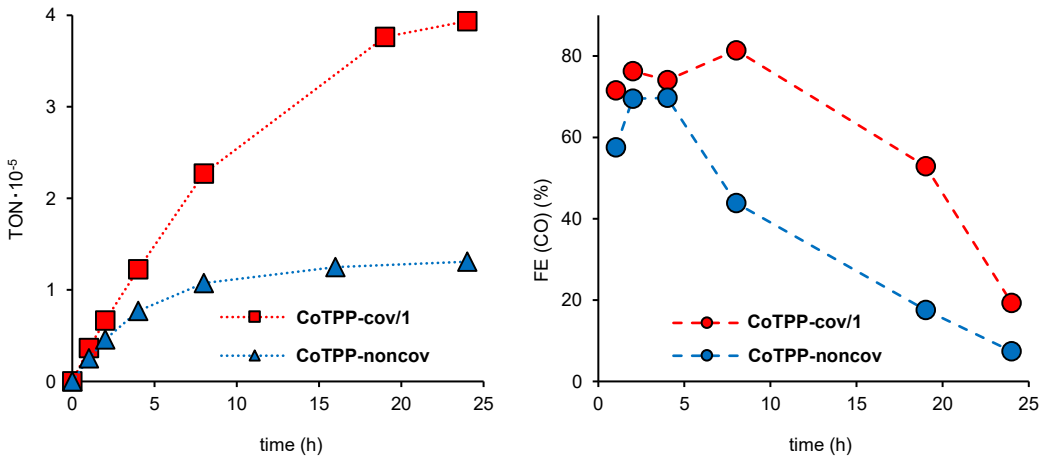

Figure A33. (a) TON and (b) FE (CO) during 24 h long CPE on **CoTPP-cov/1** and **CoTPP-noncov**.

A19. Homogeneous nature of ORR redox couple observed on CoTPP-noncov

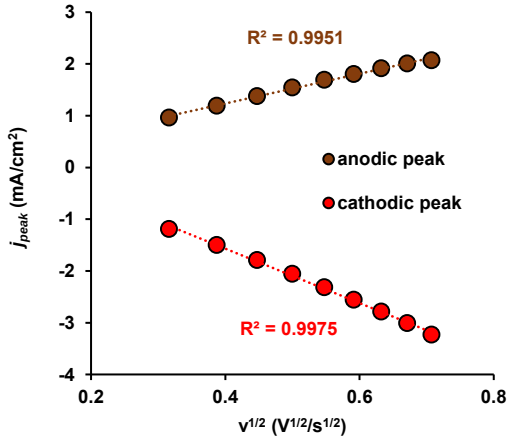

Figure A34. Dependence of ORR peak current on square root of the scan rate observed on **CoTPP-noncov** in 0.1M KOH.

A20. FTIR spectroscopy of CoTPP deactivation products

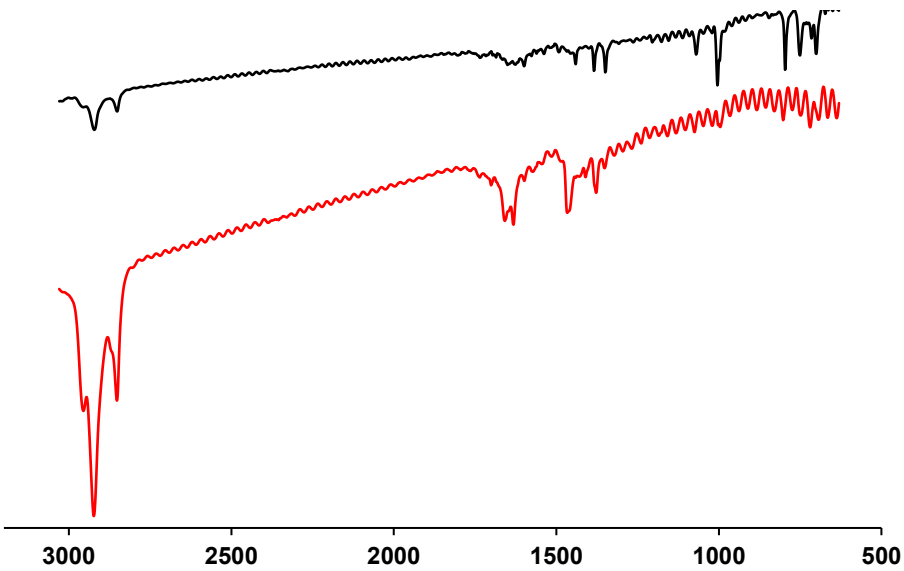

Figure A35. FTIR spectra of pure CoTPP (black trace) and its deactivation products after CO_2ERR (red trace).

A21. NMR ^{1}H of organics extracted from the electrolyte after CO_2ERR

Extraction of organics from electrolyte with CH_2Cl_2 and the following removal of the solvent also gave colourless substance which was found in the blank experiment. Clearly, no signals corresponding to CoTPP were detected as it is ether absent in the mixture the amount is below the NMR detection limit.

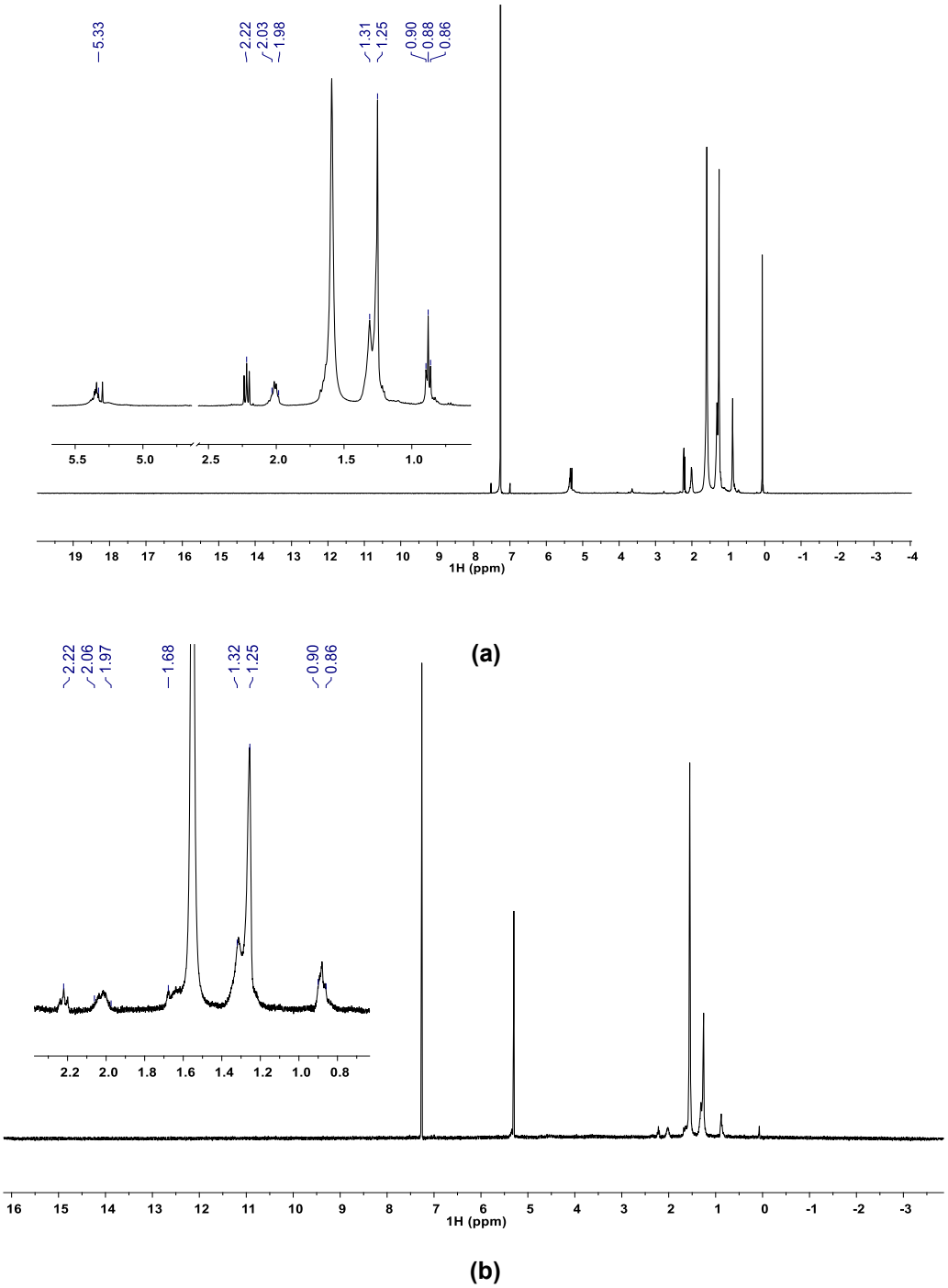

Figure A36. ^{1}H NMR spectra of the products extracted from the electrolyte after CO_2ERR on (a) **CoTPP-noncov** and (b) **CoTPP-cov/1**. No CoTPP signals were found in both cases. The only organics detected were the products of carbon fabric reduction.

A22. NMR spiking experiment

As free-base tetraphenylporphyrin has an ^{1}H NMR spectrum very similar to the one of deactivation product, we performed a spiking experiment to additionally confirm absence of Co loss during electrolysis. To do that, an ^{1}H NMR spectrum of CoTPP deactivation products was recorded (green trace in the Figure A37a), then a crystal of TPP was added to the same tube and the new spectrum was observed (red trace in the Figure A37a). The result shows clear difference in *β*-CH shifts of the **component X** and TPP (Figure A37a) and the appearance of characteristic NH signal after TPP addition (Figure A37b) thus excluding demetallation during CO_2ERR as a possible decomposition pathway.

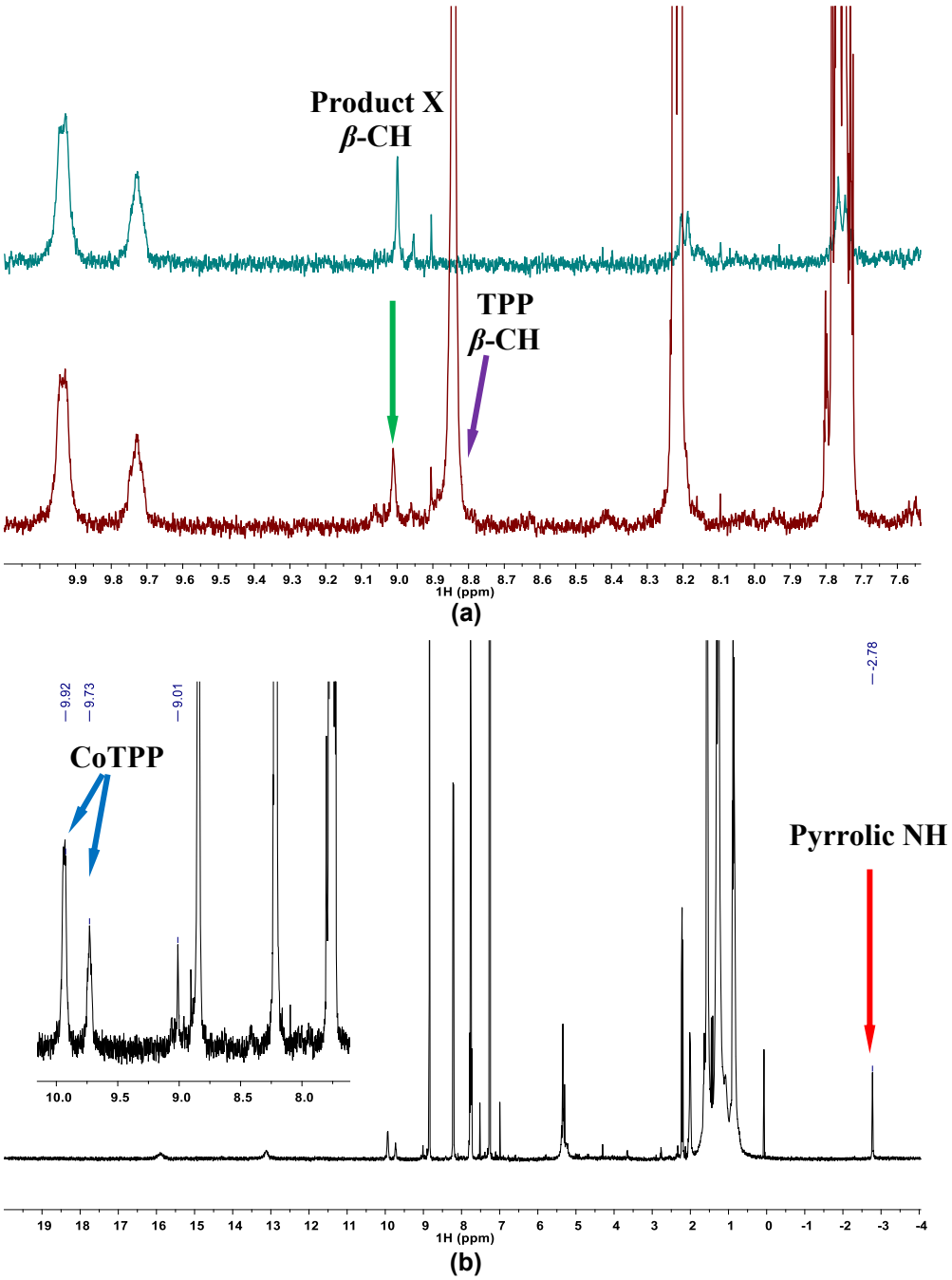

Figure A37. (a) ^{1}H NMR spectrum of CoTPP deactivation products before (green trace) and after addition of TPP (red trace); (b) full spectrum of the mixture of **component X** and TPP.

A23. Blank CPE on bare carbon cloth

Standard 4 h long CO_2ERR was performed on a 4 cm^2 bare carbon cloth electrode at -1.05 V vs NHE. The organics were washed off with CH_2Cl_2 and the solvent was removed. Small amount of colourless residue was collected and transferred to NMR tube. The resulting spectrum is shown in Figure A38. Clearly, signals of alkenyl and aliphatic protons originate from the products of reductive decomposition of carbon fabric itself. Notably, the same NMR pattern was found even for carbon cloth which was previously repetitively washed for 24 h with boiling trifluoroacetic acid, chlorobenzene and chloroform. Thus, we could ascribe the appearance of aliphatic signals to the reduction of carbon cloth itself rather than to impurities present on the surface.

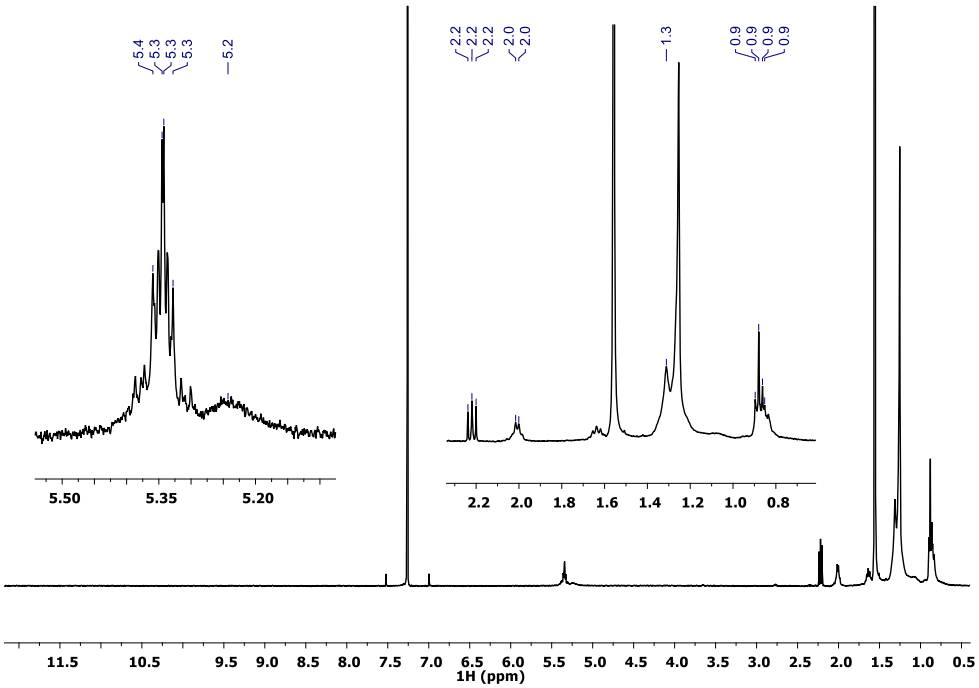

Figure A38. ^{1}H NMR spectrum of organics extracted from the surface of bare carbon cloth electrode after its exposure to standard conditions of CO_2ERR (CD_3OD, 400.1 MHz).

Probably, the reduction of carbon itself is facilitated by the presence of nitrogen in the structure as ^{15}N HSQC experiment performed on CoTPP decomposition products shows presence of three types of NH groups (Figure A39).

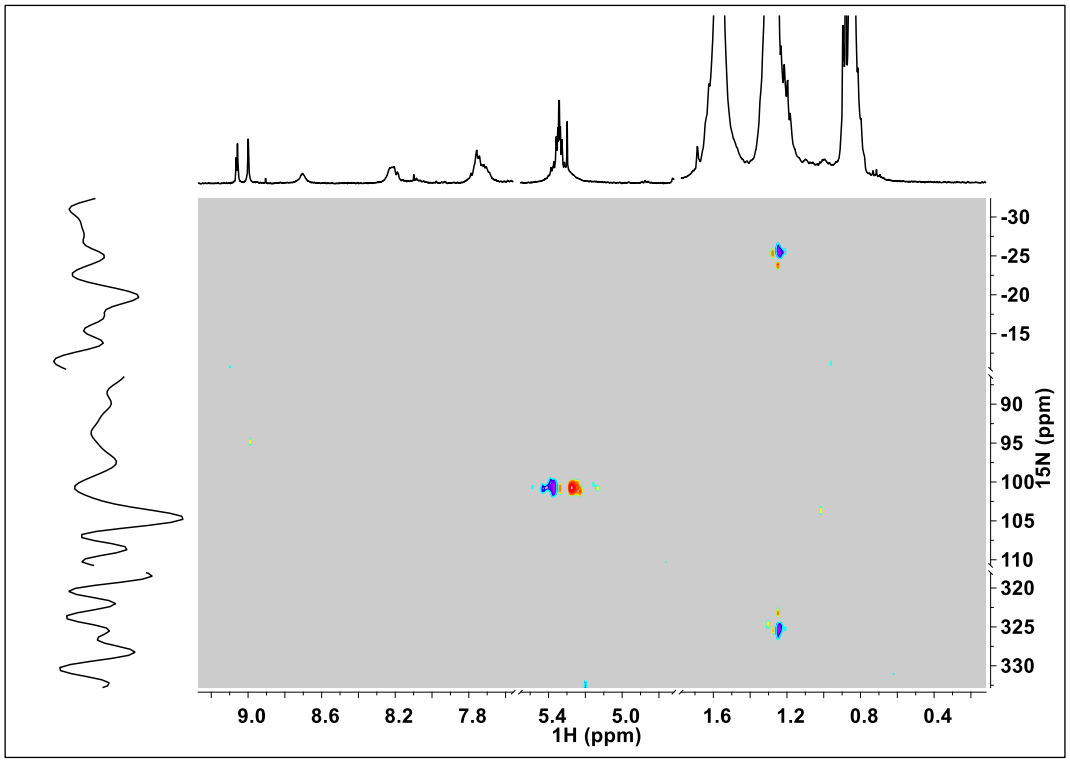

Figure A39. ^{15}N HSQC NMR of CoTPP decomposition products

A24. Deactivation in CO_2-free medium and in fully deuterated electrolyte

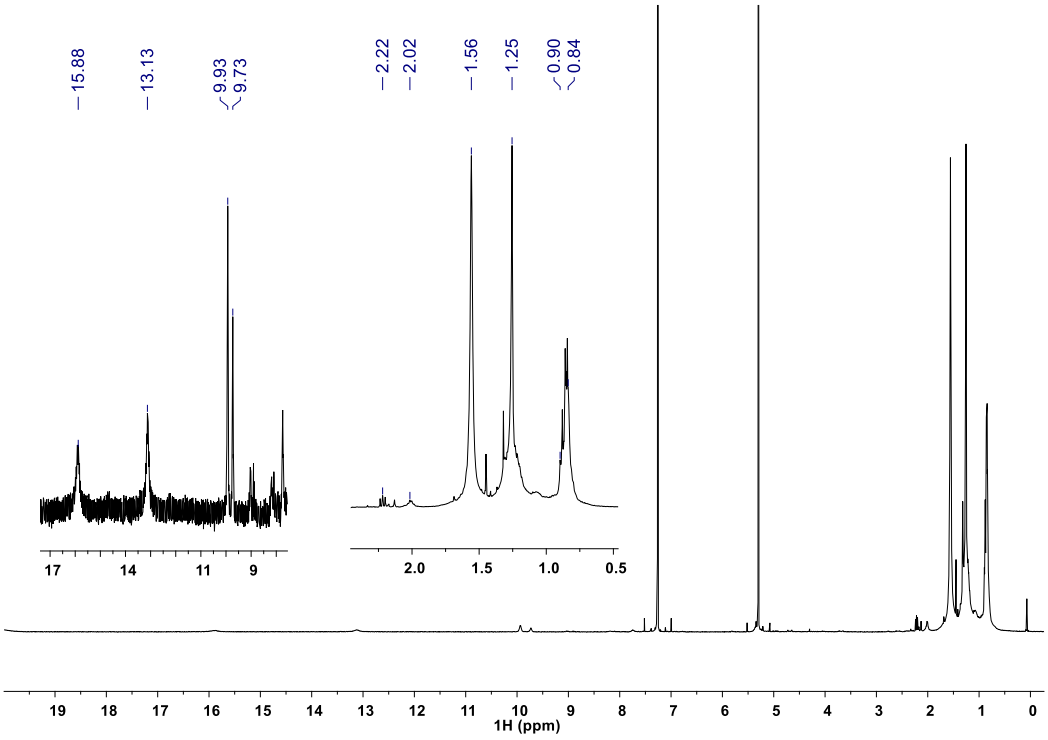

Figure A40. NMR ^{1}H of CoTPP after electrolysis in degassed 0.1 M $KClO_4$.

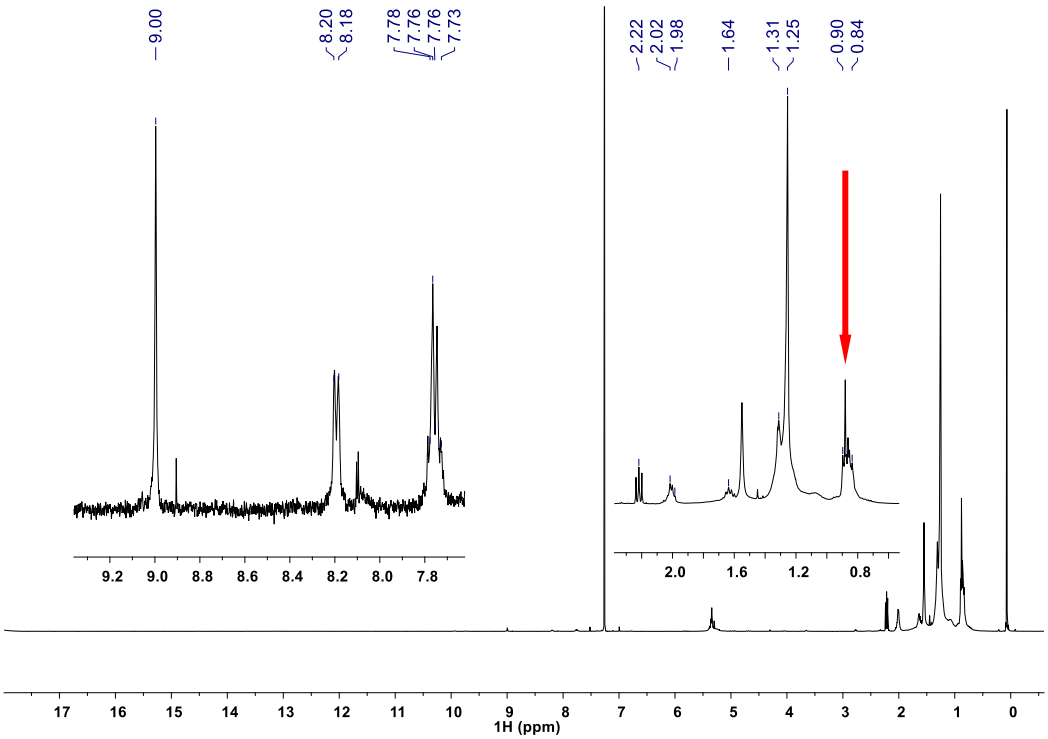

Figure A41. NMR ^{1}H of CoTPP after electrolysis in CO_2-saturated 0.5 M $KDCO_3$ in D_2O. The peak showing decrease of intensity compared with the reaction performed in protonated solvent is shown with arrow.

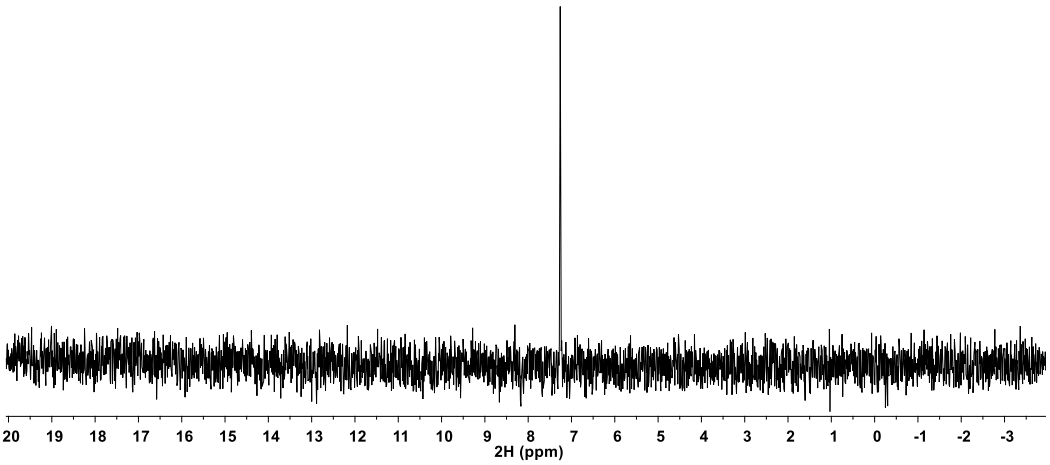

Figure A42. NMR ^{2}D of CoTPP after electrolysis in fully deuterated system.

A25. COSY and NOESY NMR spectra of CoTPP deactivation products

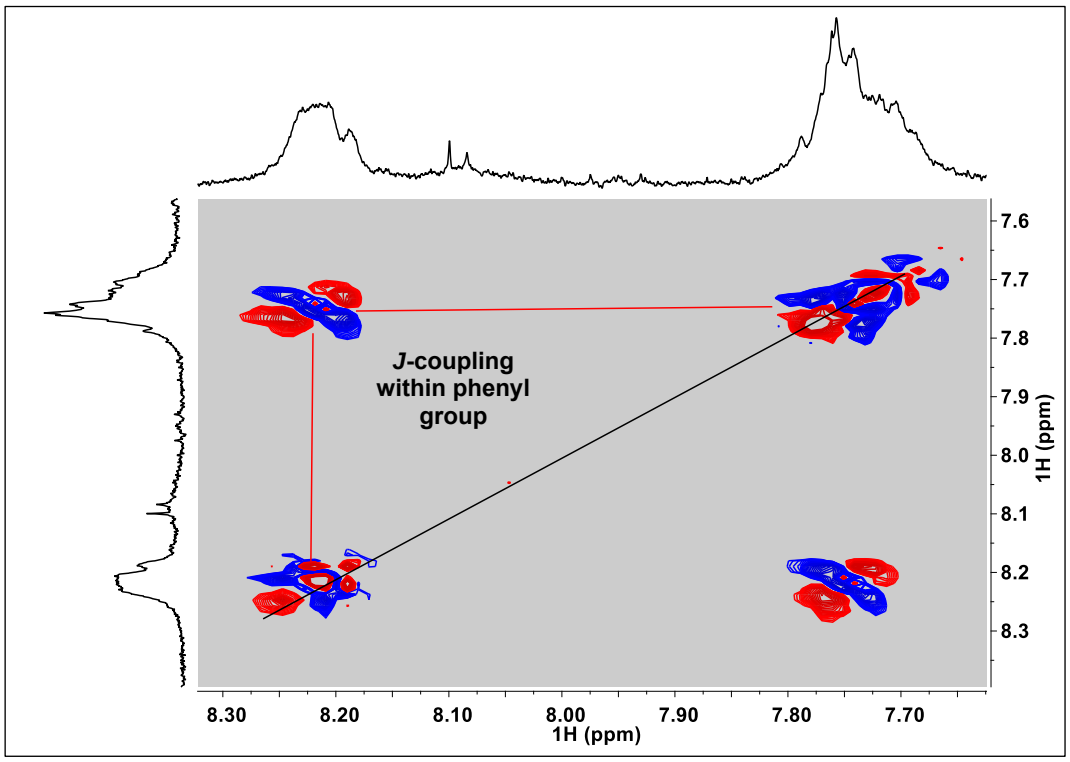

Figure A43. COSY NMR of CoTPP decomposition products.

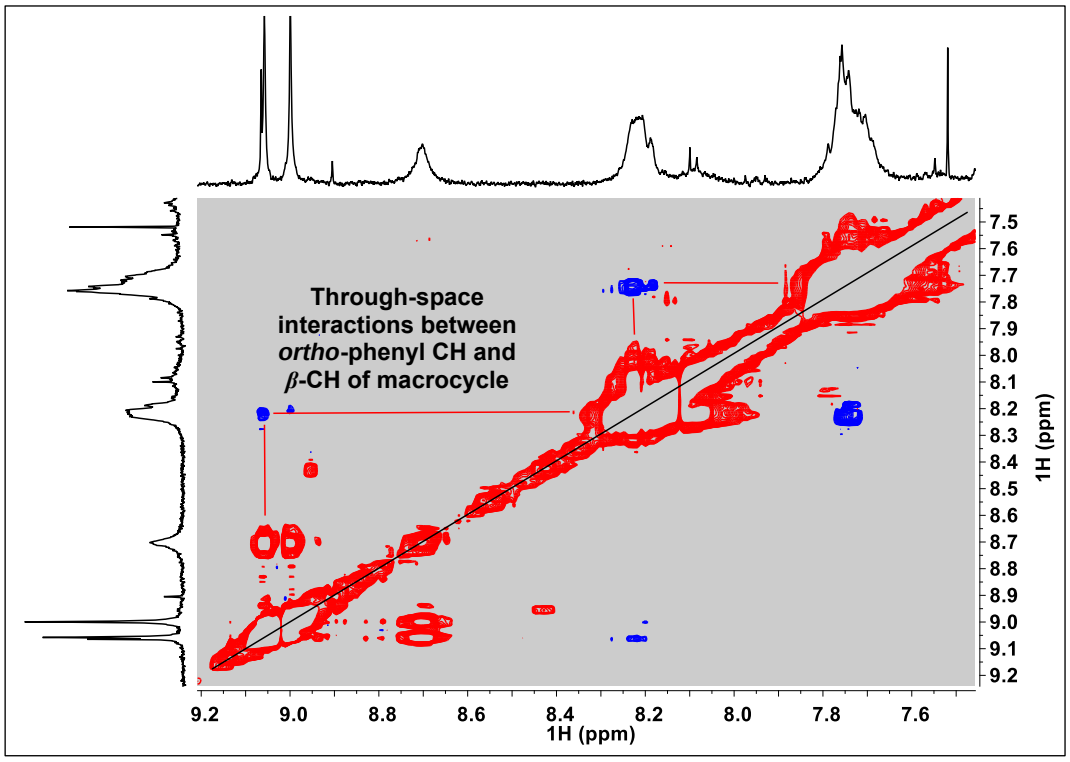

Figure A44. NOESY NMR of CoTPP decomposition products.

A26. Spectra and electrochemical behaviour of [Co^{III}TPP]

It is known that CoTPP could be oxidised to [Co^{III}TPP]L where L is a negatively charged monodentate ligand. We suspected that this oxidation might take place on the surface of electrode immediately upon completion of electrolysis and influence catalytic activity of the complex. To test this hypothesis we synthesised [Co^{III}TPP]Cl using the methodology reported earlier[5] and studied its behaviour.

To see if this complex is formed during CO_2ERR, we performed NMR ^{1}H analysis of the resulting product (Figure A45). Clearly, there are no wide singlets at 8.63, 8.23, 7.78 and 7.73 ppm in the spectra of deactivation products which means that Co^{III} porphyrin is an unlikely deactivation product (see the main text, Figure 6.1).

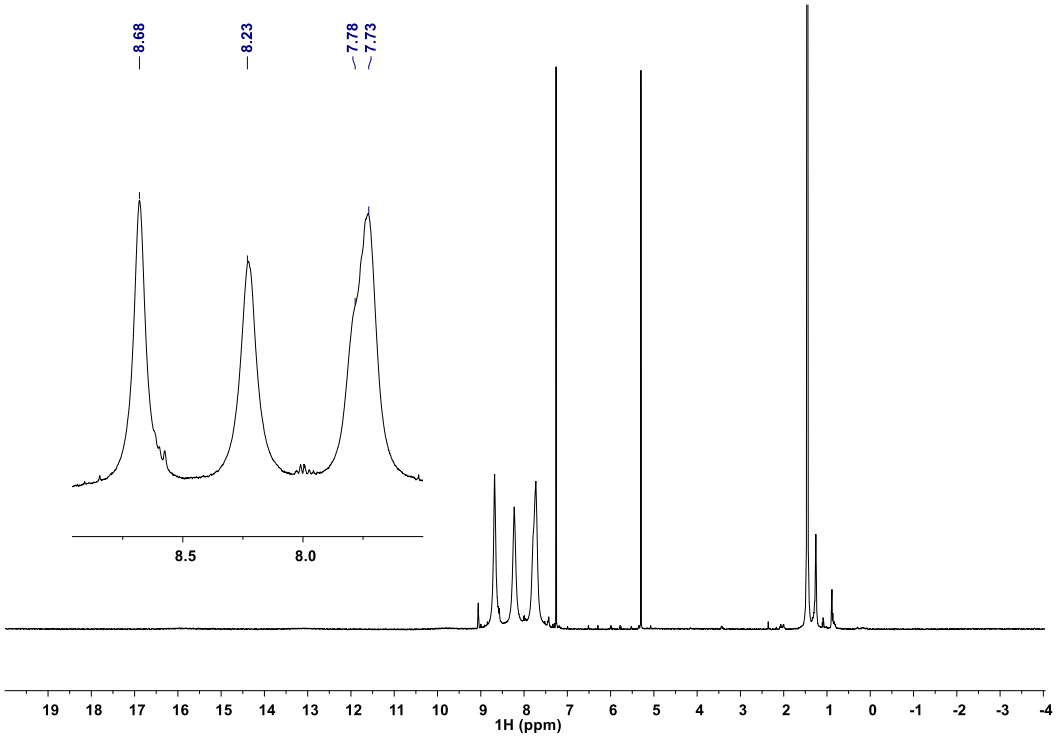

Figure A45. NMR ^{1}H of [Co^{III}TPP]Cl, 400.1 MHz ($CDCl_3$).

Further, we studied its electrochemical behaviour in aqueous and non-aqueous media using CV. Even though CV of [Co^{III}TPP]Cl in DMF is similar to the one recorded for CoTPP, its catalytic activity in aqueous electrolytes is inferior compared to Co^{II}TPP, most probably due to slow loss of the axial ligands (-Cl and -OH_2) upon reduction. This is possible considering that reductions are ligand-centred and any additional ligands coordinated to the metal core are detrimental for catalysis in aqueous medium as we have already shown on the example of pyridine.

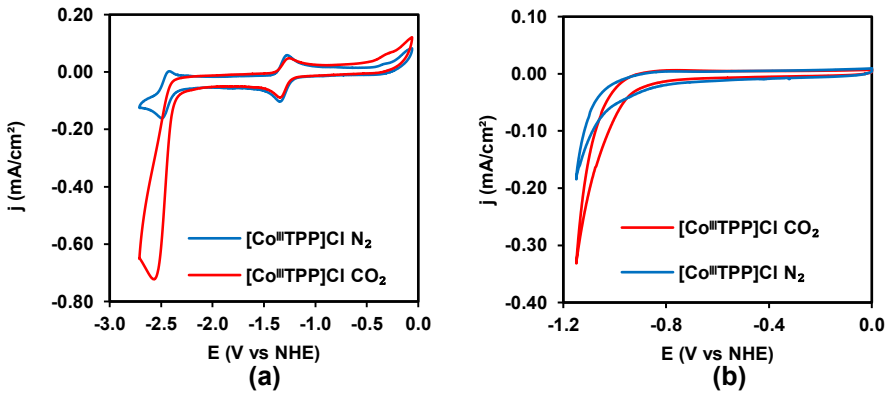

Figure A46. CV of [Co^{III}TPP]Cl in the degassed (blue line) and CO_2-saturated (red line) solvents: (a) DMF; (b) water.

A27. Performance of Co[TPP-(OMe)$_8$] at -1.10 V vs NHE

Additionally, we attempted to improve the CO_2ERR rate on **Co[TPP-(OMe)$_8$]** via increase of electrode potential to -1.10 V vs NHE. The application of only 50 mV more negative potential led to increase of FE (CO) to 12 % in the first CPE and 6 times higher CO production rate (Figure A47). However, stability started to suffer under these conditions, and the reaction rate again dropped by 55 % by the third run. Thus, the catalyst with bulky donating groups was very durable, however this was restricted to low reaction rate only. This drop of stability at higher reaction rate might stem from the increase of pH in the proximity of reaction centre which, as we found earlier, may lead to the migration of oxygen from CO_2.

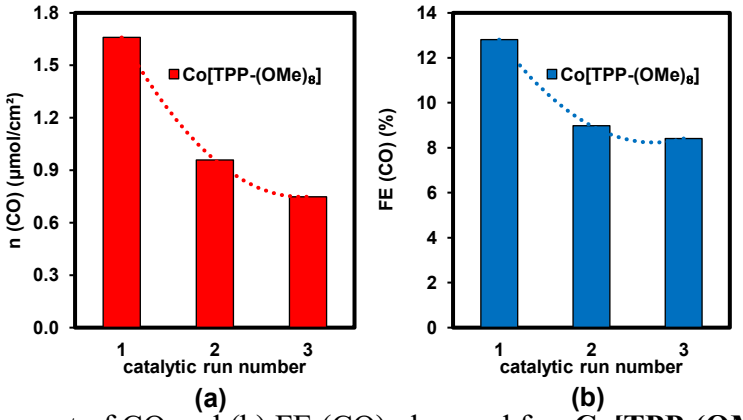

Figure A47. (a) amount of CO and (b) FE (CO) observed for **Co[TPP-(OMe)$_8$]** during three 4 h long catalytic runs in aqueous electrolyte.

A28. Stability and activity of Co[TPP-(OMe)$_3$(OH)$_5$]

We also studied activity and stability of **Co[TPP-(OMe)$_3$(OH)$_5$]** prepared through the partial demethylation of **TPP-(OMe)$_8$** with the following metalation of free-base porphyrin (Figure A47). We assumed that the presence of several bulky substituents would increase the activity of the catalyst to the levels comparable to **Co[TPP-(OH)$_8$]** and retain stability of **Co[TPP-(OMe)$_8$]**.

The resulting catalyst showed the activity intermediate between **Co[TPP-(OMe)$_8$]** and **Co[TPP-(OH)$_8$]**. CVs also show increase of current density upon saturation of electrolyte with CO_2 while FE (CO) in CPE was better than for both analogues. Even though stability of the

catalyst was also better that that of CoTPP, it was still similar to that of **Co[TPP-(OH)8]** with the total activity decrease of 42% over three 4 h long catalytic runs at -1.05 V vs NHE.

To sum up, this approach furnished a catalyst with relatively low activity and did not provide significant improvement in the catalyst lifetime.

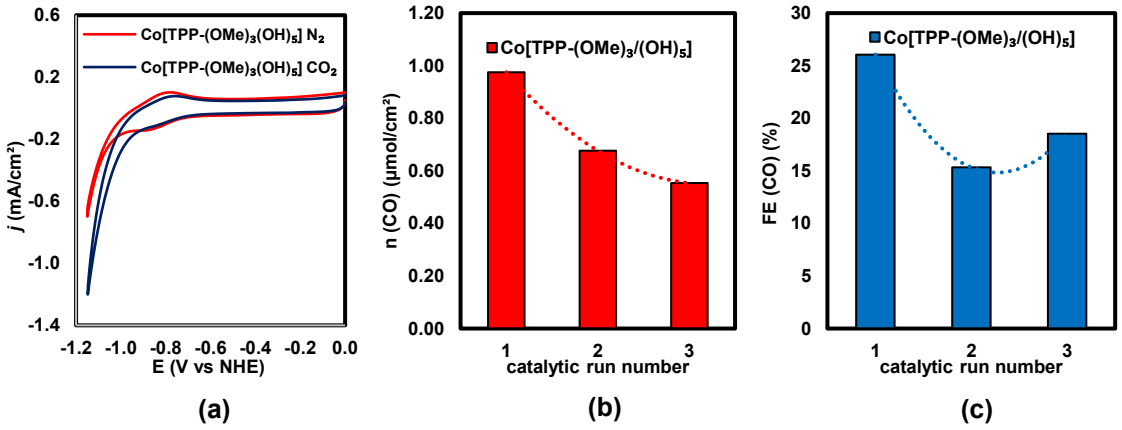

Figure A48. (a) CV of **Co[TPP-(OMe)3(OH)5]** in degassed (blue line) and CO_2-saturated (red line) 0.5 M $KHCO_3$ electrolyte; (b) amount of CO and (c) FE (CO) observed during three 4 h long catalytic runs in aqueous electrolyte.

A29. References

[1] Picot, M.; Nicolas, I.; Poriel, C.; Rault-Berthelot, J.; Barrière, F., On the nature of the electrode surface modification by cathodic reduction of tetraarylporphyrin diazonium salts in aqueous media, *Electrochem. Comm.* **2012,** 20, 167-170

[2] Brulé, E.; de Miguel, Y. R.; Hii, K. K., Chemoselective epoxidation of dienes using polymer-supported manganese porphyrin catalysts, *Tetrahedron* **2004,** 60 (28), 5913-5918

[3] David, J. G.; Kumaravelu, G.; Alastair, S.; Kate, F.; Hamish, M.; Steven, P., Ultra-nanocrystalline diamond electrodes: optimization towards neural stimulation applications, *J. Neur. Eng.* **2012,** 9 (1), 016002

[4] Li, Z. Q.; Lu, C. J.; Xia, Z. P.; Zhou, Y.; Luo, Z., X-ray diffraction patterns of graphite and turbostratic carbon, *Carbon* **2007,** 45 (8), 1686-1695

[5] Jiang, X.; Gou, F.; Chen, F.; Jing, H., Cycloaddition of epoxides and CO2 catalyzed by bisimidazole-functionalized porphyrin cobalt(iii) complexes, *Green Chem.* **2016,** 18 (12), 3567-3576